Universidad Autónoma de Madrid
Escuela politécnica superior


Proyecto fin de carrera

# FILTER DESIGN IN COAXIAL CAVITIES

Ing. Telecomunicación

Ana Morán López
Julio 2015

# FILTER DESIGN IN COAXIAL CAVITIES

AUTOR: Ana Morán López
TUTOR: Jorge A. Ruiz Cruz


Grupo de Radiofrecuencia: Circuitos, Antenas y Sistemas
Dpto. de Tecnología Electrónica y de las Comunicaciones
Escuela Politécnica Superior
Universidad Autónoma de Madrid
Julio 2015

# Abstract

A classical topic in Telecommunication Engineering is filter design at microwave frequencies. It constitutes a complex problem and therefore the whole process is divided into several stages, whose analysis is the general aim of this study.

Firstly the approximation problem is addressed by means of the generalised Chebychev method. After a process of finite transmission zeros allocation is carried out, the design polynomials are obtained. They meet the specifications typically given in the frequency domain.

From the design polynomials of the preceding stage the synthesis of the coupling matrix is developed. The coupling matrix stores information which can be directly translated into useful equivalent circuits upon which filter design at microwave frequencies is based. Sometimes there are values (i.e. called couplings) that must be annihilated in order to obtain a practical circuit topology. Towards that end matrix rotations are introduced.

Regarding physical filter design, this study raises three different approaches. In the context of lowpass filters, a stepped impedance filter is designed in coaxial technology. Both circuital and full-wave optimization are introduced under this scenario. With respect to bandpass filters, several waveguide direct-coupled filters are designed. Their full-wave responses are optimized for the sake of improvement. Finally, in the same scenario of bandpass filter design a further step is taken, and a method based on sequential stages is proposed. It is applied over a combline filter in the S-Band for mobile communications.

Budget and time constraints have prevented us from doing the manufacturing process, which could be addresses in the near future.

# Keywords

Filter design, power insertion loss method, generalised Chebychev method, coupling matrix, rotations, stepped impedance filter, direct-coupled bandpass filter, waveguide, iris, microwave cavity, resonator , combline filter, optimization, optimization method by stages.

# Resumen

Un escenario típico en Ingeniería de Telecomunicación es el diseño de filtros de radiofrecuencia. Es un problema complejo, por lo que habitualmente se aborda en varias etapas. El análisis de las mismas es el propósito general de este trabajo.

En primer lugar se decide resolver el problema de la aproximación por medio del método generalizado de Chebychev. Tras el establecimiento de los pertinentes ceros de transmisión finitos, este método obtiene los polinomios de diseño. La respuesta asociada a dichos polinomios cumple las especificaciones de diseño, típicamente dadas a través de una máscara en el dominio de la frecuencia.

En la siguiente etapa de diseño se enmarca la síntesis de la matriz de acoplos. La información numérica que almacena esta matriz se traduce directamente en un equivalente circuital. El diseño de filtros de radiofrecuencia sienta sus bases en la aproximación de estructuras de radiofrecuencia a modelos equivalentes, por lo que la matriz de acoplos se convierte en una herramienta de gran utilidad. Se introduce adicionalmente el concepto de rotación como proceso adicional de eliminación de acoplos. Dicho proceso puede ser requerido para obtener una implementación sencilla en las estructuras típicas de radiofrecuencia.

Con respecto a la realización física de filtros, se plantean tres aproximaciones. En el contexto de los filtros paso bajo se diseña un filtro de secciones cortas en coaxial. En este escenario se introducen tanto la optimización circuital como la electromagnética. Con respecto a los filtros paso banda, se diseñan varios filtros de cavidades de acoplos directos. Una vez finalizado su diseño se lleva a cabo un proceso adicional de optimización para mejorar sus prestaciones. Finalmente, en este mismo escenario de aproximaciones paso banda se propone un método basado en subdivisión de etapas. Dicho método se aplica en el diseño de un filtro combline en banda S para comunicaciones móviles.

Por limitaciones de tiempo y presupuesto no se ha llevado a cabo la fabricación de ningún prototipo, quedando esta tarea como objetivo a desarrollar en un futuro cercano.

# Palabras clave

Diseño de filtros, método de las pérdidas de inserción, método de Chebychev generalizado, matriz de acoplos, rotaciones, filtro de secciones cortas, filtro paso banda de acoplos directos, guía de onda, iris, cavidad , resonador , filtro combline, optimización, método de optimización por etapas.

# Agradecimientos

Teleco es una carrera exigente, pero muy bonita. Llega uno a la meta satisfecho, pero casi sin suelas (y con los pies empezados, si me apuras). En teleco varias veces al año uno se ve sometido a tal aliasing de tareas, que al final uno se pregunta por qué no existe un Nyquist académico que sirva de referencia. En teleco, varias veces al mes uno cree ingenuamente que ha alcanzado su punto de compresión a 1 dB. Teleco puede hasta hacer mella en tu lenguaje: cuando a mi me preguntan por qué no veo películas gore ya no sé si decir que mi sensibilidad es alta o baja.

Con este panorama, supongo que a alguien en su sano juicio le deberían entrar ganas de echarse a correr al meterse en teleco: pero de echarse a correr en dirección contraria a la meta. Y sin embargo, si uno tiene la osadía de elegir teleco y no arrepentirse, a lo largo de la carrera se conocen personas que le dan sentido a tu esfuerzo. En este punto, en el que me hallo rozando la cinta del final del recorrido con la yema de los dedos, no puedo evitar echar la vista atrás, y sentir que al menos, en este espacio limitado, he de daros las gracias.

A ti Jorge, por no cortarme las alas cuando quise abrir nuevos caminos en el proyecto, pero a la par saber frenar esa inquietud descarada que me caracteriza, enseñándome la importancia de saber qué guerras librar. Por enseñarme que lo perfecto es enemigo de lo óptimo. Por transmitirme la idea de que decidir es vivir, y no un desequilibrio incómodo que resolver.

A los demás profes del RFCAS. Especialmente a ti, Jose Luis, porque tuyo es el mérito de teñirme el pensamiento de radiofrecuencia en cuarto de carrera, hasta el punto de haber decidido finalizar la carrera en RFCAS. Por volcarte conmigo aun sin estar trabajando juntos en el grupo.Y a ti Juan, porque aunque no me iniciaras en el mundillo, desde luego conseguiste avivar mi interés. Y eso, en los últimos cursos, que es cuando precisamente uno toma consciencia de todas esas cosas chulas en las que trabajan de los distintos grupos de la Escuela, dista mucho de ser fácil. Y por supuesto Juan, porque en este año de proyecto siempre le has dado un toque divertido a los momentos de descanso.

A dos grandes profesores: Chema y Jose, porque a raíz de este año de proyecto puedo decir que, además de ser grandes profesores, sóis grandísimas personas. A vosotros os debo muchos minutos este año ... y yo encantada de resolver mi deuda. Quería también darle las gracias a otros profesores con los que he tenido un contacto más breve, y quizás más académico, pero el suficiente como para decir que esta Escuela no sería lo mismo sin ellos. Y por supuesto a ti, Susana. Sin duda imaginaba el día de mi presentación contigo en primera fila, pero la vida a veces es así, caprichosa. Gracias por todo tu apoyo, donde quiera que estés.

A Pablo S., porque siempre has tenido palabras de ánimo para los momentos de bajón, y bromas incesantes para los de celebración. Por estar siempre dispuesto a ayudar y a escuchar, sin importar ni el lugar ni el momento (salvo si es viernes a las 14h y el asunto tiene que ver con alguno de los pozos de la radiofrecuencia, sólo entonces la palabra lunes se te dibuja en la sonrisa ;) ).

A mis compañeros de laboratorio, porque habéis conseguido que me sienta en familia. No quiero convertir este párrafo en una larga y aburrida enumeración de nombres, dada la tropa que hemos coincidido este año. Lo sabéis, y me atrevo a decir que hasta lo habéis olido en los días de mayor overbooking. Bromas a parte, lo que quería deciros, es que al menos la mitad de mi proyecto, si no más, es vuestra compañía, risas y empatía (¡y tapeos!). Porque cuando uno trabaja a gusto las cosas salen, no solas, pero sí más fácilmente.

Al resto de amigos que me llevo de la carrera, más allá de las fronteras del RFCAS. Álex y Elena: con vosotros he vivido todo un contraste de momentos a raíz de las prácticas, que resumiré en estrés, algo de miedo, pero sobre todo en muchas risas y satisfacción. Me habéis ayudado a crecer como persona, me habéis acompañado en este viaje que ha hecho que de esta carrera salga una persona mucho más madura que la que entró hace ya algunos años. Alicia, Carol, Pablo B., Pablo P. y por supuesto Luis: la verdad es que no recuerdo en qué momento decidieron cruzarse nuestros caminos, pero lo que sí que sé es que me alegro mucho de que se hayan cruzado. Hemos pasado muy buenos momentos juntos, y de forma sincera espero que, en el caos particular de nuestras vidas quede siempre algo de espacio para seguir disfrutando juntos.

A todos mis amigos, y especialmente a mis dos amigas de toda la vida Cris y Celia, porque las cenas de comida china y cháchara a vuestro lado no tienen precio.

A Pedro, Antonio y Miguel, porque habéis hecho de mi beca un paseo muy agradable. Especialmente a ti, Pedro, tengo que decirte que no sabes lo que me alegra haber conocido a alguien con el mismo sentido del humor, y a la vez con el mismo hambre de conocimiento. Sólo por las conversaciones que hemos mantenido creo que merece la pena haber sido radiados ;).

A mi familia, por apoyarme en lo personal y en lo académico, y ofrecerme su cariño, calor y consejo desde que tengo consciencia de mi persona. Y sin desmerecer a nadie por particularizar en esta ocasión, me gustaría agradecerle a mi madre su lucha por seguir con nosotros, y a Kiko por cuidar de ella cuando no podíamos estar en casa. Eres una valiente, mamá. Y a ti, fiel compañero, te voy a querer siempre en mi recuerdo.

Volviendo al punto donde comencé, a teleco, quisiera cerrar este espacio con una reflexión personal.

Conozco a amigos que se quedaron en el camino, a pesar de que se esforzaron. Estos mismos amigos se habrían convertido en perfectos asesinos en serie si en esos momentos de frustración les hubieran dicho que "lo importante era participar". Yo misma habría bufado a quien me hubiera dicho que "querer es poder", mientras me hervía el cerebro en la 24h tratando de entender alguna de las cincuenta transformadas de nuestra carrera. Seguro que un estudio de la universidad no se cuál, ha demostrado que las frases populares en teleco disminuyen la esperanza de vida de quienes las dicen.

Como estas dos frases se me ocurren más. Sin embargo, tras todo este recorrido, me doy cuenta de que en realidad sólo son frases vacías si no se completan. Que quizás no sean malas frases en sí mismas, y que tal vez sean simplemente saber popular desdibujado fruto de un boca a oreja mal transmitido. En efecto, querer no es poder, a secas. Querer es poder encontrar una meta. Y qué importante es esto, pues para poder centrar nuestros esfuerzos en una dirección, primero hay que conocer cuál es. Y que lo importante no es participar, a secas. Lo importante es participar de la vida, pero desde la consciencia de que muchas veces es injusta. Y que a pesar de los sinsabores, y esto lo diré para los que atraviesan momentos de desencanto, la vida puede ser tan gratificante que sólo por esos momentos, el poder ser los actores de nuestra historia es un auténtico regalo.

Teleco es una carrera exigente, pero muy bonita. Bonita por sus contenidos, pero bonita también por las personas que conforman tu circunstancia mientras corres hacia la meta.

*Ana Morán*
*Julio 2015*

*Dicen que el tiempo todo lo cura,*
*que vuela el recuerdo a cualquier parte,*
*mas concédeme Susana la duda,*
*porque yo, en mi cordura,*
*prometo no olvidarte.*

# Contents

# List of Figures

# List of Tables

# 1 Introduction

## 1.1 Motivation

The purpose of this work is to study the design of filters at microwave frequencies (i.e. from 300 MHz to 300 GHz). Microwave filters are passive devices in charge of the selection of signals in the frequency domain, rejecting noise and interfering signals to the largest extent possible. These type of filters are typically found in the front-end of high-frequency transceivers of diverse systems such as radar, satellite TV or microwave links.

Those systems are usually subject to very restrictive specifications, demanding high-performance filters. From the electrical point of view, the desirable features can be summarized as: high selectivity, low insertion losses in the passband, wide free-spurious window, and good power handling capability. From a mechanical point of view, weight and volume can be critical depending on the target system.

This work is entitled "Filter design in coaxial cavities" , as it aims at designing a combline cavity bandpass filter. However, this technical term refers to a particular kind of physical structure, and filter design is far from "just" solving the physical dimensions of a structure. As figure 1.1 shows, the whole design process entails other stages upon which the task of finding out dimensions is built. In high-performance systems, each stage is key when it comes to producing a design that meets the given specifications. In fact, each of those stages has such complexity that it is considered a different area of expertise.

Nevertheless, they are not isolated and to succeed in the design process each stage must take into account the following ones. The main aim of this work is to gain a theoretical and practical global view of the process, bringing together those areas of knowledge. The last stage, i.e. the one responsible for filter manufacturing, is beyond the scope of this work due to budget and time constraints.

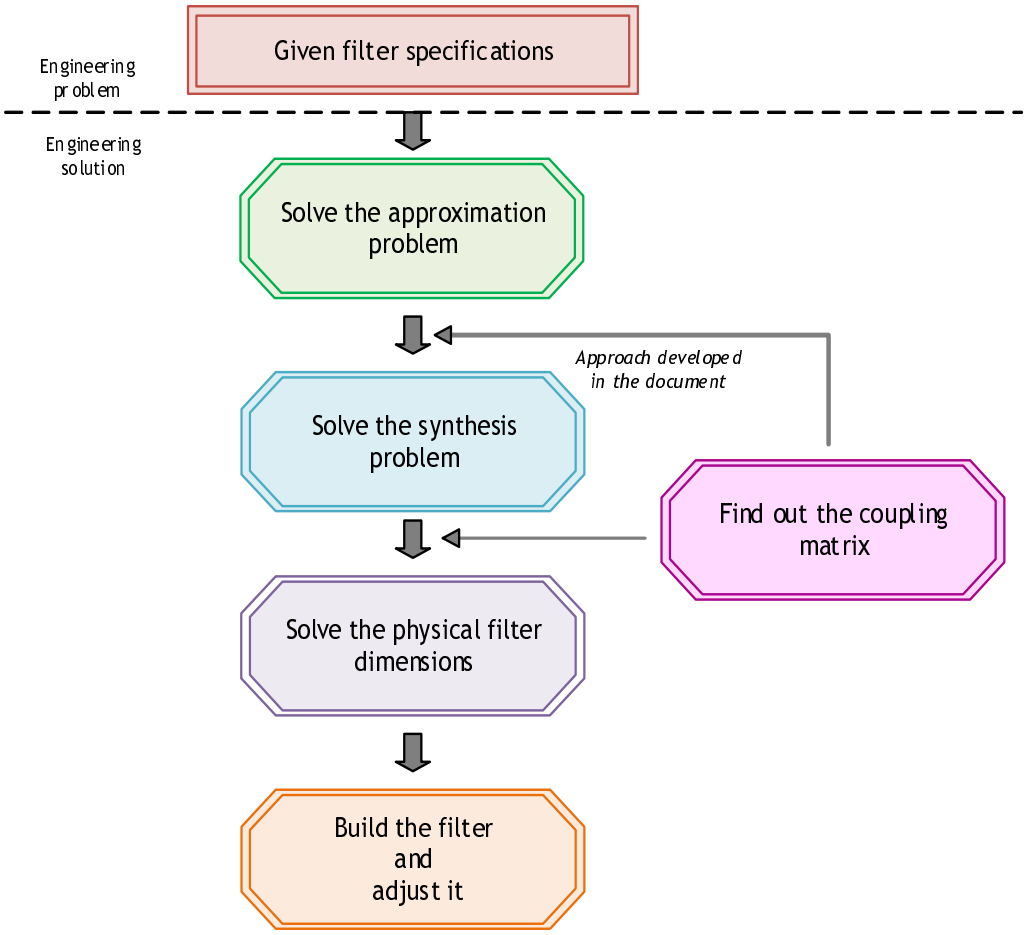


**Figure 1.1: Stages in filter design**

## 1.2 Goals and structure of the document

This document is organised according to the aforementioned stages involved in filter design. Each chapter can gather one or several goals as follows:

⇒ Chapter 2 addresses the theory of approximation (i.e. the power insertion loss method), where a rational function is found to meet the specifications of a desired frequency response, in terms of both amplitude and phase. In this chapter the properties that the design polynomials must fulfil are given. The relationship between the S parameters typically used to characterise radio-frequency devices and such design polynomials is shown. Then, the generalised Chebychev method is presented as a valuable tool to provide the designer freedom to set finite transmission zeros that can even lead to asymmetrical responses. The goal of this chapter is to develop this method in MATLAB code to evidence its awesome capabilities and flexibility. Four examples are given at the end of the chapter.

⇒ Chapter 3 is devoted to the coupling matrix theory. In this case, the theory presented is a goal in itself. Although explanations related to the coupling matrix can be easily found in technical books (e.g. in [1], [2]), it can be difficult to follow them as usually information is spread over several chapters, and more than one method is presented. Only after studying and gathering all the information it was possible to develop a MATLAB-based software. This tool finds out the values of the coupling matrix associated to a given polynomial response. Some examples are given at the end of the chapter.

⇒ Chapters 4 and 5 deal with both stages of synthesis and physical filter realization. Lowpass radiofrequency filters are studied in the former, whereas bandpass filters are included in the latter.

The synthesis problem is presented in the first section of both chapters since lumped element networks constitute the reference upon which the models that lead to a physical filter realization at microwave frequencies are based. Chapter 5 also includes a brief section where rotations as a means of topology transformation are introduced. Software in MATLAB is again developed and several examples are shown.

In chapter 4, the main objective is to design a stepped impedance filter in coaxial technology. Chapter 5 aims at studying a bandpass approach based on inverter networks and use it to design several filters in different technologies. The problem of a uniform dielectric change is addressed as well.

⇒ Finally, chapter 6 focuses on designing a high-performance narrowband combline cavity filter. This kind of filter is usually designed in the S Band (i.e. from 1.5 GHz to 4 GHz) for mobile base stations. The goal of this chapter is to develop a method to efficiently design filters where the characterization of the discontinuities between resonators is not always affordable. This method is based on the strategic subdivision of the whole design problem into minor sequential stages.

Optimization becomes a fundamental tool to accomplish this task, since the physical dimensions in the intermediate stages must ideally lead to the match between the full wave response of the partial structure and its equivalent circuital response. Otherwise this task can be extremely demanding and clearly unpractical (i.e. by means of purely manual adjustment).

# 2
# Polynomial Synthesis

The first step in filter design is to find a function capable of meeting certain specifications. Those specifications at microwave frequencies are given through a power mask, in terms of the S parameters (also known as scattering parameters). This chapter addresses this concept and links it to the polynomial world, where the approximation process can be developed. Classical polynomial functions generally pursue one of these three objectives: flatness, selectivity (in magnitude) or linear phase response (i.e. flat group delay). However, a versatile approximation called the generalised Chebychev method allows the designer to cope with both selectivity and linear phase response problems until a trade-off is achieved. Due to its flexibility, this study aims at developing it theoretically and implementing it in MATLAB afterwards. Some examples are included at the end of this chapter in order to gain a practical understanding of its capabilities.

## 2.1 S parameters overview

At microwave frequencies, the use of currents and voltages under a common understanding is not always possible. In addition, the measurement of those magnitudes is a difficult task. In this context power begins to play a primary role, and S parameters arise.
In an N-port network, each port has one incident power wave ($a_i$) and one reflected power wave ($b_i$),which are defined as follows:

$$a_i = \frac{V_i + Z_{0i} i_i}{\sqrt{8Re\{Z_{0i}\}}} \quad b_i = \frac{V_i - Z_{0i}^* i_i}{\sqrt{8Re\{Z_{0i}\}}} \tag{2.1}$$

Those waves are defined concerning the reference plane $t_i$, where the characteristic impedance is $Z_{0i}$ (see figure 2.1). Depending on the nature of $Z_{0i}$ - i.e. complex or real - the scattering parameters belong to a problem of generalised or non generalised power waves. Throughout this work the consideration of the non generalised case for the practical designs suffices.

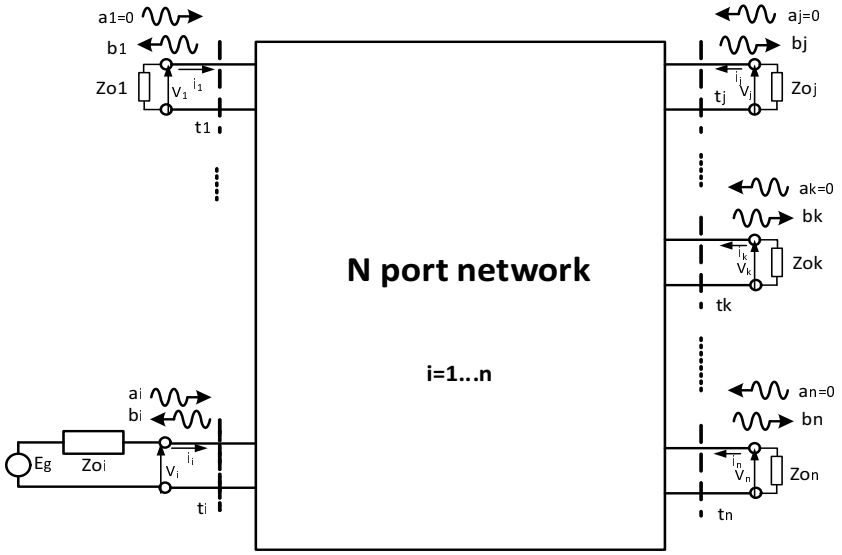


**Figure 2.1: Multiport network**

The S parameter matrix relates the incident and reflected waves just described:

$$\begin{bmatrix} b_1 \\ b_2 \\ \dots \\ b_n \end{bmatrix} = \begin{bmatrix} S_{11} & S_{12} & \dots & S_{1n} \\ S_{21} & S_{22} & \dots & S_{2n} \\ \dots & \dots & \dots & \dots \\ S_{m1} & S_{m2} & \dots & S_{mn} \end{bmatrix} \cdot \begin{bmatrix} a_1 \\ a_2 \\ \dots \\ a_n \end{bmatrix} \tag{2.2}$$

In order to obtain a specific parameter $S_{ij}$ from the scattering matrix, it is necessary to annihilate the incident waves that do not correspond to the port under analysis. To that end, each port is loaded with its reference impedance $Z_{0i}$, so that:

$$V_i = -i_i Z_{0i} \Longleftrightarrow a_i = 0 \tag{2.3}$$

Then,

$$S_{ij} = \left.\frac{b_j}{a_i}\right|_{a_k=0, k\neq i} \tag{2.4}$$

After this brief overview, a key concept must be remarked: S parameters can be used to characterize any network (including those used at low frequencies). However their advantages are mainly exploited in microwave devices.

## 2.2 Polynomial functions in quadripoles

This section shows the link between S parameters and polynomial functions in quadripoles.

### 2.2.1 Transmission function and reflection coefficient

First of all, as this section is focused on quadripoles, the expressions of the previous section must be applied to a two port network (see figure 2.2) with reference impedances $R_g$ and $R_L$.

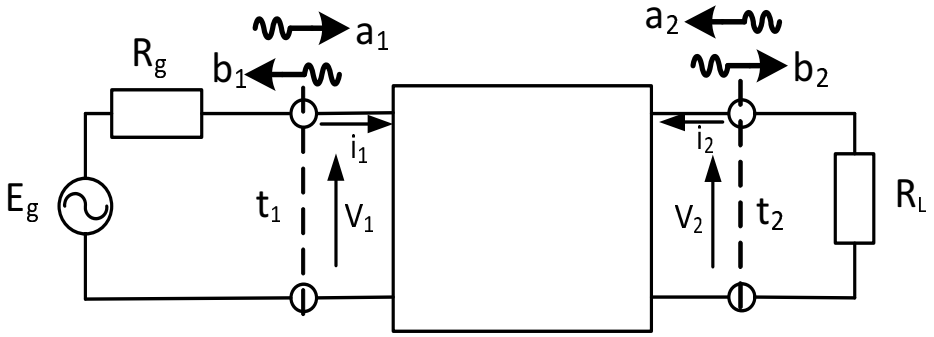


**Figure 2.2: Two port network**

Using equation 2.4 for a two port network, S parameters in a quadripole are:

$$S_{11} = \left.\frac{b_1}{a_1}\right|_{a_2=0} \quad S_{12} = \left.\frac{b_1}{a_2}\right|_{a_1=0} \quad S_{21} = \left.\frac{b_2}{a_1}\right|_{a_2=0} \quad S_{22} = \left.\frac{b_2}{a_2}\right|_{a_1=0} \tag{2.5}$$

This section will be focused on parameters $S_{11}$ and $S_{21}$, where the excitation is set at port one. Note that the same reasoning is valid for parameters $S_{21}$ and $S_{22}$ just by putting the source at port two. Another definition of the incident power wave $a_1$ is given in this section, so that a better understanding would be gained:

$$\left.\begin{array}{l} a_1 = \frac{V_1 + R_g i_1}{\sqrt{8Re\{R_g\}}} \\ V_1 = E_g - R_g i_1 \end{array}\right\} a_1 = \frac{E_g}{\sqrt{8Re\{R_g\}}} = \sqrt{P_{dg}} \tag{2.6}$$

In the previous expression $a_1$ is presented as the square root of the maximum power available in the system, that is, the power produced by the generator. At the same time, the power delivered to the load can be expressed in terms of the incident and reflected waves at port two:

$$P_2 = \mid b_2 \mid^2 - \mid a_2 \mid^2 \tag{2.7}$$

If one keeps in mind the two immediately preceding definitions, now it is easy to understand parameter $S_{21}$ as a ratio between power delivered to the load at port two, and power available by generator (since $a_2$ is annihilated by loading port two with $R_L$):

$$\mid S_{21} \mid^2 = \left.\frac{\mid b_2 \mid^2}{\mid a_1 \mid^2}\right|_{a_2=0} = \frac{P_2}{P_{dg}}, \tag{2.8}$$

The inverse square root of that powers' relationship is what in general is called the transmission function:

$$|H(s)|_{s=j\omega} = \sqrt{\frac{P_{dg}}{P_2}} = \left|\frac{1}{S_{21}(s)}\right|_{s=j\omega} \tag{2.9}$$

Likewise, $S_{11}$ parameter is found to be a ratio between power reflected to the source load at port one and power available by the generator:

$$|\ S_{11}\ |^2 = \left.\frac{|\ b_1\ |^2}{|\ a_1\ |^2}\right|_{a_2=0} = \frac{P_{ref,port1}}{P_{dg}}, \tag{2.10}$$

The square root of the prior result is called reflection coefficient, and it is usually depicted by letter $\rho$ and using the s variable of the Laplace transform:

$$|\rho(s)|_{s=j\omega} = \sqrt{\frac{P_{ref,port1}}{P_{dg}}} = |S_{11}(s)|_{s=j\omega} \tag{2.11}$$

Finally, the transmission function and the reflection coefficient can be expressed in terms of characteristic polynomials:

$$\rho(s) = \frac{F(s)}{E(s)}, \quad H(s) = \frac{E(s)}{P(s)}, \tag{2.12}$$

It is important to highlight that in the preceding definitions:

⇒ The roots of $F(s)$ are known as reflection zeros, i.e. points of maximum power transmission. In some literature they can also be referred as attenuation zeros.

⇒ The roots of $P(s)$ are known as transmission zeros, i.e. points where power transmission does not exist.In some literature they can also be referred as attenuation poles.

⇒ The roots of $E(s)$ are the natural frequencies of the network, i.e. frequencies where a non-zero response is ideally obtained without any excitation.

Further information about this polynomials is detailed in subsection 2.2.3 .

### 2.2.2 Characteristic function

In the previous subsection it was important to present the linkage between the transmission function, the reflection coefficient and their corresponding S parameters. Moreover, at the same time it was important to present them as power ratios. Yet there is another parameter left, referred to as the characteristic function:

$$K(s) = \rho(s) \cdot H(s) = \frac{F(s)}{E(s)} \cdot \frac{E(s)}{P(s)} = \frac{F(s)}{P(s)} \tag{2.13}$$

The relationship between the characteristic and the transmission function is shown in equation 2.14. Almost the same expression (except for a normalization that is explained at the end of

section 2.3, and a particularization in $j\omega$ axis) is found in books focused on the filter realization process, but usually named as power loss ratio in spite of transmission function.

$$| H(s) |^2 = 1 + | K(s) |^2 \tag{2.14}$$

In order to evidence the utility of this definition the equation of Feldkeller must be introduced:

$$|E(s)|^2 = |F(s)|^2 + |P(s)|^2 \tag{2.15}$$

As it can be seen, Feldkeller equation shows that polynomials $E(s)$, $F(s)$ and $P(s)$ are not independent. Since transmission zeros (roots of $P(s)$) are points of nonexistent transmission and reflection zeros (roots of $F(s)$) are points of maximum power transmission , it seems reasonable to focus the design effort on establishing them conveniently in the characteristic function recently introduced. Once these zeros and their respective polynomials are found, $E(s)$ is then directly synthesized using equation 2.15.

Another approach would be to choose the natural frequencies associated with $E(s)$ and then to select the transmission or the reflection zeros, but due to its simplicity classical filter design develops its theory in terms of maximum and minimum power transmission rather than in natural frequencies whose response is not directly translated into the power shape mask of the device under analysis. The characteristic function arises in that context.

### 2.2.3 Properties of the design polynomials

From now on, we will refer to $E(s)$, $P(s)$ and $F(s)$ as the design polynomials. They are involved in the process of filter design since they define together the desired whole frequency response. Their definition, in the end, concerns the distribution of both the reflected and the transmitted power.

These design polynomials can not adopt any form provided their ultimate goal is to synthesize a physical network. Thus, they must respect some properties, whose proof is not the purpose of this document (the underlying theory is complex enough to treat it separately). Nevertheless, the aim of this subsection is to provide an initial guideline to facilitate the future comprehension of the transformations done in a typical ladder network and as well the placement of the transmission zeros in the generalised Chebychev method treated in section 2.3 .

The constraints imposed to $E(s)$, $F(s)$ and $P(s)$ have to do with the fact that in order to guarantee that the impedance function $Z(s)$ of a two port network is a positive real function (i.e. $\Re\{Z(s)\} \geq 0 \iff \Re\{s\} \geq 0, \quad Z(s) \in \Re \iff s \in \Re$), their coefficients must remain real. To understand why this constraint of the impedance function directly affects the design

polynomials it is important to keep in mind that, in the end, both the transfer function $H(s)$ and the reflection coefficient $\rho(s)$ can be written directly in terms of $Z(s)$ by relating the currents and voltages in the circuit with the impedance parameters.

The properties of the design polynomials that ensure a positive real impedance function are:

⇒ The roots of $F(s)$ lie symmetrically on the imaginary axis in the passband region (see figure 2.3.a.)

⇒ The roots of $P(s)$ can lie on the imaginary axis (figure 2.3b.) or on the real axis (figure 2.3.c.) as long as they occur symmetrically. They can also form a complex quad in the $s$ plane (figure 2.3.d.).

⇒ $E(s)$ is a strict Hurwitz polynomial, that is, its roots lie on the left half of the s plane.

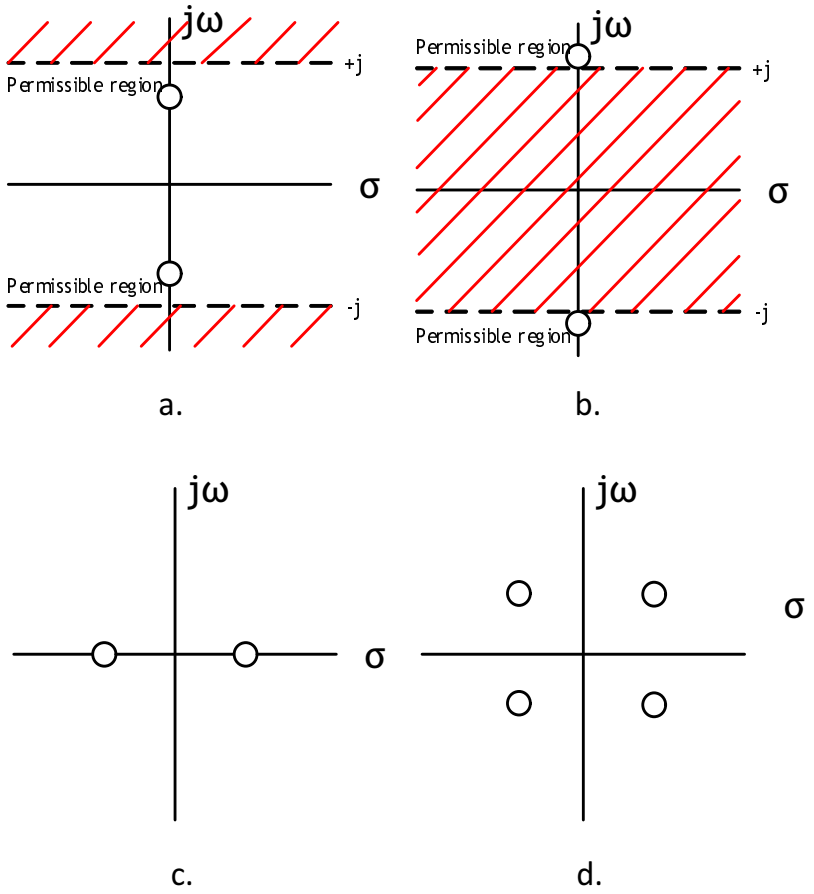


**Figure 2.3: Permissible zero locations of F(s) (a. on the jω axis) and P(s) (b. on the jω axis, c. on the real axis, d. as a complex quad)**

The classical filtering functions are born under the previous assumptions. At this point, however, the next two questions arise: *«Would it be possible to modify the preceding basis*

*without breaking the rules of circuit theory? Would it improve anything?»*. The answers of both questions are, of course, yes. It can be proved (and again, it is not done in this document), that, as long as $Z(s)$ is a real positive function, it is not possible to achieve an asymmetric filter response. However, a positive function (i.e. $\Re\{Z(s)\} \geq 0 \Longleftrightarrow \Re\{s\} \geq 0$) does, and asymmetric responses can turn out interesting since they provide the filter designer more freedom in the synthesis process.

In order to pursue this objective, a frequency-invariant reactive element must be added.This element will not produce a realizable lowpass filter, but a bandpass or stopband one. The key will be to include this element as a frequency offset [3].

In this context, the design polynomials can yield complex coefficients and therefore their properties have changed:

⇒ The roots of $F(s)$ must lie along the imaginary axis, but the symmetry condition about the real axis is no longer needed (figure 2.4.a.).

⇒ The roots of $P(s)$ can appear as pairs of zeros located symmetrically with respect to the imaginary axis (figure 2.4.b., but when they are placed in the imaginary axis no pairs are needed (figure 2.4.c.).

⇒ $E(s)$ remains as a strict Hurwitz polynomial (figure 2.4.d. ).

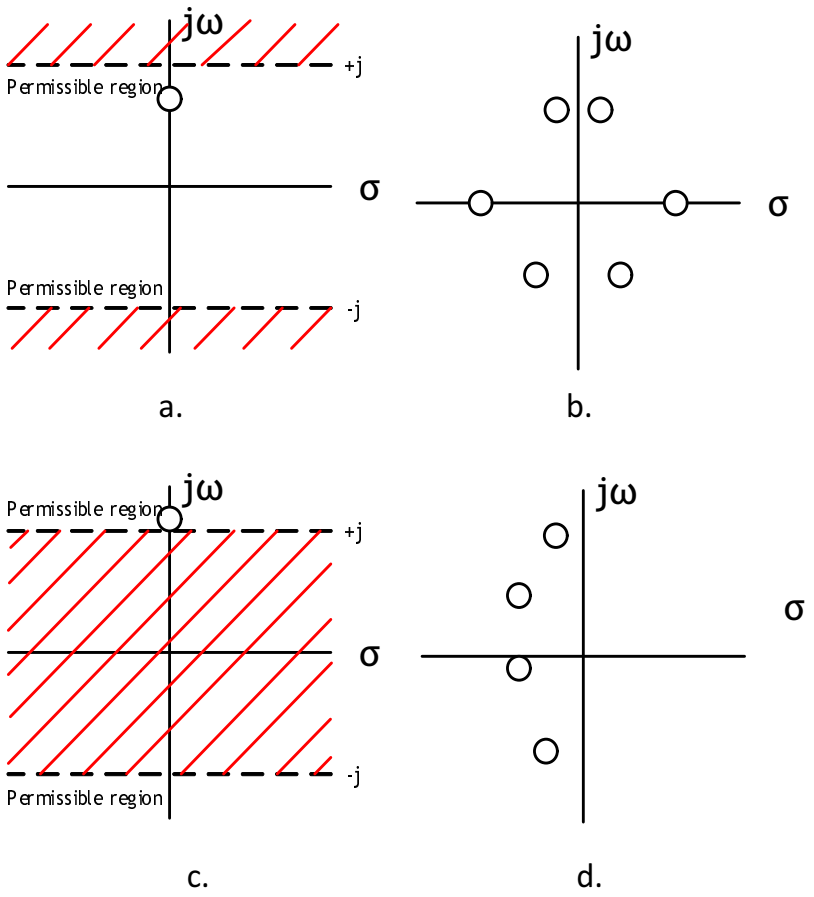


**Figure 2.4: Permissible zero locations of F(s) (a. on the j $\omega$ axis), P(s) (b. on the j$\omega$ axis, c. as pairs symmetrically located) and E(s) (d.)**

The proof of the properties of the design polynomials can be found out in [4] for positive real functions and in [1] for positive functions.

## 2.3 Generalised Chebychev method

The approximation theory copes with the problem of finding the appropriate polynomial functions which satisfy a given power specification mask. There are several approximations studied and applied in filter design - i.e. the Butterworth function, the Chebychev approximations or the elliptic function just to name a few. Notwithstanding, the purpose of this chapter is not to describe all these methods, but to focus on one: the generalised Chebychev method.

The ideal polynomial function would achieve a maximally flat and a linear phase response in the passband, and at the same time optimum selectivity in the transition passband-rejection band. Unless the filter presents a poor level of reflection in its passband, flatness as a property does not represent a problem for the designer. However, selectivity and phase linearity are well-known opposed goals. Classic functions such as Rhodes or Bessel focus on the phase response, whereas the all-pole Chebychev functions or responses based on Jacobi elliptic functions pursue selectivity.

In contrast, the generalised Chebychev method becomes a powerful tool since it has great versatility in the sense that it is possible to pursue a trade-off between selectivity and phase linearity without changing the polynomial function. Such compromise is achievable since the location and number of transmission zeros is chosen by the designer, and is only limited by the filter order and the synthesis tool used afterwards (see chapter ...). Its versatility will be evidenced in four practical cases in section 6.3.

The characteristic function $K(\omega)$ defined in this method is:

$$K(\omega) = \cosh\left[\sum_{n=1}^{N} \cosh^{-1}\left(\frac{\omega - \frac{1}{\omega_n}}{1 - \frac{\omega}{\omega_n}}\right)\right] \quad , \text{ with N filter order} \tag{2.16}$$

The preceding equation satisfy the following properties, which define a typical Chebychev function:

$$\begin{aligned} &1. \quad \mid K(\omega) \mid \leq 1, \mid \omega \mid \leq 1 \\ &2. \quad \mid K(\omega) \mid > 1, \mid \omega \mid > 1 \end{aligned} \tag{2.17}$$

Replacing equation 2.16 with its identity $K(\omega) = \cosh\left[\sum_{n=1}^{N} ln(x_n + \sqrt{x_n^2(\omega) - 1})\right]$ (where $x_n = \frac{\omega - \frac{1}{\omega_n}}{1 - \frac{\omega}{\omega_n}}$ ) and following a process of rearrangement described in [1], the subsequent expression is achieved:

$$K(\omega) = \frac{\prod_{n=1}^{N}\left[(\omega - \frac{1}{\omega_n}) + \omega'\sqrt{1 - \frac{1}{\omega_n^2}}\right] + \prod_{n=1}^{N}\left[(\omega - \frac{1}{\omega_n}) - \omega'\sqrt{1 - \frac{1}{\omega_n^2}}\right]}{2 \cdot \prod_{1}^{N}(1 - \frac{\omega}{\omega_n})} \tag{2.18}$$

If equation 2.18 is compared with equation 2.13, it is clear that:

⇒ The denominator of equation 2.18 is directly $P(\omega)$.

⇒ Although $F(\omega)$ is formed by the sum of two polynomials (given by the two productories), no reflection zeros need to be specified, since they are directly set once transmission zeros are selected.

The numerator of the previous equation can be written strategically as:

$$Num[K(\omega)] = \frac{G_N(\omega) + G_N^{'}(\omega)}{2} \tag{2.19}$$

where

$$\begin{aligned} &1.\quad G_N(\omega) = \prod_{n=1}^{N} \left[ (\omega - \frac{1}{\omega_n}) + \omega^{'} \cdot \sqrt{1 - \frac{1}{\omega_n^2}} \right] \\ &2.\quad G_N^{'}(\omega) = \prod_{n=1}^{N} \left[ (\omega - \frac{1}{\omega_n}) - \omega^{'} \cdot \sqrt{1 - \frac{1}{\omega_n^2}} \right] \end{aligned} \tag{2.20}$$

At the same time, term $G_N(\omega)$ is divided into two polynomials:

$$G_N(\omega) = U_N(\omega) + V_N(\omega) \tag{2.21}$$

One of the polynomials is written in terms of variable $\omega$ and the other in terms of the transformed frequency variable $\omega^{'} = \sqrt{\omega^2 - 1}$:

$$\begin{aligned} &1.\quad U_N(\omega) = u_0 + u_1\omega + u_2\omega^2 + ...u_N\omega^N \\ &2.\quad V_N(\omega) = \omega^{'}(v_0 + v_1\omega + v_2\omega^2 + ...v_N\omega^N) \end{aligned} \tag{2.22}$$

With the preceding assumptions, a recursive technique is carried out. The first term in which the process is built is:

$$G_1(\omega) = (\omega - \frac{1}{\omega_1}) + \omega^{'} \cdot \sqrt{1 - \frac{1}{\omega_1^2}} = U_1(\omega) + V_1(\omega) \tag{2.23}$$

When the second term is calculated using the previous one (i.e. equation 2.23 ), the result can be again split into a term in variable $\omega$ ($U_2$) and another one in variable $\omega^{'}$ ($V_2$), as shown in equation 2.24. It is important to realise that the double product of $\omega^{'}$ turns into an expression of variable $\omega$ rather than of variable $\omega^{'}$.

$$\begin{aligned} G_2(\omega) &= G_1 \cdot \left[ (\omega - \frac{1}{\omega_2}) + \omega^{'} \cdot \sqrt{1 - \frac{1}{\omega_2^2}} \right] = \\ &= \underbrace{U_1 \cdot (\omega - \frac{1}{\omega_2}) + V_1 \cdot \omega^{'} \sqrt{1 - \frac{1}{\omega_2^2}}}_{U_2(\omega)} + \underbrace{V_1 \cdot (\omega - \frac{1}{\omega_2}) + U_1 \cdot \omega^{'} \sqrt{1 - \frac{1}{\omega_2^2}}}_{V_2(\omega)} \end{aligned} \tag{2.24}$$

Using the previous result $G_3(\omega)$ is then calculated, and so on. Thus, in general the auxiliary

polynomials $U_N(\omega)$ and $V_N(\omega)$ are calculated as:

$$\begin{aligned} &1. \quad U_{i+1}(\omega) = U_i \cdot (\omega - \frac{1}{\omega_{i+1}}) + V_i \cdot \omega' \sqrt{1 - \frac{1}{\omega_{i+1}^2}} \\ &2. \quad V_{i+1}(\omega) = V_i \cdot (\omega - \frac{1}{\omega_{i+1}}) + U_i \cdot \omega' \sqrt{1 - \frac{1}{\omega_{i+1}^2}} \end{aligned} \tag{2.25}$$

Doing the same process for $G_N'(\omega)$, it is obtained that $U_N'(\omega) = U_N(\omega)$ and $V_N'(\omega) = -V_N(\omega)$. Then, equation 2.19 turns out to be $Num[K(\omega)] = U_N(\omega) = F(\omega)$, and therefore the roots of $F(\omega)$ can be found by simply calculating the roots of $U_N(\omega)$.

Although at this point the key tools to accomplish the task of implementing the general Chebychev method have been provided, there is another detail to take into account. Without any loss of generality, after the whole process it is necessary to go a step further and normalize. Thus, S parameters turn out to be:

$$\bar{S}_{11}(s) = \frac{F(s)/\epsilon_f}{E(s)}, \quad \bar{S}_{21}(s) = \frac{P(s)/\epsilon_p}{E(s)}, \tag{2.26}$$

where $\epsilon_f$ and $\epsilon_p$ are real constants in charge of normalizing $F(s)$ and $P(s)$ respectively, such that $\mid S_{11}(s) \mid$ and $\mid S_{21}(s) \mid$ are $\leq 1$ at any value of $s = j\omega$.

Finally, it must be remarked that as a generalised method, deriving the all-pole Chebychev response from it is a must. Indeed, if all the prescribed transmission zeros $\omega_n$ approach infinity, $K_N(\omega)$ degenerates to the well-known all-pole function:

$$K(\omega)\Big|_{w_n \to \infty} = \cosh\left[N \cosh^{-1}(\omega)\right] \tag{2.27}$$

## 2.4 Applied filter design examples

Section 2.3 presented a generalised method based on Chebychev polynomials which allows to set finite transmission zeros. Moreover, their number is not subjected to the filter order as in other polynomial functions: only a fixed upper limit determined exclusively by the filter order and the synthesis method must be guaranteed (see chapter 3). In the hereto work a software tool which implements the aforementioned method is developed in MATLAB. Four examples are presented.

Perhaps the most evident use of finite transmission zeros is to increase the selectivity of the filter response. Figure 2.5 shows an all-pole (i.e. $P(\omega) = 1$) fifth order Chebychev filter response, with $15\,dB$ of reflection. From now on in this section given examples will use the same specifications so that comparison is easily made.

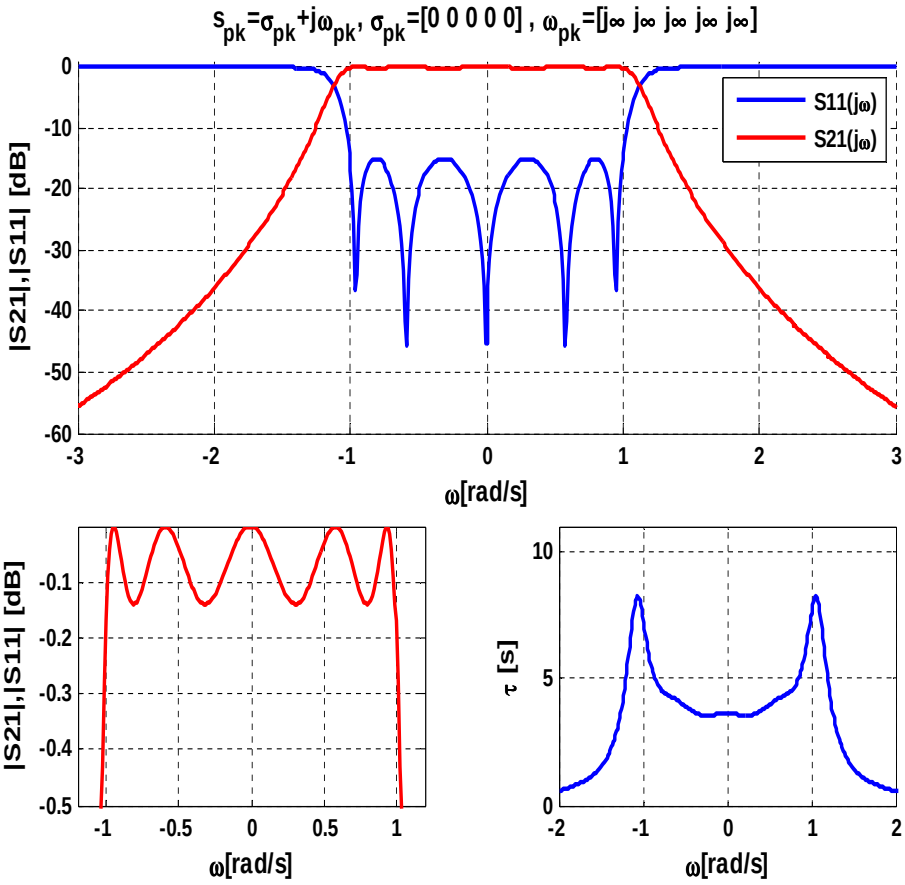


**Figure 2.5: All-pole Chebychev response. N=6, RL=15dB.**

Alternatively, figure 2.6 shows the filter response obtained by setting two finite transmission zeros at $s = \pm 1.5j$. At first glance, figures 2.5 and 2.6 evidence the improvement achieved in terms of selectivity thanks to finite transmission zeros. Thus, it must be remarked that it is an essential property since, given a power mask, this technique allows to reduce the filter order, making it possible not only to reduce the size of the filter, but to reduce its losses.

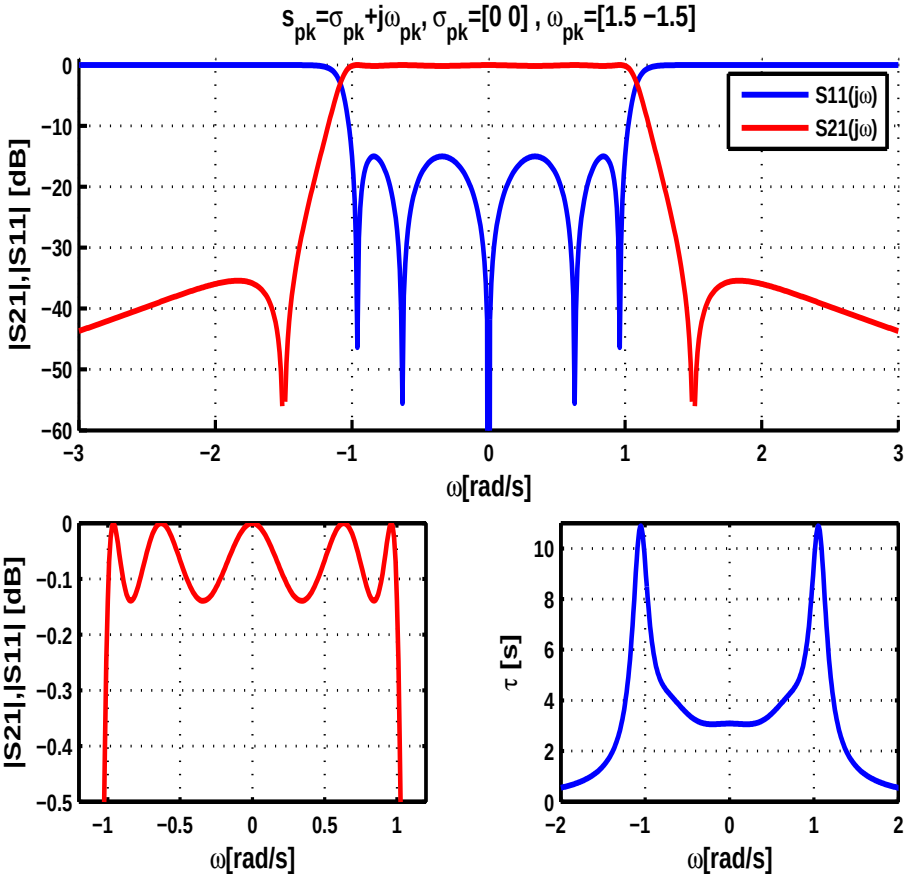


**Figure 2.6: Example 1.**
**Chebychev response with transmission zeros**
**in the imaginary axis. N=5, RL=15dB.**

However, in subsection 2.2.3 it was mentioned that $P(s)$ has more flexibility on its zero locations. Indeed, setting finite transmission zeros in the imaginary axis can lead to an undesired group delay response (i.e. a non linear phase response). Figure 2.7 shows, by comparison with figure 2.6, how finite transmission zeros located on the real axis ($s = \pm 1.5$) act as equalizers since they improve the group delay ripple.

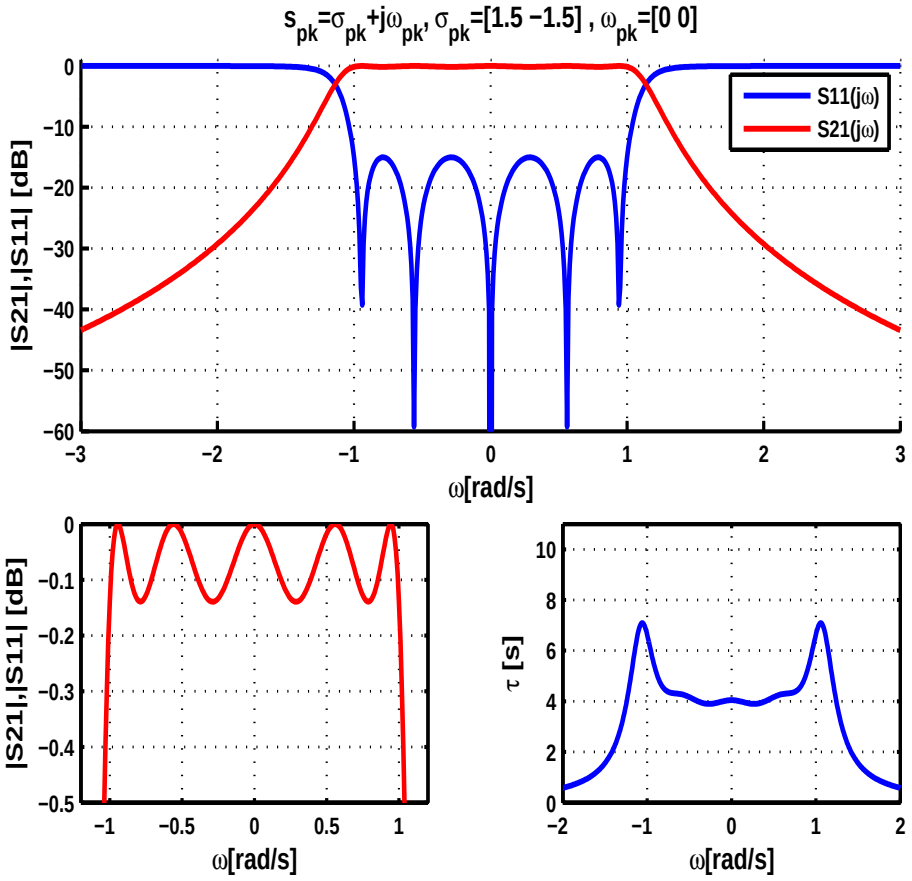


**Figure 2.7: Example 2.**
**Chebychev response with transmission zeros in the real axis. N=5, RL=15dB.**

At this point, in order to evidence the versatility of the method, a Chebychev polynomial response is formed with a complex quad of four finite transmission zeros set at $s = \pm 1.5 \pm 1.5j$. The phase linearity and selectivity shown in figure 2.8, are both worse than the better case shown, but better than the worse one. Therefore, the designer can pursue a trade-off with the same polynomial method.

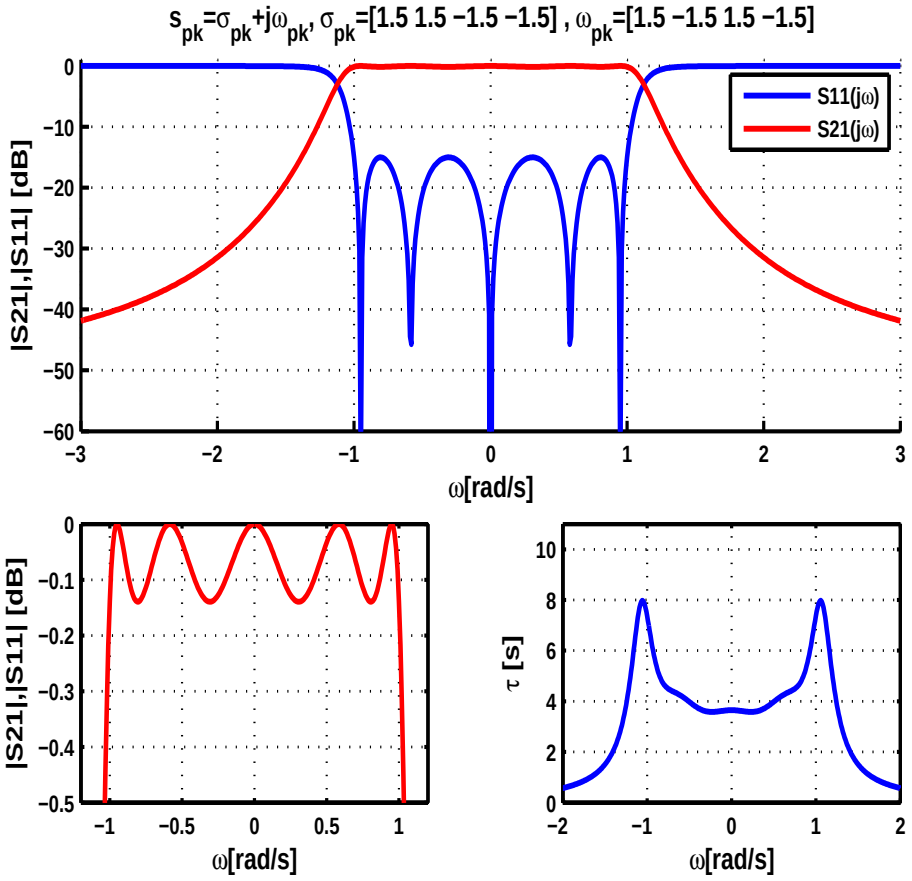


**Figure 2.8: Example 3.**
**Chebychev response with transmission zeros**
**as a complex quad. N=5, RL=15dB.**

And last but not least, there is an additional degree of freedom, which makes the generalised Chebychev method a powerful tool: asymmetry. This property is highly desirable since the filter complexity can be noticeably reduced. Figure 2.9 shows an example with a finite transmission zero set at $s = 1.5j$.

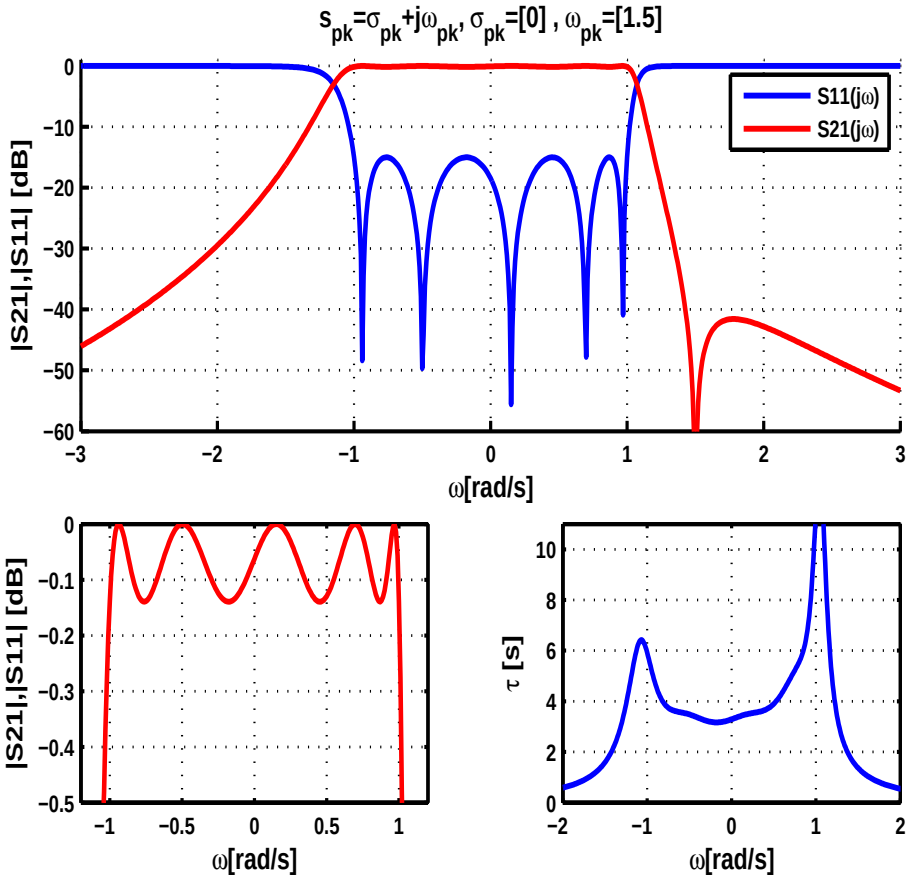


**Figure 2.9: Example 4.**
**Asymmetric Chebychev response.**
**N=5, RL=15dB.**

Finally, figure 2.10 gathers the location of the roots of the design polynomials in the preceding examples. Their associated polynomials are shown in tables 2.1 to 2.4.

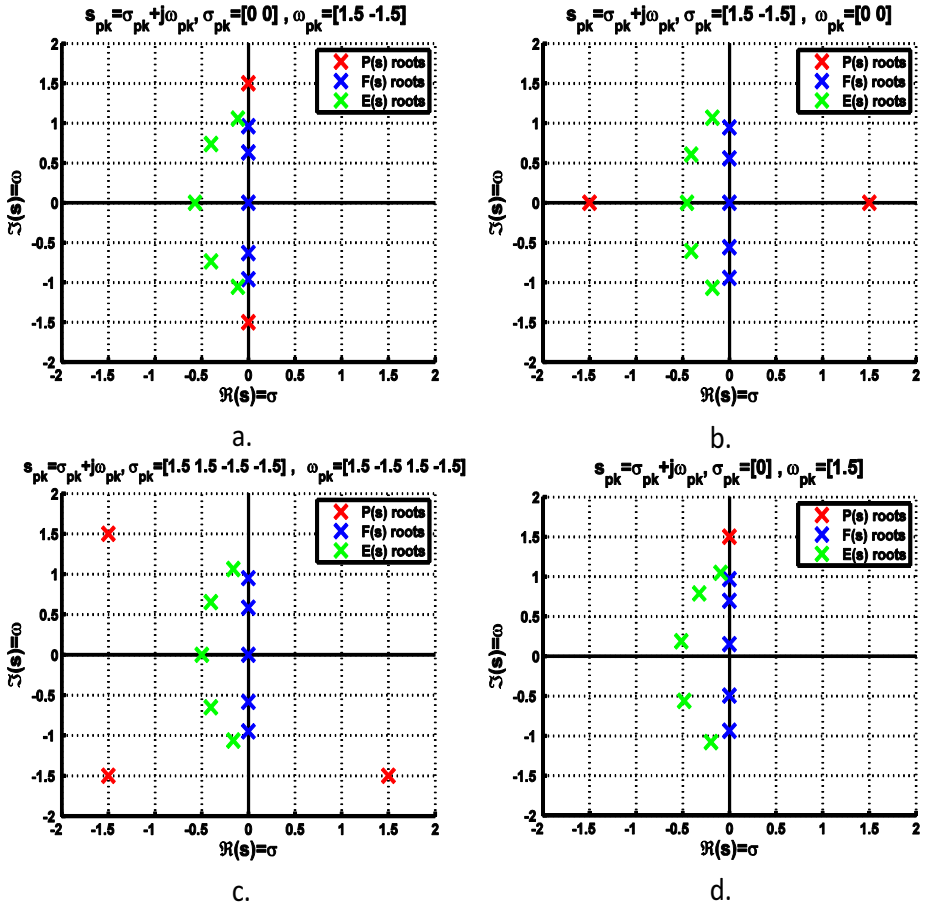


**Figure 2.10: Root map of generalised Chebychev examples. a. Example 1. b. Example 2. c. Example 3. d. Example 4.**

| Coefficients ($\epsilon_p = 4.95, \epsilon_f = 1$) | | | |
|---|---|---|---|
| $c_{k=}$ | P(s) | F(s) | E(s) |
| **0** | 2.25 | 0 | 0.45 |
| **1** | 0 | 0.37 | 1.40 |
| **2** | 1 | 0 | 2.21 |
| **3** | | 1.32 | 2.60 |
| **4** | | 0 | 1.60 |
| **5** | | 1 | 1 |

**Table 2.1: Example 1.**

| Coefficients ($\epsilon_p = 7.88, \epsilon_f = 1$) | | | |
|---|---|---|---|
| $c_{k=}$ | P(s) | F(s) | E(s) |
| **0** | −2.25 | 0 | 0.29 |
| **1** | 0 | 0.28 | 1.15 |
| **2** | 1 | 0 | 2.07 |
| **3** | | 1.20 | 2.55 |
| **4** | | 0 | 1.64 |
| **5** | | 1 | 1 |

**Table 2.2: Example 2.**

| Coefficients ($\epsilon_p = 59.62, \epsilon_f = 1$) | | | |
|---|---|---|---|
| $c_{k=}$ | P(s) | F(s) | E(s) |
| **0** | 20.25 | 0 | 0.34 |
| **1** | 0 | 0.31 | 1.24 |
| **2** | 0 | 0 | 2.12 |
| **3** | 0 | 1.24 | 2.57 |
| **4** | 1 | 0 | 1.63 |
| **5** | | 1 | 1 |

**Table 2.3: Example 3.**

| Coefficients ($\epsilon_p = 3.78, \epsilon_f = 1$) | | | |
|---|---|---|---|
| $c_{k=}$ | P(s) | F(s) | E(s) |
| **0** | 1.5 | $-0.05j$ | $0.29 - 0.27j$ |
| **1** | $j$ | 0.28 | $1.15 - 0.69j$ |
| **2** | | $-0.38j$ | $2.05 - 0.93j$ |
| **3** | | 1.21 | $2.52 - 0.65j$ |
| **4** | | $-0.38j$ | $1.62 - 0.38j$ |
| **5** | | 1 | 1 |

**Table 2.4: Example 4.**

# 3
# The Coupling Matrix

Once the design polynomials are found, the next stage is to establish a link between the approximation theory and circuit realization. Here matrices play a paramount role, specially the coupling matrix, whose synthesis is analysed in this chapter. Each element of the coupling matrix represents how the elements are coupled in the future circuit network. Although circuit realization will not be presented until the next chapter, sometimes circuit diagrams will be included in order to illustrate where the different matrices arise.

The implemented MATLAB code puts this theory into practice, and six examples are shown.At the end of the chapter the $N+2 \times N+2$ coupling matrix is briefly mentioned, as a valuable tool to overcome the $N \times N$ coupling matrix shortcomings.

## 3.1 ABCD matrix overview

S parameters presented in section 2.1 provide useful definitions to characterize multiport networks at microwave frequencies. However, they are not unique. In practice, circuits can be represented by other parameters such as the admittance parameters ($Y$ matrix), the impedance parameters ($Z$ matrix) or the transmission parameters (treated in this section, commonly named as $ABCD$ parameters). The choice of using one or another depends on the specific problem to solve. Of course all of them must lead to the same solution, but the difficulty in finding the solution may not be the same (it can be compared to solve a physic problem with the inappropriate coordinate system).

In particular, ABCD parameters are useful when there is a cascade connection of several two port networks, as in figure 3.1.

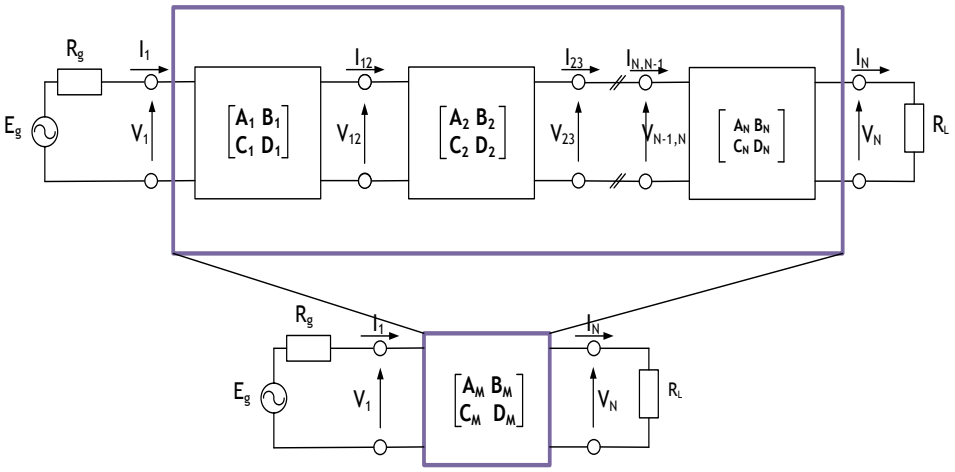


**Figure 3.1: Cascade connection of two port networks**

In that case, the following property is fulfilled:

$$\begin{bmatrix} A_M(s) & B_M(s) \\ C_M(s) & D_M(s) \end{bmatrix} = \begin{bmatrix} A_1(s) & B_1(s) \\ C_1(s) & D_1(s) \end{bmatrix} \cdot \begin{bmatrix} A_2(s) & B_2(s) \\ C_2(s) & D_2(s) \end{bmatrix} \cdots \begin{bmatrix} A_N(s) & B_N(s) \\ C_N(s) & D_N(s) \end{bmatrix} \tag{3.1}$$

Thus, if one can divide the whole problem into well-known two-port network blocks (i.e. their corresponding equivalent matrices), finding the response of the whole network is simply a problem of solving matrix products. This saves the designer from solving too many (although linear) equations. In [5] there can be found some of the most common circuits used in practice as subblocks.

Unlike S parameters, ABCD parameters are not usually used in multiport problems, and do not work directly with power but with currents and voltages, as shown in equation 3.2. And unlike impedance and admittance parameters, the current at the output port is conveniently considered positive when it is drawn inwards and not outwards. This allows an easier matrix product when cascading (otherwise it would be necessary to include a sign change in each step).

$$\begin{bmatrix} V_1 \\ I_1 \end{bmatrix} = \begin{bmatrix} A(s) & B(s) \\ C(s) & D(s) \end{bmatrix} \cdot \begin{bmatrix} V_2 \\ I_2 \end{bmatrix} \tag{3.2}$$

In order to obtain each S parameter it was necessary to load all the ports (except the one at which excitation was applied) with the associated reference impedance. In this case, the corresponding port must be short-circuited or opened in order to solve the specific ABCD parameter:

$$A = \left.\frac{V_1}{V_2}\right|_{I_2=0} \quad B = \left.\frac{V_1}{I_2}\right|_{V_2=0} \quad C = \left.\frac{I_1}{V_2}\right|_{I_2=0} \quad D = \left.\frac{I_1}{I_2}\right|_{V_2=0} \tag{3.3}$$

Finally, there is one aspect that require clarification. In the brief S parameter overview in

chapter 2, it was mentioned that S parameters at microwave frequencies overcome the problem of currents and voltages definitions. In that sense the reader may think that this section constitute an undesired step backwards. However, chapters 4 and 5 will evidence that filter design at microwave frequencies is realised via equivalent circuits where currents and voltages have an universal definition. Afterwards, ABCD parameters are translated into S parameters, so that the circuit behaviour can be expressed in terms of power, where there is no ambiguity whatever the RF technology is used.

## 3.2 Impedance and admittance matrix overview

Although admittance matrix will not be used in the filter realization stage explained in chapters 4 and 5, it becomes here a fundamental tool to accomplish the task of linking the polynomial world seen in the preceding chapter and the synthesis world. For that reason its matrix definition is here presented:

$$\begin{bmatrix} I_1 \\ I_2 \\ ... \\ I_N \end{bmatrix} = \begin{bmatrix} Y_{11}(s) & ... & Y_{1N}(s) \\ Y_{21}(s) & ... & Y_{2N}(s) \\ ... & ... & ... \\ Y_{M1}(s) & ... & Y_{MN}(s) \end{bmatrix} \cdot \begin{bmatrix} V_1 \\ V_2 \\ ... \\ V_N \end{bmatrix} \tag{3.4}$$

If a two port network is considered specifically, the different admittance parameters are recovered by short-circuiting each port at a time:

$$Y_{11} = \frac{I_1}{V_1}\bigg|_{V_2=0} \quad Y_{12} = \frac{I_1}{V_2}\bigg|_{V_1=0} \quad Y_{21} = \frac{I_2}{V_1}\bigg|_{V_2=0} \quad Y_{22} = \frac{I_2}{V_2}\bigg|_{V_1=0} \tag{3.5}$$

Another way to reveal how a circuit works through voltages and currents is via the impedance matrix, whose matrix definition is shown in equation 3.6.

$$\begin{bmatrix} V_1 \\ V_2 \\ ... \\ V_N \end{bmatrix} = \begin{bmatrix} Z_{11}(s) & ... & Z_{1N}(s) \\ Z_{21}(s) & ... & Z_{2N}(s) \\ ... & ... & ... \\ Z_{M1}(s) & ... & Z_{MN}(s) \end{bmatrix} \cdot \begin{bmatrix} I_1 \\ I_2 \\ ... \\ I_N \end{bmatrix} \tag{3.6}$$

In this case, in order to obtain the different parameters in a two port network an open circuit condition must be imposed at the port opposed to the excitation, as in the next equation set:

$$Z_{11} = \frac{V_1}{I_1}\bigg|_{I_2=0} \quad Z_{12} = \frac{V_1}{I_2}\bigg|_{I_1=0} \quad Z_{21} = \frac{V_2}{I_1}\bigg|_{I_2=0} \quad Z_{22} = \frac{V_2}{I_2}\bigg|_{I_1=0} \tag{3.7}$$

## 3.3 Synthesis process of the NxN coupling matrix

### 3.3.1 Design polynomials and circuit matrices

In this subsection the relationship between the design polynomials synthesized in chapter 2 and both admittance and transmission parameters is presented. Since a physical implementation is desired, relating somehow the polynomials that achieve the desired transfer function with circuit parameters is a must.

Firstly, the example found in [1] is here followed. It will lead to the transmission polynomials of a typical filter ladder structure. Although physical implementations are not introduced until chapters 4 and 5, it is difficult to separate knowledge into completely isolated areas. Due to this, at this point this structure is used for the procedure without proving that it corresponds to a filter network.

Suppose then the third order low-pass filter of figure 3.2, implemented with the inverter model that will be seen in the next chapter.

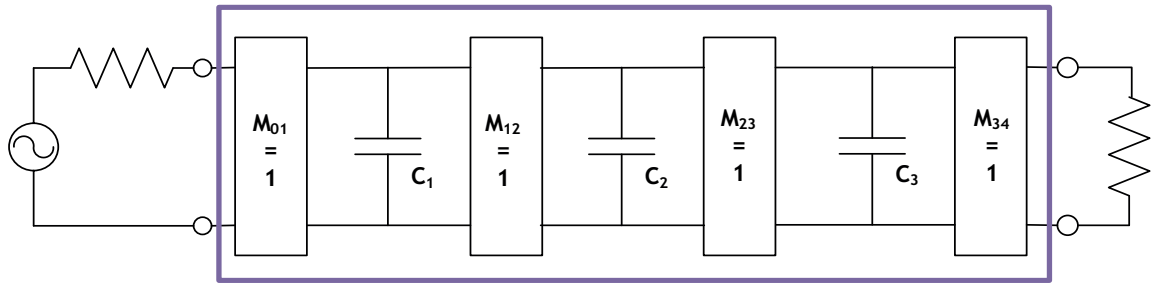


**Figure 3.2: Third order lowpass example**

The transmission matrix of shunt capacitors is:

$$\begin{bmatrix} A(s) & B(s) \\ C(s) & D(s) \end{bmatrix} = \begin{bmatrix} 1 & 0 \\ sC_i & 1 \end{bmatrix} \tag{3.8}$$

Whereas the one associated with the unit inverters is:

$$\begin{bmatrix} A(s) & B(s) \\ C(s) & D(s) \end{bmatrix} = \begin{bmatrix} 0 & j \\ j & 0 \end{bmatrix} \tag{3.9}$$

In order to get the whole filter response in terms of the ABCD matrix, the following cascading must be done:

$$\begin{bmatrix} A(s) & B(s) \\ C(s) & D(s) \end{bmatrix} = \begin{bmatrix} 0 & j \\ j & 0 \end{bmatrix} \cdot \begin{bmatrix} 1 & 0 \\ sC_1 & 1 \end{bmatrix} \cdot \begin{bmatrix} 0 & j \\ j & 0 \end{bmatrix} \cdot \begin{bmatrix} 1 & 0 \\ sC_2 & 1 \end{bmatrix} \cdot \begin{bmatrix} 0 & j \\ j & 0 \end{bmatrix} \cdot \begin{bmatrix} 1 & 0 \\ sC_3 & 1 \end{bmatrix} = \begin{bmatrix} 1 + s^2C_1C_2 & s(C_1 + C_3) + s^3C_1C_2C_3 \\ sC_2 & 1 + s^2C_2C_3 \end{bmatrix} \tag{3.10}$$

As it was mentioned in section 2.2.3, to take the case of complex coefficients into account it is necessary to put a shunt frequency-independent element next to each capacitor (see figure 3.3).

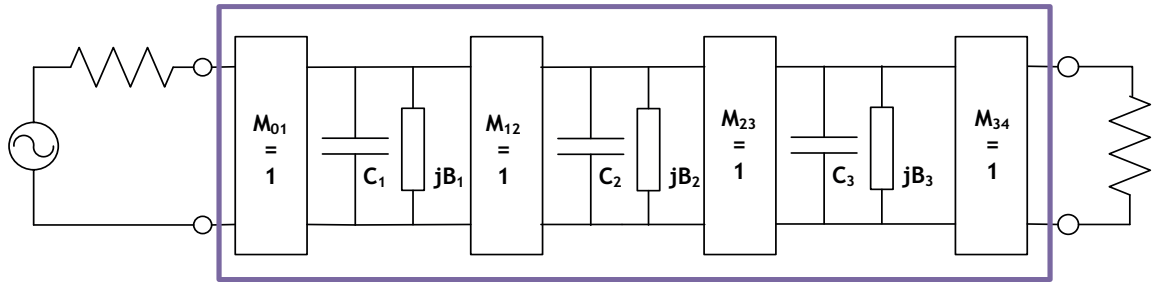


**Figure 3.3: Asymmetric third order lowpass example**

If $sC_i$ is replaced with $sC_i + jB_i$ in the polynomials of equation 3.10, it is obtained:

$$\begin{aligned}
A(s) &= 1 + (sC_1 + jB_1)(sC_2 + jB_2) = (1 - B_1B_2) + js(C_1B_2 + C_2B_1) + s^2C_1C_2 \\
B(s) &= sC_1 + jB_1 + sC_3 + jB_3 + (sC_1 + jB_1) \cdot (sC_2 + jB_2) \cdot (sC_3 + jB_3) = \\
&= -j(B_3 + B_1 - B_1B_2B_3) + s(C_3 + C_1 - B_1C_2C_3 - C_3B_1B_2) + \\
&+ js^2(C_3C_1B_2 + C_3B_1C_2 + C_1C_2B_3 - C_1B_2B_3) + s^3C_1C_2C_3 \\
C(s) &= jB_2 + sC_2 \\
D(s) &= 1 + (sC_2 + jB_2)(sC_3 + jB_3) = (1 - B_2B_3) + js(C_2B_3 + B_2C_3) + s^2C_2C_3
\end{aligned} \tag{3.11}$$

The previous result can be generalised. Thus, for odd-degree cases:

$$\begin{aligned}
A(s) &= a_0 + ja_1s + a_2s^2 + ... + a_{N-1}s^{N-1} \\
B(s) &= jb0 + b_1s + jb_2s^2 + ...jb_{N-1}s^{N-1} + b_Ns^N \\
C(s) &= jc_0 + c_1s + jc_2s^2 + ... + c_{N-2}s^{N-2} \\
D(s) &= d_o + jd_1s + d_2s^2 + ... + d_{N-1}s^{N-1}
\end{aligned} \tag{3.12}$$

It can be seen that the coefficients of the polynomials alternate between purely real and purely imaginary (or vice versa) as the power of $s$ increases. Similarly, for even-degree cases:

$$\begin{aligned}
A(s) &= ja_0 + a_1s + ja_2s^2 + ... + a_{N-1}s^{N-1} \\
B(s) &= b0 + jb_1s + b_2s^2 + ...jb_{N-1}s^{N-1} + b_Ns^N \\
C(s) &= c_0 + jc_1s + c_2s^2 + ... + c_{N-2}s^{N-2} \\
D(s) &= jd_o + d_1s + jd_2s^2 + ... + d_{N-1}s^{N-1}
\end{aligned} \tag{3.13}$$

This generalization is given in [1], but directly in terms of the design polynomials $E(s)$ and $F(s)$ synthesised in chapter 2. From now on, in this subsection the aim is to proof that, indeed, that relationship is hold.

Firstly, it must be introduced the polynomial decomposition into an even and an odd part: any

polynomial of the form $X(s) = \sum_{k=0}^{N} (x'_k + jx''_k)s^k$ can be divided as in equation 3.14.

$$X(s) = X_{even}(s) + X_{odd}(s) \tag{3.14}$$

where

$$\begin{aligned} X_{even}(s) &= \frac{X(s) + X^*(-s)}{2} = x'_0 + jx''_1 s + x'_2 s^2 + ... \\ X_{odd}(s) &= \frac{X(s) - X^*(-s)}{2} = jx''_0 + x'_1 s + jx''_2 s^2 + ... \end{aligned} \tag{3.15}$$

Secondly, the input impedance of the equivalent quadripole network is written in terms of the design polynomials $E(s)$ and $F(s)$:

$$Z_{in}(s) = \frac{E(s) + F(s)/\epsilon_r}{E(s) - F(s)/\epsilon_r} \tag{3.16}$$

If the polynomial decomposition shown in equations 3.14 and 3.15 is applied not to a single polynomial but to the whole numerator (and denominator) of equation 3.16 :

$$Z_{in}(s) = \frac{E(s) + F(s)/\epsilon_r}{E(s) - F(s)/\epsilon_r} = \frac{N_{even}(s) + N_{odd}(s)}{D_{even}(s) + D_{odd}(s)} \tag{3.17}$$

where

$$\begin{aligned} N_{even}(s) &= \Re(e_0 + f_0/\epsilon_r) + j\Im(e_1 + f_1/\epsilon_r)s + \Re(e_2 + f_2/\epsilon_r)s^2 + ... \\ N_{odd}(s) &= j\Im(e_0 + f_0/\epsilon_r) + \Re(e_1 + f_1/\epsilon_r)s + j\Im(e_2 + f_2/\epsilon_r)s^2 + ... \\ D_{even}(s) &= \Re(e_0 - f_0/\epsilon_r) + j\Im(e_1 - f_1/\epsilon_r)s + \Re(e_2 - f_2/\epsilon_r)s^2 + ... \\ D_{odd}(s) &= j\Im(e_0 - f_0/\epsilon_r) + \Re(e_1 - f_1/\epsilon_r)s + j\Im(e_2 - f_2/\epsilon_r)s^2 + ... \end{aligned} \tag{3.18}$$

Thirdly, the next two equations must be taken into account, which are formed just by factoring out equation 3.17:

$$\begin{aligned} Z_{in}(s) &= \frac{N_{even}(s) \cdot [1 + N_{odd}(s)/N_{even}(s)]}{D_{even}(s) + D_{odd}(s)} \quad \text{for odd-degree filters} \\ Z_{in}(s) &= \frac{N_{odd}(s) \cdot [1 + N_{even}(s)/N_{odd}(s)]}{D_{even}(s) + D_{odd}(s)} \quad \text{for even-degree filters} \end{aligned} \tag{3.19}$$

The variables $D_{even}(s)$ and $D_{odd}(s)$ are here ignored because they do not take part in the following reasoning. Now another expression of the input impedance of a two port network with unity source and loading is brought here (see its derivation in appendix A):

$$Z_{in}(s) = \frac{z'_{11}(s) \cdot [1 + 1/y'_{22}(s)]}{z'_{22}(s) + 1} \tag{3.20}$$

When comparing directly equations 2.16 and 2.17, it is found that:

$$\begin{aligned} y'_{22}(s) &= \frac{N_{even}(s)}{N_{odd}(s)} \quad \text{for odd-degree filters} \\ y'_{22}(s) &= \frac{N_{odd}(s)}{N_{even}(s)} \quad \text{for even-degree filters} \end{aligned} \tag{3.21}$$

The next step in this reasoning is to find out the value of $y_{21}^{'}(s)$. An easy way to do it is through the $S$ parameter $\leftrightarrow$ $Y$ parameter transformation, where it can be seen that the numerator of the $S_{21}(s)$ parameter is the same as in the $y_{21}^{'}(s)$ parameter, and therefore, they share the same transmission zeros. If the remaining $S$ parameters transformations are checked, it can be found out that they share a common denominator. Thus, the $y_{21}^{'}(s)$ parameter can be written as:

$$\begin{aligned} y_{21}^{'}(s) &= \frac{kP(s)/\epsilon_p}{N_{odd}(s)} \quad \text{for odd-degree filters} \\ y_{21}^{'}(s) &= \frac{kP(s)/\epsilon_p}{N_{even}(s)} \quad \text{for even-degree filters} \end{aligned} \tag{3.22}$$

At this point it is time to go backwards to equations sets 3.12 and 3.13. In fact, the whole $ABCD$ matrix can not be formed only with those parameters, but needs to include a common denominator which can be factored out:

$$\begin{bmatrix} A^{'}(s) & B^{'}(s) \\ C^{'}(s) & D^{'}(s) \end{bmatrix} = \frac{1}{P(s)/\epsilon_p} \cdot \begin{bmatrix} A(s) & B(s) \\ C(s) & D(s) \end{bmatrix} \tag{3.23}$$

On the one hand, if the transformation between transmission parameters and admittance parameters is computed for the admittance parameter $y_{22}(s)$:

$$y_{22}(s) = \frac{A^{'}(s)}{B^{'}(s)} = \frac{A(s)\Big/P(s)/\epsilon_p}{B(s)\Big/P(s)/\epsilon_p} = \frac{A(s)}{B(s)} \tag{3.24}$$

Then, using equation sets 3.12 and 3.13:

$$\begin{aligned} y_{22}^{'}(s) &= \frac{a_0 + ja_1 s + a_2 s^2 + ... + a_{N-1}s^{N-1}}{jb0 + b_1 s + jb_2 s^2 + ...jb_{N-1}s^{N-1} + b_N s^N} \text{ , for odd-degree cases} \\ y_{22}^{'}(s) &= \frac{ja_0 + a_1 s + ja_2 s^2 + ... + a_{N-1}s^{N-1}}{b0 + jb_1 s + b_2 s^2 + ...jb_{N-1}s^{N-1} + b_N s^N} \text{ , for even-degree cases} \end{aligned} \tag{3.25}$$

Comparing equation set 3.25 with equation sets 3.18 and 3.21 it is now clear that the coefficients $a_i$ and $b_i$ are formed by the sum of polynomials $E(s)$ and $F(s)$.

On the other hand, the transformation for the admittance parameter $y_{21}(s)$ is:

$$y_{21}(s) = \frac{-1}{B^{'}(s)} = \frac{-P(s)/\epsilon_p}{B(s)} \tag{3.26}$$

Using again equation sets 3.12 and 3.13:

$$y_{21}^{'}(s) = \frac{-P(s)/\epsilon_p}{jb0 + b_1 s + jb_2 s^2 + ...jb_{N-1}s^{N-1} + b_N s^N} \text{ , for odd-degree cases}$$
$$y_{21}^{'}(s) = \frac{-P(s)/\epsilon_p}{b0 + jb_1 s + b_2 s^2 + ...jb_{N-1}s^{N-1} + b_N s^N} \text{ , for even-degree cases} \tag{3.27}$$

Comparing with equation sets 3.18 and 3.27, it is clear again that $b_i$ is formed from the sum of the design polynomials $E(s)$ and $F(s)$. With respect to polynomials $C(s)$ and $D(s)$, their expressions are not here derived since it is more tedious and the coupling matrix treated in subsection 3.3.3 can be obtained from $y_{21}(s)$ and $y_{22}(s)$.

To end with, it is important to remark that all the expressions derived in this subsection assume a unitary loading condition. Additional scaling must be done if different loads are needed.

### 3.3.2 Admittance matrix of a multicoupled network

This subsection needs to use the circuit diagram of figure 3.4 which will be explained in the next chapter.It is important to remember that since circuit realization is a stage built upon the stage of synthesis, those areas sometimes need from each other and it is impossible to isolate explanations. At this point it is not going to be explained what kind of elements constitute this network, and all is required to know is that it depicts a circuit network where each loop can be connected to the others.

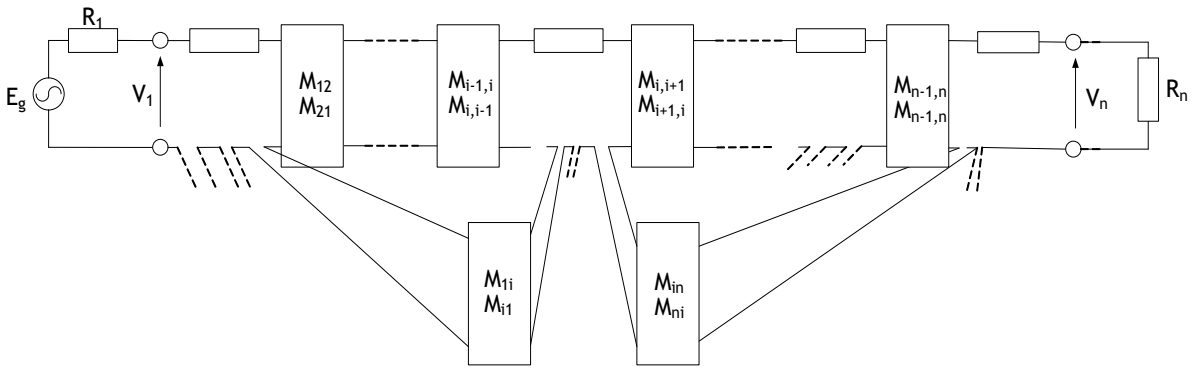


**Figure 3.4: Circuit diagram of a multicoupled network**

In order to avoid jumping from one chapter to another in this document, in this subsection the next equations are solely provided. Further explanation will be found in the next chapter. Sections 3.1 and 3.2 showed that circuits can be described in terms of matrices. The impedance matrix of figure 3.4 satisfy $N$ loop equations that can be gathered in the following shorten matrix notation:

$$e_g[1, 0, 0, ...0]^t = [j\mathbf{M} + s\mathbf{I} + \mathbf{R}] \cdot [i_1, i_2, ..., i_n]^t \tag{3.28}$$

Or, in a more detailed form:

$$\begin{bmatrix} e_g \\ 0 \\ .. \\ 0 \\ 0 \end{bmatrix} = \begin{bmatrix} R_1 & 0 & ... & 0 & 0 \\ 0 & 0 & ... & 0 & 0 \\ ... & ... & ... & ... & ... \\ 0 & 0 & ... & 0 & 0 \\ 0 & 0 & ... & 0 & R_n \end{bmatrix} \cdot \begin{bmatrix} i_1 \\ i_2 \\ ... \\ i_{n-1} \\ i_n \end{bmatrix} + \begin{bmatrix} s+jM_{11} & jM_{12} & ... & jM_{1,n-1} & jM_{1,n} \\ jM_{21} & s+jM_{22} & ... & jM_{2,n-1} & jM_{2,n} \\ ... & ... & ... & ... & ... \\ jM_{n-1,1} & jM_{n-1,2} & ... & s+jM_{n-1,n-1} & jM_{n-1,n} \\ jM_{n,1} & jM_{n,2} & ... & jM_{n-1,n-1} & s+jM_{n,n} \end{bmatrix} \cdot \begin{bmatrix} i_1 \\ i_2 \\ ... \\ i_{n-1} \\ i_n \end{bmatrix} \tag{3.29}$$

Leaving alone the second addend, it is obtained:

$$\begin{bmatrix} e_g - R_1 i_1 \\ 0 \\ .. \\ 0 \\ -R_n i_n \end{bmatrix} = \begin{bmatrix} s+jM_{11} & jM_{12} & ... & jM_{1,n-1} & jM_{1,n} \\ jM_{21} & s+jM_{22} & ... & jM_{2,n-1} & jM_{2,n} \\ ... & ... & ... & ... & ... \\ jM_{n-1,1} & jM_{n-1,2} & ... & s+jM_{n-1,n-1} & jM_{n-1,n} \\ jM_{n,1} & jM_{n,2} & ... & jM_{n-1,n-1} & s+jM_{n,n} \end{bmatrix} \cdot \begin{bmatrix} i_1 \\ i_2 \\ ... \\ i_{n-1} \\ i_n \end{bmatrix} \tag{3.30}$$

And taking into account that $v_1 = e_g - R_1 i_1$ and that $v_n = R_n i_n$ (if the loop currents of the network in figure 3.4 are all defined clockwise), it is concluded that:

$$[v_1\, 0 \ldots 0\ -v_n]^t = [s\mathbf{I} + j\mathbf{M}] \cdot [i_1 \ldots i_n]^t \tag{3.31}$$

In order to pursue the form of an admittance matrix:

$$[v_1\, 0 \ldots 0\ -v_n]^t = \mathbf{P} \cdot [i_1 \ldots i_n]^t \longleftrightarrow [i_1 \ldots i_n]^t = \mathbf{P^{-1}} \cdot [v_1\, 0 \ldots 0\ -v_n]^t \longleftrightarrow$$

$$\begin{bmatrix} i_1 \\ i_n \end{bmatrix} = \mathbf{P^{-1}} \cdot \begin{bmatrix} v_1 \\ -v_n \end{bmatrix} \longleftrightarrow \begin{bmatrix} i_1 \\ -i_n \end{bmatrix} = \begin{bmatrix} [\mathbf{P^{-1}}]_{11} & -[\mathbf{P^{-1}}]_{1n} \\ -[\mathbf{P^{-1}}]_{n1} & [\mathbf{P^{-1}}]_{nn} \end{bmatrix} \cdot \begin{bmatrix} v_1 \\ v_n \end{bmatrix} \longleftrightarrow \begin{bmatrix} i_1 \\ -i_n \end{bmatrix} = \mathbf{Y} \cdot \begin{bmatrix} v_1 \\ v_n \end{bmatrix} \tag{3.32}$$

Equation 3.32 depicts the admittance matrix of the quadripole of figure 3.5, built from the multicoupled network of figure 3.4.

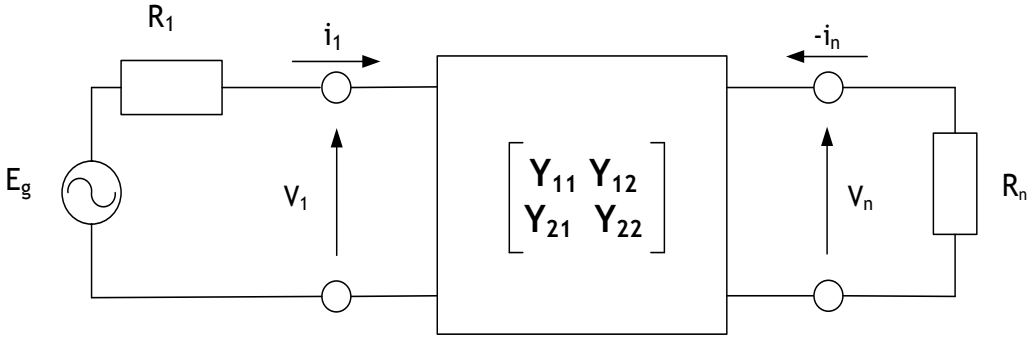


**Figure 3.5: Equivalent quadripole of a multicoupled network**

In the next subsection it will be used subscript "2" in spite of "n" for the aforementioned admittance matrix (i.e. it will be treated as a two port network and the fact that it is a multicoupled network will be omitted whenever is mathematically possible).

### 3.3.3 Final synthesis of M

The coupling matrix, which is in fact the main core of this chapter, was included in the impedance matrix (or equally, in the admittance matrix) of the multicoupled network (see equations 3.31 and 3.32). However, at this point it is not yet clear how to compute the coupling matrix ($M_{N\times N}$) from those expressions

To that end, it is necessary to resort to the property of symmetry the coupling matrix: linear algebra states that only symmetric matrices can be diagonalized by an orthogonal matrix (see appendix C for clarification). In that case, the columns of the diagonalization matrix T ($\{t_1,...,t_n\}$) form a set of eigenvectors in an orthonormal base of $\mathbb{R}^n$, and the values of the diagonal matrix $D$ are the corresponding eigenvalues. Moreover, as the coupling matrix is real, apart from symmetric, its eigenvalues are real too (check again appendix C). Then:

$$\mathbf{M} = \mathbf{T}\cdot\mathbf{D}\cdot\mathbf{T^t}, \quad \text{with D} = \text{diag}[\lambda_1,\ \lambda_2\ ,\ ...\ \lambda_n] \tag{3.33}$$

Now, the general solution for an element $i$,$j$ of an inverse eigenmatrix problem is:

$$[\mathbf{jT}\cdot\mathbf{D}\cdot\mathbf{T^t} + s\mathbf{I}]^{-1}_{ij} = \sum_{k=1}^{N}\frac{T_{ik}T_{jk}}{s-j\lambda_k} \quad i,j = 1...N \tag{3.34}$$

Appendix B proofs how this solution is achieved by means of Neumann series and evidences how this subscript generalization in matrix $T$ is done. In order to avoid getting lost in the whole process, it is advisable bearing in mind that:

⇒ Dashed admittance parameters ($y'_{ij}$) are the ones with unity source and load terminations, and therefore, are the ones directly related to the design polynomials in subsection 3.3.1 through equations 3.25 and 3.27. Only $y'_{21}$ and $y'_{22}$ will be of interest.

⇒ The dashed admittance matrix $Y'$ is a quotient of rational polynomials and can be written in terms of its residues.

⇒ The coupling matrix diagonalization is done through matrix $T$, which is formed by orthonormal vectors.

Hence,

$$\begin{aligned} y'_{21}(s) &= -[jM+sI]^{-1}_{n1} = -\sum_{k=1}^{n}\frac{T'_{nk}T'_{1k}}{s-j\lambda_k} = \sum_{k=1}^{n}\frac{r'_{21k}}{s-j\lambda_k} \\ y'_{22}(s) &= [jM+sI]^{-1}_{nn} = \sum_{k=1}^{n}\frac{T'^{\,2}_{nk}}{s-j\lambda_k} = \sum_{k=1}^{n}\frac{r'_{22k}}{s-j\lambda_k} \end{aligned} \tag{3.35}$$

And therefore,

$$T_{nk}^{'} = \sqrt{r_{22k}^{'}}$$

$$T_{1k}^{'} = \frac{r_{21k}^{'}}{T_{nk}^{'}} = \frac{r_{21k}^{'}}{\sqrt{r_{22k}^{'}}} \tag{3.36}$$

The key step now is to understand that the inverse eigenmatrix solution has led us to what is essentially a partial expansion problem. Due to that result, it has been feasible to link "the world of design polynomials" presented in chapter 2 with the admittance parameters of subsection 3.3.1, which in turn will mean a realizable filter network in chapter 5.

At this point there is a subtle fact that must be taken into account to succeed in the synthesis process of the coupling matrix: as $T$ matrix was formed by orthonormal vectors, its norm must be equal to unity ($\sum_{k=1}^{n} T_{ik}^2 = 1$).And the fact is that unfortunately the sum of the dashed admittance parameters residues(i.e. the norm of $T_{ik}$) is not necessarily equal to unity. To that purpose, as can be seen in figure 3.6,a pair of transformers must be added, which in turn will produce another admittance matrix (undashed in order to distinguish each).

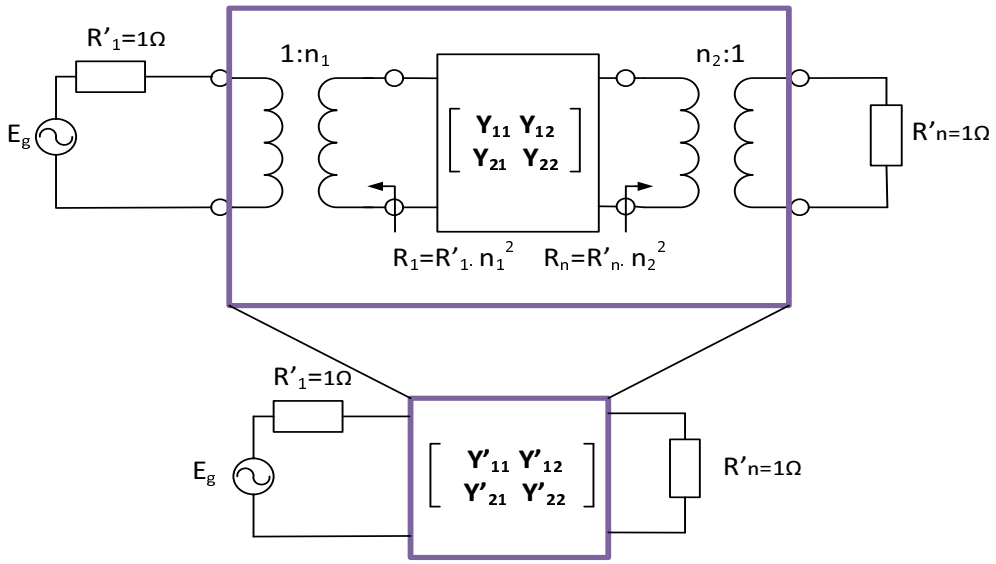


**Figure 3.6: Scaled admittance matrix transformation**

In order to figure out the relationship between both admittance matrix, the input and output transformer ratios are provided:

$$n_1 = \frac{v_1}{v_{1'}} = \frac{i_{1'}}{i_1}, \qquad n_2 = \frac{v_n}{v_{n'}} = \frac{i_{n'}}{i_n} \tag{3.37}$$

On the other hand, the equation set for the admittance parameters of both matrices are:

$$y_{11} = \left.\frac{i_1}{v_1}\right|_{v_n=0} \quad y_{1n} = \left.\frac{i_1}{v_n}\right|_{v_1=0} \quad y_{n1} = \left.\frac{i_n}{v_1}\right|_{v_n=0} \quad y_{nn} = \left.\frac{i_n}{v_n}\right|_{v_1=0}$$
$$y_{11}^{'} = \left.\frac{i_{1'}}{v_{1'}}\right|_{v_{n'}=0} \quad y_{1n}^{'} = \left.\frac{i_{1'}}{v_{n'}}\right|_{v_{1'}=0} \quad y_{n1}^{'} = \left.\frac{i_{n'}}{v_{1'}}\right|_{v_{n'}=0} \quad y_{nn}^{'} = \left.\frac{i_{n'}}{v_{n'}}\right|_{v_{1'}=0} \tag{3.38}$$

Then, using equations 3.37 and 3.38, the relationship is finally found by doing the following operations:

$$\frac{y_{11}^{'}}{y_{11}} = \frac{i_{1'}/v_{1'}}{i_1/v_1} = \frac{i_{1'}}{i_1}\cdot\frac{v_1}{v_{1'}} = n_1^2 \rightarrow y_{11}^{'} = n_1^2 y_{11}$$

$$\frac{y_{1n}^{'}}{y_{1n}} = \frac{i_{1'}/v_{n'}}{i_1/v_n} = \frac{i_{1'}}{i_1}\cdot\frac{v_n}{v_{n'}} = n_1 n_2 \rightarrow y_{1n}^{'} = n_1 n_2 y_{1n}$$

$$\frac{y_{n1}^{'}}{y_{n1}} = \frac{i_{n'}/v_{1'}}{i_n/v_1} = \frac{i_{n'}}{i_n}\cdot\frac{v_1}{v_{1'}} = n_2 n_1 \rightarrow y_{21}^{'} = n_2 n_1 y_{n1} \tag{3.39}$$

$$\frac{y_{nn}^{'}}{y_{nn}} = \frac{i_{n'}/v_{n'}}{i_n/v_n} = \frac{i_{n'}}{i_n}\cdot\frac{v_n}{v_{n'}} = n_2^2 \rightarrow y_{22}^{'} = n_2^2 y_{nn}$$

Thus:

$$\begin{bmatrix} y_{11}^{'}(s) & y_{12}^{'}(s) \\ y_{21}^{'}(s) & y_{22}^{'}(s) \end{bmatrix} = \begin{bmatrix} n_1^2 y_{11}(s) & n_1 n_2 y_{12}(s) \\ n_2 n_1 y_{21}(s) & n_2^2 y_{22}(s) \end{bmatrix} \tag{3.40}$$

Now equations 3.35 and 3.40, lead to the following expressions:

$$y_{22}(s) = \frac{y_{22}^{'}(s)}{n_2^2} = \frac{1}{n_2^2}\cdot\sum_{k=1}^{n}\frac{{T_{nk}^{'}}^2}{s-j\lambda_k} = \sum_{k=1}^{n}\frac{{T_{nk}}^2}{s-j\lambda_k} \qquad \text{,with } T_{nk} = \frac{T_{nk}^{'}}{n_2} = 1$$
$$y_{21}(s) = \frac{y_{21}^{'}(s)}{n_2 n_1} = \frac{-1}{n_2 n_1}\cdot\sum_{k=1}^{n}\frac{T_{1k}^{'}T_{nk}^{'}}{s-j\lambda_k} = -\sum_{k=1}^{n}\frac{T_{1k}T_{nk}}{s-j\lambda_k} \quad \text{,with } T_{1k} = \frac{T_{1k}^{'}}{n_1} = 1 \tag{3.41}$$

Equation 3.41 evidences that inserting a pair of transformers allows to normalize the aforementioned vectors of $T$ matrix with:

$$n_1 = \sum_{k=1}^{n} T_{1k}^{'}\,, \quad n_2 = \sum_{k=1}^{n} T_{nk}^{'} \tag{3.42}$$

With the transformer ratios now determined, the load impedances for the calculated coupling matrix must be:

$$R_a = n_1^2\,, \quad R_b = n_2^2 \tag{3.43}$$

It is important to remark that another equivalent implementation would make use of two input-output inverters in spite of transformers. Their values must be $M_{S1} = \sqrt{R_a} = n_1$ and $M_{NL} = \sqrt{R_b} = n_2$ (see figure 3.7). Inverters will be fully explained in the next chapter.

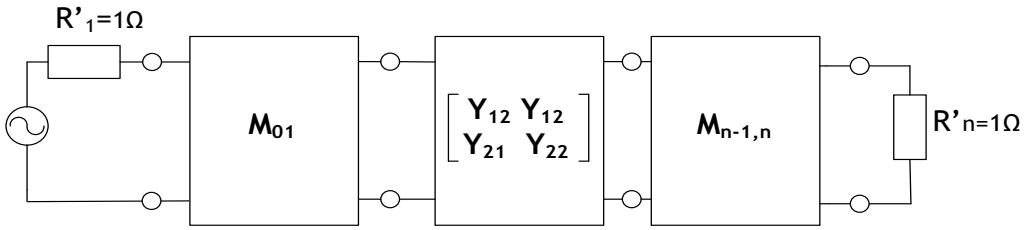


**Figure 3.7: Design with input/output inverters**

Finally, there are still two things left to complete this subsection, which clearly are now identified by looking at equation 3.33:

⇒ although $T_{1k}$ and $T_{nk}$ have been calculated, the $T$ matrix has rank $N$ and thus, $N-2$ remaining vectors need to be determined. This is the moment to call for its orthogonality property. Indeed, with the first and last rows of T determined, $N-2$ independent vectors are chosen, so that with the Gram-Schmitt orthonormalization process the remaining orthogonal rows of $T$ can be calculated.

⇒ in order to complete the coupling matrix synthesis the eigenvalues must be computed in advanced so that the diagonalization process is possible. They can be computed as the roots of the denominator polynomial $B(s)$. It must be noticed that because the coupling matrix $M_{NxN}$ is symmetric and real, the eigenvalues $\lambda_k$ are real too.

## 3.4 Applied filter design examples

The theory shown in the previous sections of this chapter is used to implement a MATLAB code which synthesises a coupling matrix given a set of design polynomials. This section aims at showing a few examples developed with that code. In this case, the design polynomials are obtained using the code implemented in the preceding chapter.

The first four matrices that are synthesised belong to the four examples presented in chapter 2 (thus, they all have N=5 and RL=15 dB). For this reason their responses are not shown again and only the numerical values are provided in A-C.

A. Coupling matrix and loading resistors for finite transmission zeros at $s = \sigma + j\omega = \pm 1.5j$.

$$R_1 = R_2 = 0.7992, \qquad M = \begin{bmatrix} 0.0000 & 0.7514 & 0.0000 & -0.0836 & 0.0000 \\ 0.7514 & 0.0000 & 0.6328 & 0.0000 & -0.0833 \\ 0.0000 & 0.6328 & 0.0000 & 0.6357 & 0.0000 \\ -0.0836 & 0.0000 & 0.6357 & 0.0000 & 0.7548 \\ 0.0000 & -0.0833 & 0.0000 & 0.7548 & 0.0000 \end{bmatrix} \tag{3.44}$$

B. For finite transmission zeros at $s = \sigma + j\omega = \pm 1.5$.

$$R_1 = R_2 = 0.8192, \qquad M = \begin{bmatrix} 0.0000 & -0.7802 & 0.0000 & -0.0496 & 0.0000 \\ -0.7802 & 0.0000 & -0.5709 & 0.0000 & -0.0496 \\ 0.0000 & -0.5709 & 0.0000 & -0.5710 & 0.0000 \\ -0.0496 & 0.0000 & -0.5710 & 0.0000 & -0.7804 \\ 0.0000 & -0.0496 & 0.0000 & -0.7804 & 0.0000 \end{bmatrix} \tag{3.45}$$

C. For finite transmission zeros at $s = \sigma + j\omega = \pm 1.5 \pm 1.5j$.

$$R_1 = R_2 = 0.8132, \qquad M = \begin{bmatrix} 0.0000 & 0.4149 & 0.0000 & 0.6537 & 0.0000 \\ 0.4149 & 0.0000 & 0.1701 & 0.0000 & -0.6541 \\ 0.0000 & 0.1701 & 0.0000 & -0.8206 & 0.0000 \\ 0.6537 & 0.0000 & -0.8206 & 0.0000 & 0.4290 \\ 0.0000 & -0.6451 & 0.0000 & 0.4290 & 0.0000 \end{bmatrix} \tag{3.46}$$

D. For finite transmission zeros at $s = \sigma + j\omega = 1.5j$.

$$R_1 = R_2 = 0.8087, \qquad M = \begin{bmatrix} -0.0205 & 0.7635 & 0.0947 & 0.0384 & 0.0000 \\ 0.7635 & 0.1000 & -0.6175 & 0.1346 & 0.0267 \\ 0.0947 & -0.6175 & 0.2001 & 0.5670 & 0.0947 \\ 0.0384 & 0.1346 & 0.5670 & 0.1230 & -0.7639 \\ 0.0000 & 0.0267 & 0.0947 & -0.7639 & -0.0206 \end{bmatrix} \tag{3.47}$$

Another two new complete examples (i.e their design polynomials, coupling matrices and responses ) are now provided. The first of the additional examples (which is the fifth given in this chapter) evidences that the nearer to the normalized cutoff frequency the finite transmission zero is placed, the higher the lobe level formed in the transmission parameter is (see figure 3.8).

E. Coupling matrix and loading resistors for a generalised Chebychev sixth-order filter,return loss 25 dB and finite transmission zeros at $s = \sigma + j\omega = -1.5j,\ 1.2j$.

$$R_1 = R_2 = 1.1901, \quad M = \begin{bmatrix} -0.0100 & 0.0601 & 0.5502 & -0.3665 & -0.6324 & 0.0000 \\ 0.0601 & 0.0440 & -0.7940 & 0.1269 & 0.1410 & -0.3259 \\ 0.5502 & -0.7940 & 0.0252 & 0.5661 & -0.3114 & 0.0387 \\ -0.3665 & 0.1269 & 0.5661 & 0.4543 & 0.3071 & -0.7395 \\ -0.6324 & 0.1410 & -0.3114 & 0.3071 & -0.3489 & 0.4313 \\ 0.0000 & -0.3259 & 0.0387 & -0.7395 & 0.4313 & -0.0100 \end{bmatrix} \tag{3.48}$$

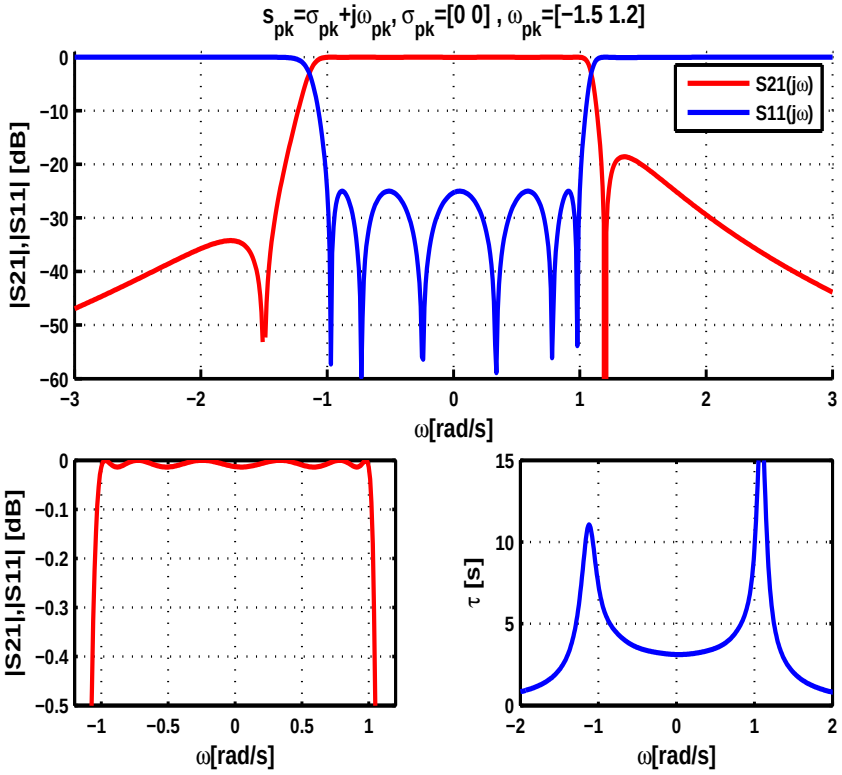


**Figure 3.8: Example 5.**

| Coefficients ($\epsilon_p = 2.198, \epsilon_f = 1$) | | | |
|---|---|---|---|
| $c_{k,k=}$ | P(s) | F(s) | E(s) |
| **0** | $1.8j$ | 0.045 | $0.789 - 0.223j$ |
| **1** | $-0.3$ | $-0.054j$ | $2.495 - 0.565j$ |
| **2** | $j$ | 0.662 | $4.424 - 0.768j$ |
| **3** | | $-0.201j$ | $5.166 - 0.696j$ |
| **4** | | 1.597 | $4.429 - 0.392j$ |
| **5** | | $-0.155j$ | $2.380 - 0.155j$ |
| **6** | | 1 | 1 |

**Table 3.1: Example 5.**

Concerning the second additional example, it shows that if it is needed to keep the finite transmission zero near the normalized frequency to pursue selectivity, an additional finite transmission should be placed (see figure 3.9) to guarantee a low transmission lobe level.

F. Coupling matrix and loading resistors for a generalised Chebychev sixth-order filter, return loss 25 dB and finite transmission zeros at $s = \sigma + j\omega = -1.2j,\ 1.2j,\ 1.4j$.

$$R_1 = R_2 = 1.1787, \qquad M = \begin{bmatrix} -0.0104 & 0.8722 & -0.1996 & -0.1541 & -0.0428 & 0.0000 \\ 0.8722 & 0.0141 & -0.2337 & 0.5045 & -0.5093 & -0.1252 \\ -0.1996 & -0.2337 & -0.7297 & 0.0391 & -0.3334 & 0.7029 \\ -0.1541 & 0.5045 & 0.0391 & 0.7787 & 0.3209 & 0.0160 \\ -0.0428 & -0.5093 & -0.3334 & 0.3209 & 0.3779 & -0.5623 \\ 0.0000 & -0.1252 & 0.7029 & 0.0160 & -0.5623 & -0.0104 \end{bmatrix} \tag{3.49}$$

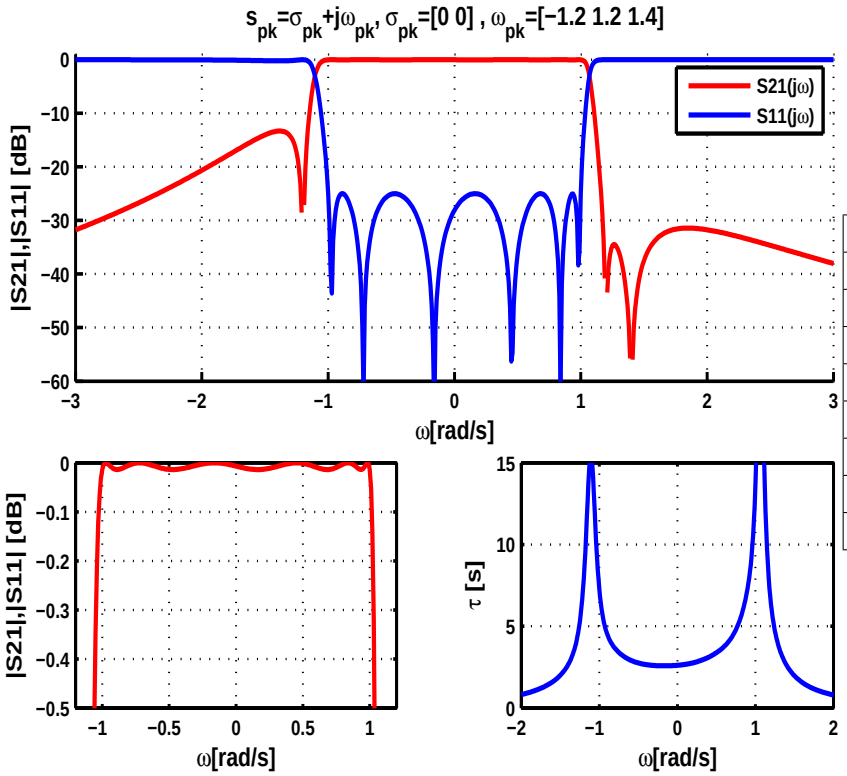


**Figure 3.9: Example 6.**

| Coefficients ($\epsilon_p = 1.862, \epsilon_f = 1$) | | | |
|---|---|---|---|
| $c_{k,k=}$ | P(s) | F(s) | E(s) |
| **0** | $-2.016j$ | 0.043 | $0.745 - 0.788j$ |
| **1** | 1.44 | $-0.179j$ | $2.499 - 1.529j$ |
| **2** | $-1.4j$ | 0.661 | $4.351 - 2.006j$ |
| **3** | 1 | $-0.586j$ | $5.089 - 1.811j$ |
| **4** | | 1.600 | $4.379 - 1.015j$ |
| **5** | | $-0.420j$ | $2.357 - 0.420j$ |
| **6** | | 1 | 1 |

**Table 3.2: Example 6.**

## 3.5 $M_{N\times N}$ constraints

The coupling matrix presented in this chapter is a powerful tool, but it has two relevant limitations:

⇒ The maximum number of finite transmission zeros that it can accommodate is $N-2$ (being $N$ the filter order).

⇒ The effect of the loads ($R_i$) over the intermediate resonators can not be considered.

As a direct consequence of these constraints the designer has less degrees of freedom in order to pursue the fulfilment of certain specifications. However, it is possible to take a further step in filter synthesis and overcome both limitations through the $M_{N\times 2+N\times 2}$ coupling matrix. The "$N+2\times N+2$" subscript used is not chosen by coincidence: it is used as opposed to the $M_{NxN}$ coupling matrix presented in this chapter, since an extra pair of rows are added (one at the top and the other at the bottom, see figure 3.10 ).

| | | | |
|---|---|---|---|
| $\mathbf{M_{1,1}}$ | $\mathbf{M_{1,2}}$ | ... | $\mathbf{M_{1,n}}$ |
| $\mathbf{M_{2,1}}$ | $\mathbf{M_{2,2}}$ | ... | $\mathbf{M_{2,n}}$ |
| $\mathbf{M_{3,1}}$ | $\mathbf{M_{3,2}}$ | ... | $\mathbf{M_{3,n}}$ |
| $\mathbf{M_{4,1}}$ | $\mathbf{M_{4,2}}$ | ... | $\mathbf{M_{4,n}}$ |
| ... | ... | ... | ... |
| $\mathbf{M_{n,1}}$ | $\mathbf{M_{n,2}}$ | ... | $\mathbf{M_{n,n}}$ |

| | | | | | |
|---|---|---|---|---|---|
| | $\mathbf{M_{S,1}}$ | $\mathbf{M_{S,2}}$ | ... | $\mathbf{M_{S,n}}$ | $\mathbf{M_{S,L}}$ |
| $\mathbf{M_{1,S}}$ | $M_{1,1}$ | $M_{1,2}$ | ... | $M_{1,n}$ | $\mathbf{M_{1,L}}$ |
| $\mathbf{M_{2,S}}$ | $M_{2,1}$ | $M_{2,2}$ | ... | $M_{2,n}$ | $\mathbf{M_{2,L}}$ |
| $\mathbf{M_{3,S}}$ | $M_{3,1}$ | $M_{3,2}$ | ... | $M_{3,n}$ | $\mathbf{M_{3,L}}$ |
| $\mathbf{M_{4,S}}$ | $M_{4,1}$ | $M_{4,2}$ | ... | $M_{4,n}$ | $\mathbf{M_{4,L}}$ |
| ... | ... | ... | ... | ... | ... |
| $\mathbf{M_{n,S}}$ | $M_{n,1}$ | $M_{n,2}$ | ... | $M_{n,n}$ | $\mathbf{M_{n,L}}$ |
| $\mathbf{M_{L,S}}$ | $\mathbf{M_{L,1}}$ | $\mathbf{M_{L,2}}$ | ... | $\mathbf{M_{L,n}}$ | |

**Figure 3.10: Comparison of the $M_{N\times N}$ and the $M_{N+1\times N+1}$ matrix structures**

Finally, another advantage of the $M_{N\times 2+N\times 2}$ coupling matrix is that its synthesis procedure uses a transversal array circuit representation in which the Gram Schmitt orthonormalization process is no longer needed.

# 4

# Physical Filter Realization I

Chapters 4 and 5 focus on the physical realization of filters (i.e. the synthesis problem). Both chapters are divided in two main sections: one on low-frequency filter design and the other on microwave filters. Such division is needed as filter design at microwave frequencies is based on the circuital theory of lumped elements, born in the context of low frequencies. This chapter addresses lowpass designs.

The first section shows how lowpass ladder networks arise once the approximation problem has been solved, and introduces the concept of duality and denormalization. The second section is focused on microwave filter design, where the lumped elements are no longer valid and therefore making it convenient to resort to more suitable structures (i.e. the ones in general called distributed elements). Two lowpass approaches typically used at microwave frequencies are presented: Richards' transformation and the stepped impedance filter. A filter design based on the latter approach is carried out. Once the physical dimensions are known its full-wave response is obtained using CST Microwave Studio. The concept of optimization is introduced and applied throughout this case study.

## 4.1 Introduction to low-frequency filter design

The first step towards physical filter realization at microwave frequencies is to study the low-pass circuit model composed of lumped elements (i.e. inductors and capacitors). This model will be used as the starting point of the approaches seen in section 4.2.

### 4.1.1 Ladder networks

LC ladder networks have their origin in Cauer's dissertation, published in 1926. He completed the properties associated with the two-kind realizable impedances functions (i.e. LC, RC, RL)

in which Foster had been working two years before, and suggested new topologies. Whereas Foster used partial expansions, where impedance (Foster I) or admittance (Foster II) poles were subtracted, Cauer used continued fraction expansion about infinity (Cauer I) or about zero (Cauer II), alternating impedance and admittance subtractions leading to ladder structures. Those topologies are canonical (i.e. they use the minimum number of physical elements) as they remove each pole completely. In 1931, Brune introduced the concept of positive-real functions (in which classical filter network theory is currently built) and applied this concept for the realization of RLC networks.

All this work took into account one-port networks. It was nearly a decade after, between 1938 and 1941, when Cocci, Darlington and Cauer developed independently a new general insertion loss theory (as opposed to the image parameters design)[1]. When it was shown that such impedances met the appropriate conditions to be developed in terms of Cauer's canonical LC networks, the well-known two-port ladder networks applied to filters arised.

As opposed to Foster, Cauer synthesis uses "simple branches" where only one type of lumped element is used (namely capacitors or inductors in the filter networks here treated). Those kind of ladders can hold functions where all transmission zeros are set at infinity, or all at the origin. The former ladder adopts Cauer-I configuration, and the latter the Cauer-II topology (see figure 4.1).

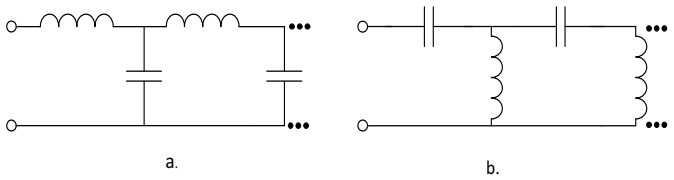


**Figure 4.1: Lumped ladder networks. a.Cauer I b.Cauer II**

In fact figure 4.1.a. is the well-known ladder used as a starting point in filter synthesis, where the capacitors and inductors are placed in shunt and series branches respectively (whereas figure b. corresponds to a highpass structure, as will be seen in subsection 5.1.1). At first glance it can be seen that a transmission zero is created when series arms are open or when shunt arms hold a short, and that both situations happen at infinity frequency. Thus, somehow this topology has a low-pass nature. However, it is obvious that a low-pass filter must accomplish certain requirements in a whole band, and not at a single specific frequency.

At this point it is worth once again to recall the importance of the role of the power insertion loss method, as it provides manifold functions to meet the desired frequency requirements. The

[1] in fact, the first attempts towards insertion loss theory date from Norton's insertion-loss functions applied to constant resistance filter pairs (published in 1937).

selected function is then translated into specific values of the lumped elements of the two-port Cauer-I ladder network. This is possible as the power insertion loss ends with the designed reflection coefficient being translated into the driving-point impedance, which allows continued fraction expansion as certain properties of the location of zeros were respected.

The achieved values are usually represented by letter $g$, as in figure 4.2. Letter $g_0$ is used for the source load, and always adopts unity value, whereas letter $g_{n+1}$ is used for the end-load and its value is subjected to the approximation function used. It is worth to mention that classical filter functions usually provide formulas to skip the aforementioned expansion process.

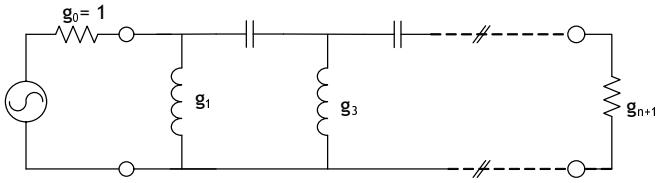


**Figure 4.2: Ladder lumped lowpass filter**

To end with, it is important to mention that the most classical filter functions (e.g. Butterworth, Chebychev, and so on), which set all their transmission zeros at infinity are also known as all-pole functions-i.e. with all their transmission zeros at infinity.

### 4.1.2 The duality principle

Actually, given the $g_i$ parameters associated to a certain low-pass frequency response, figure 4.2 is not the only possible configuration. Indeed, the duality principle allows to use the configuration seen in figure 4.3 and obtain the same frequency response.

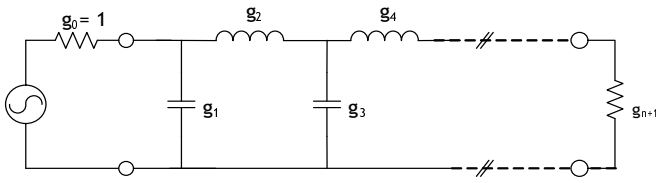


**Figure 4.3: Dual ladder lumped lowpass filter**

Duality is described in terms of the impedance and admittance parameters. If two networks are dual, it means that, given the undashed impedance parameters of one, and the dashed admittance parameters of the other:

$$\begin{aligned} Z_{ii}/Z_0 &= Y_{ii}^{'}/Y_0^{'} \\ Z_{ij}/Z_0 &= -Y_{ij}^{'}/Y_0^{'}, \end{aligned} \tag{4.1}$$

assuming $Z_0$ and $Y_0$ equal to unity for a normalized case. Equation 4.1 implies that an inductor of x henries is the dual of a capacitance of x farads, that a resistance of x ohms is the dual

of a conductance of x mohs, that a short circuit is the dual of an open circuit, that a series connection is the dual of a parallel connection and so on. Two dual networks produce the same filtering response.

Thanks to duality, there are always two topologies that can be used conveniently depending on the situation (i.e. one starting with a shunt branch and the other one with a series branch).

### 4.1.3 Impedance scaling

The polynomial functions used to meet given specifications can be directly translated into certain topologies, such as the ladder networks seen in subsection 4.1.1. This is possible to address as those polynomial functions are conceived under certain properties concerned with realizability.However, input and output impedances seen from where the filter is going to be placed usually differ considerably from the common low values reached "purely" by means of the insertion loss method (i.e. $g_0$ and $g_{n+1}$). To cope with this problem, it is introduced the concept of impedance scaling.

The impedance matrix of a network in which each dipole is characterised by its impedance matrix $Z_i$ can be written as in equation 4.2, where $z_0$ is a diagonal matrix with the characteristic impedances of each port.

$$\mathbf{S} = (\mathbf{z_0}^{-\frac{1}{2}} \cdot \mathbf{Z} \cdot \mathbf{z_0}^{-\frac{1}{2}} - \mathbf{I}) \cdot (\mathbf{z_0}^{-\frac{1}{2}} \cdot \mathbf{Z} \cdot \mathbf{z_0}^{-\frac{1}{2}} + \mathbf{I})^{-1} \tag{4.2}$$

Now another network (denoted with dashed parameters) is obtained by changing the reference impedance of each port. This operation includes the two extreme dipoles, which in fact implies a change in the impedances at the input and output of the network considered as a whole. Although that is exactly what we are looking for, not only all the intermediate reference impedances must be scaled ($\mathbf{z_0'} = R_0\mathbf{z_0}$), but each dipole of the network (i.e. $Z_i' = R_0 Z_i$, and hence, $\mathbf{Z}' = R_0\mathbf{Z}$).
Only then,

$$\mathbf{z_0}'^{\frac{-1}{2}} \cdot \mathbf{Z}' \cdot \mathbf{z_0}'^{\frac{-1}{2}} = \mathbf{z_0}^{\frac{-1}{2}} R_0^{\frac{-1}{2}} \cdot \mathbf{Z} \cdot R_0 \mathbf{z_0}^{\frac{-1}{2}} R_0^{\frac{-1}{2}} = \mathbf{z_0}^{\frac{-1}{2}} \cdot \mathbf{Z} \cdot \mathbf{z_0}^{\frac{-1}{2}} \tag{4.3}$$

And therefore, $\mathbf{S}' = \mathbf{S}$, which implies that it is possible to maintain the desired frequency response if the input and output impedances of the whole network are changed by properly scaling the elements that constitute the network.

It is important to highlight that this reasoning is developed in terms of a single load value (i.e. $R_0$). If the source load differs from the end load, the designer will need to use additional circuits such as transformers or inverters (the latter ones will be seen in subsection 5.1.2).

Finally, a low-pass filter needs as well to be denormalized in terms of frequency. However, to avoid repetition, the whole concept of frequency denormalization will be introduced in the next chapter, in the context of bandpass filters realization. A complete table, taking into account both operations (i.e. impedance and frequency scaling) will be given then.

## 4.2 Radio-frequency filter design

For the first time in this document it is treated the problem of the physical filter realization at microwave frequencies. For that reason the first subsection is included in this chapter: to provide a general view of nature of the problem,

### 4.2.1 Statement of the problem

Chapters 2 and 3, together with section 4.1, and the section for bandpass filters included in chapter 5 (section 5.1), reveal a robust theory for filter design. It allows to synthesize a physical lumped network which ideally behaves exactly as a desired (lowpass/bandpass/bandstop)[2] polynomial response. Any deviation from the desired response is due to losses associated with non-ideal conductors and dielectric materials, circuital tolerances and/or undesired interaction between lumped elements because of a space limitation and a poor isolation between packages.

Nevertheless, as the development of society boosted the use of higher frequencies, problems (or "engineering challenges" to make it sound better) appeared. The main problem of lumped elements is rooted in pure physical constraints: realizable capacitors and inductors can not behave as such over the whole range of frequencies due to the existence of parasitics. Figure 4.4 shows two typical equivalent models of a real capacitor and a real inductor respectively. Both of them have a resonant frequency(the former $f_0 = \frac{1}{2\pi\sqrt{ESL \cdot C}}$ and the latter $f_0 = \frac{1}{2\pi}\sqrt{\frac{1}{LC} - \frac{R^2}{L^2}}$), where the capacitor begins to behave as an inductor and vice versa.

There are many equivalent models depending on the type of inductor or capacitor used(e.g. the equivalent circuit model given in figure 4.4.b. is the one of a typical air core inductor, but ferromagnetic core inductors use a different equivalent circuit model). These models even depend on the type of mounting (e.g. surface mounting in a PCB usually includes additional capacitances to ground). Anyhow, the idea is clear: the ideal value of a lumped element which is related to an ideal linear response has an upper (or even a lower) limit associated with physical fabrication.

[2] A highpass filter, as opposed to the remaining types of filters, is by definition unreachable (see the remark on the parasitics of lumped elements in the same subsection) and therefore it is not here included.

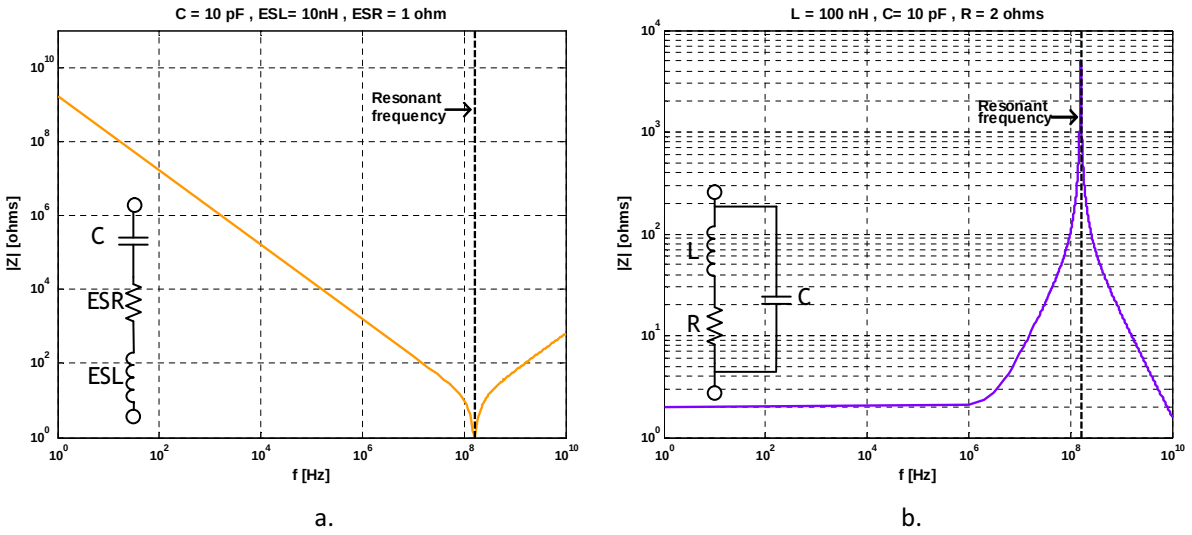


**Figure 4.4: Two examples of the behaviour of a. a real capacitor b. a real inductor**

There is another reason why lumped elements are superseded by distributed elements (i.e. transmission lines) at high frequencies: the relationship between frequency and distance between elements. When frequency is increased and the distance between lumped elements is comparable to the wavelength, it becomes mandatory to consider voltages and currents as waves, or even to take into account the propagation of the electromagnetic fields involved. Therefore, models which include those physical effects are needed.

In view of these constraints, filter design at microwave frequencies needed to develop its own theory. However, as it will be seen through the next subsections in this chapter, it is built over the well-known classical theory concepts. The price to pay is that filter design at microwave frequencies is not as accurate as in lumped networks. It is generally based on approaches which are valid at a narrow range of frequencies (when not at a single one, as in imittance inverters).

### 4.2.2 Lowpass approaches

Lowpass approaches are based on the replacement of each lumped element by a transmission line with suitable length, characteristic impedance and in some cases termination. Since the distributed elements are placed one next to the other without any space in between, actually the filter designer does not need to worry explicitly about the propagation phenomena of currents and voltages.

Two typical low-pass approaches used in microwave filter design are now presented. At the end of the section differences between them are underlined.

**Richards' transformation**

In order to explain how this transformation works, firstly it is recalled the expression of the input impedance of a transmission line of length $d$, characteristic impedance $Z_0$, and loaded with an impedance of value $Z_L$:

$$Z_{in} = Z_0 \frac{Z_L + jZ_0 \tan(\beta d)}{Z_0 + jZ_L \tan(\beta d)} \tag{4.4}$$

If the mentioned transmission line is open-ended (i.e. $Z_L = \infty$), and its length is chosen as $d = \lambda_c/8$, the input admittance of equation 4.4 at a given frequency $f_c$ turns out to be:

$$Y_{in}\Big|_{f_c} = jY_0 \tan(\beta_c d) \overset{\tan(\frac{\pi}{4})=1}{=} jY_0 \tag{4.5}$$

Whereas if the same transmission line(see equation 4.4) is short-ended (i.e. $Z_L = 0$), and its length is again chosen as $d = \lambda_c/8$, the input impedance at a given frequency $f_c$ becomes:

$$Z_{in}\Big|_{f_c} = jZ_0 \tan(\beta_c d) \overset{\tan(\frac{\pi}{4})=1}{=} jZ_0 \tag{4.6}$$

Equation 4.5 evidences that at a single frequency $f_c$ a capacitor can be replaced by an open-ended transmission line of length $d = \lambda_c/8$ and characteristic admittance $Y_0 = \omega_c C$ since:

$$jY_0 = j\omega_c C \longleftrightarrow Y_0 = w_c C \tag{4.7}$$

Similarly, equation 4.6 shows that at a single frequency $f_c$ an inductor can be replaced by a short-ended transmission line of length $d = \lambda_c/8$ and characteristic impedance $Z_0 = \omega_c L$ since:

$$jZ_0 = j\omega_c L \longleftrightarrow Z_0 = w_c L \tag{4.8}$$

It is important to notice that the length of the transmission lines is $\lambda_c/8$ in order to let the term $tan(\beta_c d)$ in equations 4.5 and 4.6 disappear.It is required since the impedance of either an inductor or capacitor behave linearly with frequency. Similarly equations 4.7 and 4.8 use a particular frequency $\omega_c$ and not $\omega$, since capacitors and inductors do not behave as constants over the whole range of frequencies.

Although it is clear that this approach works at a single frequency, any filter design involves a range of frequencies. And at this point is when the filter designer comes across with the harsh reality: if a wider range of frequencies is considered, the same open-ended transmission line of length $d = \lambda_c/8$ behaves as $Y_{in} = jY_0 tan(\beta d)$, and the short-ended $\lambda_c/8$ transmission line

as $Z_{in} = jZ_0 \tan(\beta d)$. Thus, this transformation depends on the linearity around $f_c$ that the *tangent* function can provide.And what is more, because the tangent is a periodic function, unlike a classical lumped filter network, Richards' transformation leads to a periodic response of period $4 \cdot \omega_c$.The filter designer must take into account this periodic behaviour to meet the desired specifications (i.e. a particular power mask).

As the reader may have noticed, so far it has not been mentioned the term "lowpass", since Richards' transformation is focused on the replacement of individual lumped elements. However, actually this approach is only used for lowpass filters, because:

⇒ in a high-pass design periodicity is much worse, as even without the replicas the obtained filter response is bandpass and not highpass (otherwise it is conceptually impossible for replicas to appear).

⇒ at the scene of bandpass and bandstop filters there are better approaches which do not replace individually capacitors and inductors but whole resonant circuits formed by both lumped elements.

Figure 4.5 provides an easy and short MATLAB example of the circuital response of the Richards' transformation used to design a sixth-order Chebychev lowpass filter with 20 dB of return loss, R0=50 ohms and fc=2GHz. According to the frequency scaling used for a lumped element network ,which for convenience will be seen in subsection 5.1.1, the characteristic admittance of the open-ended transmission lines of equation 4.7 becomes:

$$Y_0 = \omega_c C = \frac{g_c}{R_0}, \text{ with } C = \frac{g_c}{\omega_c R_0} \tag{4.9}$$

With respect to the characteristic impedance of the short-ended transmission lines of equation 4.8:

$$Z_0 = \omega_c L = g_L R_0, \text{ with } L = \frac{g_L R_0}{\omega_c} \tag{4.10}$$

Figure 4.6 depicts the normalized lumped network and the distributed network after carrying out Richards' transformation.

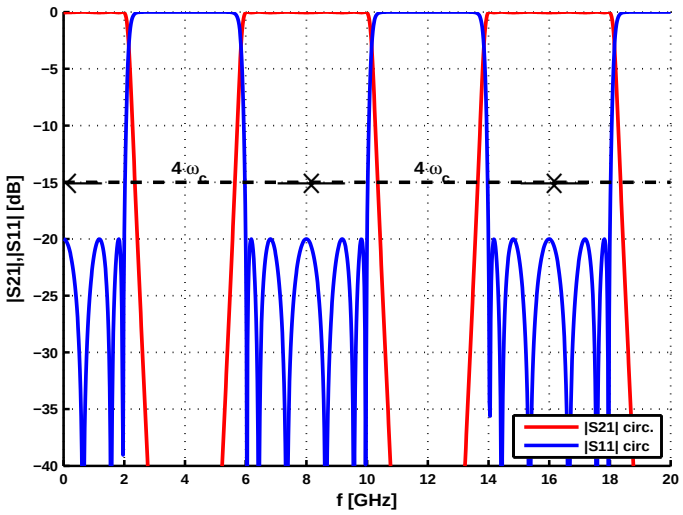


**Figure 4.5: Richards' response for a sixth-order Chebychev lowpass filter (fc=2GHz, RL=20 dB, R0=50 ohms)**

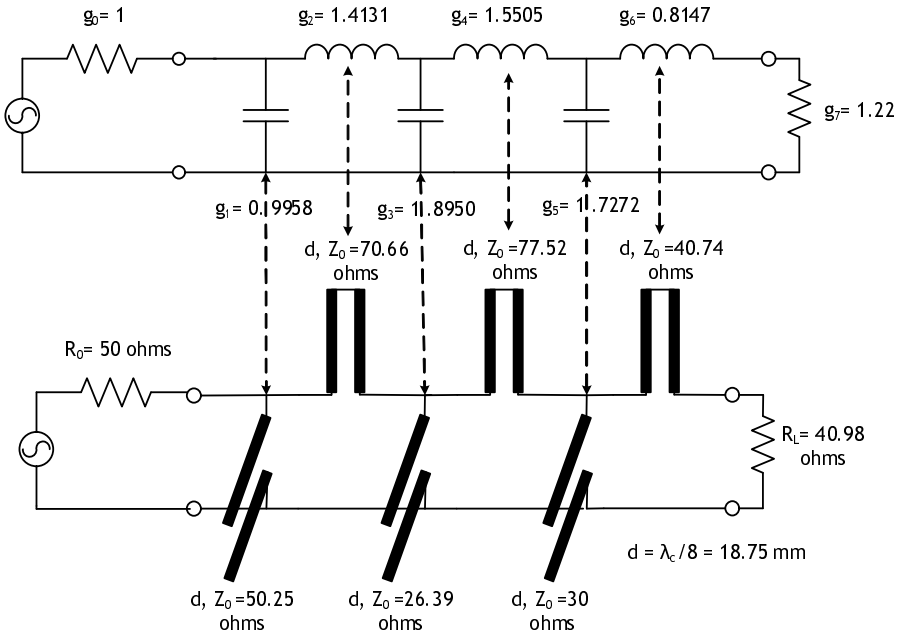


**Figure 4.6: Richards' circuital transformation for a sixth-order Chebychev lowpass filter (fc=2GHz, RL=20 dB, R0=50 ohms)**

Finally, it must be mentioned that Kuroda identities, which are detailed in [5], can be used to transform the distributed network into an equivalent one with only series or shunt transmission lines (also called stubs in this configuration). This transformation sometimes is needed since transmission lines is (and again is here remarked) a circuital approach. This means that, when choosing a specific means of transmission to materialise the physical circuit, sometimes it is not possible to realize it (e.g. a microstrip means of transmission can not synthesise series stubs).

**The stepped impedance filter**

Another useful approach for radio-frequency filters is the stepped impedance design. Firstly it is recalled the ABCD matrix of a transmission line seen as a quadripole (see figure 4.7):

$$ABCD_{trans.line} = \begin{bmatrix} \cos(\theta) & jZ_0 \sin(\theta) \\ jY_0 \sin(\theta) & \cos(\theta) \end{bmatrix} \tag{4.11}$$

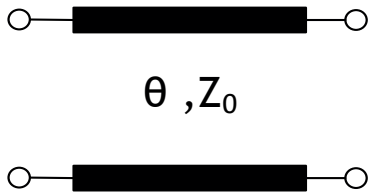


**Figure 4.7: Transmission line as a quadripole**

If $\theta << 1$, then $\cos(\theta) \approx 1$ and $\sin(\theta) \approx \theta$, and hence equation 4.11 becomes:

$$ABCD_{trans.line}\Big|_{\theta<<1} \approx \begin{bmatrix} 1 & jZ_0\theta \\ jY_0\theta & 1 \end{bmatrix} \tag{4.12}$$

Now two cases are considered:

(a) The electrical length of the transmission line remains short (i.e. $\theta << 1$), and its characteristic impedance is selected with a very high value (i.e. $Z_0 \uparrow\uparrow$). Then, equation 4.12 can be computed as:

$$ABCD_{trans.line}\Big|_{\theta<<1,\, Z_0\uparrow\uparrow} \approx \begin{bmatrix} 1 & jZ_0 \\ 0 & 1 \end{bmatrix} \tag{4.13}$$

(b) The electrical length of the transmission line remains short (i.e. $\theta << 1$), but in this case its characteristic impedance is selected with a very low value (i.e. $Z_0 \downarrow\downarrow$). Then, 4.12 can be written as:

$$ABCD_{trans.line}\Big|_{\theta<<1,\, Z_0\downarrow\downarrow} \approx \begin{bmatrix} 1 & 0 \\ jY_0 & 1 \end{bmatrix} \tag{4.14}$$

Looking carefully at the two preceding matrices ( 4.13 and 4.14 ), and comparing them with the transmission matrix of a series impedance and of a shunt admittance respectively, it can be seen that a short transmission line with high characteristic impedance can be used to replace a series inductor, and a short transmission line with low characteristic impedance can be used to

replace a shunt capacitor respectively:

$$(a) \qquad \begin{bmatrix} 1 & jZ_0\theta \\ 0 & 1 \end{bmatrix} = \begin{bmatrix} 1 & j\omega L \\ 0 & 1 \end{bmatrix} \longleftrightarrow Z_0\theta = \omega L$$
$$(b) \qquad \begin{bmatrix} 1 & 0 \\ jY_0\theta & 1 \end{bmatrix} = \begin{bmatrix} 1 & 0 \\ j\omega C & 1 \end{bmatrix} \longleftrightarrow Y_0\theta = \omega C \tag{4.15}$$

Finally it is worth to remark two major differences regarding Richards' transformation:

⇒ This method is specifically designed for lowpass filters. Richards' transformation allows to replace inductors and capacitors individually, and no matter if they are placed at shunt or series branches. Its performance in other types of filters (i.e. high-pass/bandpass/bandstop) limits its use to lowpass filters, but conceptually there is not restriction to use it in those designs. However, the stepped impedance method only find approaches for series inductors and shunt capacitors, and hence can only form a lowpass topology.

⇒ Unlike Richards' transformation, the stepped impedance method is not focused at a single frequency (review equations 4.15.a. and b.)

Subsection 4.2.3 provides a complete (i.e. circuital and full-wave) design of a lowpass filter using this approach.

### 4.2.3 Lowpass applied filter design

This subsection focuses on the stepped impedance filter. Although subsection 4.2.2 explains how a transmission line of certain length and characteristic impedance can behave as a reactance (inductor or capacitor depending on the latter feature), the design formulas have not been given yet. Therefore, the first step is to deduce two expressions from equations 4.15a. and b. Since usually fabrication in a particular technology imposes stronger restrictions on transversal dimensions rather than on length, it is decided to obtain the lengths of the transmission lines given the selected characteristic impedances, and not the other way around.

Hence, the length of a transmission line that behaves as an inductor can be derived as:

$$\theta = \frac{\omega L}{Z_{high}} \qquad \longleftrightarrow \qquad \beta_g d_L = \frac{\omega L}{Z_{high}} \qquad \overset{L=\frac{g_L R_0}{\omega_c}}{\longleftrightarrow} \qquad d_L = \frac{\lambda_g}{2\pi} \cdot \frac{f}{f_c} \cdot \frac{g_L R_0}{Z_{high}} \qquad \longleftrightarrow$$

$$d_L = \frac{1}{2\pi f\sqrt{\mu\epsilon}} \cdot \frac{f}{f_c} \cdot \frac{g_L R_0}{Z_{high}} = \frac{g_L}{2\pi} \cdot \frac{R_0}{Z_{high}} \cdot \frac{1}{f_c\sqrt{\mu\epsilon}} \tag{4.16}$$

On the other hand, if the transmission line is required to behave as a capacitor:

$$\theta = \frac{\omega C}{Y_{high}} = \omega C Z_{low} \quad \longleftrightarrow \quad \beta_g d_C = \omega C Z_{low} \quad \overset{C=\frac{g_C}{R_0\omega_c}}{\longleftrightarrow} \quad = d_C = \frac{\lambda_g}{2\pi} \cdot \frac{f}{f_c} \cdot \frac{g_C Z_{low}}{R_0} \longleftrightarrow$$

$$d_C = \frac{1}{2\pi f\sqrt{\mu\epsilon}} \cdot \frac{f}{f_c} \cdot \frac{g_C Z_{low}}{R_0} = \frac{g_C}{2\pi} \cdot \frac{Z_{low}}{R_0} \cdot \frac{1}{f_c\sqrt{\mu\epsilon}} \tag{4.17}$$

With the two preceding equations the designer can begin to work. In this subsection the response of a fifth-order Chebychev lumped element filter with 15 dB of return loss, cut-off frequency of 2 GHz and $R_0 = 50$ ohms is used to set the desired power mask (see figure 4.8).

Firstly it is used MATLAB in order to study the theoretical behaviour of a stepped impedance filter depending on the selected characteristic impedances. Figure 4.9.a. shows that if extremely high and low impedances are chosen, the filter behaves as the lumped filter, as expected. However, this choice is not advisable because:

⇒ If the selected characteristic impedance is very high, losses in the real design will greatly increase.

⇒ If it is very low, higher order modes start being a problem.

Figure 4.9.b. depicts how the filter response gradually improves as the characteristic impedances $Z_{high}$ and $Z_{low}$ are more differentiated.

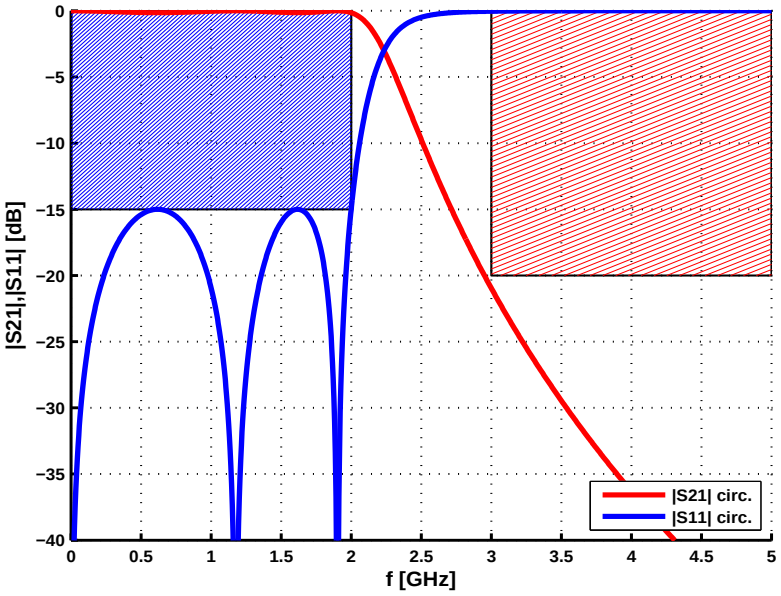


**Figure 4.8: Fifth-order Chebychev lumped lowpass filter (fc=2GHz, RL=15 dB, R0=50 ohms) and its corresponding power mask**

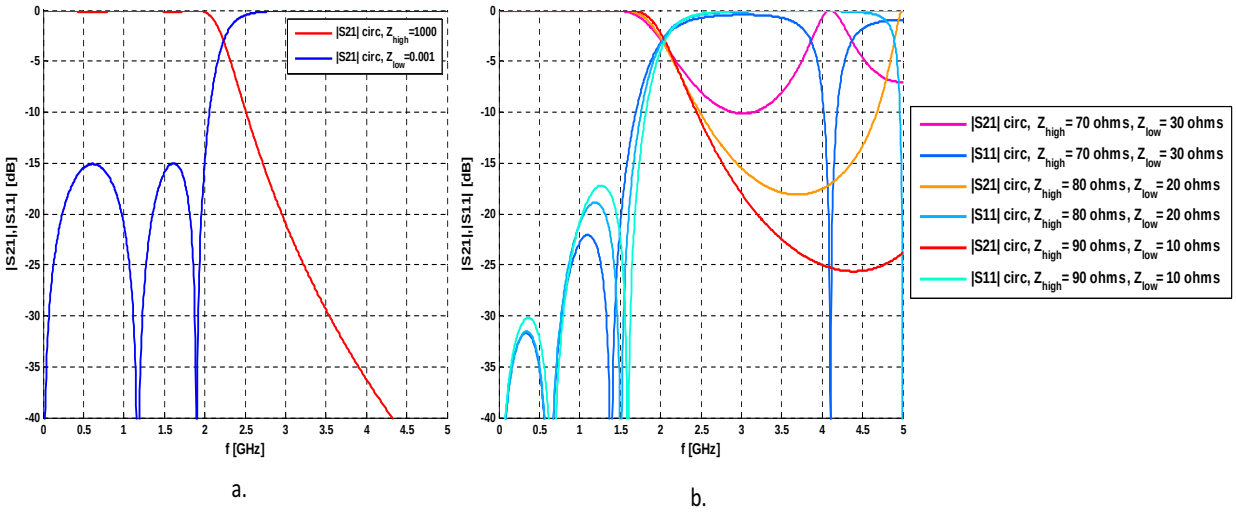


**Figure 4.9: Fifth-order Chebychev stepped impedance filters (fc=2GHz,RL= 15 dB, R0=50 ohms).a.Extreme impedance values b.Moderate values**

Reference [2] advises to select $Z_{low} < R_0 < Z_{high}$, and for that reason it is chosen $Z_{high} = 100$ ohms and $Z_{low} = 10$ ohms as a starting point (recall $R0 = 50$ ohms).The corresponding lengths (calculated using equations 4.16 and 4.17) for that choice are gathered in table 4.1.

| $d_{L1}[mm]$ | $d_{C2}[mm]$ | $d_{L3}[mm]$ | $d_{C4}[mm]$ | $d_{L5}[mm]$ |
|---|---|---|---|---|
| 14.7 | 6.5 | 24.6 | 6.5 | 14.7 |

**Table 4.1: Design table of the fifth-order Chebychev stepped impedance filter (fc=2GHz,RL= 15 dB, R0=50 ohms)**

However, none of the attempts which kept the values of $Z_{high}$ and $Z_{low}$ close enough to those initial values succeeded in satisfying the specifications.Since plotting one figure each time impedance is changed is clearly unpractical, it is created a visual interface based on MATLAB GUI (see figure 4.10). It is important to notice that at this point five additional sliders depicting the lengths of the filter sections have been added. The reason is quite simple: although equations 4.16 and 4.17 show that the lengths are computed using the selected impedances, in fact the designer can treat them as independent variables if it is required. Indeed, the designer can directly use equation 4.11 to design. In other words, if the transmitted and the reflected power do not meet the requirements changing the characteristic impedances (as it was the case), it is preferable to pursue the desired response selecting the impedances and the lengths separately rather than directly increase the filter order. Furthermore, the filter does not need to keep symmetry and in this case it is decided to use sections with no restrictions on them.

Before going on, it is worth to highlight that there are some drawbacks that make advisable to begin with equations 4.16 and 4.17 and not with equation 4.11, although the filter designer gains more degrees of freedom using 4.11. On the one hand, more degrees of freedom imply to increase the complexity of the problem, and on the other hand, there is one parameter that the designer will not be able to use for its own benefit: the cutoff frequency.

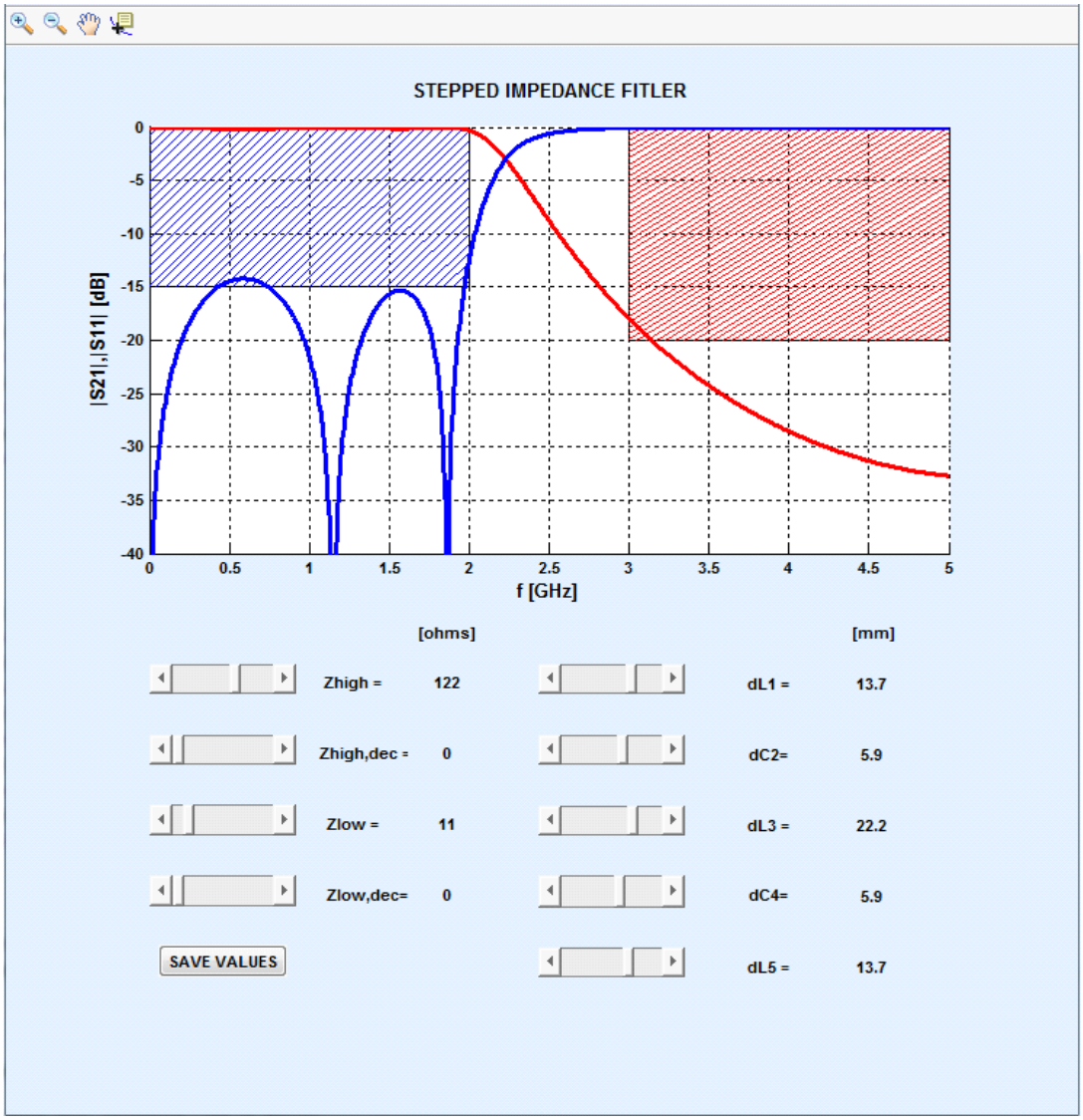


**Figure 4.10: MATLAB design window for a fifth-order Chebychev stepped impedance filter (example values).RL=15 dB, R0=50 ohms.**

After several attempts none combination of impedances and lengths succeeds. Before increasing the filter order, it is decided to use circuital optimization via MATLAB for the first time in the hereto work. Optimization is the process of minimizing a given scalar objective function (i.e. the cost function), which depends on the design parameters. This function is chosen so that a wrong selection of the variables (i.e. the design parameters) would give a strong growth of the cost function.

In the stepped impedance filter, the variables are the same design parameters as the ones considered in the graphic interface (i.e. the two characteristic impedances and the five section lengths). Regarding the cost function, it is used the well-known least square objective function, applied to the mask sections set in figure 4.8 (see equation 4.18).

$$y(Z_{high}, Z_{low}, d_{L_1}, d_{C_2}, d_{L_3}, d_{C_4}, d_{L_5}) = r + t \qquad \text{where}$$

$$r \begin{cases} (|S_{11}(f)| - 10^{\frac{-15}{20}})^2 & 0 \leq f \leq 2 \text{ GHz and } |S_{11}(f)| > -15\,dB \\ 0 & rest \end{cases} \tag{4.18}$$

$$t \begin{cases} (|S_{21}(f)| - 10^{\frac{-20}{20}})^2 & 3 \leq f \leq 5 \text{ GHz and } |S_{21}(f)| > -20\,dB \\ 0 & rest \end{cases}$$

In the preceding definition of the cost function it can be seen that a negative evaluation value indicates that the corresponding specification is satisfied (i.e. adds zero to the cost function), whereas a positive value means that there is an error that needs to be corrected (i.e. error since the squared difference is added to the cost function and the optimization process pursues minimization). Once the optimization process is carried out (using the *fminsearch* algorithm of MATLAB), the following design parameters are obtained:

| $Z_{high}[ohms]$ | $Z_{low}[ohms]$ | $d_{L1}[mm]$ | $d_{C2}[mm]$ | $d_{L3}[mm]$ | $d_{C4}[mm]$ | $d_{L5}[mm]$ |
|---|---|---|---|---|---|---|
| 221.50 | 5.40 | 6.9 | 3.3 | 11.3 | 3.4 | 6.7 |

**Table 4.2: Optimized values for stepped impedance Chebychev filter (N=5 RL=15 dB)**

Although the filter response now fits the power mask (see figure 4.11a.), the impedance values found are considered too high and low respectively, as values near 10 and 100 ohms were pursued. At this point it is decided to increase the filter order. Since the optimization software routine is already written, it is directly used in this case (rather than use again a graphic interface). The obtained response is shown in figure 4.11.b., and the design variables are gathered in table 4.3.

| $Z_{high}[ohms]$ | $Z_{low}[ohms]$ | $d_{L1}[mm]$ | $d_{C2}[mm]$ | $d_{L3}[mm]$ | $d_{C4}[mm]$ | $d_{L5}[mm]$ | $d_{C6}[mm]$ |
|---|---|---|---|---|---|---|---|
| 99.70 | 10.53 | 13.1 | 6.2 | 23.5 | 6.6 | 23.4 | 4 |

**Table 4.3: Optimized values for stepped impedance Chebychev filter (N=6, RL=15 dB, R1=50 ohms R2=71.6 ohms)**

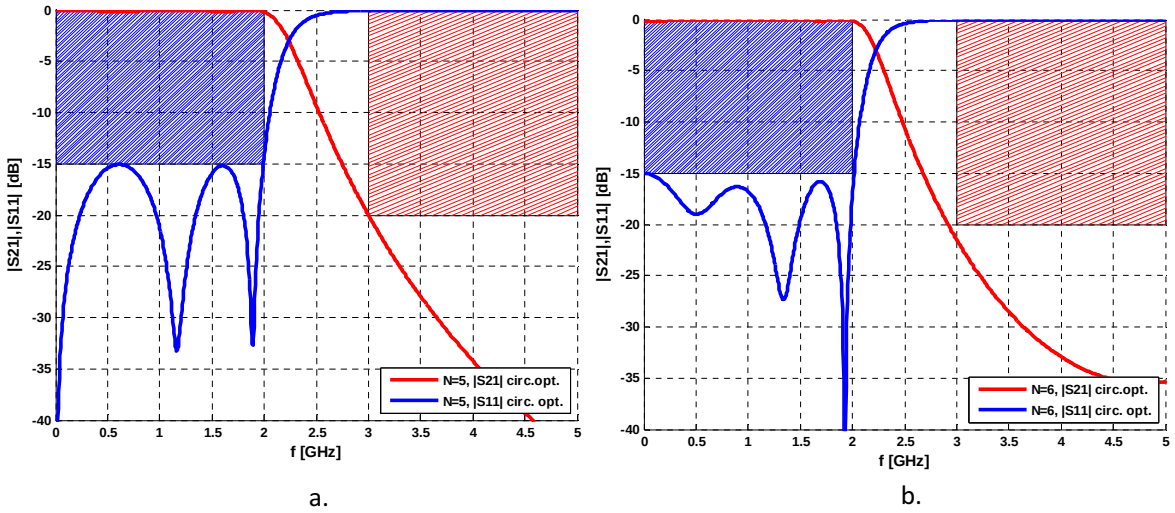


**Figure 4.11: Two circuital optimized Chebychev stepped impedance filters (RL=15 dB, R0=50 ohms). a. N=5 b.N=6**

In this case the characteristic impedances are close enough to 100 and 10 ohms respectively, and for that reason this design is considered valid. However, as the design parameters are purely circuital, the final filter realization is not attained yet. The specific technology selected for this sort of filter is coaxial, with air as dielectric (i.e.$\epsilon_r = 1$). Obviously air makes the filter unrealizable, as the inner conductors are air-suspended. However, this design is acceptable for academic purposes. The use of another dielectric would only involve to multiply the physical dimensions by a constant factor known in advance. This issue is explained in the last example of subsection 5.2.1.

Lengths of table 4.3 can be directly used as physical parameters, since the coaxial acts as a transmission line. Concerning the characteristic impedances, using equation 4.19 they are directly translated into a physical transversal size (being b and a the outer and inner radius respectively) [5].

$$Z_0^{coaxial} = \frac{60}{\sqrt{\epsilon_r}} \cdot ln\left(\frac{b}{a}\right) \tag{4.19}$$

Since equation 4.19 provides a radius relationship, there seem to be infinite solutions for this problem. In fact there are, but apart from the earlier mentioned considerations about power handling and higher order modes, there is another slight nuance: the radius selection of the narrow and wide sections must not block power transmission (see figure 4.12). To that end, it is decided to maintain the same outer radius(b=10mm) and only vary the inner one.

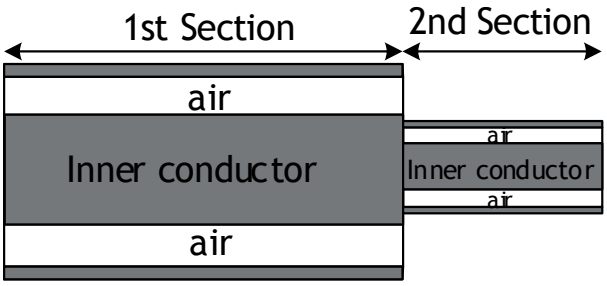


**Figure 4.12: Short-circuit due to a wrong radius selection**

It is important to remark as well that, due to the even order of the Chebychev filter, the required filter end load value is 71.6 ohms in spite of 50 ohms (as $g_7 = 1.4326$ and not 1). Hence, an additional transformer would need to be included in a real design in order to fully satisfy the specifications.The appearance together with the physical dimensions of the filter are shown in figure 4.13 Now and hereinafter the outer conductor is not depicted. Here the inner conductor is highlighted with diagonal lines. The rest of the structure depicts the air.

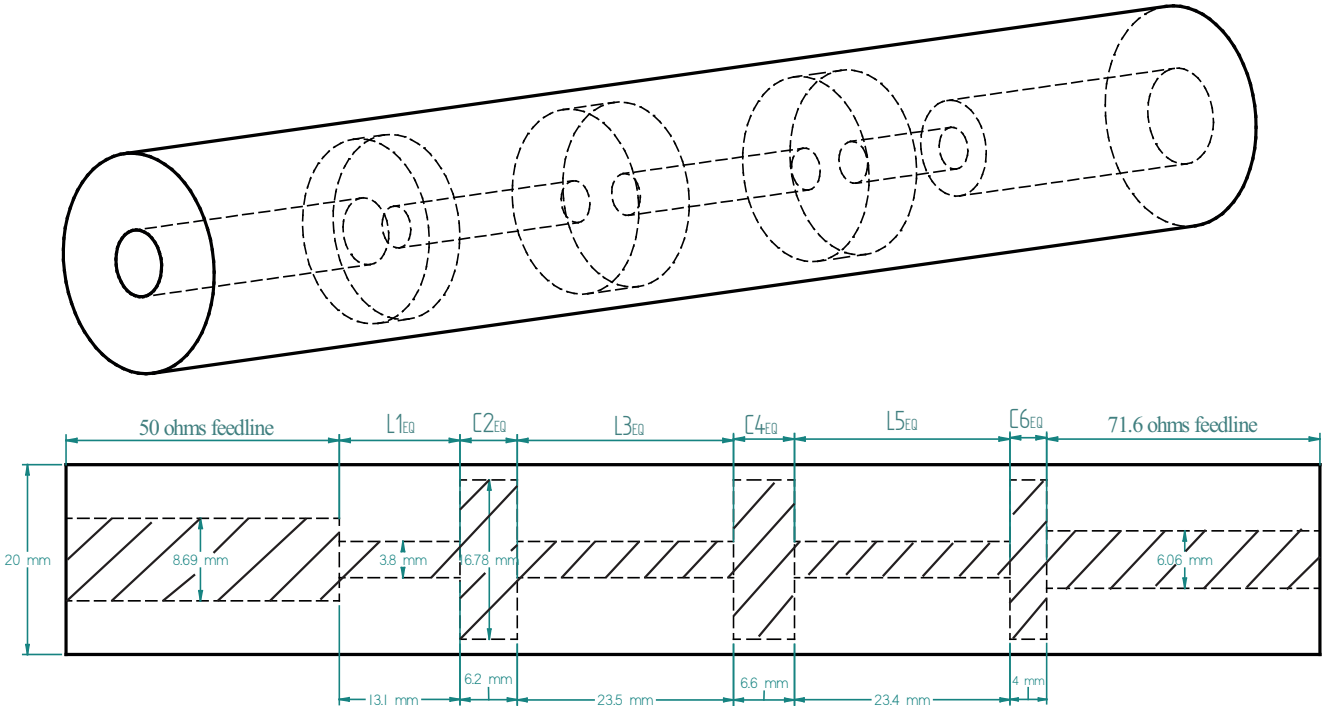


**Figure 4.13: Structure of the initial stepped impedance Chebychev filter (N=6, RL=15, R1=50 ohms R2=71.6)**

The full-wave response obtained with CST Microwave Studio is depicted in figure 4.14. Figure 4.15 overlaps the desired power mask with the full-wave response. Since it obviously violates the specifications, the physical dimensions need to be optimized in the full-wave simulator.

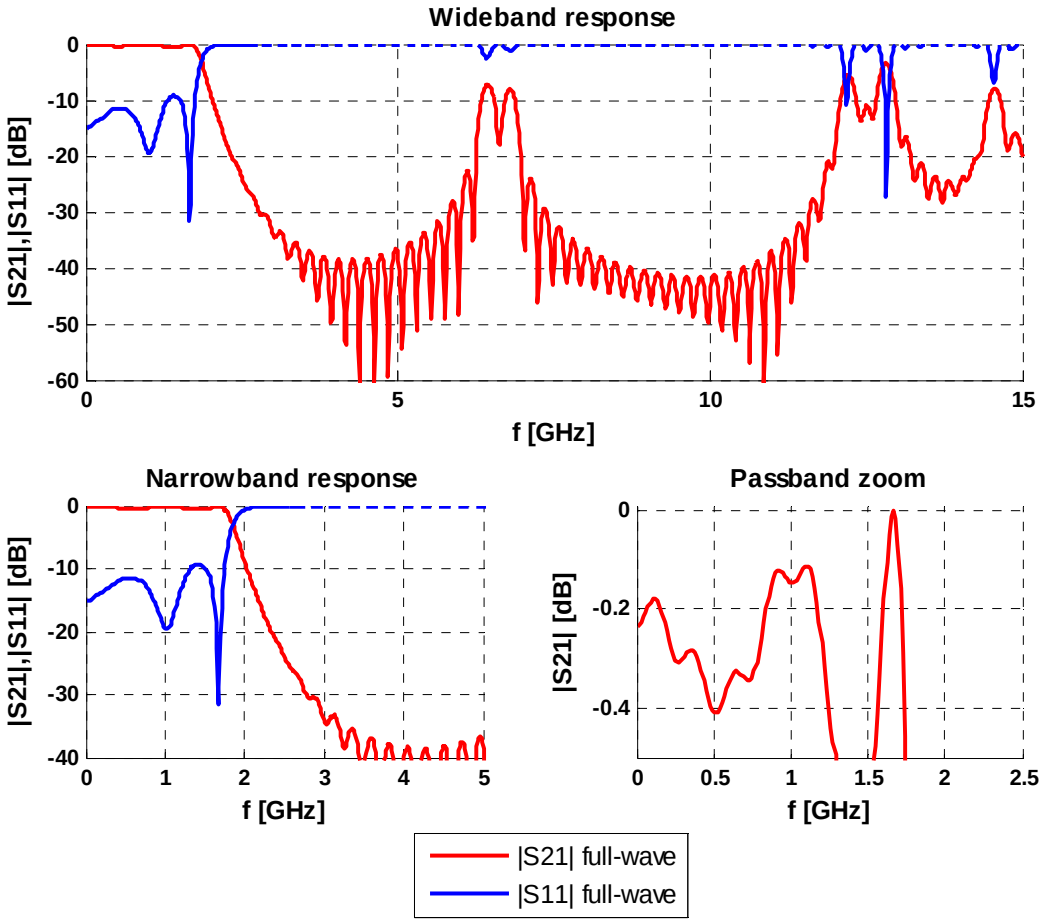


**Figure 4.14: Full-wave response of the initial stepped impedance Chebychev filter (N=6, RL=15 dB, R1=50 ohms, R2=71.6 ohms)**

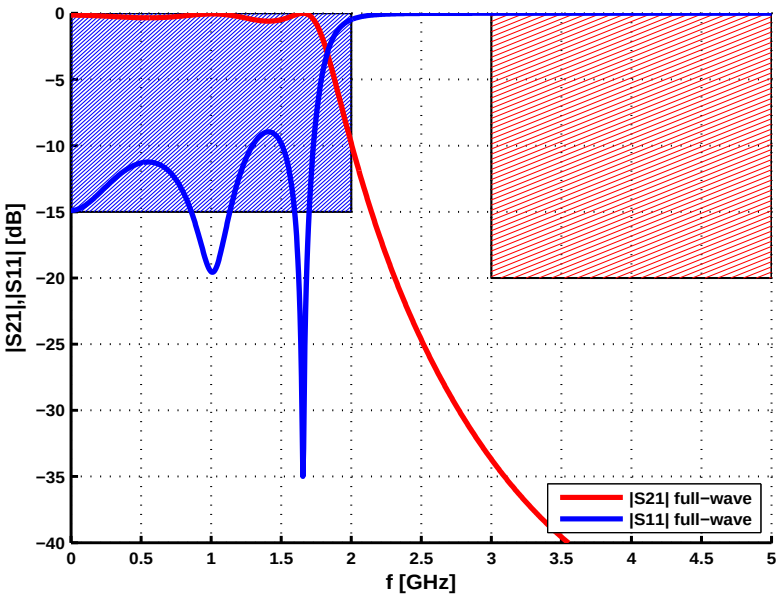


**Figure 4.15: Full-wave response of the initial stepped impedance Chebychev filter (N=6, RL=15 dB, R1=50 ohms, R2=71.6 ohms) and the objective mask**

The algorithm selected in CST MWS to carry out the optimization process is the one called "Trust Region Framework". It is defined exactly the same mask as the one violated in figure 4.15 (which was obviously the mask set in figure 4.8). The physical dimensions obtained are shown in figure 4.16. Using equation 4.19 it can be seen that the achieved radius provide values of 99.64 ohms ($Z_{high}$) and 10.53 ohms ($Z_{low}$).

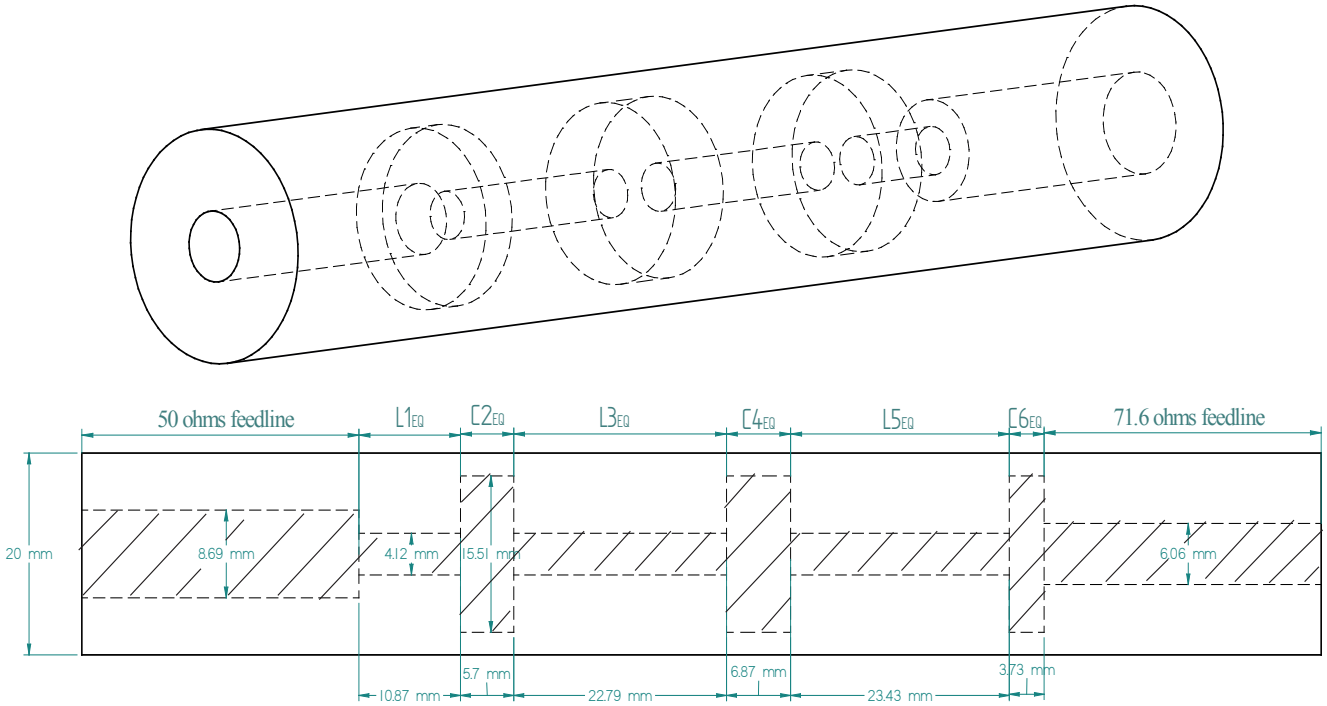


**Figure 4.16: Structure of the optimized stepped impedance Chebychev filter (N=6, RL=15 dB, R1=50 ohms, R2=71.6 ohms)**

With respect to the full-wave response of the final filter, it is depicted in figure 4.17. Finally figure 4.18 overlaps the optimized response with the desired power mask, which is in this case satisfied as it was expected.

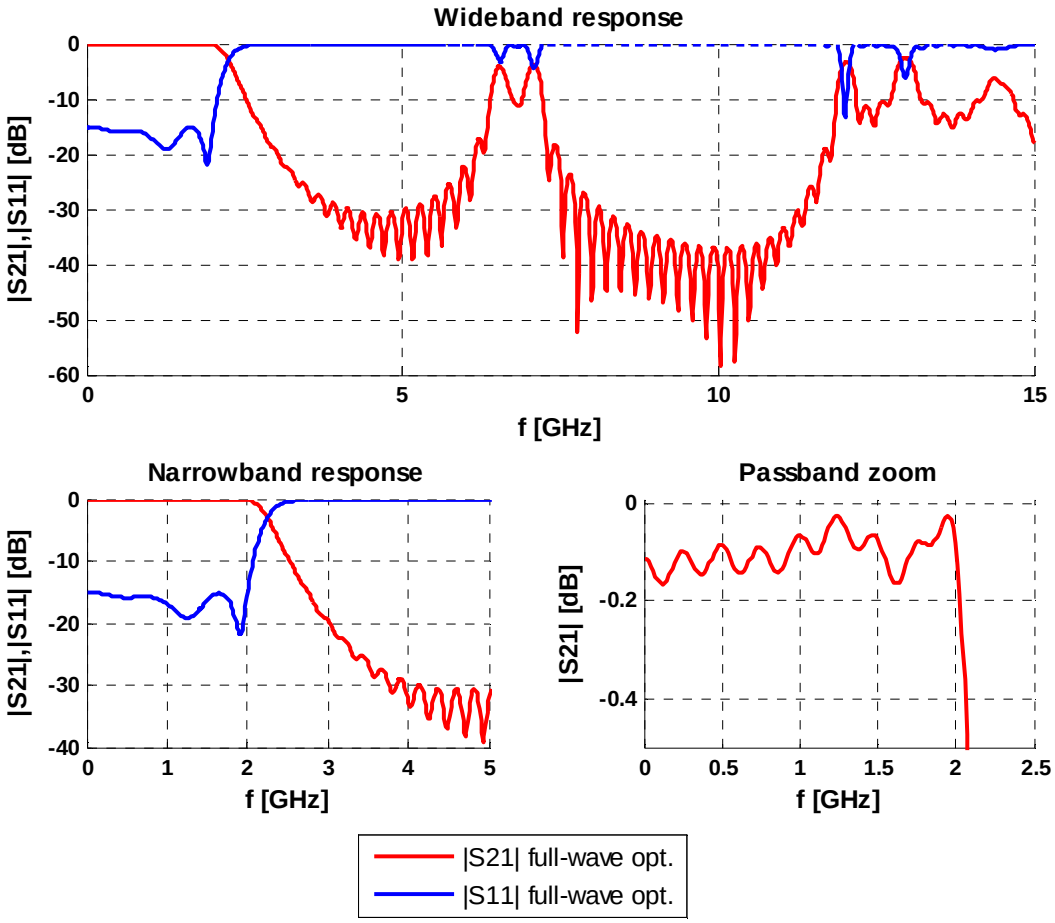


**Figure 4.17: Full-wave response of the optimized stepped impedance Chebychev filter (N=6, RL=15dB, R1=50 ohms, R2=71.6 ohms)**

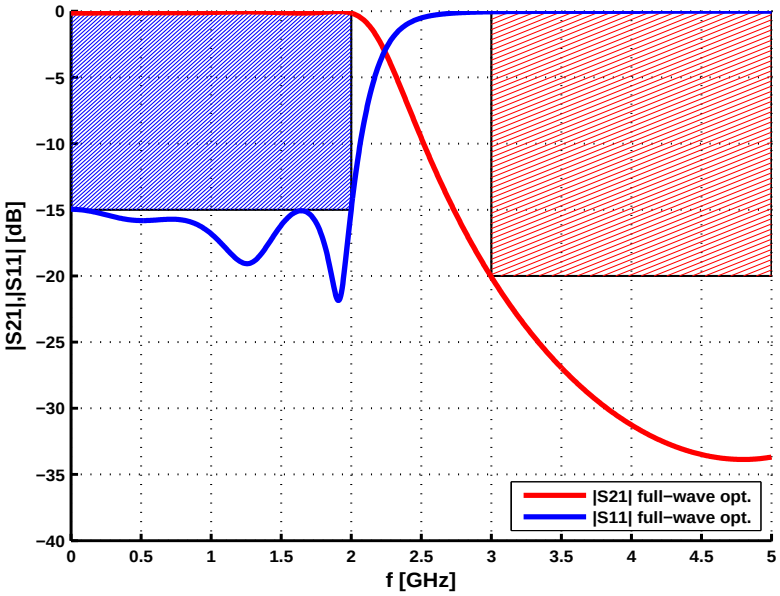


**Figure 4.18: Full-wave response of the optimized stepped impedance Chebychev filter (N=6, RL=15 dB, R1=50 ohms, R2=71.6 ohms) and the objective mask**

# 5

# Physical Filter Realization II

Lowpass filter realization was treated in chapter 4. However, lowpass filters are not the most popular filters at microwave frequencies. Since microwave frequencies cover the range between 300 MHz and 300 GHz, bandpass filters are the ones widely used. This chapter is focused on this kind of filters.

The second section addresses microwave bandpass filter design. A useful approach to such kind of filters is presented, and three design examples are developed. The full-wave responses are obtained using again the commercial CAD tool CST Microwave Studio. In two out of the three designs a further step of optimization is carried out in order to improve their initial response.

## 5.1 Low-frequency filter design for bandpass networks

The previous chapter introduced the network theory related to lowpass filters based on lumped elements. In order attain the corresponding bandpass networks, some transformations must be carried out: not only to obtain the desired response over a new range of frequencies, but also to achieve certain topologies which can be realized at microwave frequencies. Such transformations are presented in this section.

### 5.1.1 Frequency scaling

Impedance scaling was treated in subsection 4.1.3. However, whether the values obtained from the polynomial responses (the aforementioned $g_i$, with $i = 0...n+1$, being n the filter order) are scaled to allow another loading value, or not, the designer comes across with a normalized low-pass response - i.e. with $\omega$=1 rad/s as the cutoff frequency. In order to overcome such limitation, frequency scaling is presented.

Chapter 2 presented the transmission function, among others, as a function to describe the desired frequency response in a lossless two-port filter. It was also mentioned that many books use the concept of power loss ratio instead ($P_{LR} = \frac{1}{|S_{21}(\omega)|^2} = |H(\omega)|^2$). Such power loss ratio can be written as a function which depends on the impedances of each lumped element of the network:

$$P_{LR}(\omega) = f_{circ}(Z_1(\omega), Z_2(\omega), ...) \tag{5.1}$$

Then, it is defined the next frequency transformation:

$$\omega = f(\omega^{'}) \qquad \longleftrightarrow \qquad \omega^{'} = f^{-1}(\omega) \tag{5.2}$$

If the new impedance (admittance) function can be expressed as $Z_i^{'}(\omega^{'}) = Z_i(f(\omega^{'}))$ , then the frequency response of the new network will be the same as in the original network but transformed in frequency:

$$P_{LR}^{'}(\omega^{'}) = f_{circ}(Z_1^{'}(\omega^{'}), Z_2^{'}(\omega^{'}), ...) = f_{circ}(Z_1(f(\omega')), Z_2(f(\omega')), ...) = P_{LR}(f(\omega^{'})) = P_{LR}(\omega) \tag{5.3}$$

In the preceding expressions, the original network expressed in terms of variable $\omega$, depicts a normalized low-pass filter. Variable $\omega^{'}$ can be used to define a high-pass, bandpass or a bandstop response. Figure 5.1.1 attempts to show intuitively how any frequency transformation moves the power insertion loss function along the frequency axis without distorting its shape.

In [6] it can be found the pole movement after a bandpass frequency transformation is carried out . However, it must be remarked that at this step it is not necessary to find out if their new locations contravene certain properties: practical realizability is guaranteed since inductor/capacitor immittances are directly obtained. Appendix D proofs what kind of lumped elements must replace the lowpass normalized lumped elements in order to obtain the desired lowpass/highpass/bandpass/bandstop response.

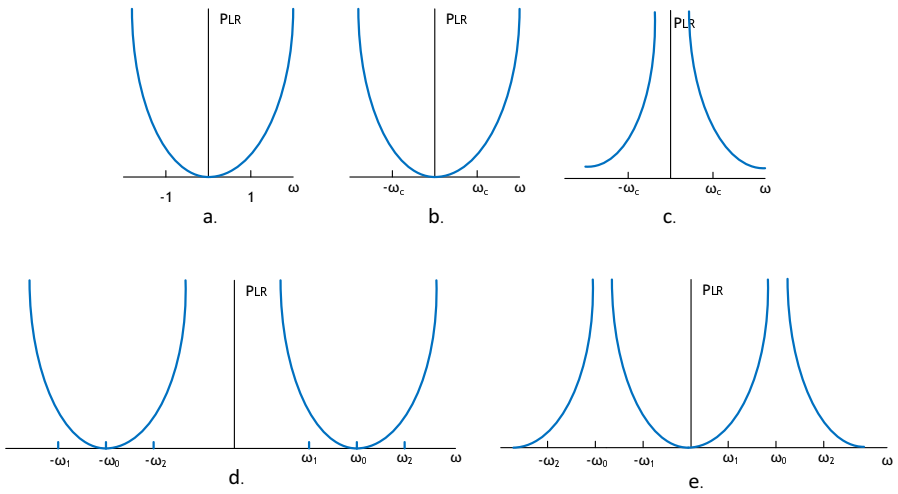


**Figure 5.1: Power loss ratio a.Normalized lowpass filter. b.Lowpass filter. c.Highpass filter. d.Bandpass filter. e.Bandstop filter**

Figure 5.2 summarizes the obtained results in appendix D, and includes impedance scaling in the derived formulas.

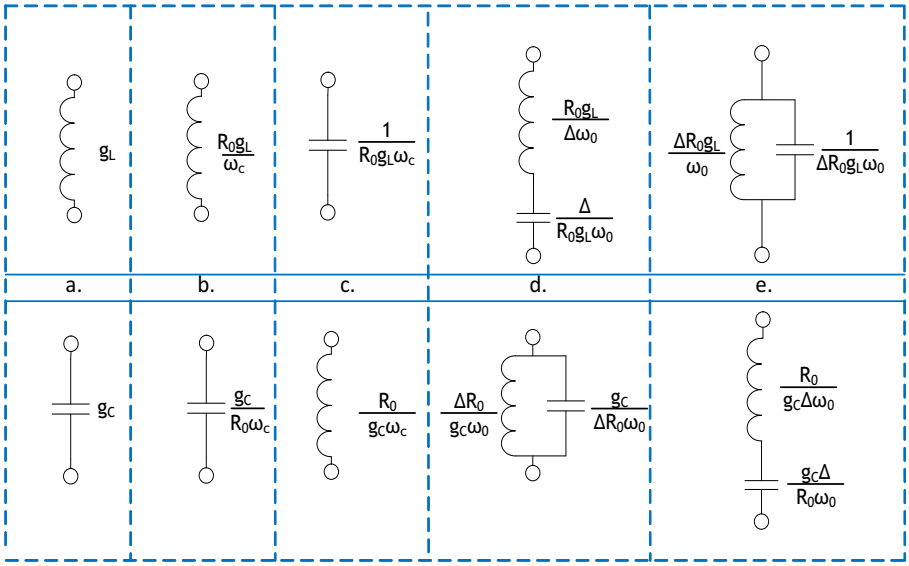


**Figure 5.2: Design table for impedance and frequency scaling. a.Normalized values. b. Lowpass. c.Highpass. d.Bandpass. e.Bandstop.**

### 5.1.2 Immittance inverters

The concept of inverter is not related to a particular circuit, but to a specific function: it inverts the immittance of an arbitrary load (see figure 5.3). Furthermore, if it is an ideal inverter this behaviour is maintained at all frequencies.

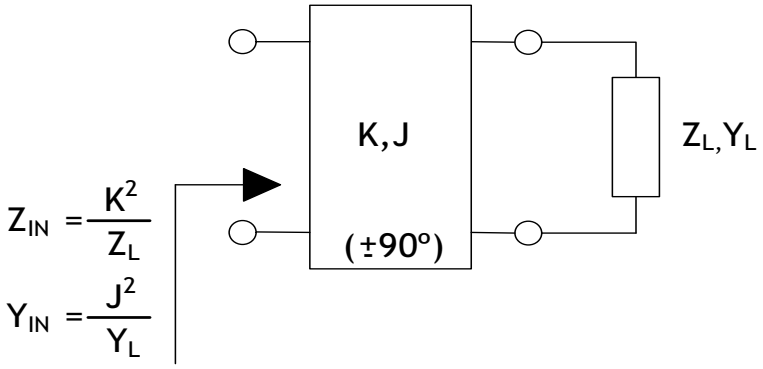


**Figure 5.3: Immitance inverter**

The essential role that the inverter model plays in microwave filter design will be evidenced in subsection 5.2.1. This lumped inverter model attains an homogeneous network where all the lumped elements are located in series (or in shunt) branches.

Figure 5.4 shows the values that are needed to transform a given lumped bandpass network into

an equivalent inverter model where the lumped elements and the two loads can be chosen by the filter designer.The key to reach such topology with such degrees of freedom is to transform partial blocks of the circuit, guaranteeing that the ABCD matrix that corresponds to the transformed partial block acquires the same values as the original one. Only the last step uses the concept of seen impedances. Other references like [7], do not use ABCD matrices but seen impedances from the beginning.

One of the objectives of this work was to be able of deducing the formulas shown in figure 5.4. Towards that end, appendix E details the procedure by means of a third-order filter example. It is not included in the herein subsection since the chapter becomes less readable.

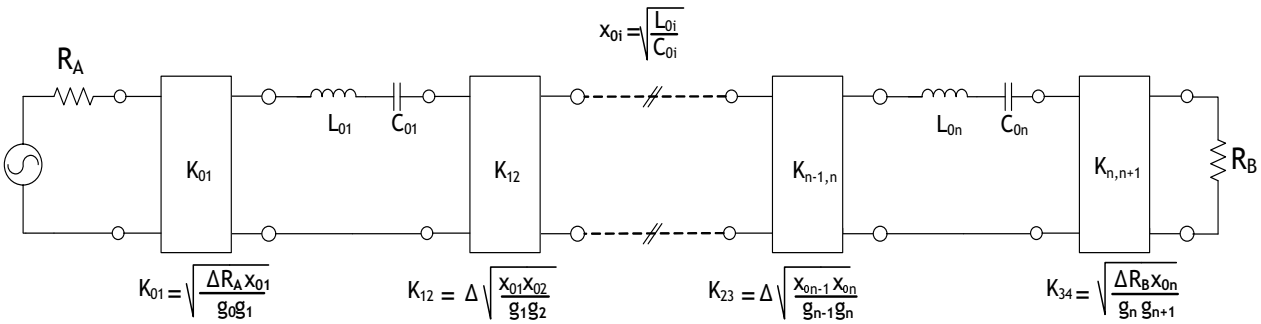


**Figure 5.4: Bandpass inverter ladder network**

The underlying concept of the mentioned procedure is equivalency. Two M-port networks (for M>1) are said to be equivalent when their corresponding matrices are equal. Unlike duality (seen in section), equivalence is not set in terms of a specific kind of matrix (e.g. in terms of the impedance matrix) since the equivalence in one type of matrix (whatever it is, e.g. the impedance matrix) implies the equivalence in the other types of matrices (admittance matrix, transmission matrix, and so on).

### 5.1.3 Multicoupled networks

Bandpass ladder networks with the same topology as in figure 5.4 can be used when all the transmission zeros of the polynomial lowpass response are set at infinity (and therefore are called all-pole networks as well). Finite transmission zeros can also be found in ladder networks, but they are achieved by means of the zero shifting technique (also known as pole weakening). Further information can be found in [8], under the name of mid-shunt and mid-series elements (see figure 5.5). In the hereto work this method is not developed as those topologies are not feasible with the type of structures used at microwave frequencies.

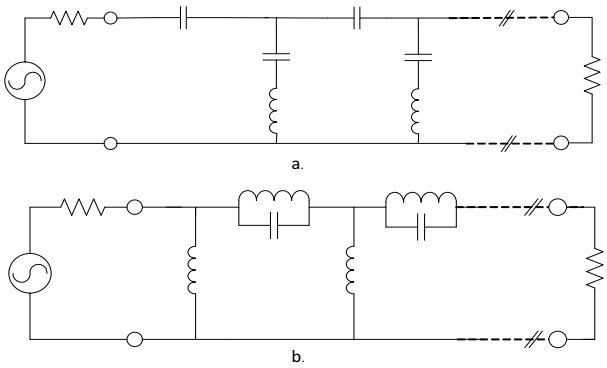


**Figure 5.5: a.Mid-shunt network example b.Mid-series network example**

Nevertheless, the multicoupled networks introduced in section 3.3.2 lead to structures that are extensively used at microwave frequencies.They are a generalization of the ladder inverter networks seen in subsection 5.1.2, since any loop can be connected to any other. This kind of structure allows to synthesize finite transmission zeros studied in chapter 2. Figure 5.6 depicts a multicoupled network that does not take into account the source and load interactions. Such kind of structure can be synthesized from an NxN coupling matrix (seen in chapter 3). If the source and load interactions need to be considered, then the Nx2 coupling matrix must be used instead and two additional loops (one at the beginning and another one at the end) are included.

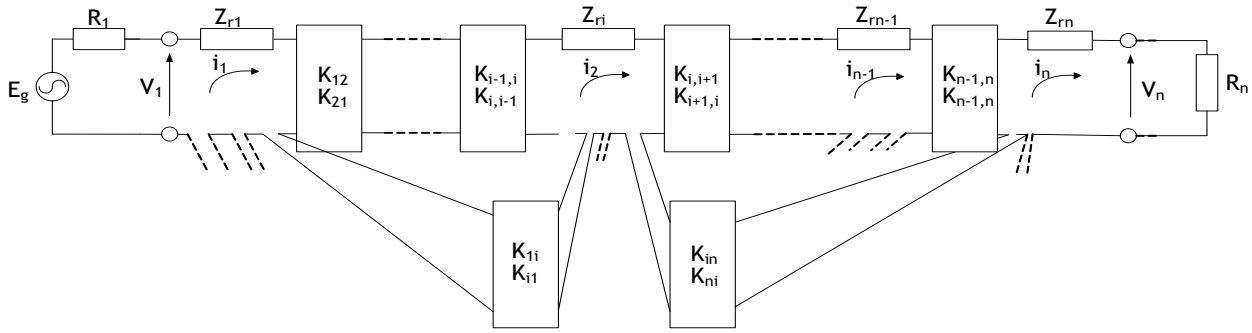


**Figure 5.6: Multicoupled network**

It is now time to introduce for the first time the meaning of the structure of such coupling matrix, at least from the circuital point of view. The complete understanding will be achieved in chapter 6 where it will be explained from the fields side. Using the transmission matrix associated with an inverter (see subsection 5.1.2), the following equation can be written:

$$v_a = (-jK)i_b, \tag{5.4}$$

where $K > 0$ for $+90°$ and $K < 0$ for $-90°$, $v_a$ depicts the voltage of one of the quadripole ports, and $i_b$ the current of the remaining port defined towards the inverter. By means of equation

5.4 the multicoupled network of figure 5.6 can be described with the following equations, where it is assumed that all the loop currents are defined clockwise:

$$\begin{aligned}
&\text{When k=1 : } = z_{rk}i_k + \sum_{p=k+1}^{n}\Big[(-jK_{kp})\cdot(-i_p)\Big] = v_1 \\
&\text{With k=2...n-1 : } \sum_{p=1}^{k-1}\Big[-(-jK_{kp})i_p\Big] + z_{rk}i_k + \sum_{p=k+1}^{n}\Big[(-jK_{kp})\cdot(-i_p)\Big] = 0 \\
&\text{When k=n : } = \sum_{p=1}^{k-1}\Big[-(-jK_{kp})i_p\Big] + z_{rk}i_k = -v_n
\end{aligned} \tag{5.5}$$

The preceding expressions give positive products, and therefore they can be written in the following simplified matricial form:

$$\begin{bmatrix} v_1 \\ 0 \\ .. \\ 0 \\ -v_n \end{bmatrix} = \begin{bmatrix} z_{r1} & jK_{12} & ... & jK_{1,n-1} & jK_{1,n} \\ jK_{21} & z_{r2} & ... & jK_{2,n-1} & jK_{2,n} \\ ... & ... & ... & ... & ... \\ jK_{n-1,1} & jK_{n-1,2} & ... & z_{rn-1} & jK_{n-1,n} \\ jK_{n,1} & jK_{n,2} & ... & jK_{n-1,n-1} & z_{rn} \end{bmatrix} \cdot \begin{bmatrix} i_1 \\ i_2 \\ ... \\ i_{n-1} \\ i_n \end{bmatrix} \tag{5.6}$$

Equation 5.6 is the same as the equation 3.31 seen in the previous chapter if $K_{ij} = M_{ij}$ and $z_{rk} = s + jM_{ii}$. On the one hand, $K_{ij} = M_{ij}$ can be directly equal, it is a matter of mathematical notation and origins: letter $M$ was used when Atia and Williams presented for the first time the concept of the coupling matrix in [9], whereas letter $K$ belongs to the mathematical development in terms of inverters. In both cases the elements of the matrix are called couplings in general, and in particular:

⇒ The coupling elements placed at the main diagonal of the matrix (i.e., the ones with equal subscripts, $M_{ii}(K_{ii})$), are named the self-couplings.

⇒ The coupling elements with consecutive subscripts are named main couplings. Any network built with only this kind of elements will have a ladder topology.

⇒ The rest of the couplings are known as cross couplings, and they appear when finite transmission zeros are needed.

On the other hand, when the coupling matrix seen in chapter 3 is directly synthesized from the polynomials of chapter 2, $z_{rk}$ depicts a unity inductor. In case the response is asymmetric, this inductor is in the series branch together with the FIR element (recall subsection 2.2.3). Therefore only self-couplings arise when the response is asymmetric. When a frequency transformation is carried out from the lowpass to a bandpass filter, $z_{rk}$ becomes a series resonator (review appendix D), and in case the frequency response is asymmetric, the FIR element is absorbed as a frequency offset associated to that particular resonator. It is important to underline that, since all the couplings are frequency-independent, the shape of the function in frequency that the coupling matrix shows at zero frequency is simply moved into the new bandpass frequency. This allows once again not to design different polynomials from the ones designed at lowpass frequencies when pursuing a bandpass frequency response.

### 5.1.4 Multicoupled networks and their practical realizability

So far section 5.1 has only treated lumped bandpass networks - i.e. the ones suitable only at low-frequencies. However, at microwave frequencies not all the topologies are practical. Indeed,the designer can apply the design equations of microwave filter theory and find the appropriate physical dimensions, but be incapable of materializing those dimensions in a physical structure.

Inline topologies do not involve, itself, problems of practical realizability. Inline is the technical word used for filters which only have main couplings (see subsection 5.1.3), and for that reason each resonator is surrounded only by the corresponding two adjacent ones. In other words, the inverter ladder network seen in subsection 5.1.2 is in fact an inline topology.

Conversely, only certain structures with cross-couplings are practical. In this context, several topologies have been studied in the theory of microwave filter design. One of them is the well-known folded form, shown in figure 5.7 (where circles depict resonators and the lines that connect them the couplings allowed).

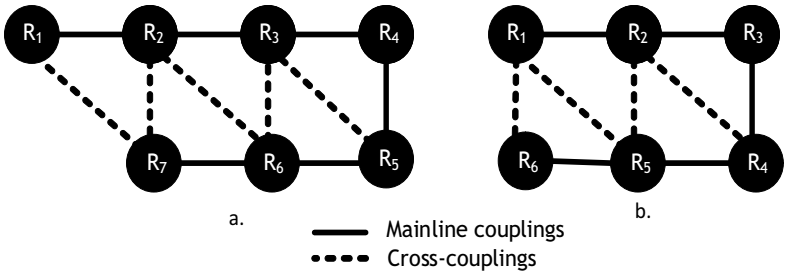


**Figure 5.7: Folded form**
**a.Odd example b.Even example**

In order to achieve the mentioned folded form, the coupling matrix obtained from the synthesis process needs to be transformed. The specific algorithm for coupling matrix reduction is detailed in [1], and therefore the whole explanation is not here repeated. However, the main ideas are in this work pointed out.

Coupling matrix reduction is based on the use of similarity transformations (i.e. matrix rotations),where it is involved a rotation matrix $\mathbf{R}$. The rotation of a coupling matrix $\mathbf{M_i}$ is carried out by doing the following operation:

$$\mathbf{M_{i+1}} = \mathbf{R_{i+1}} \cdot \mathbf{M_i} \cdot \mathbf{R_{i+1}^t} \tag{5.7}$$

As the eigenvalues of matrix $\mathbf{M_i}$ are preserved in $\mathbf{M_{i+1}}$, the same frequency response is guaranteed. The rotation matrix is formed by an identity matrix in which four of the elements are replaced by a trigonometric expression (i.e. $cos(\theta)$ or $\pm sin(\theta)$). The specific value of the angle (i.e. the rotation angle), and the location of such trigonometric expressions depends on the

specific step in the algorithm. Essentially the algorithm defines the proper locations and the values of the rotation angles that lead to the annihilation of the undesired coupling elements of the matrix.In the seventh-order filter of figure 5.7.a. an example of rotation matrix would be:

$$\mathbf{R} = \begin{bmatrix} 1 & 0 & 0 & 0 & 0 & 0 & 0 \\ 0 & 1 & 0 & 0 & 0 & 0 & 0 \\ 0 & 0 & cos(\theta) & -sin(\theta) & 0 & 0 & 0 \\ 0 & 0 & sin(\theta) & cos(\theta) & 0 & 0 & 0 \\ 0 & 0 & 0 & 0 & 1 & 0 & 0 \\ 0 & 0 & 0 & 0 & 0 & 1 & 0 \\ 0 & 0 & 0 & 0 & 0 & 0 & 1 \end{bmatrix} \tag{5.8}$$

And the associated rotation angle would be computed as:

$$\theta = -tan^{-1}\left(\frac{M_{k4}}{M_{k3}}\right) \quad \text{or} \quad \theta = tan^{-1}\left(\frac{M_{3k}}{M_{4k}}\right), \tag{5.9}$$

depending whether the coupling that is going to be annihilated takes part of one of the steps associated with rows (first expression) or columns (second expression).

At this point, it is shown the topology that it is associated with the four examples of chapter 2 immediately after the synthesis process of the coupling matrix synthesis carried out in chapter 3. The first example had the transmission zeros located in $\pm 1.5j$, the second one in $\pm 1.5$, the third one in $\pm 1.5 \pm 1.5j$ and the last one in $1.5j$. The first three example have couplings $M_{14}$,$M_{41}$, $M_{25}$ and $M_{52}$ greater than zero, apart from the mainline couplings. As can be seen in figure 5.8.a., that topology is not realizable at microwave frequencies. Regarding the last example, the result is even worst in terms of realizability (see figure 5.8.b.), since all the couplings are greater than zero except $M_{15}$ and $M_{51}$.

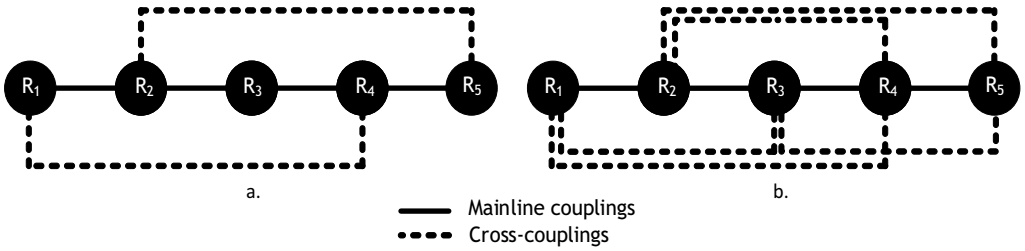


**Figure 5.8: Initial topologies of the examples of chapters 2 and 3 a.Examples A,B and C b.Example D**

Using the algorithm described in [1] it is developed a code in MATLAB. After its application, the four mentioned examples show the following coupling matrices respectively:

A. Transformed coupling matrix and loading resistors for finite transmission zeros at $s = \sigma + j\omega = \pm 1.5j$.

$$R_1 = R_2 = 0.7992, \qquad M = \begin{bmatrix} 0.0000 & 0.7560 & 0.0000 & 0.0000 & 0.0000 \\ 0.7560 & 0.0000 & 0.5586 & 0.0000 & -0.1663 \\ 0.0000 & 0.5586 & 0.0000 & 0.7018 & 0.0000 \\ 0.0000 & 0.0000 & 0.7018 & 0.0000 & 0.7410 \\ 0.0000 & -0.1663 & 0.0000 & 0.7410 & 0.0000 \end{bmatrix} \tag{5.10}$$

B. For finite transmission zeros at $s = \sigma + j\omega = \pm 1.5$.

$$R_1 = R_2 = 0.8192,\ M = \begin{bmatrix} 0.0000 & 0.7818 & 0.0000 & 0.0000 & 0.0000 \\ 0.7818 & 0.0000 & 0.6060 & 0.0000 & 0.0990 \\ 0.0000 & 0.6060 & 0.0000 & 0.5336 & 0.0000 \\ 0.0000 & 0.0000 & 0.5336 & 0.0000 & 0.7757 \\ 0.0000 & 0.0990 & 0.0000 & 0.7757 & 0.0000 \end{bmatrix} \tag{5.11}$$

C. For finite transmission zeros at $s = \sigma + j\omega = \pm 1.5 \pm 1.5j$.

$$R_1 = R_2 = 0.8132, \qquad M = \begin{bmatrix} 0.0000 & 0.7743 & 0.0000 & 0.0000 & 0.0000 \\ 0.7743 & 0.0000 & -0.6017 & 0.0000 & 0.0165 \\ 0.0000 & -0.6017 & 0.0000 & -0.5834 & 0.0000 \\ 0.0000 & 0.0000 & -0.5834 & 0.0000 & 0.7745 \\ 0.0000 & 0.0165 & 0.0000 & 0.7745 & 0.0000 \end{bmatrix} \tag{5.12}$$

D. For finite transmission zeros at $s = \sigma + j\omega = 1.5j$.

$$R_1 = R_2 = 0.8087, \qquad M = \begin{bmatrix} -0.0205 & 0.7703 & 0.0000 & 0.0000 & 0.0000 \\ 0.7703 & -0.0287 & 0.5299 & -0.2752 & 0.0000 \\ 0.0000 & 0.5299 & 0.4804 & 0.5298 & 0.0000 \\ 0.0000 & -0.2752 & 0.5298 & -0.0287 & 0.7702 \\ 0.0000 & 0.0000 & 0.0000 & 0.7702 & -0.0206 \end{bmatrix} \tag{5.13}$$

As can be seen in the preceding matrices, now those examples are physically realizable using a folded form (see figure 5.9)

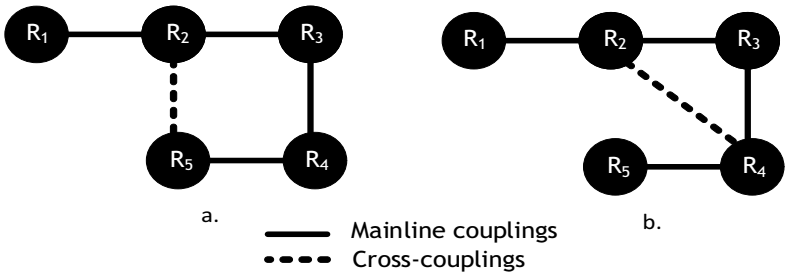


**Figure 5.9: Final topologies of the examples of chapters 2 and 3 a.Examples A,B and C b.Example D**

## 5.2 Radio-frequency filter design in bandpass filters

Following the same structure of chapter 4, once the network theory for lumped elements is presented, the approach for filter design at microwave frequencies is studied.

### 5.2.1 Bandpass approach

At microwave frequencies, once again filter design can be addressed by means of transmission lines approaches. However, in this kind of filters, an underlying concept emerges: resonance. Indeed, a transmission line with certain features of length, termination and characteristic impedance can behave as a series (shunt) resonator over a range of frequencies. Those approaches are not included in this chapter for the sake of brevity.

The concept of resonance allows the designer to go a step further and avoid transmission line approaches, which are less suitable for waveguides. The theory is developed in terms of fields instead, and it is focused on the calculation of the resonant modes of a cavity, computed imposing the boundary conditions in a closed cavity. The boundary conditions, which allow certain modes to be present at specific structures, are based on the tangential and normal behaviour of the electric and magnetic field in the structure interface.

Cutoff frequency arises when transversal boundary conditions are set.All microwave passive devices use this sort of conditions, but they are not unique. In fact, microwave filters use longitudinal boundary conditions as well. In this case, the concept of resonant frequency emerges.

Any waveguide cavity (see figure 5.10) is said to be resonant if under ideal conditions (i.e. lossless conditions) an hypothetical electromagnetic field can stay without any external input, just by transferring energy repeatedly between the magnetic and the electric fields. A closed enclosure satisfies this requirement.

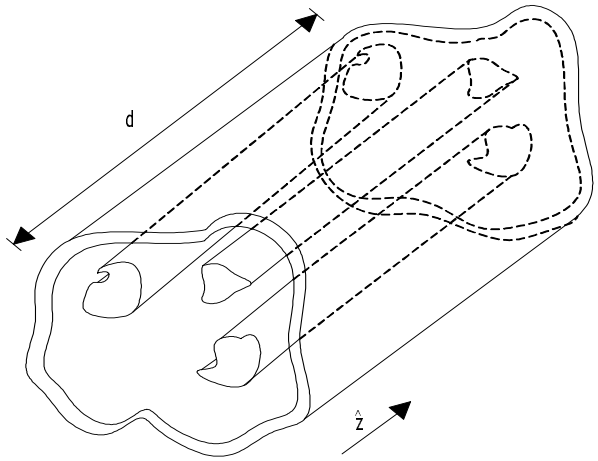


**Figure 5.10: Arbitrary waveguide**

The electric and magnetic fields in an arbitrary waveguide (i.e. with arbitrary contour and arbitrary number of inner conductors) can be written as:

$$\begin{aligned}\vec{E} &= \sum_n \left[ (\varsigma^+ e^{-\gamma_n z} + \varsigma^- e^{+\gamma_n z})\vec{e_t} + (\varsigma^+ e^{-\gamma n z} - \varsigma^- e^{+\gamma_n z}) \right] e_z \hat{z} \\ \vec{H} &= \sum_n \left[ (\varsigma^+ e^{-\gamma_n z} - \varsigma^- e^{+\gamma_n z})\vec{h_t} + (\varsigma^+ e^{-\gamma_n z} + \varsigma^- e^{+\gamma_n z}) \right] h_z \hat{z}\end{aligned} \tag{5.14}$$

If the arbitrary waveguide under consideration is a completely closed cavity, and the longitudinal boundary conditions are set:

$$\vec{E_t}\Big|_{z=0} = 0 \qquad \longleftrightarrow \qquad \sum_n (\varsigma^+ + \varsigma^-)\vec{e_t} = 0 \qquad \longleftrightarrow \qquad \varsigma^+ = -\varsigma^- \tag{5.15}$$

$$\vec{E_t}\Big|_{z=d} = 0 \qquad \longleftrightarrow \qquad \sum_n (\varsigma^+ e^{-\gamma_n z} + \varsigma^- e^{+\gamma_n z})\vec{e_t} = 0 \qquad \longleftrightarrow \qquad \varsigma^- = -e^{-2\gamma_n d}\varsigma^+ \tag{5.16}$$

Using the result obtained in equation 5.15 in 5.16:

$$\varsigma^- = e^{-2\gamma_n d}\varsigma^- \qquad \longleftrightarrow \qquad e^{-2\gamma_n d} = 1 \qquad \longleftrightarrow \qquad \gamma_n d = jq\pi \text{ with } q = 0, 1, 2... \tag{5.17}$$

According to the definition of the propagation constant:

$$\gamma_n d = \sqrt{k_{cn}^2 - \omega^2 \mu\epsilon}\, d = jq\pi \tag{5.18}$$

From equation 5.18, it is derived:

$$f_{res} = \frac{1}{2\pi\sqrt{\mu\epsilon}} \sqrt{k_{cn}^2 + \left(\frac{q\pi}{d}\right)^2} = \sqrt{f_{cn}^2 + \left(\frac{q}{2d\sqrt{\mu\epsilon}}\right)^2} \text{ with } q = 0, 1, 2... \tag{5.19}$$

Parameter $f_{cn}$ in equation 5.19 is the cutoff frequency obtained according to the transversal boundary conditions. Its value will be greater than zero except from TEM modes. It is worth to point out the next two ideas, implicit in equations 5.18 and 5.19:

⇒ In order to allow resonance, the mode depicted by subscript $n$ must be above its cutoff frequency.

⇒ Each mode (depicted by subscript $n$) has infinite resonant frequencies (indexed by letter $q$).

Up until now waveguide microwave resonators have been described. It is now clear that if a microwave cavity is designed to have a desired resonant frequency, it can play a similar role to a lumped element resonator (at least if it is only considered its fundamental resonant mode). However, the previous analysis only took into account a single cavity. Since lumped bandpass filters include several resonators, it is not enough in order to attain a microwave filter. It is obvious that for that purpose several cavities are needed ( in fact as much as the resonators needed-i.e. as much as the filter order), and they somehow need to be coupled in a similar way that resonators share circuit nodes in a low frequency network.

Classical microwave filter theory models discontinuities with equivalent circuits that are included afterwards in the circuital network between resonators. As an example, figure 5.11 depicts the equivalent circuit of the typical discontinuity used in microstrip direct coupled filters. This may seem useless since it could be thought that the new circuital network is not forced to have the desired lumped element filter response. However, actually it is not useless at all. The key is that the equivalent circuit is forced to be an inverter. In that case, whenever the discontinuities between cavities (microwave resonators) adopt the desired inverter value, the structure will ideally act as a bandpass filter, as in subsection 5.1.2.

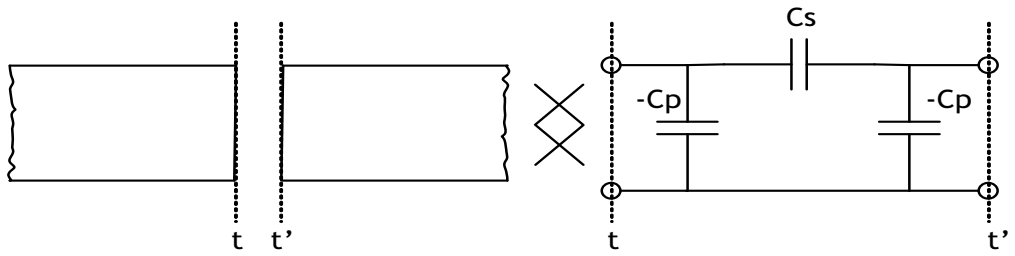


**Figure 5.11: Typical microstrip discontinuity and its circuital characterization**

### 5.2.2 Bandpass applied filter designs

Classical microwave filter design used formulas to approach the values of the lumped elements that form the inverters. This had a major drawback: the trickier a discontinuity is, the more complicated the formulas become. Nowadays, the outstanding development of CAD tools has changed the way radiofrequency designers work. The concepts remain, but formulas are no longer needed. In this work it will be followed the derivation in [1].

First of all, it is vital to understand that any T network can be expressed in terms of the S parameters (see equation 5.20 and figure 5.12 ).

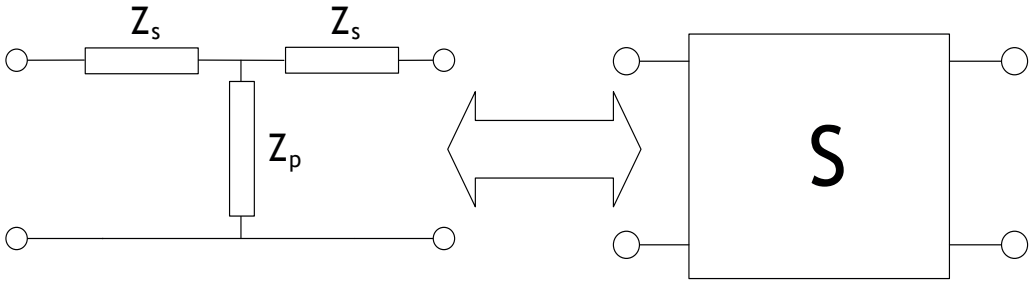


**Figure 5.12: T network as a quadripole characterized by S parameters**

$$\frac{Z_s}{Z_0} = \frac{1 - S_{12} + S_{11}}{1 - S_{11} + S_{12}}, \qquad \frac{Z_p}{Z_0} = \frac{2S_{12}}{(1 - S_{11})^2 - S_{12}^2} \tag{5.20}$$

Secondly, as it was mentioned earlier the designer can avoid to find out the formulas that characterize a discontinuity by means of a full-wave simulator. This CAD tool translates the fields into scattering parameters, which can be used by the designer to set a T equivalent circuit network. This is the reason why dispersion parameters become here essential, although impedance or transmission parameters are usually chosen to describe this topology. They allow to characterize any discontinuity regardless of its shape.

At this point, a direct coupled cavity structure can be modelled as the circuit in figure 5.13, where the waveguides are depicted by transmission lines, and the couplings by the T networks just calculated.

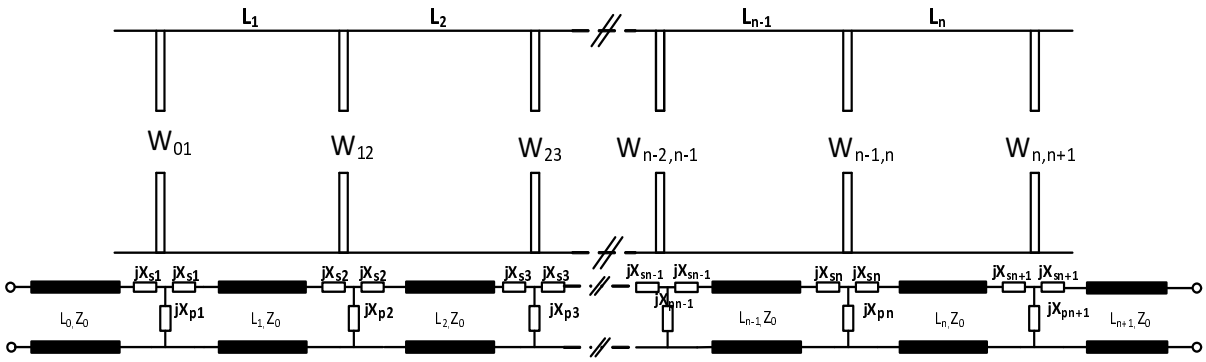


**Figure 5.13: Direct-coupled waveguides and the equivalent circuit model**

However, in subsection 5.2.1 it was remarked that not any discontinuity leads to a filter, and that the model that the radiofrequency designer keeps in mind is the one seen in subsection 5.1.2. Since not all T-networks behave as inverters, a further step must be taken, and two transmission lines are added on each side of the network (see figure 5.14) so that the network of figure 5.12 is transformed into an inverter.

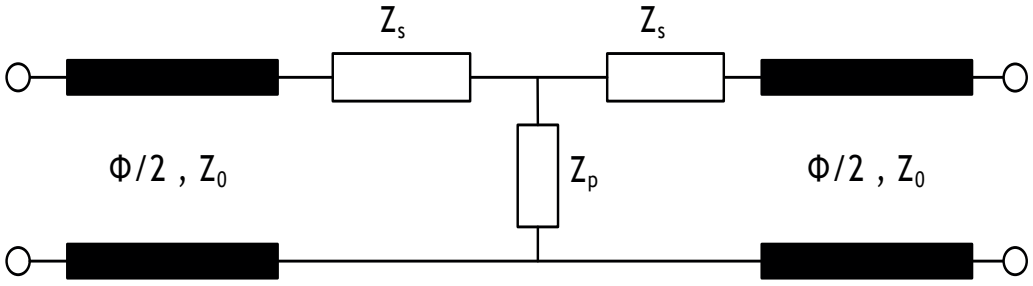


**Figure 5.14: Inverter model used to design a direct-coupled bandpass filter**

However, in order to preserve the equivalent circuit of figure 5.13, two more additional transmission lines need to be added as in figure 5.15. Their length is absorbed into the

waveguide cavities (i.e. the adjacent lines).

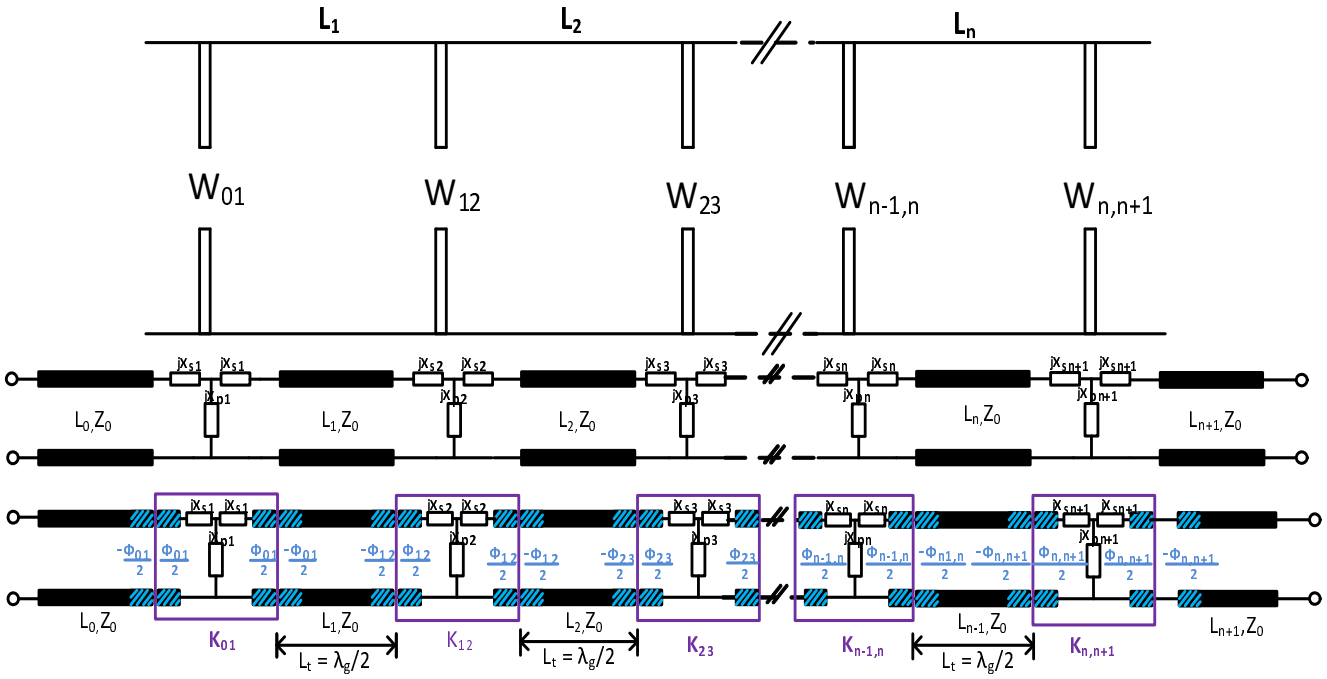


**Figure 5.15: Complete development to achieve the inverter model for a direct-coupled bandpass filter**

It is important to notice that in figure 5.15 the generic impedances of figure 5.14 have been replaced by reactances, as it is impossible to achieve inversion if the involved impedances have real values. This immittances adopt values greater or lower than zero depending on the coupling structure used. Likewise, the electrical lengths of the added transmission lines can increase or decrease the length of the waveguide resonators.

Two bandpass filters are now designed using the aforementioned concepts. A third one is included to show how to address a change in the dielectric. However, as opposed to the lowpass applied filter design developed in subsection 4.2.3, in the hereto subsection the emphasis on the design procedure makes the power mask specification be secondary. However, at the end of the two first examples the structures will be optimized to improve their initial responses.

### Rectangular waveguide direct-coupled bandpass filter

In order to put into practice the theory explained, it is suggested to design a fourth-order Chebychev filter with RL=-20 dB and R0=50 ohms, using rectangular waveguide means of transmission. The centre frequency is set at 11 GHz, with f1=10.85 GHz and f2=11.15 GHz.

The first step is to choose the mode that will be in charge of the power transmission from one port to the other at the specified range of frequencies. This mode is named the fundamental mode.

Since the waveguides are treated as cavities, the fundamental mode has three subscripts.The first two have to do with the transversal variation, whereas the last one has to do with the longitudinal variation. In this design, the mode chosen as fundamental is the one with less variations and the first to propagate -i.e. $TE_{101}$.

The cross section of the waveguide must be properly chosen in order to guarantee that only the fundamental mode propagates in the bandpass region. The selected waveguide has a=22.86 mm and b=10.16 mm (WR90), and is filled with air. Therefore, the fundamental mode has a cutoff frequency of:

$$fc_{TE10} = \frac{1}{2a\sqrt{\mu\epsilon}} = 6.56\,\text{GHz} \tag{5.21}$$

The single-mode bandwidth (strictly speaking for the worst case) is 6.56 GHz, as can be seen in the mode chart of figure 5.16.

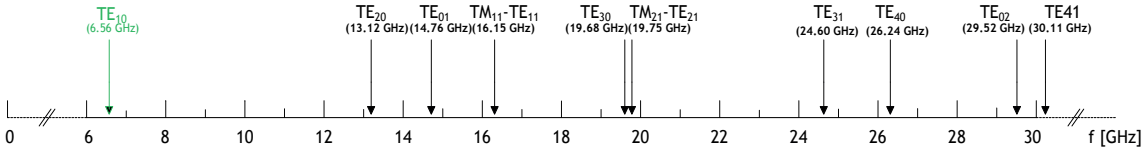


**Figure 5.16: Mode chart WR-90 waveguide**

Now the initial length of the cavity (i.e. before it is modified by the inverter) must be chosen. In order to use mode $TE_{101}$ it is used equation 5.19 with $q = 1$:

$$j\beta L_t = jq\pi \qquad \overset{q=1,}{\longrightarrow} \qquad L_t = \frac{\pi}{\beta} \qquad \overset{\beta=\frac{2\pi}{\lambda_g}}{\longleftrightarrow} \qquad L_t = \frac{\lambda_{g0}}{2} \tag{5.22}$$

where the wavelength of the waveguide is calculated as:

$$\lambda_{g0} = \frac{c}{\sqrt{f_0^2 - fc_{TE10}^2}} = 34\,\text{mm}, \qquad \text{with } c = \frac{1}{\sqrt{\mu\epsilon}} \text{ and } f_0 = 11\,\text{GHz} \tag{5.23}$$

Once the waveguide resonators have been chosen, the designer must focus on the coupling structure. The selected iris (i.e. type of aperture) for this design has the same height of the waveguide (b=10.16 mm), and only varies its width (see figure 5.17 ). In order to characterize this discontinuity by means of the full-wave simulator CST MWS, the waveguide ports must be de-embedded.

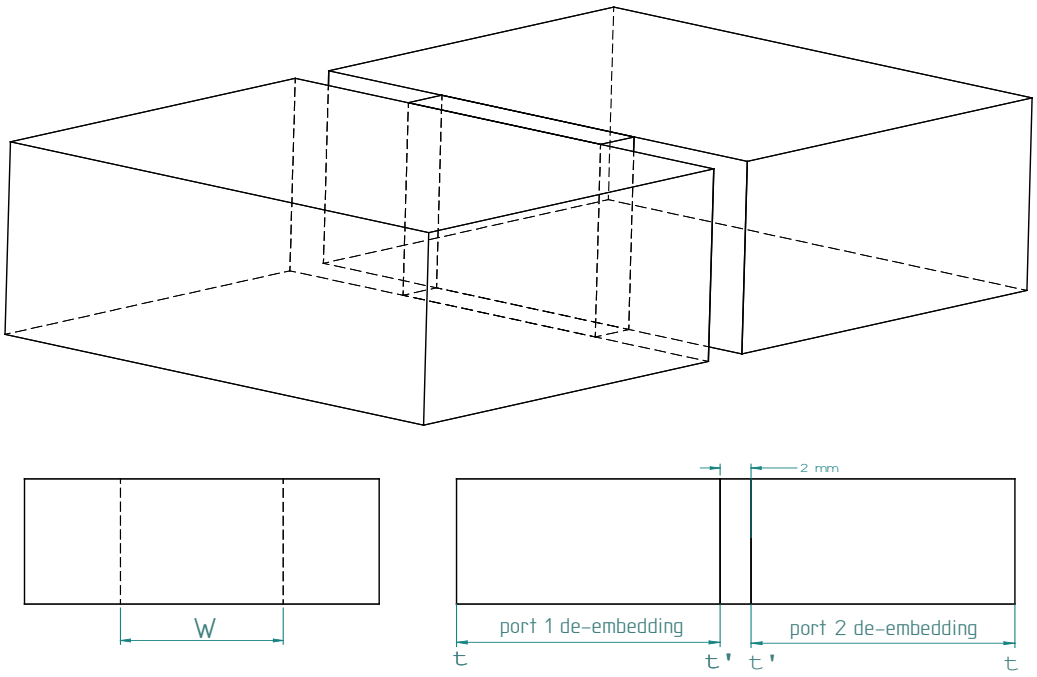


**Figure 5.17: Structure for full-wave iris characterization (WR90 waveguide)**

This kind of iris has an inductive behaviour, and therefore the T-network is characterised as in figure 5.18.

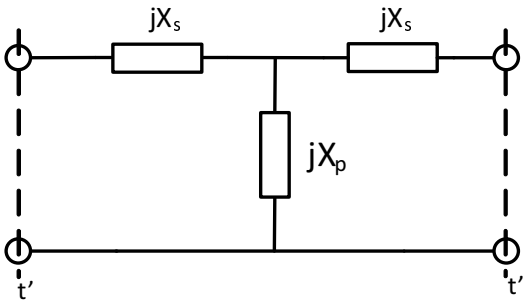


**Figure 5.18: Inductive T network**

Hence, equation 5.20 turns out to be:

$$\frac{jX_s}{Z_0} = \frac{1 - S_{12} + S_{11}}{1 - S_{11} + S_{12}}, \qquad \frac{jX_p}{Z_0} = \frac{2S_{12}}{(1 - S_{11})^2 - S_{12}^2} \tag{5.24}$$

Several simulations are carried out in the full-wave solver CST Microwave Studio. The iris width is varied getting the following results of figure 5.19.

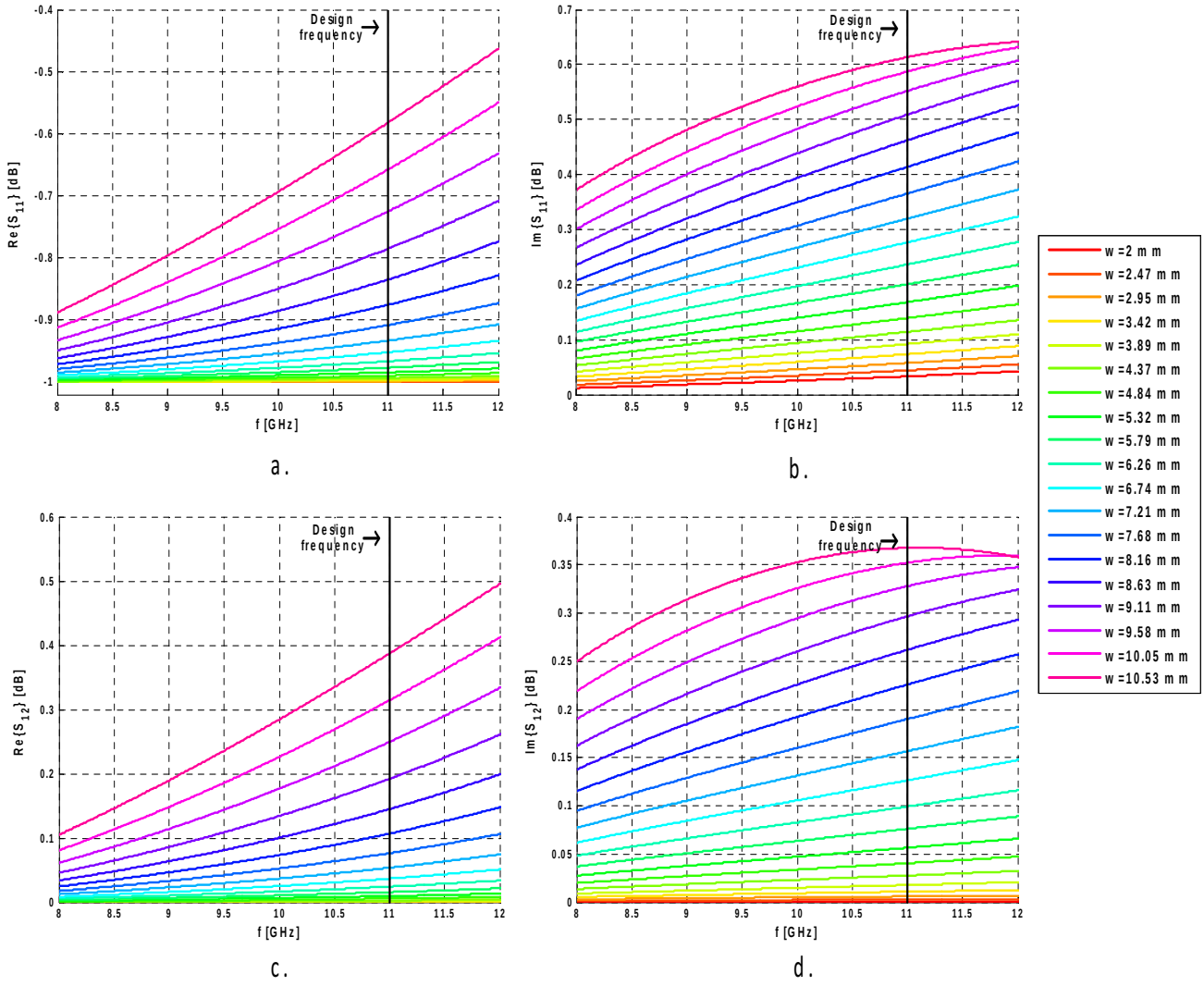


**Figure 5.19: Full-wave iris characterization (WR90)**
**a.** $\Re\{S_{11}\}$ **b.** $\Im\{S_{11}\}$
**c.** $\Re\{S_{12}\}$ **d.** $\Im\{S_{12}\}$

As soon as $X_p$ and $X_s$ are computed at $f_0$ (with the results given in figure 5.19 and equation 5.24), the electrical lengths which transform the equivalent T-network into an inverter circuit (recall figure 5.14) must be calculated. The formulas given in [1] are used to work out their values:

$$A. \qquad \phi = -\tan^{-1}\left(\frac{2X_p}{Z_0} + \frac{X_s}{Z_0}\right) - \tan^{-1}\left(\frac{X_s}{Z_0}\right)$$
$$B. \qquad \frac{K}{Z_0} = \left| tan\left(\frac{\phi}{2} + \tan^{-1}\left(\frac{X_s}{Z_0}\right)\right)\right| \tag{5.25}$$

The values of $X_s$, $X_p$, $\phi$, and $K$ are shown in table 5.1.

| W[mm] | $X_s$[ohms] | $X_p$[ohms] | $\phi$[rad] | K[ohms] |
|---|---|---|---|---|
| 2.00 | 0.0161 | 0.0005 | −0.0332 | 0.0005 |
| 2.47 | 0.0207 | 0.0014 | −0.0442 | 0.0014 |
| 2.95 | 0.0258 | 0.0030 | −0.0575 | 0.0030 |
| 3.42 | 0.0313 | 0.0055 | −0.0735 | 0.0055 |
| 3.89 | 0.0372 | 0.0090 | −0.0921 | 0.0089 |
| 4.37 | 0.0432 | 0.0140 | −0.1143 | 0.0139 |
| 4.84 | 0.0495 | 0.0206 | −0.1398 | 0.0205 |
| 5.32 | 0.0560 | 0.0289 | −0.1692 | 0.0287 |
| 5.79 | 0.0624 | 0.0393 | −0.2025 | 0.0389 |
| 6.26 | 0.0690 | 0.0519 | −0.2400 | 0.0512 |
| 6.74 | 0.0755 | 0.0674 | −0.2828 | 0.0661 |
| 7.21 | 0.0820 | 0.0857 | −0.3299 | 0.0833 |
| 7.68 | 0.0884 | 0.1074 | −0.3825 | 0.10354 |
| 8.16 | 0.0948 | 0.1335 | −0.4416 | 0.1269 |
| 8.63 | 0.1011 | 0.1636 | −0.5055 | 0.1532 |
| 9.11 | 0.1073 | 0.1990 | −0.5748 | 0.1825 |
| 9.58 | 0.1133 | 0.2416 | −0.6506 | 0.2157 |
| 10.052 | 0.1191 | 0.2899 | −0.7285 | 0.2508 |
| 10.53 | 0.1247 | 0.3479 | −0.8112 | 0.2892 |
| 11.00 | 0.1300 | 0.4178 | −0.8973 | 0.3306 |

**Table 5.1: Iris characterization in the WR90 waveguide**

Up until now a process of analysis has been carried out. It can be summarized in figure 5.20.

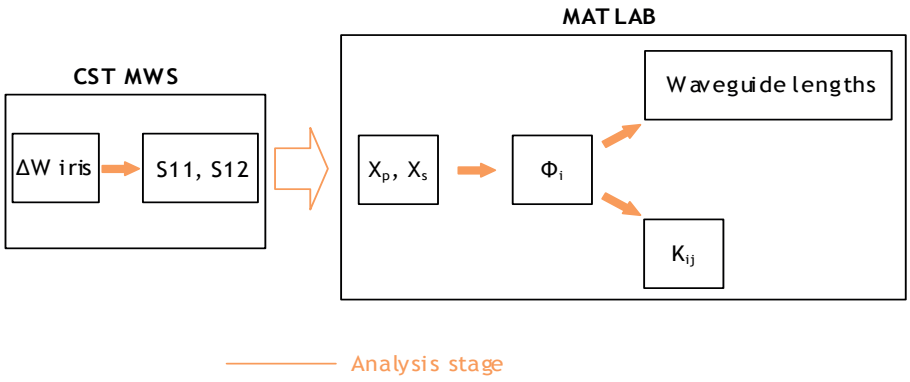


**Figure 5.20: Analysis stage in a direct-coupled bandpass filter design**

This stage of analysis provides the designer enough data to characterize the discontinuity behaviour. The next step for the filter designer is to synthesize the properly physical dimensions of the filter. Those physical dimensions are attained using the data gathered in the analysis stage, together with the theoretical inverter values (see section 5.1.2) and the theo-

retical waveguide lengths ($\lambda_{g0}/2$). In other words: given the theoretical inverter values of the lumped bandpass inverter model, the designer chooses the widths of the irises and the electrical lengths which gave an inverter value in equation 5.25.b. close to the desired one.

Regarding the absorbed electrical lengths, they are translated into physical waveguide lengths using equation 5.26:

$$\frac{\phi_{ij}}{2} = \beta_g d_{ij} \qquad d_{ij} = \frac{\phi_{ij}/2}{\beta_g} \tag{5.26}$$

Therefore, the final length of each waveguide cavity is computed as:

$$L_i = \frac{\lambda_{g0}}{2} + \frac{\phi_{i-1,i}}{2\beta_g} + \frac{\phi_{i,i+1}}{2\beta_g}, \qquad \text{with } \phi_i, \phi_{i+1} < 0 \tag{5.27}$$

Figure 5.21 summarizes the synthesis and analysis processes that must be followed to design a direct-coupled bandpass filter based on the inverter model.

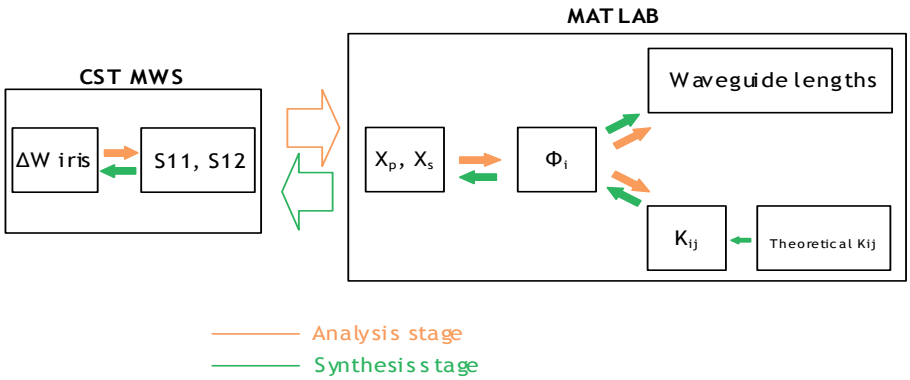


**Figure 5.21: Analysis and synthesis stages in a direct-coupled bandpass filter design**

In order to choose the values of $K$ that are closest to the theoretical values, two graphics are plotted in figure 5.22.

The overlapped crosses belong to twenty iris simulated values. Due to the smooth form of the data plotted, it is decided to use MATLAB to interpolate values (using the *interp1* function). That way, less simulations are needed an it is possible to find closer values to the desired ones, getting therefore a trade-off between accuracy and computational time.

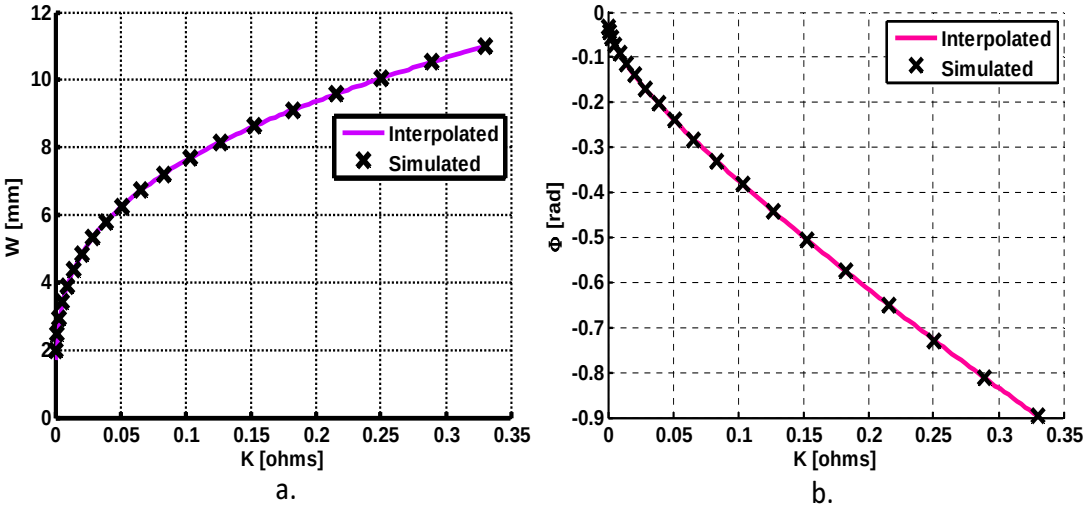


**Figure 5.22: a. Inverter value - Iris width**
**b. Inverter value - Electrical length**

Figures 5.22.a and b can be used as a look-up tables, so that together with the theoretical formulas shown in subsection 5.1.2, the design physical filter values are obtained. However, in fact the aforementioned two plots are here shown only for academic purposes. Actually in the hereto work MATLAB is used to get the precise values, avoiding to depend on how good the designer is capable to select graphic values. It is highly advisable to proceed that way to keep clear of errors. Results are gathered in table 5.2.

| $\mathbf{K_{theoretical}}$**[ohms]** | $\mathbf{K_{simulated}}$**[ohms]** | **W[mm]** | $\phi$**[rad]** |
|---|---|---|---|
| 0.2985 ($K_{01}$) | 0.2976 | 10.62 | $-0.8288$ ($\phi_{01}$) |
| 0.0699 ($K_{12}$) | 0.0694 | 6.83 | $-0.2921$ ($\phi_{12}$) |
| 0.0518 ($K_{23}$) | 0.0529 | 6.32 | $-0.2451$ ($\phi_{23}$) |
| 0.0699 ($K_{34} = K_{12}$) | 0.0694 | 6.83 | $-0.2921$ ($\phi_{34} = \phi_{12}$) |
| 0.2985 ($K_{45} = K_{01}$) | 0.2976 | 10.62 | $-0.8288$ ($\phi_{45} = \phi_{01}$) |

**Table 5.2: Design table I for the $WR90$ waveguide direct-coupled bandpass filter (N=4,RL=20dB,R0=50 ohms,f0=11GHz,$\triangle = 2.73\%$)**

Physical lengths are computed using equation 5.27 and shown in figure 5.23,which shows three views of the final filter design (perspective, top view and side view) .

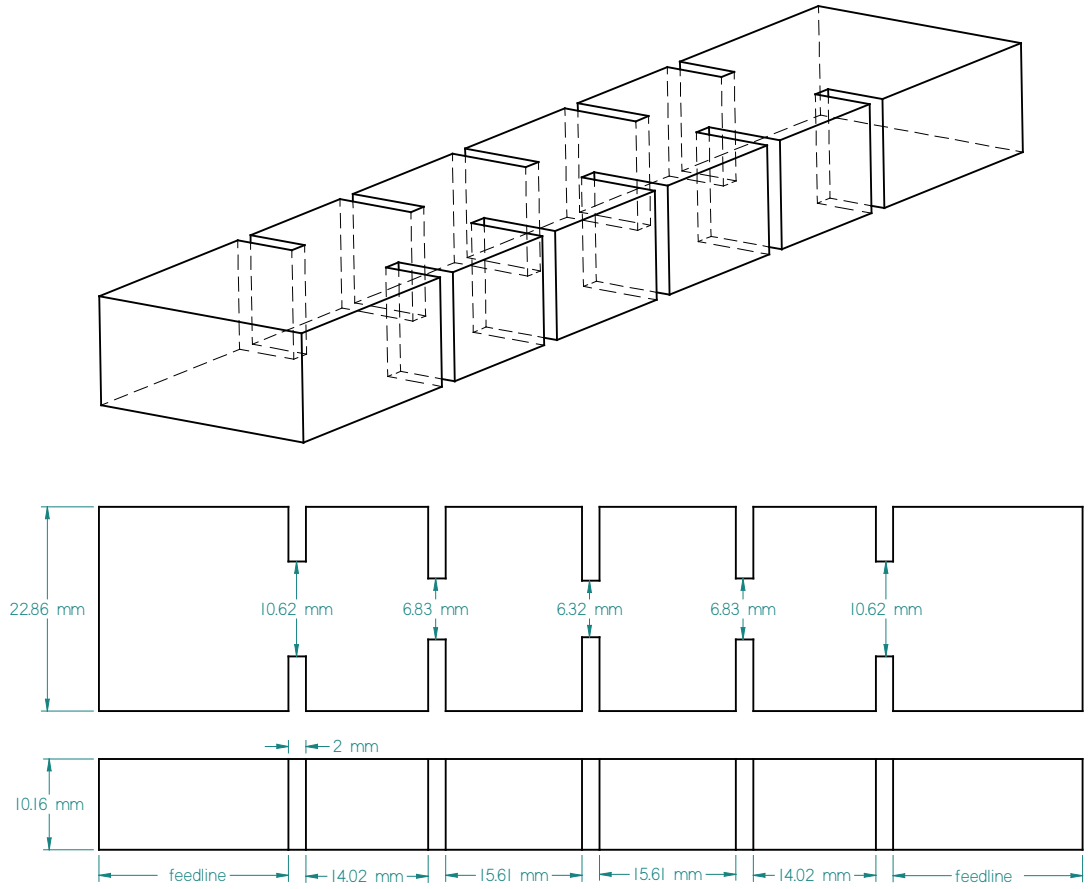


**Figure 5.23: Structure of the initial WR90 direct-coupled bandpass Chebychev filter design (N=4, RL=20dB, R0=50 ohms, f0=11 GHz,** $\triangle = 2.73\%$**)**

The attained filter response is shown in figure 5.24. Figure 5.25 compares the response of the equivalent lumped bandpass filter with the full-wave response achieved. Although the four zeros are preserved, since their level is lower than the desired 20 dBs of return loss, the direct coupled waveguide filter has poorer rejection (i.e. poorer selectivity).

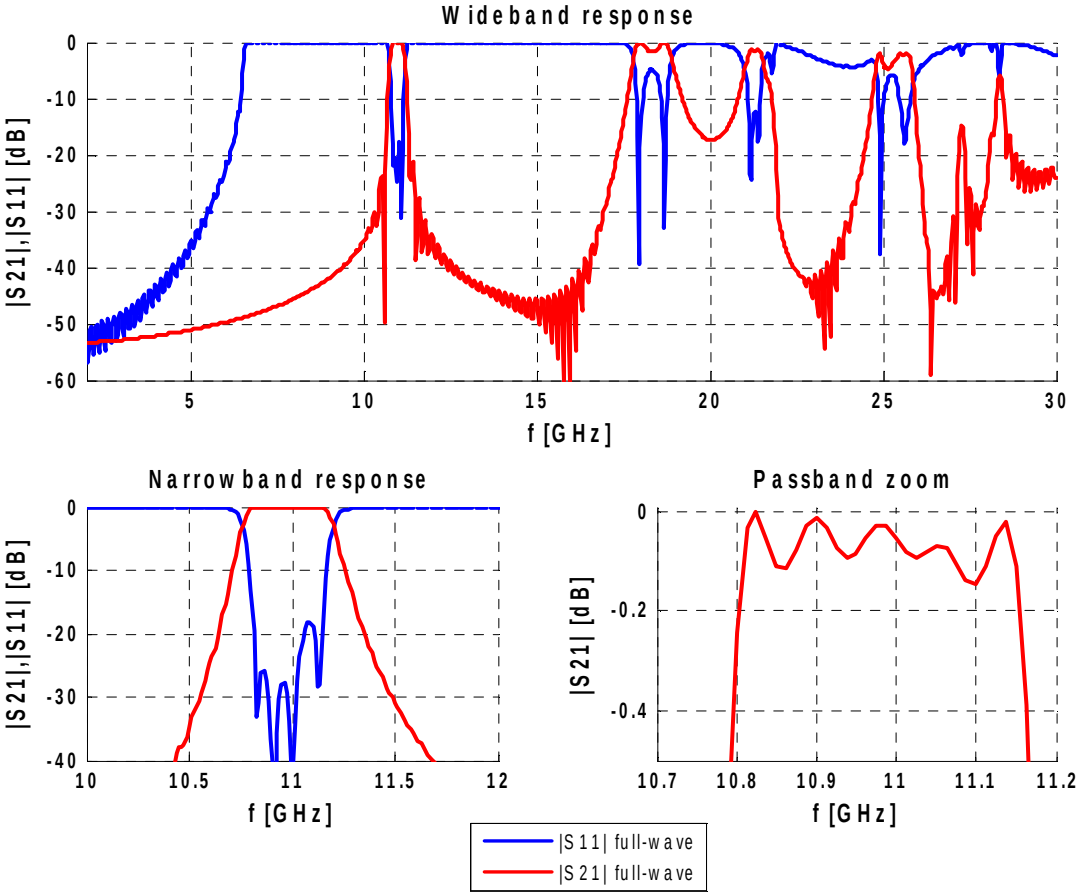


**Figure 5.24: Full-wave response of the initial WR90 direct-coupled bandpass Chebychev filter design (N=4, RL=20dB, R0=50 ohms, f0=11 GHz, $\triangle = 2.73\%$)**

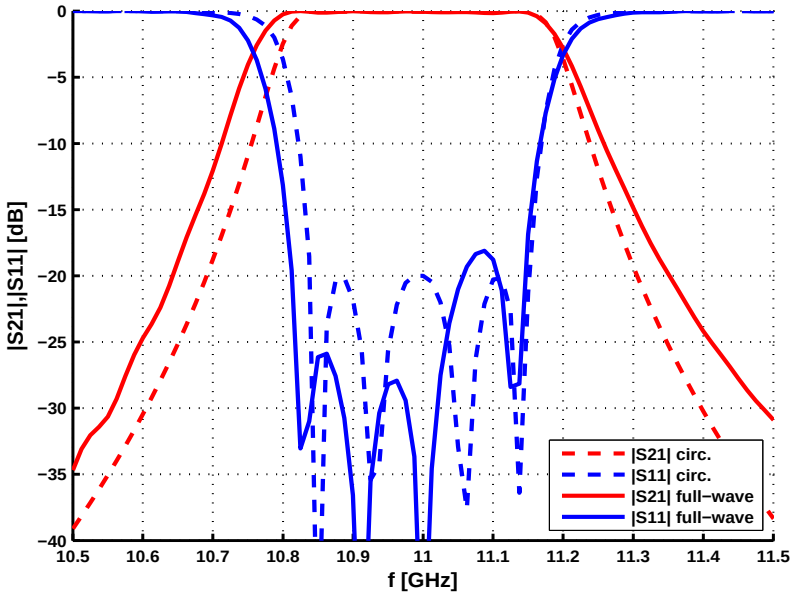


**Figure 5.25: Full-wave response of the initial WR90 direct-coupled bandpass Chebychev filter design (N=4, RL=20dB, R0=50 ohms, f0=11 GHz, $\triangle = 2.73\%$) and the equivalent lumped network response**

In order to improve the filter response, the same algorithm used in subsection 4.2.3 (i.e. the "Trust Region Framework" algorithm) is used in this design. Only the iris widths and the cavity lengths are used as optimization variables (i.e. the transversal dimension of the rectangular waveguide is preserved). The final dimensions are shown in figure 5.26

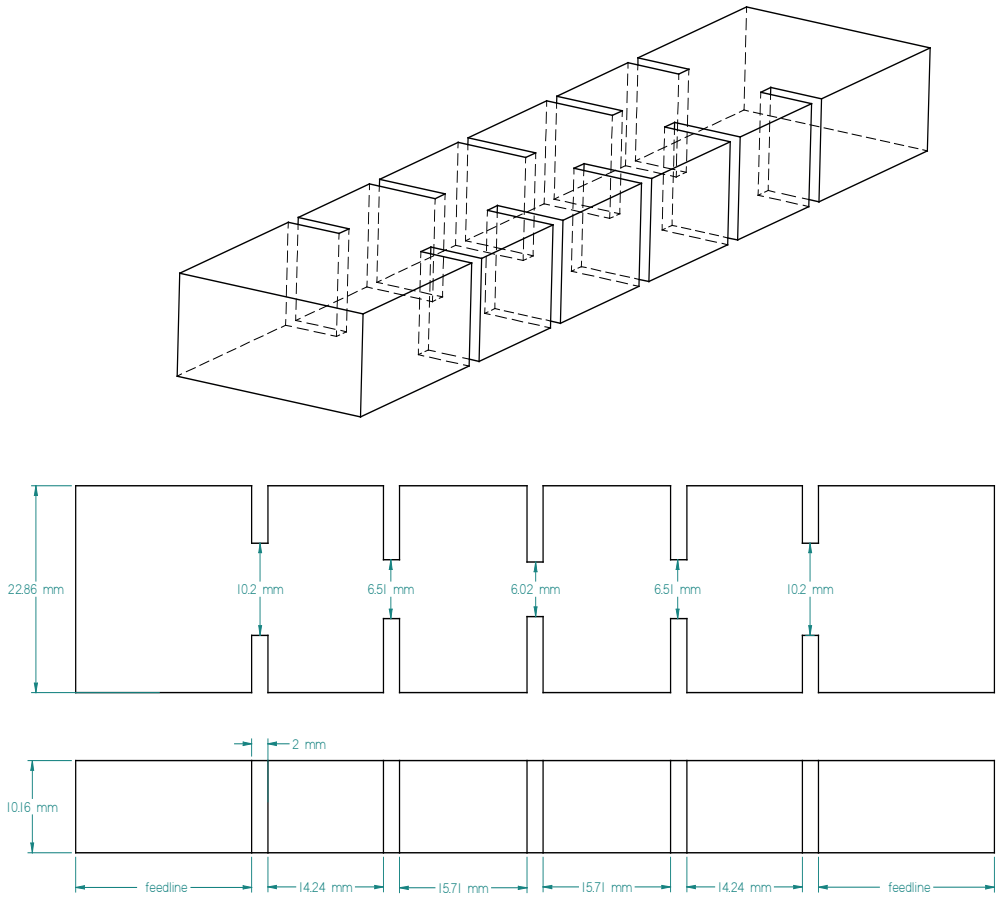


**Figure 5.26: Structure of the optimized WR90 direct-coupled bandpass Chebychev filter design (N=4, RL=20dB, R0=50 ohms, f0=11 GHz, $\triangle = 2.73\%$)**

The full-wave response obtained with those dimensions is given in figure 5.27. Figure 5.28 shows the meaningful improvement of the filter response, as it is very close to the lumped equivalent network.

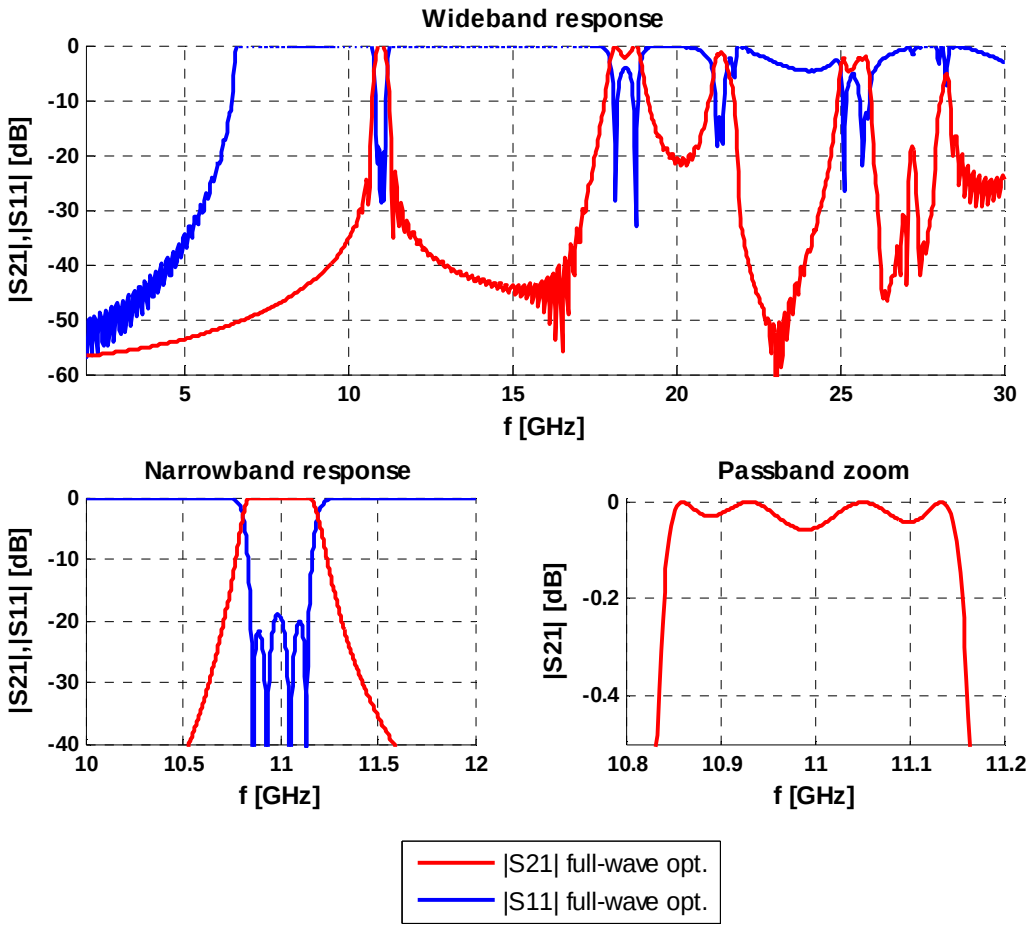


**Figure 5.27: Full-wave response of the optimized WR90 direct-coupled bandpass Chebychev filter design (N=4, RL=20dB, R0=50 ohms, f0=11 GHz, $\triangle = 2.73\%$)**

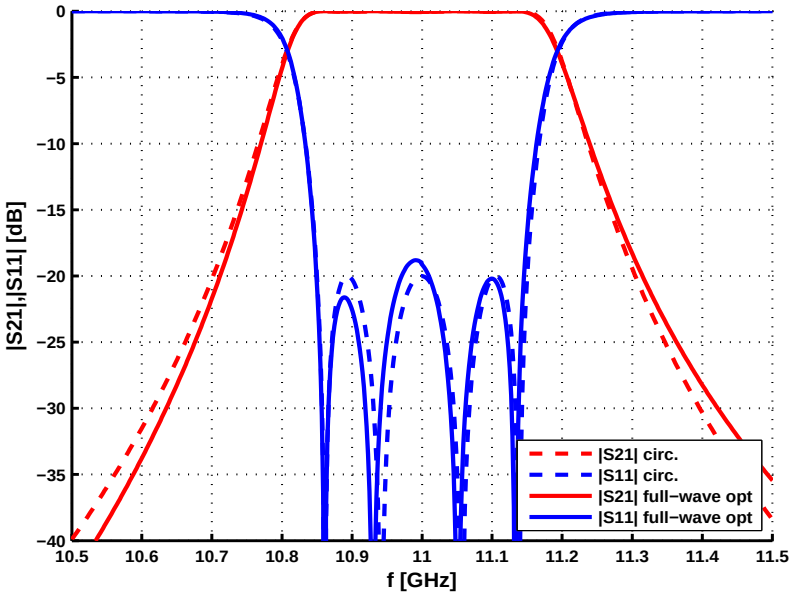


**Figure 5.28: Full-wave response of the initial WR90 direct-coupled bandpass Chebychev filter design (N=4, RL=20dB, R0=50 ohms, f0=11 GHz, $\triangle = 2.73\%$) and the equivalent lumped network response**

**Circular waveguide direct-coupled bandpass filter with circular irises**

This second example aims at designing a fourth-order direct-coupled Chebychev bandpass filter with the same specifications as in the preceding design, except for the return loss, which is now set to 25 dBs. Thus, $R_0$ remains equal to 50 ohms, f0=11 GHz, f1=10.85 GHz and f2=11.15 GHz. Concerning the specific means of transmission, it is chosen a circular waveguide of radius a=10mm.

According to the transversal dimension, the selected fundamental mode $TE_{11}$ has a cutoff frequency of:

$$f_{c_{TE11}} = \frac{1.841}{2\pi a\sqrt{\mu\epsilon}} = 8.79 \text{ GHz}. \tag{5.28}$$

Thus, in view of the mode chart of figure 5.29, in the worst scene possible the monomode bandwidth is equal to 2.69 GHz.

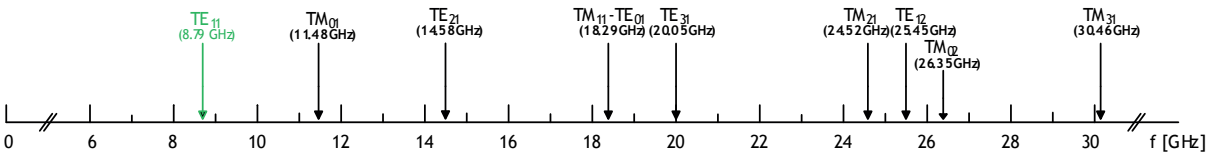


**Figure 5.29: Mode chart circular waveguide a=10mm**

Taking now into account the longitudinal dimension, the chosen fundamental mode becomes the $TE_{111}$, as it is decided to use the mode with less longitudinal variations.That mode results in the shortest cavity lengths, whose value is calculated as $L_t = \lambda_{g_0}/2$ with $\lambda_{g_0}/2$ as:

$$\lambda_{g_0} = \frac{c}{\sqrt{f_0^2 - f_{c_{TE_{11}}}}} = 45.4 \text{ mm, being } f_0\text{=11 GHz and } c = \frac{1}{\sqrt{\mu\epsilon}} \tag{5.29}$$

Now it is time to begin with iris characterization. The selected iris in this design is circular as well. Figure 5.30 shows its appearance. Once again the full-wave simulator (i.e. CST Microwave Studio) must include a de-embedding in the ports of the structure, since the phase information is in this method of design vital.

Figures 5.31.a. to d. provide the information acquired in this stage of analysis of the discontinuity. Using equations 5.24, and the two formulas of equation 5.25, the values of $X_s$,$X_p$, $\phi$ and $K$ are computed and shown in table 5.3.

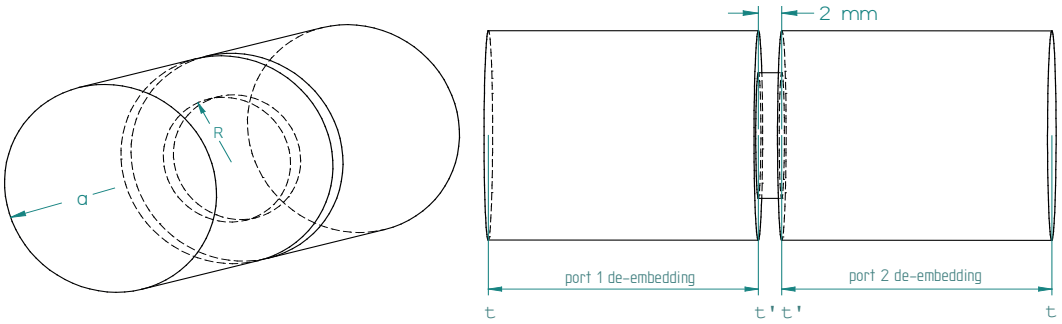


**Figure 5.30: Structure for full-wave iris characterization (circular iris, circular waveguide a=10mm)**

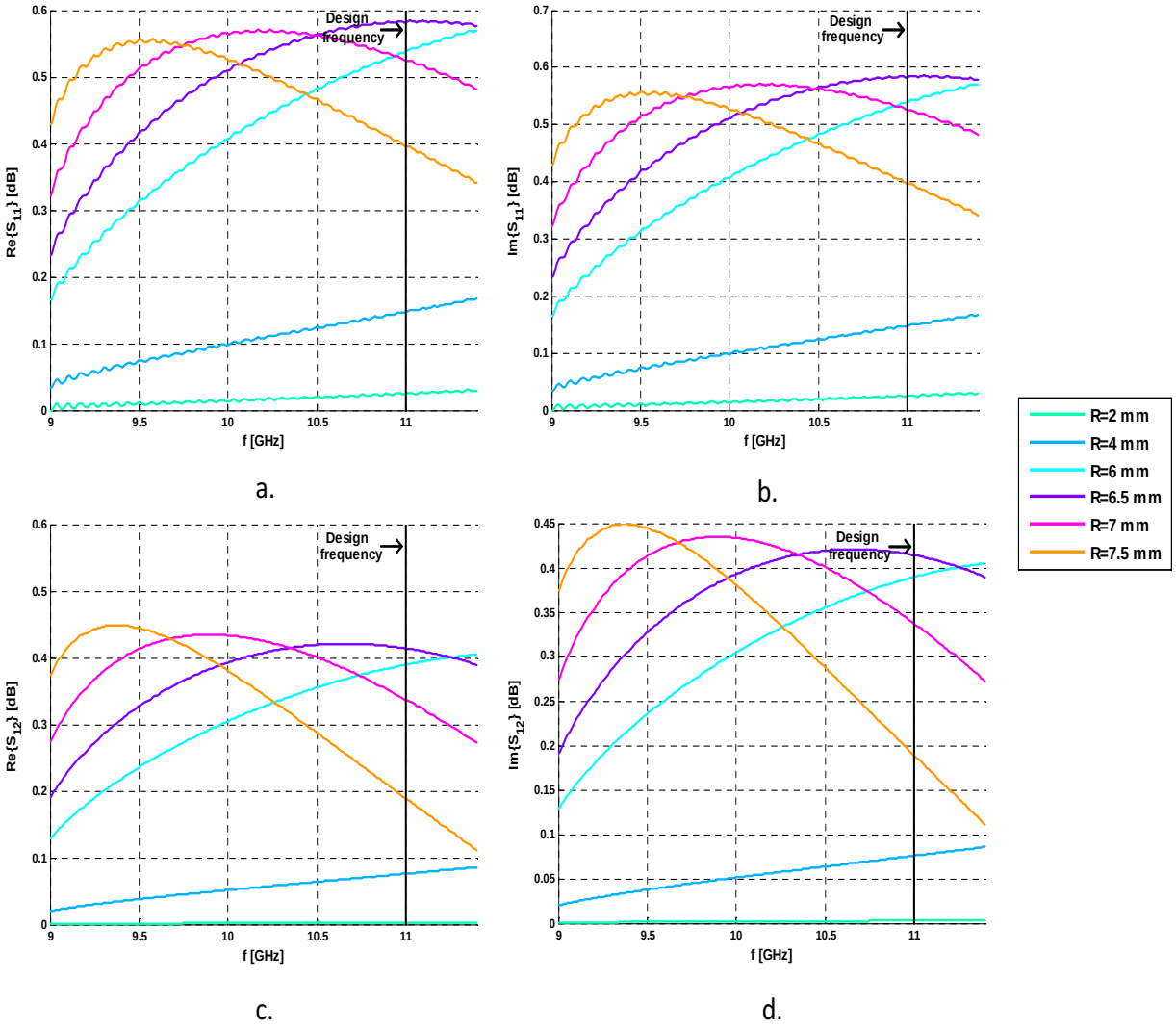


**Figure 5.31: Full-wave circular iris characterization (circular iris, circular waveguide a=10mm)**

**a.** $\Re\{S_{11}\}$ **b.** $\Im\{S_{11}\}$
**c.** $\Re\{S_{12}\}$ **d.** $\Im\{S_{12}\}$

| R[mm] | $X_s$[ohms] | $X_p$[ohms] | $\phi$[rad] | K[ohms] |
|---|---|---|---|---|
| 2 | 0.0107 | 0.0014 | −0.0242 | 0.0014 |
| 4 | 0.0356 | 0.0387 | −0.1480 | 0.0384 |
| 6 | 0.0746 | 0.3013 | −0.6697 | 0.2664 |
| 6.5 | 0.0851 | 0.4900 | −0.9017 | 0.3833 |
| 7 | 0.0951 | 0.8238 | −1.1446 | 0.5175 |
| 7.5 | 0.1050 | 1.4933 | −1.3626 | 0.6504 |

**Table 5.3: Iris characterization in circular waveguide (a=10mm)**

Figures 5.32.a. and b depict the look-up tables that are going to be processed in MATLAB pursuing the best values for the design (i.e. iris radius R and electrical length). It is important to underline that in this example less full-wave samples (i.e. depicted in figure 5.32 with overlapped crosses) are used. Moreover, the wide gap between the second and the third sample is set on purpose to check whether using MATLAB interpolation leads to inaccurate results or not. It can be seen in table 5.4 that two out of the three different inverter values are precisely in between samples two and three.

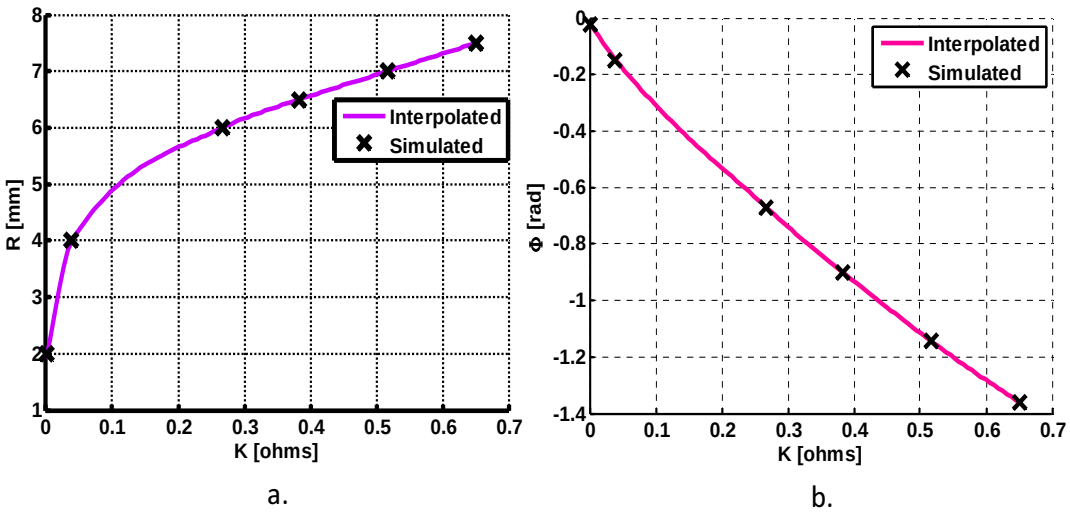


**Figure 5.32: a. Inverter value - Iris radius**
**b. Inverter value - Electrical length**

| $K_{theoretical}$[ohms] | $K_{simulated}$[ohms] | W[mm] | $\phi$[rad] |
|---|---|---|---|
| 0.3972 ($K_{01}$) | 0.3968 | 6.55 | −0.927 ($\phi_{01}$) |
| 0.1237 ($K_{12}$) | 0.1236 | 5.13 | −0.365 ($\phi_{12}$) |
| 0.0917 ($K_{23}$) | 0.0911 | 4.79 | −0.287 ($\phi_{23}$) |
| 0.1237 ($K_{34} = K_{12}$) | 0.1236 | 5.13 | −0.365 ($\phi_{34} = \phi_{12}$) |
| 0.3972 ($K_{45} = K_{01}$) | 0.3968 | 6.55 | −0.927 ($\phi_{45} = \phi_{01}$) |

**Table 5.4: Design table I for circular waveguide (a=10 mm, circular iris) direct-coupled bandpass Chebychev filter design (N=4,RL=25dB,R0=50 ohms,f0=11GHz,$\triangle = 2.73\%$)**

Using the preceding electrical lengths and equation 5.27, the final physical lengths (i.e. the corrected ones) of the circular waveguide cavities are computed. Therefore the dimensions of the designed filter are given in figure 5.33.

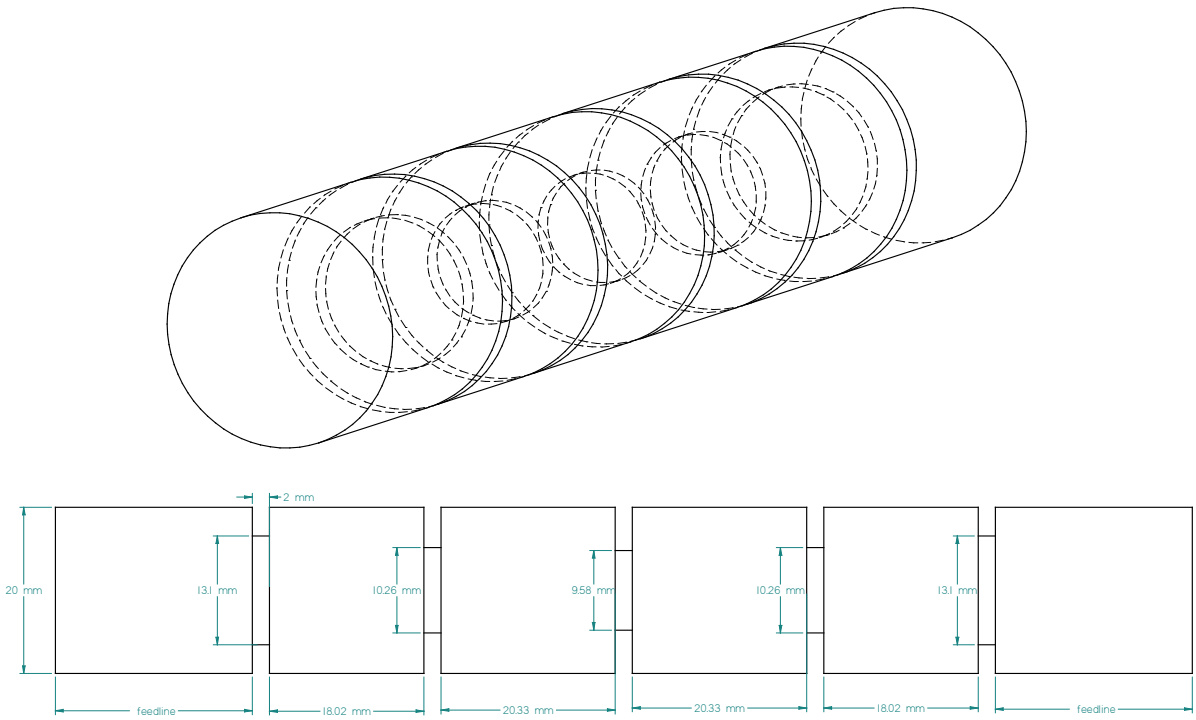


**Figure 5.33: Structure of the initial circular waveguide(a=10 mm, circular iris) direct-coupled bandpass Chebychev filter design (N=4,RL=25dB,R0=50 ohms,f0=11GHz, $\triangle = 2.73\%$)**

The frequency response of the structure above is shown in figure 5.34. Figure 5.35 compares the equivalent lumped bandpass network with the achieved filter response of the microwave filter. Due to the results obtained, it is clear that the interpolation used in MATLAB to avoid full-wave simulations is accurate enough. In fact, it is concluded that it can be used even less samples to characterise the iris in future designs, which will save some valuable time.

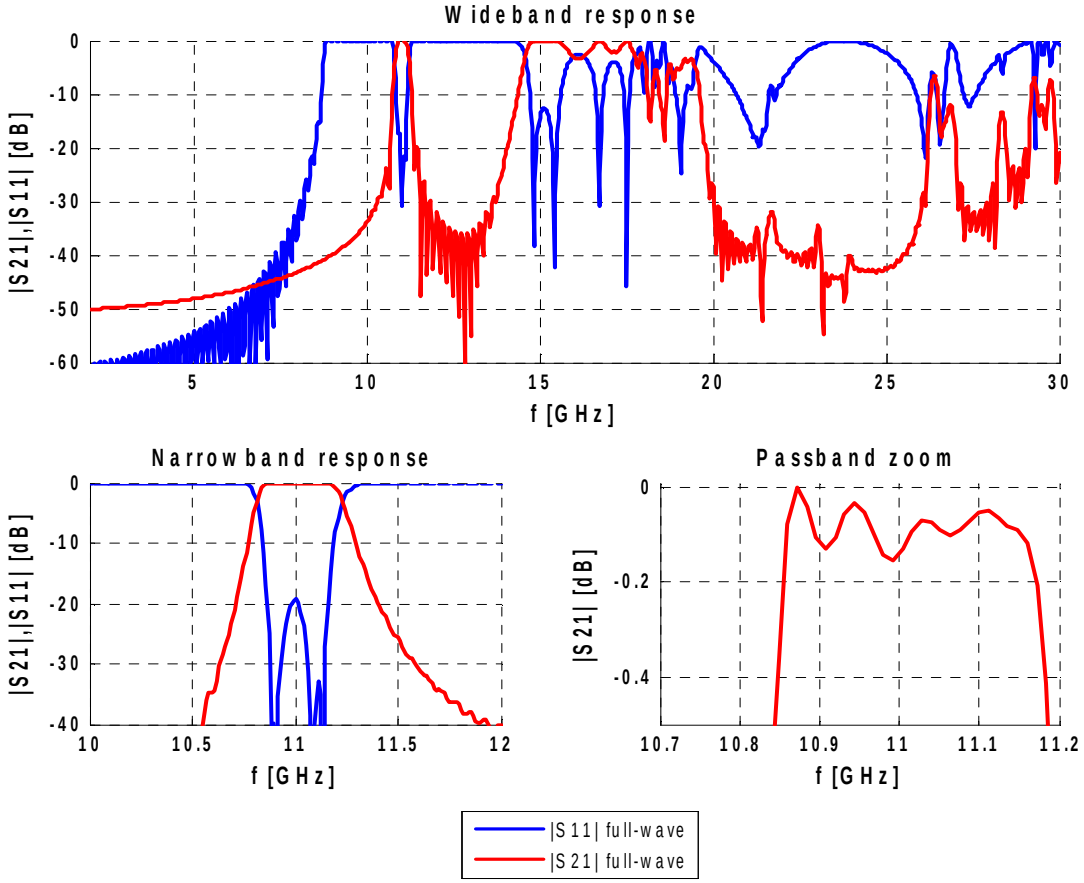


**Figure 5.34: Full-wave response of initial circular waveguide (a=10 mm, circular iris) direct-coupled bandpass Chebychev filter design (N=4,RL=25dB,R0=50 ohms,f0=11GHz, $\triangle = 2.73\%$)**

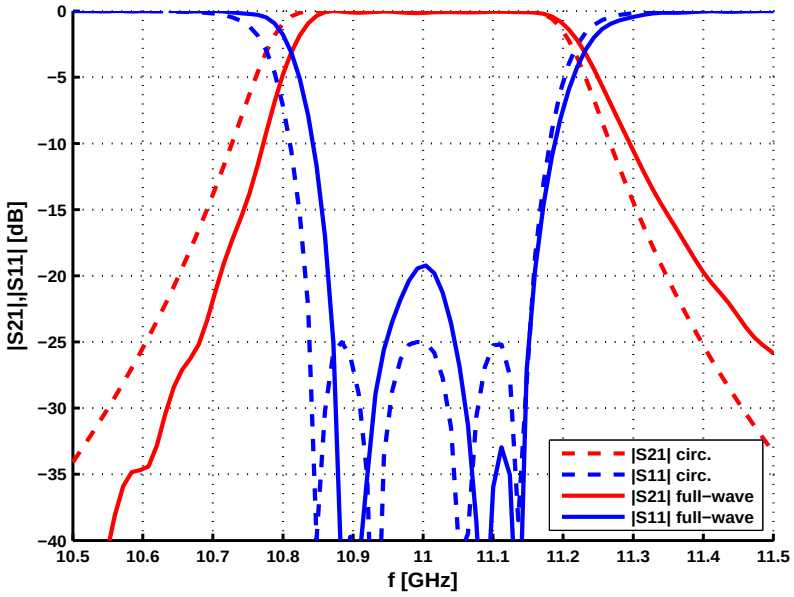


**Figure 5.35: Full-wave response of initial circular waveguide (a=10 mm, circular iris) direct-coupled bandpass Chebychev filter design (N=4,RL=25dB,R0=50 ohms,f0=11GHz, $\triangle = 2.73\%$) and the equivalent lumped network response**

The frequency response of the initial filter design can be improved through optimization. The Trust Region Framework leads to the dimensions gathered in figure 5.36. Once again the transversal dimension of the waveguide (i.e. a= 10 mm) is preserved, and only the waveguide cavities and the iris widths are considered as optimization variables.

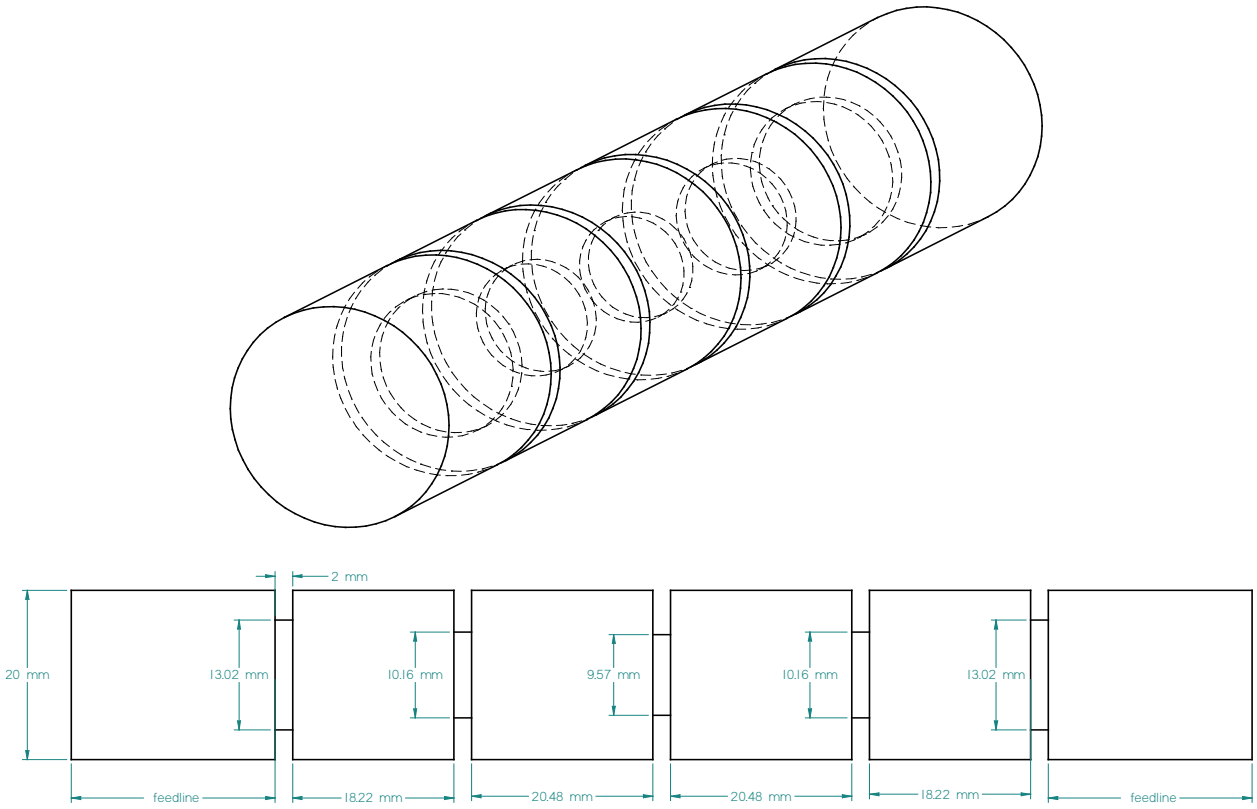


**Figure 5.36: Structure of the optimized circular waveguide(a=10 mm, circular iris) direct-coupled bandpass Chebychev filter design (N=4,RL=25dB,R0=50 ohms,f0=11GHz, $\triangle = 2.73\%$)**

The final response of the optimized filter can be found in figure 5.37. Figure 5.38 evidences that the optimization process has recovered the four academic reflection zeros. However, selectivity is not as good as in the rectangular filter, and hence a further improvement would include filter desymmetrization in order to provide more degrees of freedom to the optimizer (although this does not guarantee to achieve this purpose, however).

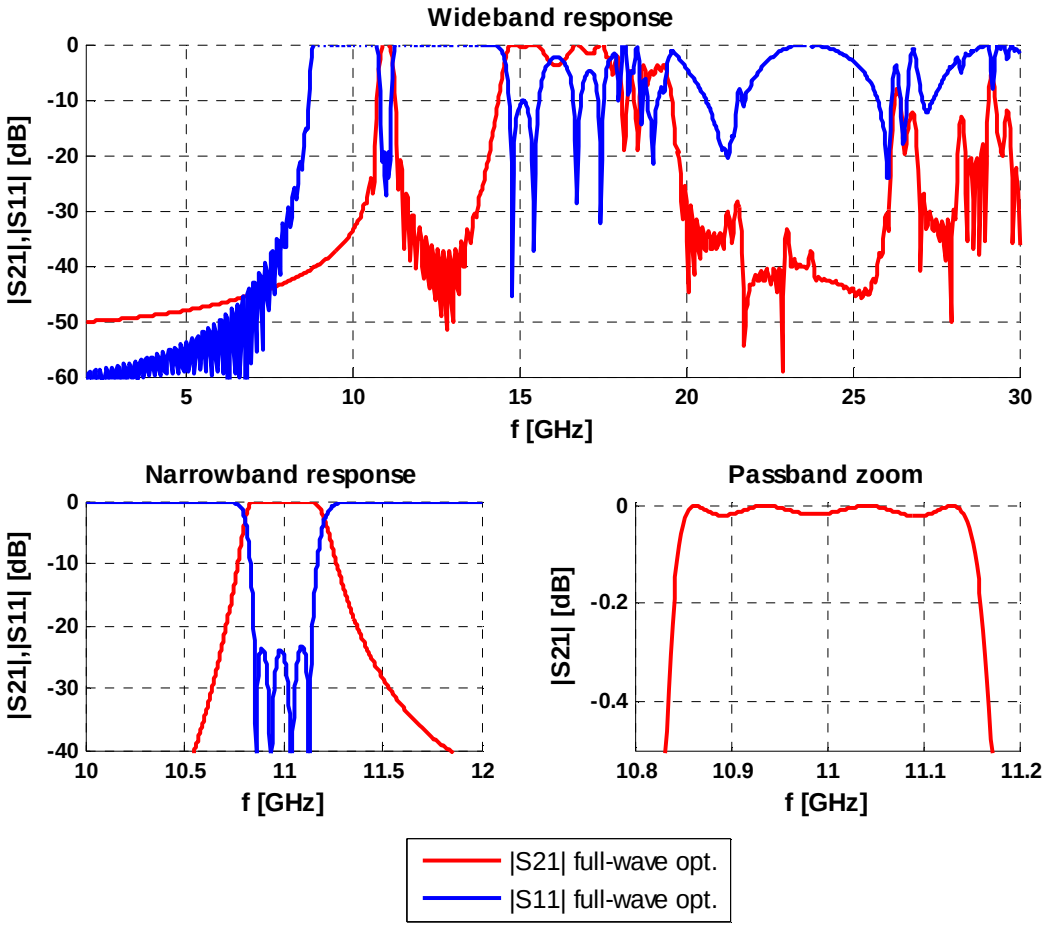


**Figure 5.37: Full-wave response of optimized circular waveguide (a=10 mm, circular iris) direct-coupled bandpass Chebychev filter design (N=4,RL=25dB,R0=50 ohms,f0=11GHz, $\triangle = 2.73\%$)**

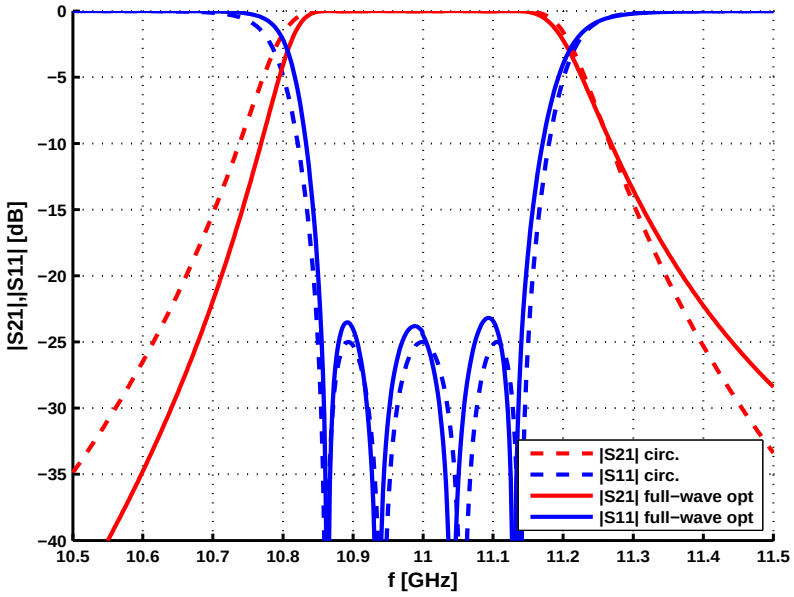


**Figure 5.38: Full-wave response of initial circular waveguide (a=10 mm, circular iris) direct-coupled bandpass Chebychev filter design (N=4, RL=25dB, R0=50 ohms, f0=11GHz, $\triangle = 2.73\%$) and the equivalent lumped network response**

**Circular waveguide direct-coupled bandpass filter with coaxial irises**

The first of the bandpass examples was a guideline that put into practice the theoretical concepts of the current direct-coupled bandpass (and based on inverters) method (i.e. current since it uses CAD tools and not theoretical formulas for discontinuity characterization). The second example was carried out to show that the procedure is not subjected to a specific means of transmission, and therefore the same steps as in the previous design were followed.

This third example will be based on a circular waveguide with coaxial irises, and is not going to show again each design step, since the procedure can be understood with the two preceding examples. It aims at show that a (complete) change in the dielectric of a structure only leads to physical dimension scaling. The easiest way to understand this is through the cut-off and the resonant frequencies involved in the filter response. Hence, the cutoff frequency of the fundamental mode $TE_{11}$ in the circular waveguide with coaxial irises considered is:

$$f^1_{c_{TE_{11}}} = \frac{1.841}{2\pi a_1 \sqrt{\mu\epsilon_0\epsilon_{r1}}} \tag{5.30}$$

Now the dielectric is changed, and therefore equation 5.30 becomes:

$$f^2_{c_{TE_{11}}} = \frac{1.841}{2\pi a_2 \sqrt{\mu\epsilon_0\epsilon_{r2}}} \tag{5.31}$$

If the same dimensions are used, i.e. $a_2 = a_1$, it is clear from equations 5.30 and 5.31 that $f^1_{c_{TE_{11}}} \neq f^2_{c_{TE_{11}}}$. However, if $a_2$ is properly scaled, the value of the original cutoff frequency is preserved:

$$a_2 = a_1\sqrt{\frac{\epsilon_{r1}}{\epsilon_{r2}}} \longleftrightarrow f^2_{c_{TE_{11}}} = \frac{1.841}{2\pi a_2\sqrt{\mu\epsilon_0\epsilon_{r2}}} = \frac{1.841}{2\pi a_1\sqrt{\frac{\epsilon_{r1}}{\epsilon_{r2}}}\sqrt{\mu\epsilon_0\epsilon_{r2}}} = f^1_{c_{TE_{11}}} \tag{5.32}$$

The same kind of operations can be done in the resonant frequency formula, which was given in equation 5.19. The resonant frequency of the original filter (i.e. the one with dielectric constant $\epsilon_{r1}$) is written as:

$$f^1_{res_{TE_{111}}} = \sqrt{\left(\frac{1.841}{2\pi a_1\sqrt{\mu\epsilon_0\epsilon_{r1}}}\right)^2 + \left(\frac{q}{2d_1\sqrt{\mu\epsilon_0\epsilon_{r1}}}\right)^2} \tag{5.33}$$

Whereas the resonant frequency of the same filter with a different dielectric $\epsilon_{r2}$ is:

$$f^2_{res_{TE_{111}}} = \sqrt{\left(\frac{1.841}{2\pi a_2\sqrt{\mu\epsilon_0\epsilon_{r2}}}\right)^2 + \left(\frac{q}{2d_2\sqrt{\mu\epsilon_0\epsilon_{r2}}}\right)^2} \tag{5.34}$$

Hence, $f^2_{res_{TE_{111}}} = f^1_{res_{TE_{111}}}$ if and only if $a_2 = a_1\sqrt{\frac{\epsilon_{r1}}{\epsilon_{r2}}}$ and $d_2 = d_1\sqrt{\frac{\epsilon_{r1}}{\epsilon_{r2}}}$:

$$f^2_{res_{TE_{111}}} = \sqrt{\left(\frac{1.841}{2\pi a_1\sqrt{\frac{\epsilon_{r1}}{\epsilon_{r2}}}\sqrt{\mu\epsilon_0\epsilon_{r2}}}\right)^2 + \left(\frac{q}{2d_1\sqrt{\frac{\epsilon_{r1}}{\epsilon_{r2}}}\sqrt{\mu\epsilon_0\epsilon_{r2}}}\right)^2} = f^1_{res_{TE_{111}}} \tag{5.35}$$

Figure 5.39 provides the dimensions of a direct-coupled bandpass filter with the same specifications as in the second example, which uses air as dielectric. As before, the outer conductor is not shown, and inner conductors on the side view are filled with diagonal lines for clarification. The rest of the structure depicts the air.This dielectric choice is made on purpose, as well as the coaxial type of iris, since again this design would not be realizable for the same reason as in the stepped impedance filter of section 4.2.3 (inner conductors would be air-suspended).

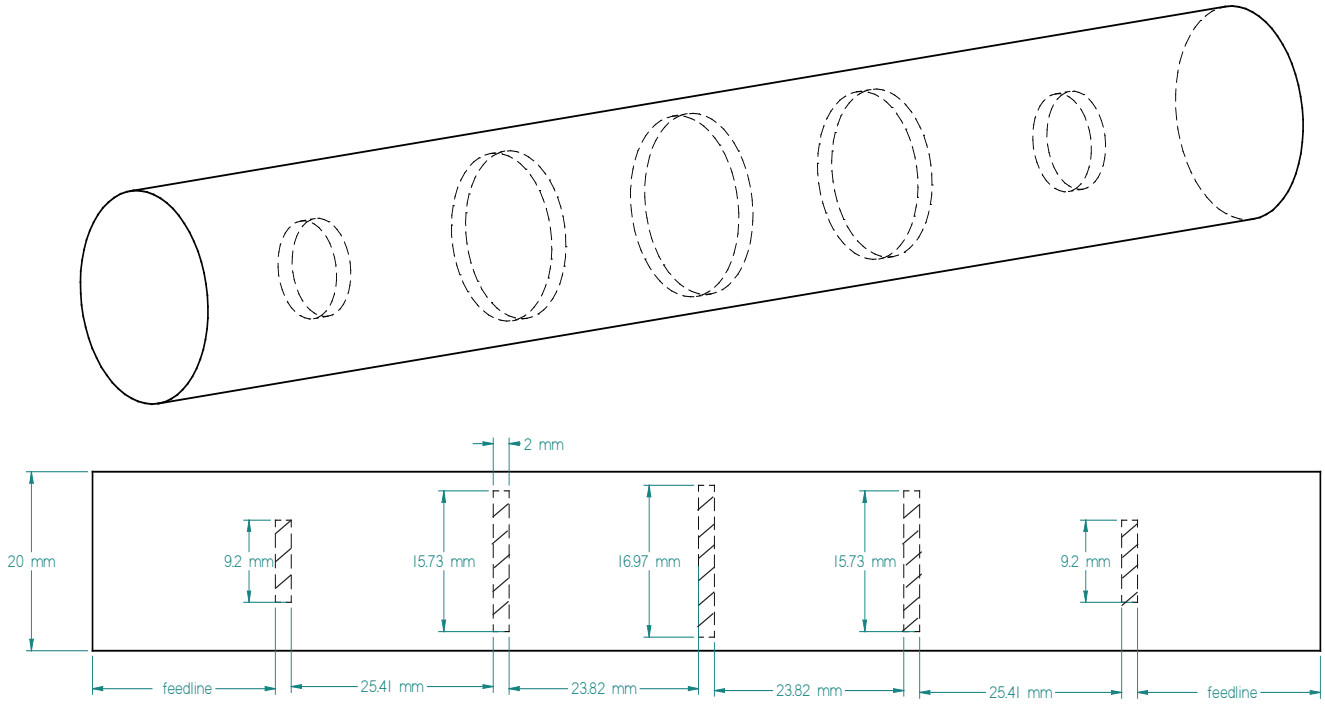


**Figure 5.39: Structure of the circular direct-coupled bandpass Chebychev filter design filled with air and coaxial irises (N=4, RL=25 dB, R0=50 ohms, f0=11GHz, $\triangle = 2.73\%$)**

Figure 5.40 shows the corresponding dimensions of the same filter with a dielectric constant of $\epsilon_r = 2.1$. Since the original design was filled with air and therefore had $\epsilon_r = 1$, the longitudinal and the transversal dimensions are divided by a factor of $\sqrt{2.1}$.

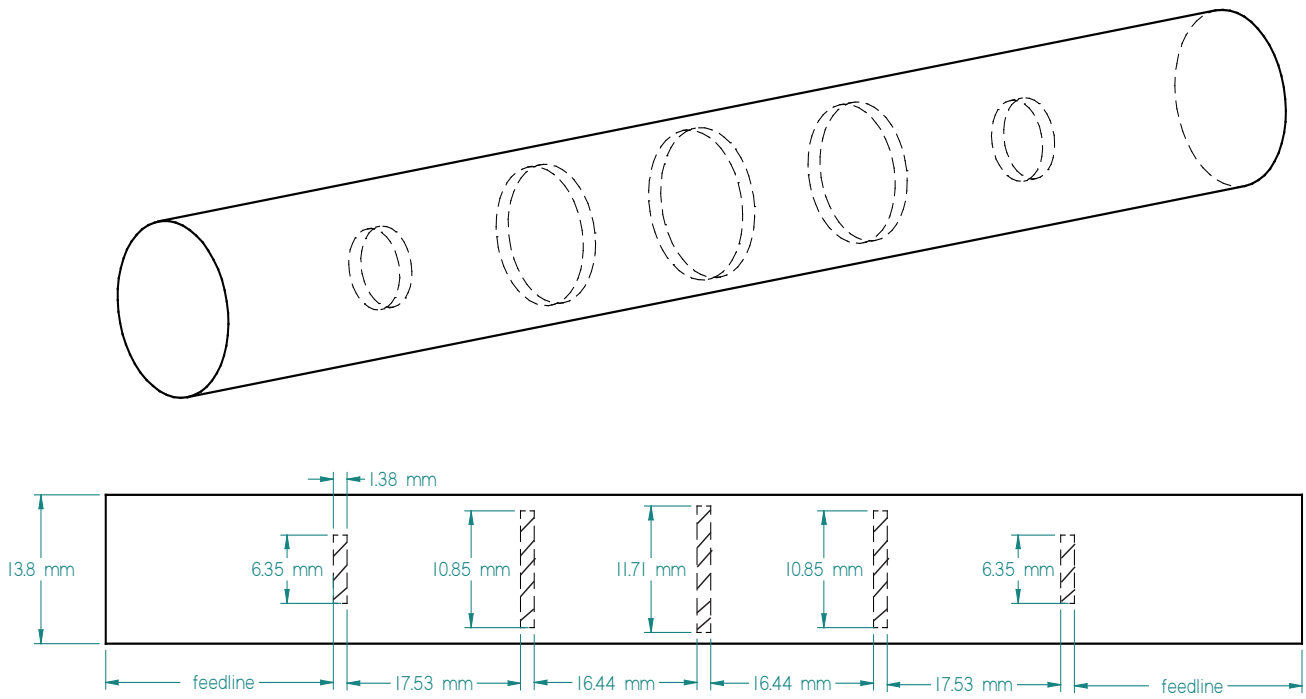


**Figure 5.40: Structure of the circular direct-coupled bandpass Chebychev filter design filled with teflon ($\epsilon_r = 2.1$) and coaxial irises (N=4, RL=25 dB, R0=50 ohms, f0=11GHz, $\triangle = 2.73\%$)**

It can be seen in the full-wave simulator that the same frequency response is achieved, which is given in figure 5.41

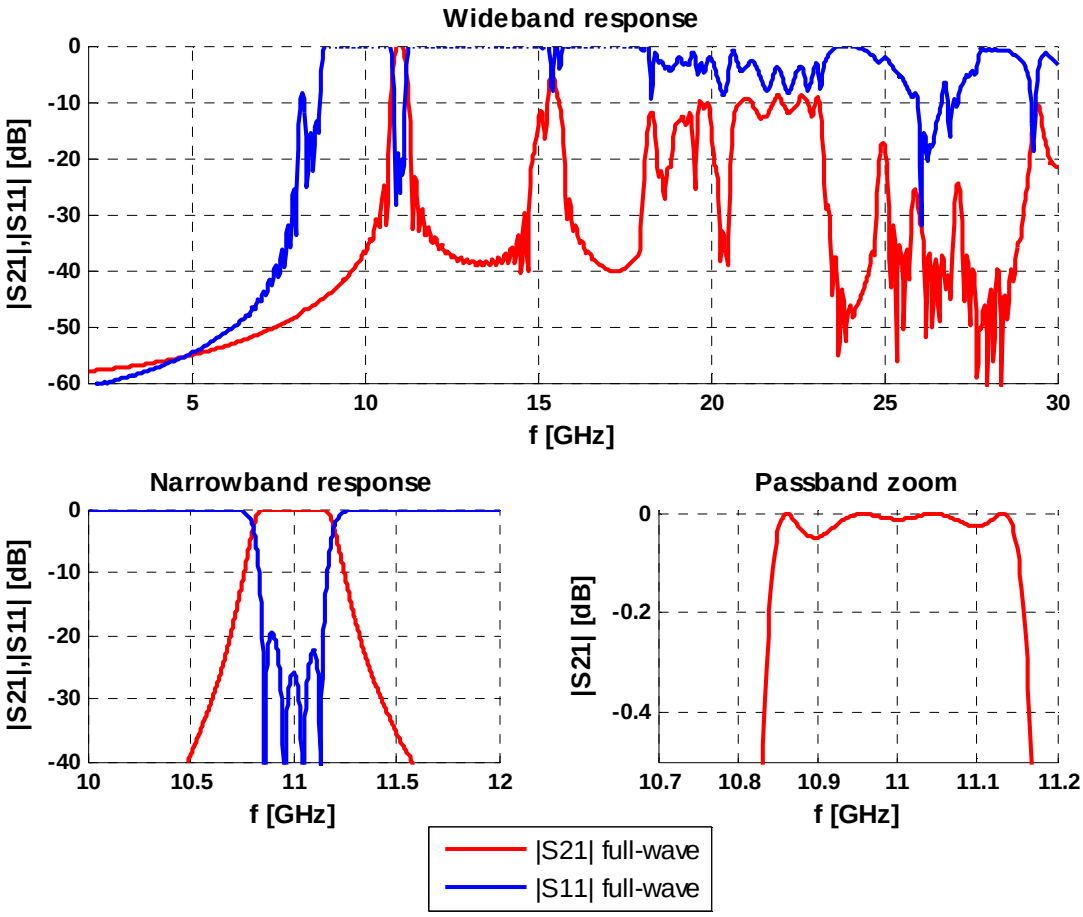


**Figure 5.41: Full-wave response of the circular direct-coupled bandpass Chebychev filter design filled with teflon ($\epsilon_r = 2.1$) and coaxial irises (N=4,RL=25 dB, R0=50 ohms, f0=11GHz, $\triangle = 2.73\%$)**

Finally, it must be reinforced the idea that although it was used a specific example of a circular waveguide filter with coaxial irises to show how scaling works, this explanation can be applied to any kind of structure. Furthermore, this kind of reasoning can be applied likewise to move the bandpass of a filter into another frequency without having to do a different design (if the fractional bandwidth is preserved and the design is not taking into account the filter losses).

# 6
# The Combline Filter

Bandpass filters are the most common filters at microwave frequencies. A specific design methodology was proposed in chapter 5. However, it involved analysing the type of discontinuity used to couple resonators. This feature makes it unsuitable for some kind of filters.

This is the case of the combline filter, whose design is the aim of this chapter. For that reason an alternative method based on sequential stages is developed here. In this scenario, optimization becomes a key tool to reach the level of refinement required in each stage. The results attained have been published in the Congress on Numerical Methods, Lisbon 2015 (in a paper entitled *"Optimization method for the design of microwave filters based on sequential stages"*).

## 6.1 The combline cavity resonator

Several microwave books describe combline filters built in planar technology (usually microstrip) [2], [10]. However, the adjective "combline" is not associated with a particular kind of technology but to a configuration of transmission line resonators resembling a comb. In fact, this work will pursue the design of a combline cavity filter, and not of a planar one. This way better performance in terms of power handling and losses is expected, although the design will be obviously bulkier and more expensive that its counterpart in printed technology.

In a microstrip filter the mode in charge of the power transmission is a quasi-TEM mode (usually directly treated as TEM). Since a combline cavity filter must be somehow based on the same principles, a TEM mode will have again the leading role. For that reason, the combline cavity must have two conductors (i.e. an internal post and the outer enclosure), in order to set a potential difference (see figure 6.1, where the inner post is depicted with dashed lines and the enclosure is depicted as in the previous chapter, with a infinitesimally thin wall). The

metallic post is shorted at one end with the enclosure, and its length is slightly shorter than a quarter of wavelength at the centre frequency of the filter [11].

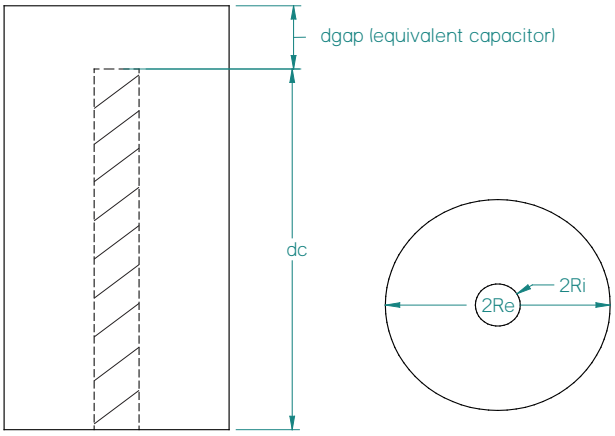


**Figure 6.1: Combline resonator**

The previous resonator can be understood with a simple circuital model: a transmission line ended in a capacitor (see figure 6.2). Such capacitor arises because of the gap formed between the end of the line and the enclosure.

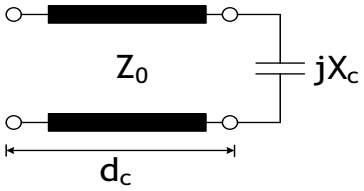


**Figure 6.2: Equivalent circuit model for a combline resonator**

This way, although chapter 5 studied the resonance frequency in terms of the fields, in this case the circuital approach is enough to find the resonance frequency. Therefore, if the circuital resonance condition is applied in figure 6.2:

$$Z_{in}(z) = Z_0 \cdot \frac{1+\rho(z)}{1-\rho(z)} = 0 \qquad \longleftrightarrow \qquad \rho(z) = -1 \qquad \longleftrightarrow \qquad |\rho(z)|e^{j\phi_L}e^{-2\beta d_c} = -1 \quad (6.1)$$

Since the magnitude of reflection coefficient $\rho_L$ of a reactive load is equal to unity, equation 6.1 leads to:

$$e^{j(\phi_L - 2\beta d_c)} = e^{j(\pi \pm 2k\pi)} \qquad \text{with k=0,1,...} \qquad \longleftrightarrow \qquad \phi_L - 2\underbrace{\beta d_c}_{\theta} = \pi \pm 2k\pi \qquad (6.2)$$

Taking into account that the load of figure 6.2 is capacitive, the reflection coefficient is computed as:

$$\rho_L = \frac{Z_L - Z_0}{Z_L + Z_0} = \frac{\frac{1}{jB} - Z_0}{\frac{1}{jB} + Z_0} = \frac{1 - jBZ_0}{1 + jBZ_0} \tag{6.3}$$

And therefore the phase of the reflection coefficient is computed as:

$$\phi_L = \tan^{-1}(-BZ_0) - \tan^{-1}(BZ_0), \tag{6.4}$$

which in turn will always have a negative value.

Regarding the electrical length associated with resonance, using equations 6.2 and 6.4 can be calculated as:

$$\theta = \frac{\phi_L - (\pi - 2k\pi)}{2} \quad \text{with k=1,...} \tag{6.5}$$

And finally, the resonance frequency can be computed from the preceding equation as:

$$f_{res} = \frac{\phi_L - (\pi - 2k\pi)c}{4\pi d_c} \quad \text{with k=1,... and } c = \frac{1}{\sqrt{\mu\epsilon}} \tag{6.6}$$

At this point, the reader can easily deduce the physical effects related to the influence of the the transmission line length and the value of the equivalent formed capacitor:

⇒ Equation 6.6 evidences that given a certain gap in the structure of figure 6.1, and therefore a specific phase of the reflection coefficient $\phi_L$, shorten the physical length $d_c$ of the transmission line produces a higher resonance frequency. Conversely, lengthen $d_c$ decreases it.

⇒ The formed gap can be compared to a parallel plate capacitor whose capacitance is inversely proportional to the distance between the plates. Thus, as the gap becomes smaller, the capacitance is increased. Again, by means of equation 6.6 it can be seen that given a certain physical length of the transmission line $d_c$, if the $d_{gap}$ is decreased the resonance frequency is decreased as well, and vice versa.

## 6.2 Statement of the design problem

In order to design a combline filter, the cavities (i.e. resonators) must be coupled by means of an open region between them. In the circuit model, these apertures, also called windows or irises are represented by inverters (recall chapter 5).

The physical dimensions involved in the design process are: the inner lengths of the posts ($L_{in}$), the height of the coaxial feed lines at the input/output ($h_f$) and the distance between

resonators ($d_{cn}$). The subscript "n" is used to reference each post and each distance since they can be different for each resonator (or pair of resonators in the case of distances).The radius of the cavities ($R_e$), the inner posts ($R_i$) and the feeds ($R_{ce}$,$R_{ci}$) are considered as fixed parameters previously set in a stage focused on the cavity design. Figure 6.3 depicts all these parameters for the physical structure representing a sixth-order filter, which can be used to synthesize a Chebychev filtering response. The filter is symmetric with respect to plane yz and plane xy, and thus, only the dimensions of half of the filter need to be specified.

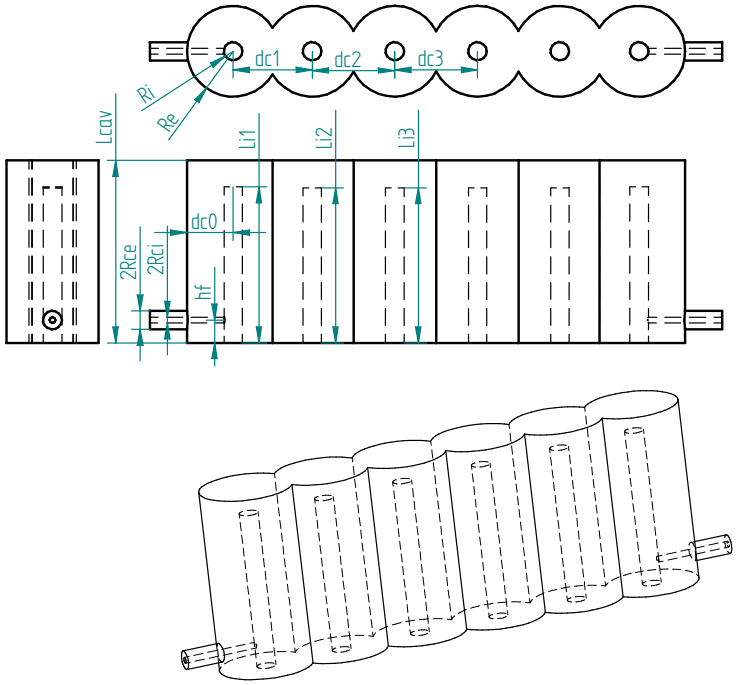


**Figure 6.3: Physical dimensions involved in the design of a combline microwave filter, and main views of the structure**

The design process must provide the physical dimensions of a structure like the one shown in figure 6.3, whose full-wave response fulfils the aimed circuital filtering response set as a goal.

### 6.2.1 The method developed

As a summary, the filter design problem can be stated as: given the coupling values ($M_{ij}$), the centre frequency ($f_0$) and the fractional bandwidth ($\triangle$) of the desired circuit filtering response, find the dimensions $L_{in}$, $h_f$, and $d_{cn}$ of a physical combline structure whose full-wave matches (approximates) it.

However, filter design of microwave cavity filters should avoid problems with a large number of variables, since full-wave responses are very time consuming and demand a lot of RAM in the computer. Hence, in spite of considering the whole design structure from the beginning,

this chapter addresses the strategy of subdividing the design process into minor stages , each of which takes into account less degrees of freedom (i.e. parameters of design) than in a direct global design. It is certainly a "divide and conquer" strategy. Each stage uses the results obtained in the previous one, which takes into account a lower number of design elements. The evolution from one stage to another occurs when the full-wave response and the one obtained from the equivalent circuit model are ideally coincident.

Furthermore, another advantage of this methodology consists in removing the need to distinguish and characterize the inverters in the structure (i.e. as in chapter 5 was done). Since the comparison involves the response of the whole simulated partial structure and the response of its equivalent circuit model, the resonator-inverter differentiation is not a requirement anymore. This method is extremely useful in that sense, since isolating the involved discontinuities and (or) characterize them is not always an affordable task. As an example, combline filters are sometimes designed with topologies where irises are not differentiated, resulting in a blurred line between resonators and inverters (see figure 6.4).

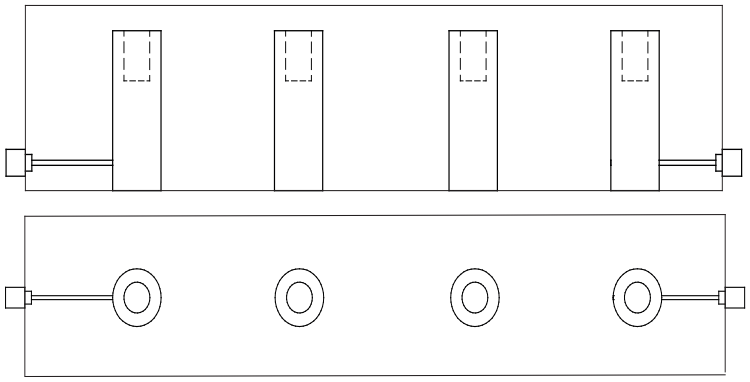

**Figure 6.4: Example of a combline filter without irises**

Just for the sake of clarification, it must be remarked that the inverters in the preceding structure (and obviously in any) are conceptually represented by the field coupling between cavities (see figure 6.5). Thus, every required circuital coupling coefficient of the coupling matrix has to do with a ratio of coupled energy to stored energy which is computed as:

$$k_{physical} = \frac{\int_v \epsilon \vec{E_1} \cdot \vec{E_2} dv}{\sqrt{\int_v \epsilon |\vec{E_1}|^2 dv \text{ x } \int_v \epsilon |\vec{E_2}|^2 dv}} + \frac{\int_v \mu \vec{H_1} \cdot \vec{H_2} dv}{\sqrt{\int_v \mu |\vec{H_1}|^2 dv \text{ x } \int_v \mu |\vec{H_2}|^2 dv}} \tag{6.7}$$

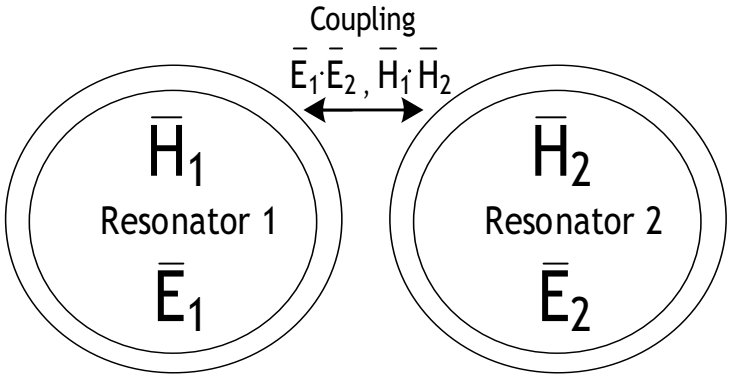


**Figure 6.5: Physical coupling conceptual diagram**

However, it is again reinforced the idea that because of the proposed design method, this physical coupling is not needed to be calculated except if the designer wants to check out if the structure used can provide the required levels of coupling [1],[2].

### 6.2.2 The role of optimization

Optimization has been used in the preceding chapter to improve the responses obtained after an initial design. However, its usage is in this method more restrictive: in this case it is not enough to obtain certain levels of power reflection or transmission (except for the last stage). In this method based on sequential stages, after a manual-coarse adjustment of the filter parameters the optimization tool is used as a process of refinement to ideally achieve the circuital partial response.

Bearing in mind that difference , again (i.e. as in the previous chapter) each stage design can be mathematically understood as a problem in which the physical parameters of the structure are variables which lead to an optimal solution – the one implementing the circuit response identified as a target. Three tools are involved in the optimization process: the cost function, the target mask and the optimization algorithm.

The physical dimensions already presented are the variables upon which the cost function is dependent. The function to be minimized is the following, comparing the full-wave and circuit responses (given by its S-parameters) at some selected critical frequencies:

$$f(\vec{x}) = \sum_{i=1}^{N} \alpha_i (|S_{21}^{full-wave}(f_i)|^2 - |S_{21}^{circuital}(f_i)|^2) + \sum_{j=1}^{M} \beta_i (|S_{11}^{full-wave}(f_i)|^2 - |S_{11}^{circuital}(f_i)|^2) \tag{6.8}$$

where $\vec{x}$ will be the optimization variables at each stage.

The previous cost function is assessed in terms of discrete frequencies conveniently chosen by the designer depending on the optimization stage [12]. These frequencies are also involved in the second tool, which is fundamental for the optimization process – the mask. This work presents

several mask types in order to attain the target circuit responses.

Finally, the algorithm [13] used to minimize the cost function is the third and last tool of the process. It must be remarked that this approach offers one main benefit: the designs show lower uncertainty levels in terms of the physical parameters of the structure as opposed to a design that take into account the full structure from the very beginning. In this way a coarse adjustment is more easily obtained as a good starting point for optimization, which in turn translates into the optimization tool being closer to the optimal solution. This does not only mean a lower number of iterations, but also that a local-deterministic algorithm suffices to obtain the desired response. This process may result in even more benefits for filters with more complex coupling arrangements.

## 6.3 Applied filter design

In order to validate the proposed design approach, a sixth-order Chebychev filter, with 20 dB of return loss is proposed. It is centred at $f_0$=2 GHz with 1% of fractional bandwidth, and the feed lines are sma connectors of 50 ohms. This would be a typical scenario for narrow-band filters used in base stations for wireless communications [14].

### 6.3.1 Cavity design

Before starting to couple the resonators following the selected stages (which will be seen in subsection 6.3.2), the resonator used in the design must be selected. Its choice pursues three main goals: to have the resonance frequency at $f_0$, to achieve a wide spurious-free window, and to reach a high unloaded quality factor (which is a ratio between the stored energy and the losses [7], [5]).

The resonator of a combline filter (seen in section 6.1) is different from other resonators such as the rectangular/circular waveguide ones seen in chapter 2, since its resonance frequencies are not analytical (and hence equation 5.19 can not be directly applied). Thus, a numerical method must be used in this case to find them, such as the one provided by the eigenmode solver of CST Microwave Studio. However,the usage of a numerical method is not synonym of a blind search. The effects of lengthening or shortening $d$ and $d_{gap}$ can be understood applying the reasoning followed in section 6.1.

One possibility to design the combline cavity is to start with $d_c = \lambda_g/4$ and an arbitrary $d_{gap}$. As it was mentioned in section 6.1, as the distance of the gap ($d_{gap}$) is larger, the capacitance formed at the end of the cavity is decreased, and therefore the loading impedance of the equivalent transmission line tends to infinity (recall the circuit model in 6.1). However, due to this behaviour it is clear that the resonance frequency $f_0$ used to compute $d = \lambda_g/4$ will

never be achieved, since an open-circuit at the end of the cavity is an idealization. However, using as well variable $d_{gap}$ the desired resonance frequency can be obtained. Indeed, section 6.1 showed that the resonance frequency can be increased as well by shortening the length $d_c$. And of course, at the same time the frequency is being adjusted, the designer must be aware of the changes in the quality factor and the spurious window in order to make appropriate decisions.

The other variables that have not been mentioned yet are the inner ($R_i$) and the outer radius ($R_e$). They can be chosen to noticeably improve the quality factor. Considering a certain outer radius, lengthening or shortening the inner radius changes the quality factor. It is not easy to predict its behaviour, since in the end it is a trade-off between how strong become the fields in the inner post (recall $|\vec{E}| \sim \frac{1}{R_i}$) and whether the inner volume of the cavity allows to store such amount of energy that it overcomes the losses in the metallic walls leading to a good quality factor, or not.

In a pure coaxial line the resonance frequency does not depend on the transversal section (i.e. on the radius). However, it is evident that in the combline cavity the resonance frequency is a little bit modified, since if the inner radius is very small the "parallel plates" formed at the end begin to disappear. For that reason, after setting the most convenient radius, the lengths of either the post or the gap need to be slightly changed again to recover the desired frequency $f_0$.

Using this strategy, the dimensions shown in figure 6.6 are set.

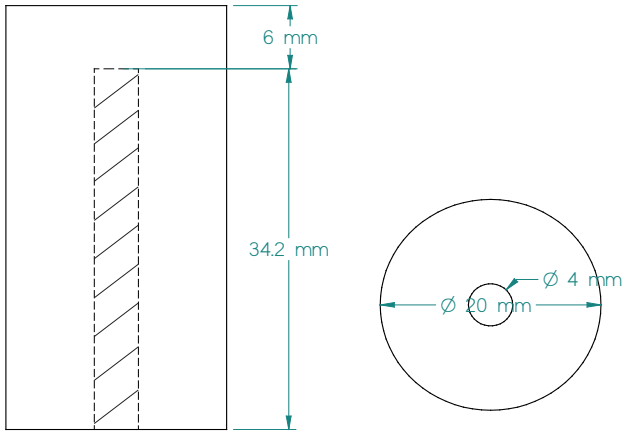


**Figure 6.6: Selected combline resonator**

However, it must be underlined that other strategies can be followed. In fact, there is not any practical reason to set $\lambda_g/4$ as the initial length of $d_c$. The designer can choose an initial length of the enclosure (i.e. $d_c + d_{gap}$, called as $L_{cav}$ in figure 6.3) and then shorten or lengthen the inner post. The lowest limit in order to choose the total height of the enclosure is approximately

at about $\lambda_g/8$.

Choosing smaller enclosures lead to more compact structures and the spurious-free window tend to be noticeably wider. On the other hand, higher quality factors are in general achieved when bigger enclosures are selected.

### 6.3.2 Strategic selection of the sequential stages

The case under consideration will be an inline structure, where the coupling matrix reduces only to the couplings between adjacent resonators. For a symmetric sixth-order filter, only three values are needed: $M_{12} = M_{56}$ ($K_{12} = K_{56}$), $M_{23} = M_{45}$ ($K_{23} = K_{45}$) and $M_{34}$ ($K_{34}$). They are mainly controlled by $d_{c1}$,$d_{c2}$ and $d_{c3}$ respectively. Input/output couplings $M_{in} = M_{out}$ are controlled by $h_f$, and the resonant frequency of the cavities will be determined by $L_{i1}$,$L_{i2}$ and $L_{i3}$. In the case under consideration $M_{12}$=0.843, $M_{23}$=0.611, $M_{34}$=0.583, $M_{in}$=$M_{out}$=1.002.

As it has already been mentioned, in each design stage a part of the structure is selected and the electromagnetic simulation is compared with the ideal circuital response correspondent to that part. It is important to select the stages so that the preceding achieved dimensions are not completely changed.

For convenience the selected stages can be represented by means of the pertinent diagram of figure 6.7, in which circles represent cavities and $M_{ij}$ ($K_{ij}$) describes the coupling (inverters in the circuit model) between resonators (as in subsection 5.1.4).

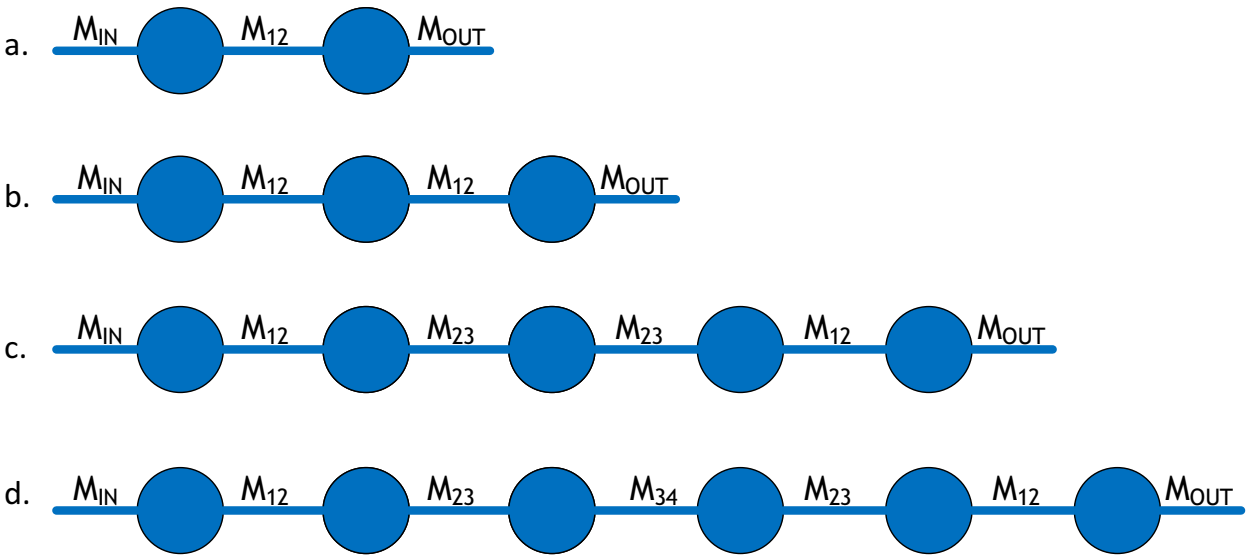


**Figure 6.7: Schematic representation of the stages of the filter design: a. first stage, b. second stage, c. third stage, d. fourth stage (final desired filter)**

### 6.3.3 The optimization tool

In subsection 6.3.4 it will be shown that the first of the stages does not need optimization, and that CST MWS is used in the second stage. However, the third of the stages was undoubtedly the more complicated. For that reason an optimization tool was developed: to gain better control of the process.

It allows to set the desired optimization parameters from a simple interface created with MATLAB GUI, to use its algorithms and finally call CST as a full wave simulator (and not as a full wave optimizer). Figures 6.8, 6.9 and 6.10, depict the three types of optimization masks that can be defined. Appendix F shows enlarged images. They will be applied in subsection 6.3.4.

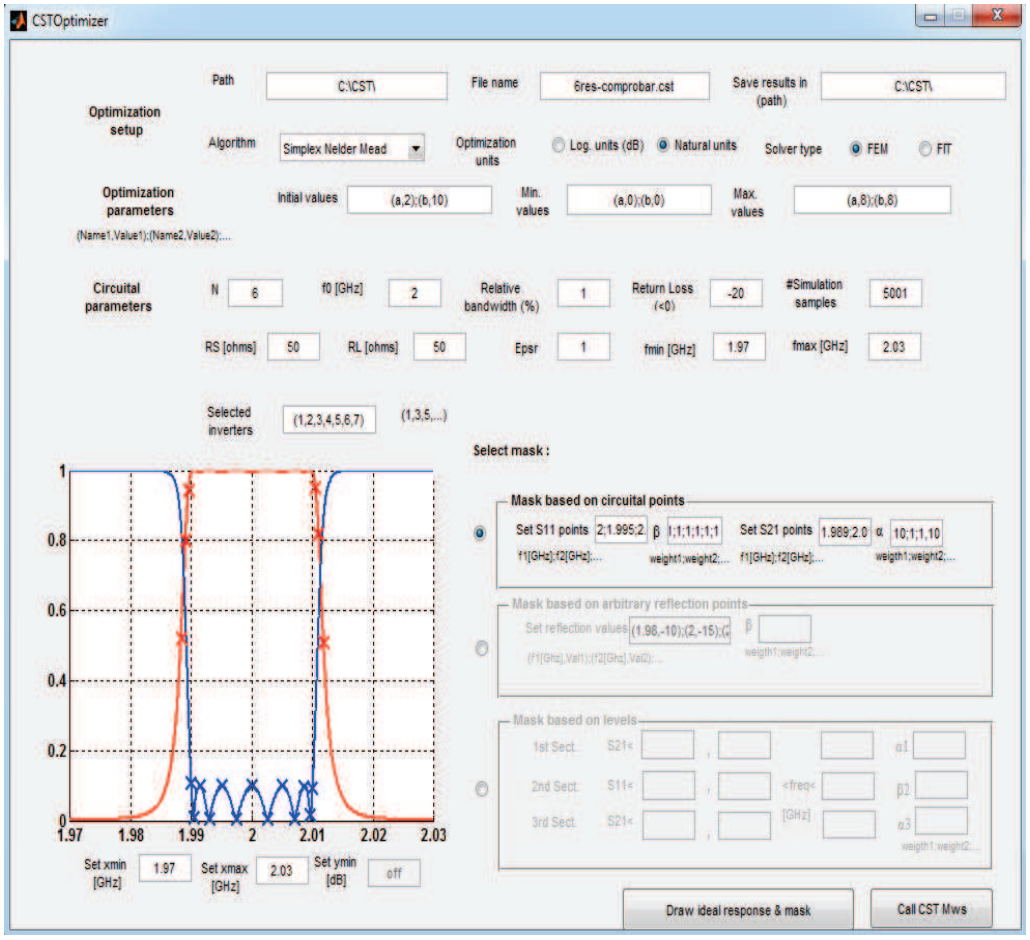


**Figure 6.8: Optimization tool first example.**

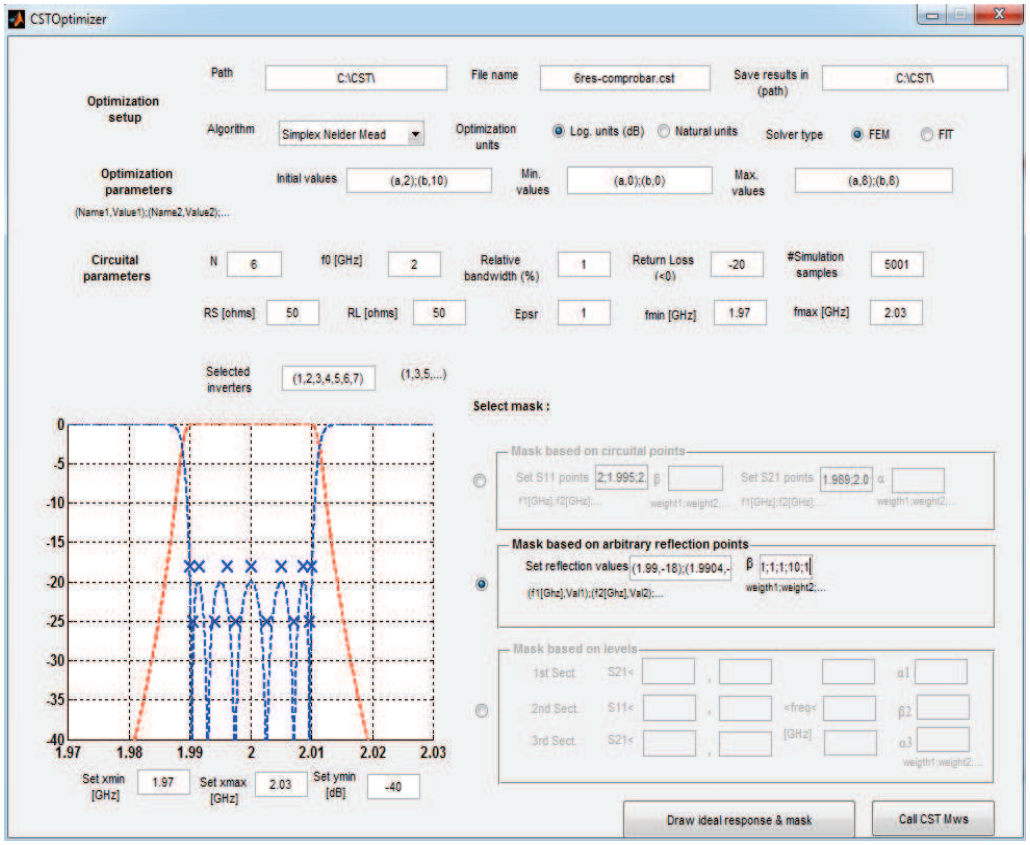


**Figure 6.9: Optimization tool second example**

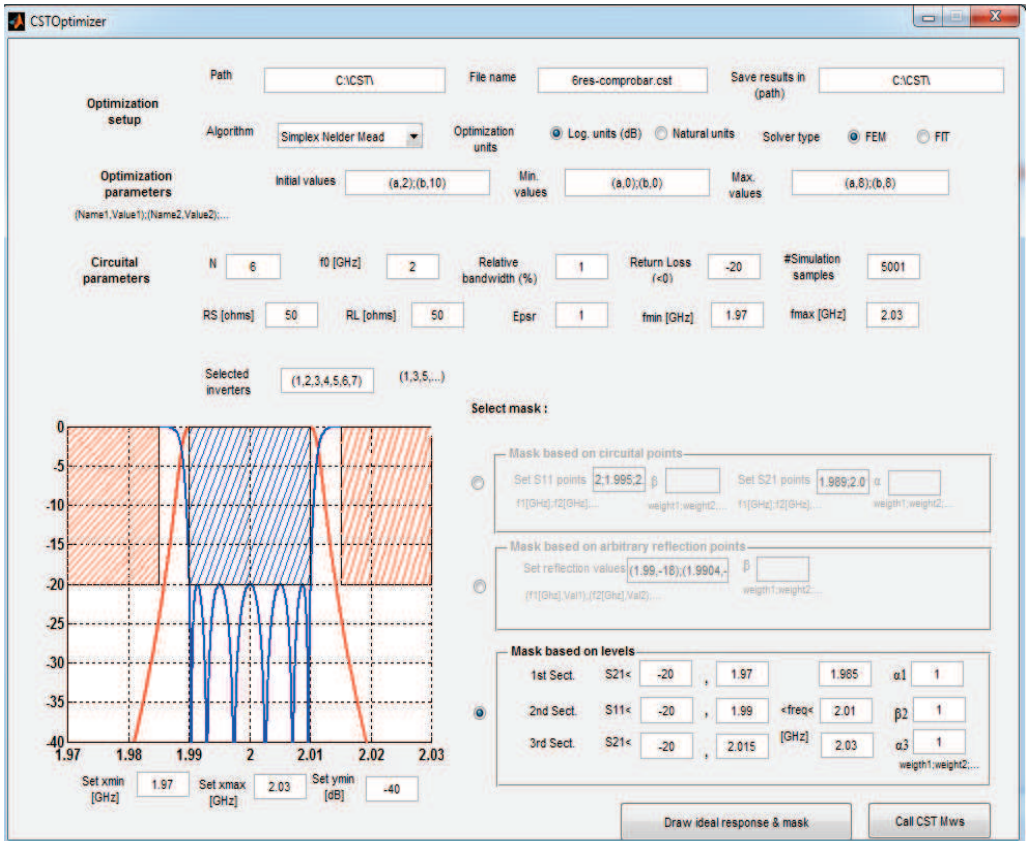


**Figure 6.10: Optimization tool third example**

### 6.3.4 Optimization process based on sequential-stages

The combination of the three optimization tools (cost function, mask and algorithm) during the fourth selected stages of design is presented below. In the stages over which the optimization process takes place, simplex algorithm by Nelder Mead is used [13], except in the second stage, in which Trust Region Framework is used.

Dimensions obtained at the end of each stage become the starting point of the next one. In all the stages, an initial task of coarse approximation of the physical parameters incorporated at that stage (and not used in previous stages) is done before the starting the optimization process. Initial values for all the variables can be found using models as those in [15],[16].

During the stages, the cost function is evaluated with the S parameters in natural units or in logarithmic (dB) units. The representation in the figures will be realized in the domain used for the optimization.

**First stage**

The first step in the design process takes exclusively into account the two resonators placed at both ends of the structure (see figures 6.7.a. and 6.11.a.) Thanks to the small number of variables present at this stage (i.e. only $h_f$, $d_{c1}$ and $L_{i1}$, because of the xy-plane symmetry of the structure), even the optimization tool can be replaced by a parametric sweep. The result is shown in figure 6.11.b., where from now on the label "f.w." refers to full wave response and the label "circ." to circuit response.

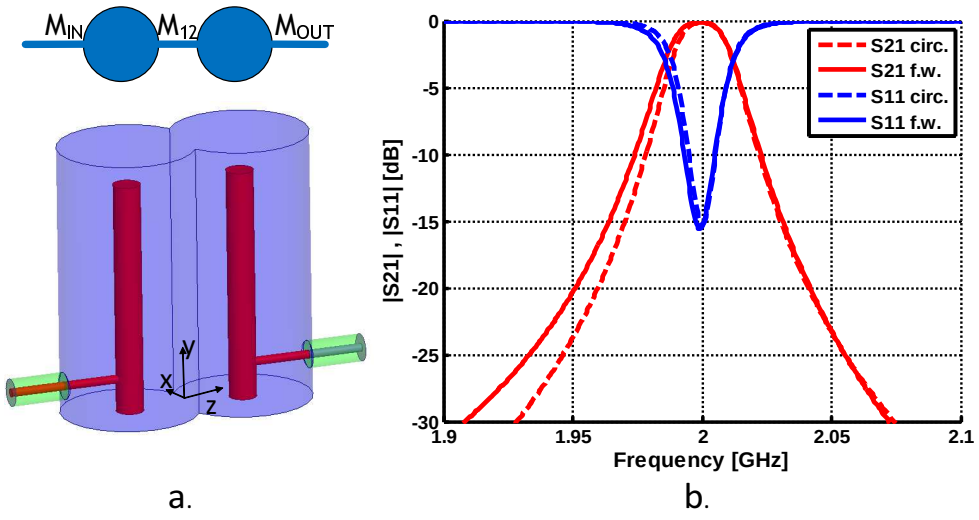


**Figure 6.11: First stage. a. Simulated physical structure b.End of the first stage**

**Second stage**

At this stage the three resonators shown in figures 6.7.b. and 6.12.a. are studied. The physical design parameters involved are $h_f$, $d_{c1}$, $L_{i1}$ and $L_{i2}$. This last variable is the only dimension that was not present at the previous stage. Thus, the goal of this stage is to set the right value for $L_{i2}$, while the values of $h_f$, $d_{c1}$,and $L_{i1}$ are slightly refined due to the loading effect of the new resonator not considered at the first stage. This is one of the advantages of this strategy: at each stage, new variables are introduced gradually, while previous ones are refined at the same time, and the complexity is increased very smoothly.

Moreover, for our particular case the target circuit response at this stage is very similar to the response of a third-order filter designed to achieve the same reflection. Since their values do not differ greatly, and the bandwidth obtained in the former is much wider than in the latter, it is decided to use a section mask based on the latter, which is less restrictive. Additional resonators incorporated in the following stages will cooperate to achieve the desired mask. In this particular premature partial stage this is not essential.

The result of the optimization process is shown in figure 6.12.b. together with the details of the mask used by sections only for the reflection. The following weights are used for the cost function by sections $\beta_{section\ 1,3,5} = 0.4$, $\beta_{section\ 2,4} = 0.75$.

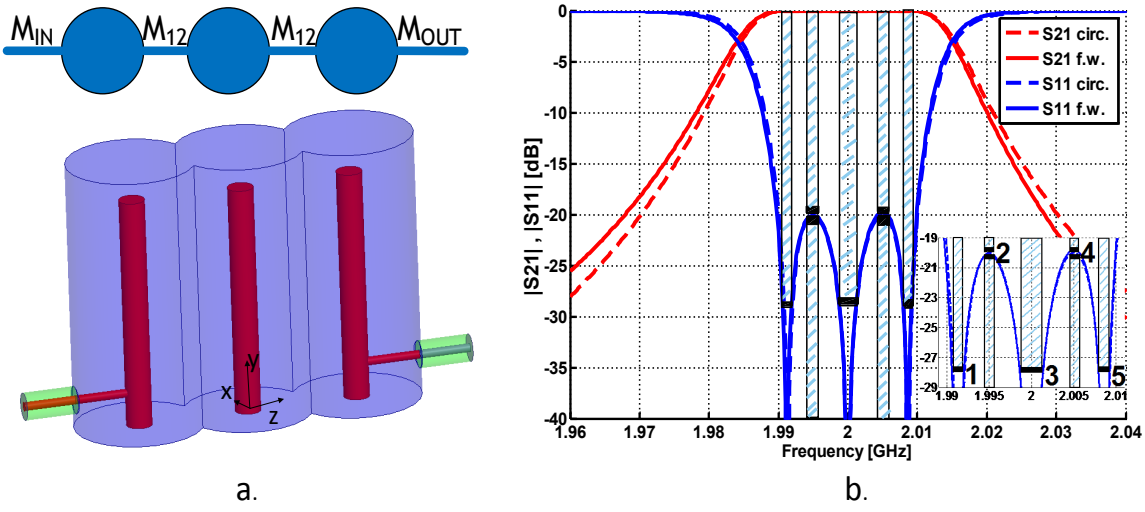


**Figure 6.12: Second stage. a. Simulated physical structure b.End of the second stage**

**Third stage**

In the third stage, the five resonators detailed in figure 6.7.c. are used. The physical design parameters involved now are $h_f$, $d_{c1}$, $d_{c2}$, $L_{i1}$, $L_{i2}$ and $L_{i3}$ (again only half of the structure because of the xy-symmetry). The physical structure associated with this stage is given in figure 6.13. Figure 6.14.a. shows the immediately preceding point to the optimization process (i.e. after the manual-coarse adjustment).

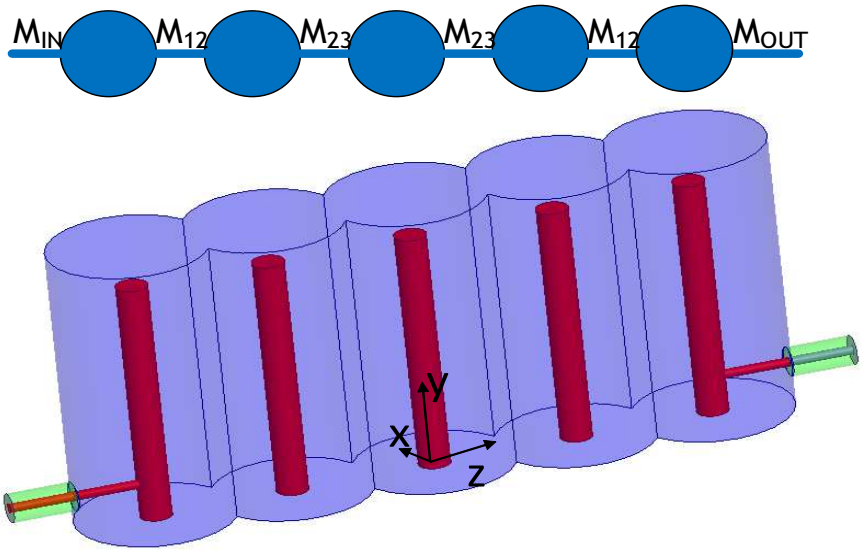


**Figure 6.13: Simulated physical structure of the third stage.**

Changing from three to five resonators entails a large variation of the loading effect seen by each resonator, which implies a more cumbersome refining process than in the previous stage. Therefore, the optimization work is carried out in several iterations by masks seeking to enhance and correct several aspects of the full-wave response until a trade-off situation is reached. In this context, it is fundamental to define suitable weights $\alpha_i$ and $\beta_i$ in the cost function. To this end dotted masks instead of section masks are widely used, since the complex nature of this stage requires a more precise control over the selected weights. When dotted masks are used, such dots are depicted by crosses on the target response to which they belong.

Figure 6.14.b. shows how a dotted circuital optimization mask overlaps with the starting point response in natural units. This mask aims at recovering the transmission bandwidth, and therefore the selected weights are $\alpha_{1...6,\neq 3,4} = 1$, $\alpha_{3,4} = 10$, $\beta_{1...11} = 1$.

Figure 6.14.c. depicts a circuital optimization mask based on levels that has been selected with the purpose of allowing the remaining two reflection zeros to appear. This aims at avoiding

that the highly restrictive dotted mask prevents them from appearing. The following weights by sections are used: $\alpha_{section\ 1} = 100$, $\alpha_{section\ 2} = 150$ , $\beta_{unique\ section} = 1$.

Figure 6.14.d. shows the response obtained after the use of the preceding mask, whose primary objective was to locate the remaining two reflection zeros. The algorithm evolution over that iteration did not show the five reflection zeros, but at least a fourth zero was obtained (figure 6.14.d. is detailed in logarithmic units for the purpose of noticeably displaying the achieved reflection zeros).

Several intermediate iterations are done with dotted circuital masks whose main goal is to obtain the remaining reflection zeros and to keep the achieved transmission bandwidth. It is important to highlight that sometimes the weights (i.e. $\alpha_i$, $\beta_i$) selected lead to the lack of one of the reflection zeros, but this iterative process requires taking such decisions in order to avoid a stalled process.

Once the reflection adjustment reaches the desired five reflection zeros without an unreasonable bandwidth widening in transmission, the response depicted in figure 6.14.e. is obtained. This response is shown overlapped with a family scanning dotted circuital optimization mask. It aims at observing the natural evolution of the algorithm in order to locate filters within the same family of solutions. To this end all dots present unit weight: $\alpha_{1...6} = 1$, $\beta_{1...11} = 1$.

Upon completion of the previous mask, the filtering response is represented in 6.14.f. It is considered a response close enough to the ideal objective circuital.

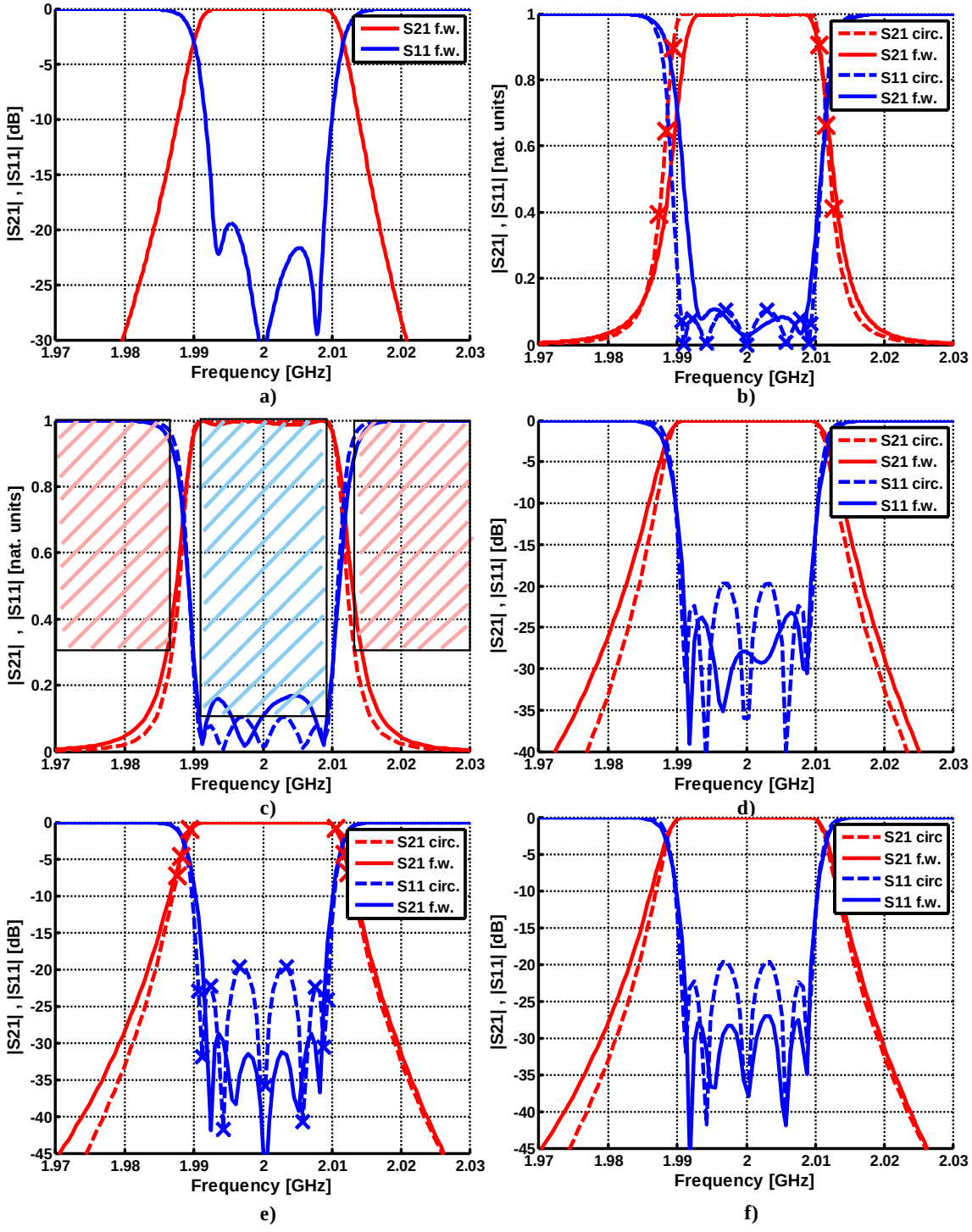


**Figure 6.14: Responses of the most representative iterations of the third stage**

**Fourth stage**

This is the fourth and last stage, where the whole filtering structure is considered. The main views of such structure can be seen in figure 6.15.

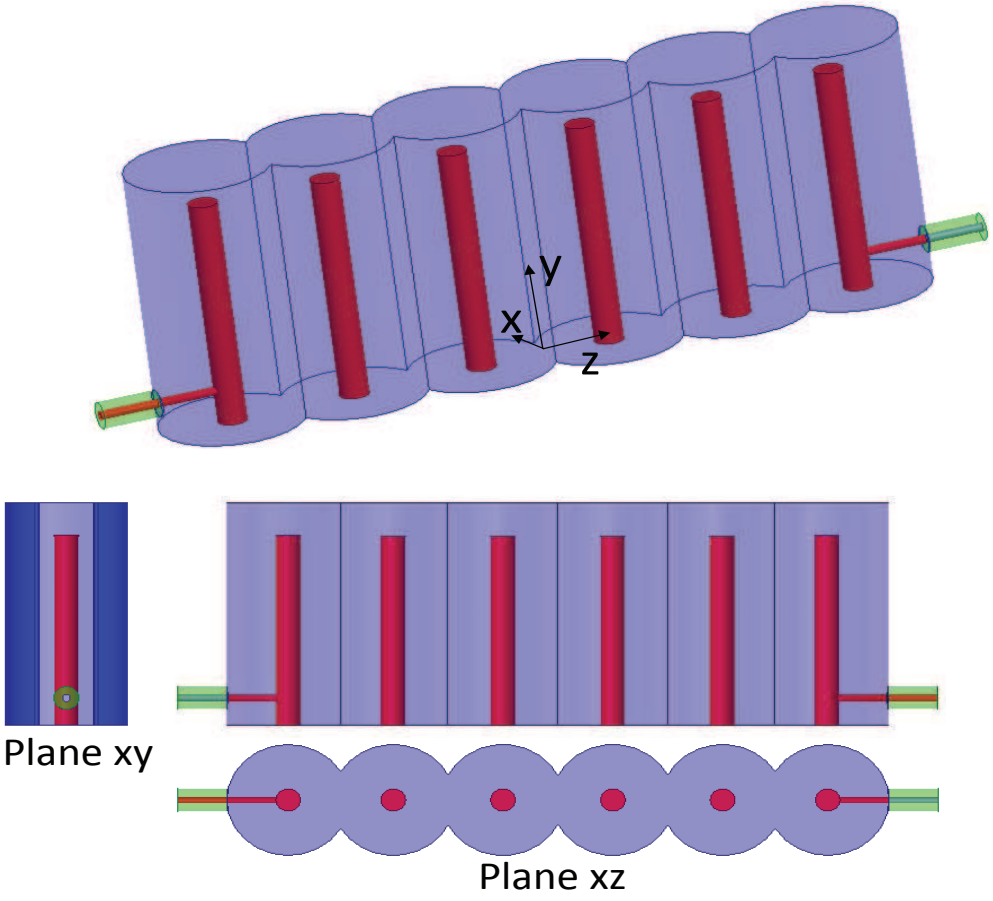


**Figure 6.15: Main views of the final filter**

Although this stage involves the same number of design parameters as in a direct global strategy (i.e. $h_f$, $d_{c1}$, $d_{c2}$, $d_{c3}$, $L_{i1}$, $L_{i2}$ and $L_{i3}$ due to the symmetry of the structure), those variables which were involved in the foregoing stage already have a value very close to the final optimal solution. This was the goal of previous stages.

The success of the method proposed in this chapter becomes evident when it is obtained the response given in figure 6.16 when the process of manual-coarse adjustment was going to be carried out (i.e. at the very beginning of that process). As it was remarked in subsection 6.2.2, the previous stages sought the best match between the partial circuital response and the full wave response. For that reason, not only the reflection level and the selectivity of the filter were pursued but the specific number of reflection zeros as well. However, at this final stage this is not mandatory as the aim of the whole filter design process from the industry side may

be formulated in terms of a mask of reflection and rejection, and not to the aforementioned zeros. In that sense this stage differs from the preceding ones, and conversely, it is similar to the optimization processes carried out in chapters 4 and 5. Therefore, if optimization had been needed at this stage, it would be perfectly correct to use a level-based mask at this stage instead.

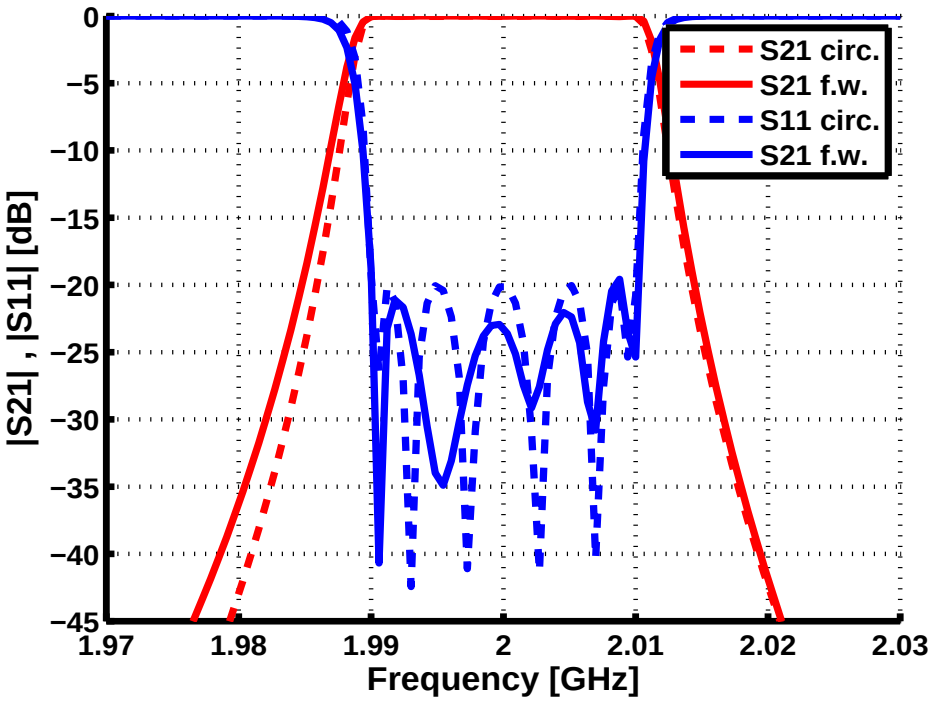


**Figure 6.16: Filter response of the final structure obtained with the proposed optimization strategy**

At this point, it is important to mention that the electromagnetic simulation software used throughout all the stages of the design process used settings oriented to the attainment of fast but relatively imprecise results. The underlying reason of this decision is that it was considered preferable to allow the optimization process to make more evaluations and therefore grant the possibility of finding out the behaviour of the selected mask to correct it if needed.

However, any final design must guarantee that the simulated response matches with reality. Accordingly, studying the convergence of the designed structure is a must. Since the FEM algorithm was used, this is directly translated into an increased number of meshing passes. Figure 6.16 shows the result achieved after the mentioned convergence process. Figure 6.17 gathers the final physical parameters of the design filter.

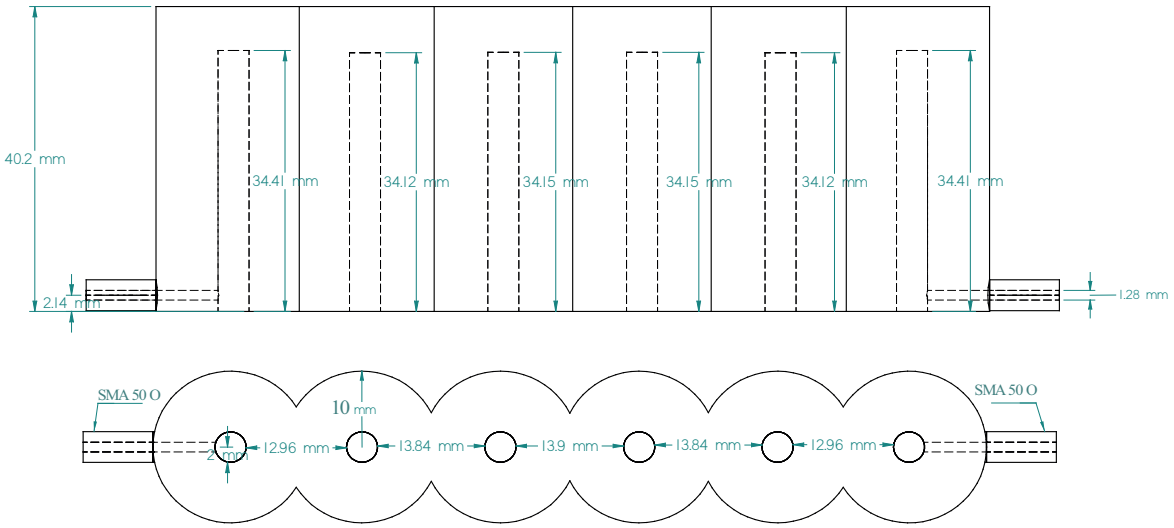


**Figure 6.17: Structure of the final combline filter ($N$=6, $R_L$=20 dB, $R_0$=50 ohms, $f_0$=2 GHz, $\triangle$=0.01, $\epsilon_r^{feeds} = 1.88$)**

# 7 Conclusions and Future Work

## 7.1 Conclusions

This work has been focused on microwave filters design. This process is divided into several stages, i.e. approximation , coupling matrix synthesis, network synthesis, selection of the proper physical dimensions and manufacturing, measurement and adjustment of the structure. All the stages but the last one (mainly due to time and economic constraints) have been addressed (with different level of depth). Therefore, this study offers a global insight of the (almost) complete design process. It has been understood the complexity the whole engineering problem involves, and it has been learnt some strategies to face it.

Chapter 2 studied the generalised Chebychev method as a tool for achieving a desired frequency response. It has been shown that this method offers the designer the flexibility to allocate finite transmission zeros pursuing a trade-off between selectivity and group delay behaviour Furthermore, it has also been proved that this method allows obtaining asymmetric responses which in turn can lead to more compact designs (i.e. a lower filter order). Following this method MATLAB code was developed and several examples were given.

Once the design polynomials were computed, the coupling matrix synthesis was studied in chapter 3. It is a powerful tool that allows identifying the influence that each resonator produces over itself as well over the remaining resonators from the given design polynomials. Moreover, it has been evidenced that its versatility resides in the fact that it is not linked to a specific technology, and therefore it can be used for both cavity and planar filters. Several validation examples using the MATLAB code developed were provided.

In addition to this, it has been shown that the initial coupling matrix synthesized sometimes does not directly translate into a typical microwave structure. Towards that end, matrix rotations were introduced and MATLAB examples were given.

After the coupling matrix that fulfils the electrical specifications of the system is computed, it has been addressed the next step in filter design: obtaining the dimensions of the physical structure that implements it. To that end, the physical structure is selected taking into account that, besides the electrical specifications, the filter will also have constraints on volume and weight, insertion losses, and power handling. In the context of physical realization, a stepped impedance filter in coaxial technology (chapter 4) , and several direct-coupled waveguide bandpass filters (chapter 5) were designed using typical approaches for microwave filters. A further step of optimization was carried out in order to improve their performance.

With this same scenario of physical filter realization a high-performance cavity combline bandpass filter for mobile base stations was designed in chapter 6 and a method based on sequential stages was proposed. It aims at subdividing the problem into minor stages, whereby less parameters are taken into account than in a direct global design. Some sections of the filter are isolated in each stage and a cost function involving the difference between the full-wave response and the desired circuital response is defined. The excellent performance of this strategy has been evidenced.

## 7.2 Future work

Improving is always possible and new things need to be done. In my view, the most interesting points to develop in the future would be the following:

⇒ Applying the knowledge gained in the area of optimization to the approximation problem. It would not imply a conceptual challenge, but it will save time when allocating the finite transmission zeros in the generalised Chebychev method in order to meet certain specifications.

⇒ Broadening the theory learnt in the context of the coupling matrix, and develop MATLAB code for the $(N+2) \times (N+2)$ coupling matrix.

⇒ Study the performance of the method of coupling extractions to design a combline filter as an alternative to the method proposed in the last chapter.

⇒ Analyzing if the use of heuristic algorithms is worth in order to overcome the problem of relative convergence. It could be interesting to study its performance as an alternative to the several optimization iterations that were needed one of the stages in the combline filter design.

⇒ Manufacturing and measuring the designed prototypes and therefore complete the whole cycle of microwave filter design. Although electromagnetic simulators are remarkably accurate nowadays, a further step of adjustment in filter design is commonly needed in order to achieve the desired response. In that sense, it is important not to underestimate this stage.

# Bibliography


[1] Richard J Cameron, Chandra M Kudsia, and Raafat R Mansour. *Microwave filters for communication systems*. Wiley-Interscience, 2007.

[2] Jia-Shen G Hong and Michael J Lancaster. *Microstrip filters for RF/microwave applications*, volume 167. John Wiley & Sons, 2004.

[3] Richard F Baum. Design of unsymmetrical band-pass filters. *Circuit Theory, IRE Transactions on*, 4(2):33–40, 1957.

[4] Gabor C Temes and Sanjit Kumar Mitra. *Modern filter theory and design*. John Wiley, 1973.

[5] David M Pozar. *Microwave engineering*. John Wiley & Sons, 2009.

[6] Herman Blinchikoff and Helen Krause. *Filtering in the time and frequency domains*. The Institution of Engineering and Technology, 2001.

[7] Robert E Collin. *Foundations for microwave engineering*. John Wiley & Sons, 2007.

[8] Vasudev K Aatre et al. *Network theory and filter design*. New Age International, 1980.

[9] Ali E Atia and Albert E Williams. Narrow-bandpass waveguide filters. *Microwave Theory and Techniques, IEEE Transactions on*, 20(4):258–265, 1972.

[10] Ian Hunter. *Theory and design of microwave filters*. Number 48. Iet, 2001.

[11] G.L. Matthaei. Comb-line band-pass filters of narrow or moderate bandwidth. *Microwave Journal*, 6:82–91, 1963.

[12] Xiaobang Shang, Wenlin Xia, and Michael J Lancaster. The design of waveguide filters based on cross-coupled resonators. *Microwave and Optical Technology Letters*, 56(1):3–8, 2014.

[13] W.T. Vetterling W. H. Press, S.A. Teukolsky and B.P.Flannery. Numerical recipes in fortran, 1986.

[14] Raafat R Mansour. Filter technologies for wireless base stations. *Microwave Magazine, IEEE*, 5(1):68–74, 2004.

[15] Chi Wang, Kawthar Zaki, et al. Full-wave modeling of electric coupling probes in combline resonators and filters. *Microwave Theory and Techniques, IEEE Transactions on*, 48(12):2459–2464, 2000.

[16] Wui-Wen Yao, Kawthar Zaki, Ali E Atia, Rafi Hershtig, et al. Full wave modeling of conducting posts in rectangular waveguides and its applications to slot coupled combline filters. *Microwave Theory and Techniques, IEEE Transactions on*, 43(12):2824–2830, 1995.

# A

# Input impedance for polynomial synthesis

The aim of this appendix is to proof a valuable expression for the input impedance of a quadripole, which will be used in the main document for polynomial synthesis purposes. Figure A.1 show the generic quadripole used for the explanation.

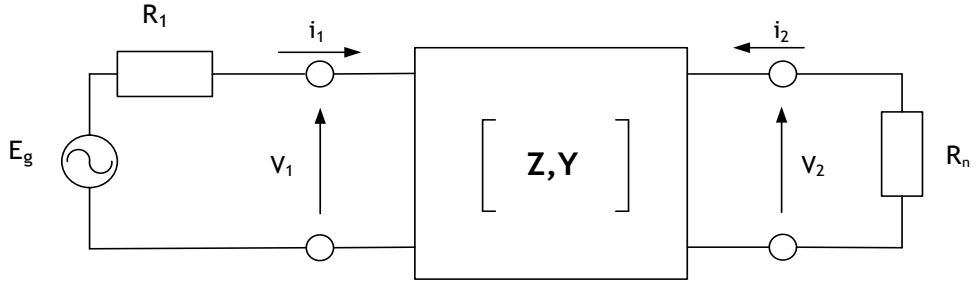


**Figure A.1: Generic quadripole**

First of all, the equation sets for both impedance and admittance parameters (equations A.1.1 - A.1.2 and A.2.1 - A.2.2 respectively )of a two port network are here reminded.

$$\begin{aligned} &1. \quad v_1 = i_1 z_{11} + i_2 z_{12} \\ &2. \quad v_2 = i_1 z_{21} + i_2 z_{22} \end{aligned} \tag{A.1}$$

$$\begin{aligned} &1. \quad i_1 = v_1 y_{11} + v_2 y_{12} \\ &2. \quad i_2 = v_1 y_{21} + v_2 y_{22} \end{aligned} \tag{A.2}$$

An additional equation is needed in order to let the output impedance $R_n$ appear:

$$v_2 = -i_2 R_n \tag{A.3}$$

Then, equation A.3 is introduced in equation A.2.2, allowing to obtain $i_2$ as:

$$i_2 = y_{21} v_1 - y_{22} R_n i_2 \quad \rightarrow \quad i_2 = \frac{v_1 y_{21}}{y_{22} R_n + 1} \tag{A.4}$$

Using equation A.4 in A.1.1:

$$v_1 = i_1 z_{11} + \frac{z_{12} y_{21} v_1}{1 + y_{22} R_n} \quad \rightarrow$$

$$Z_{in}(s) = \frac{v_1}{i_1} = \frac{z_{11}(1 + y_{22} R_n)}{1 + y_{22} R_n - z_{12} y_{21}} \overset{\div y_{22}}{=} \tag{A.5}$$

$$= \frac{z_{11}(1/y_{22}) + R_n)}{R_n + (\frac{1 - z_{12} y_{21}}{y_{22}})}$$

Now it is time to use the reciprocity property, which guarantees that:

$$\begin{aligned} &1. \quad AD - BC = 1 \\ &2. \quad z_{12} = z_{21} \end{aligned} \tag{A.6}$$

At the same time, it is convenient to take into account the table conversion between ABCD, impedance and admittance parameters:

| | $Y$ | $Z$ |
|---|---|---|
| $A$ | $-\frac{y_{22}}{y_{21}}$ | $\frac{z_{11}}{z_{21}}$ |
| $B$ | $-\frac{1}{y_{21}}$ | $\frac{\lvert z \rvert}{z_{21}}$ |
| $C$ | $-\frac{\lvert y \rvert}{y_{21}}$ | $\frac{1}{z_{21}}$ |
| $D$ | $-\frac{y_{11}}{y_{21}}$ | $\frac{z_{22}}{z_{21}}$ |

With the preceding conversion table and equation set A.6:

$$\frac{-y_{22}}{y_{21}} \cdot \frac{z_{22}}{z_{21}} + \frac{1}{y_{21}} \cdot \frac{1}{z_{21}} \quad \rightarrow$$

$$- z_{22} y_{22} + 1 = y_{21} z_{21} \quad \rightarrow \tag{A.7}$$

$$z_{22} = \frac{1 - y_{21} z_{21}}{y_{22}} = \frac{1 - y_{21} z_{12}}{y_{22}}$$

Finally, the result obtained in A.7 and the expression of $Zin(s)$ achieved in equation A.5 lead to the following final expression:

$$\boxed{Z_{in}(s) = \frac{v_1}{i_1} = \frac{z_{11}(1/y_{22}) + R_n)}{R_n + (\frac{1 - z_{12} y_{21}}{y_{22}})} = \frac{z_{11}(1/y_{22}) + R_n)}{R_n + z_{22}}} \tag{A.8}$$

# B

# Multicoupled admittance matrix decomposition

This appendix aims at proving the decomposition of the admittance matrix $Y$ of a multicoupled network into convenient sumatories. That concrete admittance matrix was defined in chapter 3 as:

$$\mathbf{Y} = \mathbf{Z^{-1}} = [j\mathbf{M} + s\mathbf{I}]^{-1} \tag{B.1}$$

At the same time, the coupling matrix M was defined as:

$$\mathbf{M} = \mathbf{T} \cdot \triangle \cdot \mathbf{T^t} \quad \text{,where} \quad \triangle = \mathbf{diag}[\lambda_k] \tag{B.2}$$

First of all, any invertible matrix can be written in terms of Neumann series (whenever it converges). Let A be a general non-singular matrix:

$$(\mathbf{A} - \mathbf{I})^{-1} \overset{1}{=} \sum_{n=0}^{\infty} \mathbf{A}^n \tag{B.3}$$

Thus, it can be written:

$$\mathbf{Y} = \mathbf{Z^{-1}} = [j\mathbf{M} + s\mathbf{I}]^{-1} = s^{-1}(\mathbf{I} + js^{-1}\mathbf{M})^{-1} = s^{-1} \sum_{n=0}^{\infty} (-js^{-1}\mathbf{M})^n =$$

$$s^{-1} \sum_{n=0}^{\infty} [(-js^{-1})^n \cdot (\mathbf{T} \triangle \mathbf{T^t})^n] \overset{2}{=} s^{-1} \sum_{n=0}^{\infty} [(-js^{-1})^n \mathbf{T} \triangle^{\mathbf{n}} \mathbf{T^t}] = \tag{B.4}$$

$$s^{-1}\mathbf{T} \sum_{n=0}^{\infty} [(-js^{-1}\triangle)^n]\mathbf{T^t} = \mathbf{T} \cdot \mathbf{D} \cdot \mathbf{T^t}$$

If matrix $D$ is developed:

$$\mathbf{D} = s^{-1}\sum_{n=0}^{\infty}[(js^{-1})^n \triangle^n] = \mathbf{diag}[D_k] = \mathbf{diag}[\frac{1}{s-j\lambda_k}] \quad \text{,where}$$
$$D_k = s^{-1}\sum_{n=0}^{\infty}[(-js^{-1}\lambda_{\mathbf{k}})^n] = s^{-1}\frac{1}{1-js^{-1}\lambda_k} = \frac{1}{s-j\lambda_k} \tag{B.5}$$

Therefore

$$\boxed{\mathbf{Y} = \mathbf{Z^{-1}} = [j\mathbf{M} + s\mathbf{I}]^{-1} = \mathbf{TDT^t} = \mathbf{T}\cdot\mathbf{diag}[\frac{1}{s-j\lambda_1}, \frac{1}{s-j\lambda_2}, ..., \frac{1}{s-j\lambda_n}]\cdot\mathbf{T^t}} \tag{B.6}$$

Now it is time to show how each element of the equation B.6 can be expressed in terms of a sumatory. Lets compute the scalar product of the aforementioned matrices:

$$\begin{bmatrix} T_{11} & T_{12} & T_{13} & ... & T_{1n} \\ T_{21} & T_{22} & T_{23} & ... & T_{2n} \\ T_{31} & T_{32} & T_{33} & ... & T_{3n} \\ ... & ... & ... & ... & ... \\ T_{n1} & T_{n2} & T_{n3} & ... & T_{nn} \end{bmatrix} \cdot \begin{bmatrix} \frac{1}{s-j\lambda_1} & 0 & 0 & ... & 0 \\ 0 & \frac{1}{s-j\lambda_2} & 0 & ... & 0 \\ 0 & 0 & \frac{1}{s-j\lambda_3} & ... & 0 \\ ... & ... & ... & ... & ... \\ 0 & 0 & 0 & ... & \frac{1}{s-j\lambda_n} \end{bmatrix} \cdot \begin{bmatrix} T_{11} & T_{21} & T_{31} & ... & T_{n1} \\ T_{12} & T_{22} & T_{32} & ... & T_{n2} \\ T_{13} & T_{23} & T_{33} & ... & T_{n3} \\ ... & ... & ... & ... & ... \\ T_{1n} & T_{2n} & T_{3n} & ... & T_{nn} \end{bmatrix} =$$

$$\begin{bmatrix} \frac{T_{11}}{s-j\lambda_1} & \frac{T_{12}}{s-j\lambda_2} & \frac{T_{13}}{s-j\lambda_3} & \cdots & \frac{T_{1n}}{s-j\lambda_n} \\ \frac{T_{21}}{s-j\lambda_1} & \frac{T_{22}}{s-j\lambda_2} & \frac{T_{23}}{s-j\lambda_3} & \cdots & \frac{T_{2n}}{s-j\lambda_n} \\ \frac{T_{31}}{s-j\lambda_1} & \frac{T_{32}}{s-j\lambda_2} & \frac{T_{33}}{s-j\lambda_3} & \cdots & \frac{T_{3n}}{s-j\lambda_n} \\ ... & ... & ... & ... & ... \\ \frac{T_{n1}}{s-j\lambda_1} & \frac{T_{n2}}{s-j\lambda_2} & \frac{T_{n3}}{s-j\lambda_3} & \cdots & \frac{T_{nn}}{s-j\lambda_n} \end{bmatrix} \cdot \begin{bmatrix} T_{11} & T_{21} & T_{31} & ... & T_{n1} \\ T_{12} & T_{22} & T_{32} & ... & T_{n2} \\ T_{13} & T_{22} & T_{33} & ... & T_{n3} \\ ... & ... & ... & ... & ... \\ T_{1n} & T_{2n} & T_{3n} & ... & T_{nn} \end{bmatrix} =$$

$$\begin{bmatrix} \frac{T_{11}T_{11}}{s-j\lambda_1} + \frac{T_{12}T_{12}}{s-j\lambda_2} + \frac{T_{13}T_{13}}{s-j\lambda_3} + ... + \frac{T_{1n}T_{1n}}{s-j\lambda_n} & \frac{T_{11}T_{21}}{s-j\lambda_1} + \frac{T_{12}T_{22}}{s-j\lambda_2} + \frac{T_{13}T_{23}}{s-j\lambda_3} + ... + \frac{T_{1n}T_{2n}}{s-j\lambda_n} & \frac{T_{11}T_{31}}{s-j\lambda_1} + \frac{T_{12}T_{32}}{s-j\lambda_2} + \frac{T_{13}T_{33}}{s-j\lambda_3} + ... + \frac{T_{1n}T_{3n}}{s-j\lambda_n} & ... & \frac{T_{11}T_{n1}}{s-j\lambda_1} + \frac{T_{11}T_{n2}}{s-j\lambda_2} + \frac{T_{11}T_{n3}}{s-j\lambda_3} + ... + \frac{T_{1n}T_{nn}}{s-j\lambda_n} \\ \frac{T_{21}T_{11}}{s-j\lambda_1} + \frac{T_{22}T_{12}}{s-j\lambda_2} + \frac{T_{23}T_{13}}{s-j\lambda_3} + ... + \frac{T_{2n}T_{1n}}{s-j\lambda_n} & \frac{T_{21}T_{21}}{s-j\lambda_1} + \frac{T_{22}T_{22}}{s-j\lambda_2} + \frac{T_{23}T_{23}}{s-j\lambda_3} + ... + \frac{T_{2n}T_{2n}}{s-j\lambda_n} & \frac{T_{21}T_{31}}{s-j\lambda_1} + \frac{T_{22}T_{32}}{s-j\lambda_2} + \frac{T_{23}T_{33}}{s-j\lambda_3} + ... + \frac{T_{2n}T_{3n}}{s-j\lambda_n} & ... & \frac{T_{21}T_{n1}}{s-j\lambda_1} + \frac{T_{22}T_{n2}}{s-j\lambda_2} + \frac{T_{23}T_{n3}}{s-j\lambda_3} + ... + \frac{T_{2n}T_{nn}}{s-j\lambda_n} \\ \frac{T_{31}T_{11}}{s-j\lambda_1} + \frac{T_{32}T_{12}}{s-j\lambda_2} + \frac{T_{33}T_{13}}{s-j\lambda_3} + ... + \frac{T_{3n}T_{1n}}{s-j\lambda_n} & \frac{T_{31}T_{21}}{s-j\lambda_1} + \frac{T_{32}T_{22}}{s-j\lambda_2} + \frac{T_{33}T_{23}}{s-j\lambda_3} + ... + \frac{T_{3n}T_{2n}}{s-j\lambda_n} & \frac{T_{31}T_{31}}{s-j\lambda_1} + \frac{T_{32}T_{32}}{s-j\lambda_2} + \frac{T_{33}T_{33}}{s-j\lambda_3} + ... + \frac{T_{3n}T_{3n}}{s-j\lambda_n} & ... & \frac{T_{31}T_{n1}}{s-j\lambda_1} + \frac{T_{32}T_{n2}}{s-j\lambda_2} + \frac{T_{33}T_{n3}}{s-j\lambda_3} + ... + \frac{T_{3n}T_{nn}}{s-j\lambda_n} \\ ... & ... & ... & ... & ... \\ \frac{T_{n1}T_{11}}{s-j\lambda_1} + \frac{T_{n2}T_{12}}{s-j\lambda_2} + \frac{T_{n3}T_{13}}{s-j\lambda_3} + ... + \frac{T_{nn}T_{1n}}{s-j\lambda_n} & \frac{T_{n1}T_{21}}{s-j\lambda_1} + \frac{T_{n2}T_{22}}{s-j\lambda_2} + \frac{T_{n3}T_{23}}{s-j\lambda_3} + ... + \frac{T_{nn}T_{2n}}{s-j\lambda_n} & \frac{T_{n1}T_{31}}{s-j\lambda_1} + \frac{T_{n2}T_{32}}{s-j\lambda_2} + \frac{T_{n3}T_{33}}{s-j\lambda_3} + ... + \frac{T_{nn}T_{3n}}{s-j\lambda_n} & ... & \frac{T_{n1}T_{n1}}{s-j\lambda_1} + \frac{T_{n2}T_{n2}}{s-j\lambda_2} + \frac{T_{n3}T_{n3}}{s-j\lambda_3} + ... + \frac{T_{nn}T_{nn}}{s-j\lambda_n} \end{bmatrix} =$$

$$= \begin{bmatrix} \sum_{k=1}^{n} \frac{T_{1k}T_{1k}}{s-j\lambda_k} & \sum_{k=1}^{n} \frac{T_{1k}T_{2k}}{s-j\lambda_k} & \sum_{k=1}^{n} \frac{T_{1k}T_{3k}}{s-j\lambda_k} & \cdots & \sum_{k=1}^{n} \frac{T_{1k}T_{nk}}{s-j\lambda_k} \\ \sum_{k=1}^{n} \frac{T_{2k}T_{1k}}{s-j\lambda_k} & \sum_{k=1}^{n} \frac{T_{2k}T_{2k}}{s-j\lambda_k} & \sum_{k=1}^{n} \frac{T_{2k}T_{3k}}{s-j\lambda_k} & \cdots & \sum_{k=1}^{n} \frac{T_{2k}T_{nk}}{s-j\lambda_k} \\ \sum_{k=1}^{n} \frac{T_{3k}T_{1k}}{s-j\lambda_k} & \sum_{k=1}^{n} \frac{T_{3k}T_{2k}}{s-j\lambda_k} & \sum_{k=1}^{n} \frac{T_{3k}T_{3k}}{s-j\lambda_k} & \cdots & \sum_{k=1}^{n} \frac{T_{3k}T_{nk}}{s-j\lambda_k} \\ \cdots & \cdots & \cdots & \cdots & \cdots \\ \sum_{k=1}^{n} \frac{T_{nk}T_{1k}}{s-j\lambda_k} & \sum_{k=1}^{n} \frac{T_{nk}T_{2k}}{s-j\lambda_k} & \sum_{k=1}^{n} \frac{T_{nk}T_{3k}}{s-j\lambda_k} & \cdots & \sum_{k=1}^{n} \frac{T_{nk}T_{nk}}{s-j\lambda_k} \end{bmatrix} \tag{B.7}$$

Thus, it can be written the next generalization:

$$\boxed{Y_{ij} = [\mathbf{T} \cdot \mathbf{diag}(\frac{1}{s-j\lambda_1}, \ldots, \frac{1}{s-j\lambda_n}) \cdot \mathbf{T^t}]_{ij} = \sum_{k=1}^{n} \frac{T_{ik}T_{jk}}{s-j\lambda_k}} \tag{B.8}$$

* * * * *

*(3) Explanation*

$$\mathbf{M} = \mathbf{T} \cdot \triangle \cdot \mathbf{T^t}$$

$$\mathbf{M}^2 = (\mathbf{T} \cdot \triangle \cdot \underbrace{\mathbf{T^t}}_{\mathbf{T^t \cdot T = I}}) \cdot (\mathbf{T} \cdot \triangle \cdot \mathbf{T^t}) = \mathbf{T} \cdot \triangle^{\mathbf{2}} \cdot \mathbf{T^t}$$

$$\mathbf{M}^3 = \mathbf{M}^2 \cdot (\mathbf{T} \cdot \triangle \cdot \mathbf{T^t}) = (\mathbf{T} \cdot \triangle^{\mathbf{2}} \cdot \underbrace{\mathbf{T^t}}_{T^t \cdot T = I}) \cdot (\mathbf{T} \cdot \triangle \cdot \mathbf{T^t}) = \mathbf{T} \cdot \triangle^{\mathbf{3}} \cdot \mathbf{T^t}$$

....

$$\mathbf{M}^n = \mathbf{T} \cdot \triangle^{\mathbf{n}} \cdot \mathbf{T^t}$$

# C

# Real symmetric matrices

This appendix aims at presenting some useful properties of the real symmetric matrices.

---

**1. Real symmetric matrices eigenvalues are always real.**

---

Let $\lambda$ be an eigenvalue of the symmetric matrix $\mathbf{A} \in \mathbb{R}^{nxn}$, with $\mathbf{x} \in \mathbb{C}^n$ its associated eigenvector:

$$\mathbf{A} \cdot \mathbf{x} = \lambda \mathbf{x} \tag{C.1}$$

Taking complex conjugates at both sides of equation C.1, it is obtained:

$$\mathbf{A}^* \cdot \mathbf{x}^* = \lambda^* \mathbf{x}^* \leftrightarrow \mathbf{A} \cdot \mathbf{x}^* = \lambda^* \mathbf{x}^* \tag{C.2}$$

Then, equation C.1 is multiplied in both sides with $(\mathbf{x}^*)^\mathbf{t}$, and the following equivalences are achieved:

$$\lambda(\mathbf{x}^*)^\mathbf{t} \cdot \mathbf{x} = (\mathbf{x}^*)^\mathbf{t} \cdot \mathbf{A} \cdot \mathbf{x} \overset{1}{=} (\mathbf{A}^\mathbf{t} \cdot \mathbf{x}^*)^\mathbf{t} \cdot \mathbf{x} \overset{2}{=} (\mathbf{A} \cdot \mathbf{x}^*)^\mathbf{t} \cdot \mathbf{x} \overset{3}{=} (\lambda^* \mathbf{x}^*)^\mathbf{t} \cdot \mathbf{x} = \lambda^* (\mathbf{x}^*)^\mathbf{t} \cdot \mathbf{x} \tag{C.3}$$

According to C.3:

$$(\lambda - \lambda^*)(\mathbf{x}^*)^\mathbf{t} \cdot \mathbf{x} = 0 \tag{C.4}$$

Since $\mathbf{x}$ is an eigenvector, at least one of its components must be different from zero:

$$(\mathbf{x}^*)^\mathbf{t} \cdot \mathbf{x} = \sum_{i=1}^{n} \mathbf{x_i}^* \cdot \mathbf{x_i} > 0 \tag{C.5}$$

Hence,

$$\lambda = \lambda^* \leftrightarrow \lambda \in \mathbb{R} \tag{C.6}$$

### 2. Eigenvectors of distinct eigenvalues of a real symmetric matrix are orthogonal

Let $\lambda_1, \lambda_2 \in \mathbb{R}$ be distinct eigenvalues of the symmetric matrix $\mathbf{A} \in \mathbb{R}^{\mathbf{nxn}}$, with their corresponding eigenvectors $\mathbf{x_1}, \mathbf{x_2} \in \mathbb{R}^{\mathbf{n}}$ such that:

$$\begin{aligned} &1. \quad \mathbf{A} \cdot \mathbf{x_1} = \lambda_1 \mathbf{x_1} \\ &2. \quad \mathbf{A} \cdot \mathbf{x_2} = \lambda_2 \mathbf{x_2} \end{aligned} \tag{C.7}$$

Equation C.7.1 is then multiplied by $\mathbf{x_2^t}$:

$$\lambda_1 \mathbf{x_2^t} \cdot \mathbf{x_1} = \mathbf{x_2^t} \cdot \mathbf{A} \cdot \mathbf{x_1} \overset{1}{=} (\mathbf{A^t} \cdot \mathbf{x_2})^{\mathbf{t}} \cdot \mathbf{x_1} \overset{2}{=} (\mathbf{A} \cdot \mathbf{x_2})^{\mathbf{t}} \cdot \mathbf{x_1} \tag{C.8}$$

Using equation C.7.2 in equation C.8:

$$(\mathbf{A} \cdot \mathbf{x_2})^{\mathbf{t}} \cdot \mathbf{x_1} = (\lambda_2 \mathbf{x_2})^{\mathbf{t}} \cdot \mathbf{x_1} = \lambda_2 \mathbf{x_2^t} \cdot \mathbf{x_1} \tag{C.9}$$

With equations C.8 and C.9, it is obtained that:

$$(\lambda_2 - \lambda_1) \mathbf{x_2^t} \cdot \mathbf{x_1} = 0 \tag{C.10}$$

Therefore, if $\lambda_1 \neq \lambda_2$, then $\mathbf{x_2^t} \cdot \mathbf{x_1} = 0$, which implies that $\mathbf{x_1}$ and $\mathbf{x_2}$ are orthogonal.

### 3. Any orthogonally diagonalizable real matrix must be symmetric

A square matrix $\mathbf{A} \in \mathbb{R}$ is orthogonally diagonalizable if there is an orthogonal matrix $\mathbf{P}$ such that $\mathbf{P^{-1}} \cdot \mathbf{A} \cdot \mathbf{P} = \mathbf{D}$ is a diagonal matrix. This is equivalent to say that $A = \mathbf{P} \cdot \mathbf{D} \cdot \mathbf{P^{-1}} = \mathbf{D}$ Recall that, as an orthonormal matrix, $\mathbf{P^{-1}} = \mathbf{P^t}$. Thus, if it is computed the following operation:

$$\mathbf{A^t} = (\mathbf{P} \cdot \mathbf{D} \cdot \mathbf{P^{-1}})^{\mathbf{t}} = (\mathbf{P^{-1}})^{\mathbf{t}} \cdot \mathbf{D} \cdot \mathbf{P^t} = \mathbf{P} \cdot \mathbf{D} \cdot \mathbf{P^{-1}} = \mathbf{A} \tag{C.11}$$

Hence, $\mathbf{A}$ must be symmetric. Moreover, $\mathbf{D}$ contains $\mathbf{A}$ real eigenvalues in its diagonal, and $\mathbf{P}$ contains the base (i.e. linearly independent) of the corresponding eigenvectors.

* * * * *

*(1) Applied properties:* $(A \cdot B)^t = B^t \cdot A^t$ *, and* $(A^t)^t = A$.
*(2) Applied property: A is symmetric.*
*(3) Use of equation C.2.*

# D

# Frequency transformations

This appendix aims at proving how the four frequency transformations used in filter design simply lead to the replacement of the lumped elements for another ones with properly values. It is important to remark that the normalized lowpass filter is considered as the starting point.

---

**Highpass transformation**

---

A highpass frequency transformation is governed by the next expression:

$$\omega = f(\omega^{'}) = \frac{-\omega_c}{\omega^{'}} \tag{D.1}$$

If the aforementioned frequency mapping is applied over an inductor:

$$Z_{Li}(f(\omega^{'})) = \frac{-jg_{L_i}\omega_c}{\omega^{'}} = \frac{1}{j\omega^{'}C_i^{'}} = Z_{Li}^{'}(\omega^{'}) \tag{D.2}$$

Hence, each inductor must be replaced by a capacitor of value $C_i^{'} = \frac{1}{g_{L_i}\omega_C}$ in order to obtain the counterpart highpass response.

Regarding capacitors, if the transformation is applied it is obtained:

$$Y_{Ci}(f(\omega^{'})) = \frac{-jg_{C_i}\omega_c}{\omega^{'}} = \frac{1}{j\omega^{'}L_i^{'}} = Y_{Ci}^{'}(\omega^{'}) \tag{D.3}$$

Therefore, each capacitor must be replaced by an inductor of value $L_i^{'} = \frac{1}{g_{C_i}\omega_C}$

**Bandpass transformation**

In this transformation the frequency mapping is:

$$\omega = f(\omega^{'}) = \frac{1}{\triangle}(\frac{\omega^{'}}{\omega_0} - \frac{\omega_0}{\omega^{'}}),\ \text{where}\ \triangle = \frac{\omega_2 - \omega_1}{\omega_0}. \tag{D.4}$$

Applying the preceding transformation over an inductor:

$$Z_{Li}(f(\omega^{'})) = \frac{jg_{L_i}}{\triangle}(\frac{\omega^{'}}{\omega_0} - \frac{\omega_0}{\omega^{'}}) = \frac{jg_{L_i}\omega^{'}}{\omega_0\triangle} + \frac{g_{L_i}\omega_0}{j\omega^{'}\triangle} = j\omega^{'}L_i^{'} + \frac{1}{j\omega^{'}C_i^{'}} = Z_{Li}^{'}(\omega^{'}) \tag{D.5}$$

Therefore each inductor must be replaced by two series lumped elements: an inductor of value $L_i^{'} = \frac{g_{L_i}}{\triangle\omega_0}$ and a capacitor of value $C_i^{'} = \frac{\triangle}{g_{L_i}\omega_0}$.

Concerning the same transformation applied over a capacitor:

$$Y_{Li}(f(\omega^{'})) = \frac{jg_{C_i}}{\triangle}(\frac{\omega^{'}}{\omega_0} - \frac{\omega_0}{\omega^{'}}) = \frac{jg_{C_i}\omega^{'}}{\omega_0\triangle} + \frac{g_{C_i}\omega_0}{j\omega^{'}\triangle} = j\omega^{'}C_i^{'} + \frac{1}{j\omega^{'}L_i^{'}} = Y_{Li}^{'}(\omega^{'}) \tag{D.6}$$

Thus, each capacitor in the network must be replaced by two shunt lumped elements: an capacitor of value $C_i^{'} = \frac{g_{C_i}}{\triangle\omega_0}$ and an inductor of value $L_i^{'} = \frac{\triangle}{g_{C_i}\omega_0}$.

**Bandstop transformation**

In order to get a bandstop transformation, the following mapping must be followed:

$$\omega = f(\omega^{'}) = \triangle(\frac{\omega_0}{\omega^{'}} - \frac{\omega^{'}}{\omega_0})^{-1},\ \text{where}\ \triangle = \frac{\omega_2 - \omega_1}{\omega_0}. \tag{D.7}$$

Thus, applying the preceding transformation over an inductor:

$$Y_{Li}(f(\omega^{'})) = \frac{1}{jg_{L_i}\triangle}(\frac{\omega_0}{\omega^{'}} - \frac{\omega^{'}}{\omega_0}) = \frac{\omega_0}{j\omega^{'}g_{L_i}\triangle} + \frac{j\omega^{'}}{g_{L_i}\omega_0\triangle} = \frac{1}{j\omega^{'}L_i^{'}} + j\omega^{'}C_i^{'} = Y_{Li}^{'}(\omega^{'}) \tag{D.8}$$

Hence, each inductor must be replaced by two shunt branches, one with an inductor and the other one with a capacitor, whose values must be $L_i^{'} = \frac{g_{L_i}\triangle}{\omega_0}$ and $C_i^{'} = \frac{1}{g_{L_i}\omega_0\triangle}$ respectively.

Doing the same transformation over a capacitor:

$$Z_{Ci} = (f(\omega^{'})) = \frac{1}{jg_{C_i}\triangle}(\frac{\omega_0}{\omega^{'}} - \frac{\omega^{'}}{\omega_0}) = \frac{\omega_0}{j\omega^{'}g_{C_i}\triangle} + \frac{j\omega^{'}}{g_{C_i}\omega_0\triangle} = \frac{1}{j\omega^{'}C_i^{'}} + j\omega^{'}L_i^{'} = Z_{Ci}^{'}(\omega^{'}) \tag{D.9}$$

Therefore, each capacitor must be replaced a series branch, where a series inductor and a series capacitor are placed, and whose values must be $L_i^{'} = \frac{1}{g_{C_i}\omega_0 \triangle}$ and $C_i^{'} = \frac{g_{C_i} \triangle}{\omega_0}$ respectively.

# E

# Bandpass inverter ladder network

The purpose of this appendix is to show how a lumped ladder bandpass network can be transformed into a lumped bandpass inverter ladder network. It will be developed a third-order filter, although these results can be generalised to an N-order filter. An equivalent procedure can be done for the dual network, as well as for a network with all shunt branches.

For the sake of readability, images associated with each of the five steps are all shown in figure E.1, which is at the end of the appendix. Therefore, there are not explicit references to figure E.1 in each step, but the reader is expected to look at the corresponding network while it is reading.

---

**Step 1**

---

Let's consider a third order bandpass filter. Hereinafter in this appendix, the superscript of each circuit value is set in accordance with the associated step. Furthermore, from now on it will be used $Z_j^i(Y_j^i)$ in order to refer to the corresponding shunt/series resonator at a particular step. Thus, the values of the lumped elements at this stage are:

$$L_1^{(1)} = \frac{\triangle}{\omega_0 g_1} \quad , \quad C_1^{(1)} = \frac{g_1}{\omega_0 \triangle}$$
$$L_2^{(1)} = \frac{g_2}{\omega_0 \triangle} \quad , \quad C_2^{(1)} = \frac{\triangle}{\omega_0 g_2}$$
$$L_3^{(1)} = \frac{\triangle}{\omega_0 g_3} \quad , \quad C_3^{(1)} = \frac{g_3}{\omega_0 \triangle}$$

And the associated impedances (admittance) are:

$$Z_1^{(1)} = j\omega L_1^{(1)} + \frac{1}{j\omega C_1^{(1)}}$$
$$Y_2^{(2)} = j\omega C_2^{(1)} + \frac{1}{j\omega L_2^{(1)}}$$
$$Z_3^{(1)} = j\omega L_3^{(1)} + \frac{1}{j\omega C_3^{(1)}}$$

$B_1^{(1)}$, $B_2^{(1)}$ and $B_3^{(1)}$ are the corresponding partial blocks (i.e. quadripoles) used as a reference in the next step. It is important to recall that due to the equivalent principle and the cascading property of the transmission (i.e. ABCD) matrices seen in subsection 3.1, if the matrix that depicts each partial block of a network keeps its values in the next step, then the circuit es equivalent and shows the same desired response. In that context, the blue arrows between steps mean that a proper transformation of the circuit elements inside a partial block is made when moving from one step to the next one. Pink arrows mean that the particular block is going to preserve its circuital elements and values in that transition, and therefore $B^i = B^{i+1}$ is directly guaranteed.

---

**Step 2**

---

In this step four inverters are introduced. Matrix $B_2^{(2)}$ is directly $B_2^{(2)} = B_2^{(1)}$, and therefore $L_2^{(2)} = L_2^{(1)}$ and $C_2^{(2)} = C_2^{(1)}$. Matrix $B_1^{(2)}$ is the result of cascading two inverters with a series resonator in the middle:

$$B_1^{(2)} = \begin{bmatrix} \frac{K_{01}^{(2)}}{K_{12}^{(2)}} & 0 \\ \frac{Z_1^{(2)}}{K_{01}^{(2)} K_{12}^{(2)}} & \frac{K_{12}^{(2)}}{K_{01}^{(2)}} \end{bmatrix} = \begin{bmatrix} 1 & 0 \\ Z_1^{(2)} & 1 \end{bmatrix} \tag{E.1}$$

In order to preserve the same response, $B_1^{(2)}$ must be equal to $B_1^{(1)}$, which is:

$$B_1^{(1)} = \begin{bmatrix} 1 & 0 \\ Y_1^{(1)} & 1 \end{bmatrix} \tag{E.2}$$

Taking into account that $Y_1^{(1)} = j\omega C_1^{(1)} + \frac{1}{j\omega L_1^{(1)}}$, it is obvious that it must be chosen $L_1^{(2)} = C_1^{(1)}$ and $C_1^{(2)} = L_1^{(1)}$ so that $Z_1^{(2)} = Y_1^{(1)}$. The values of the partial block $B_3^{(2)}$ are chosen following the same reasoning as in $B_1^{(2)}$. Thus, $L_3^{(2)} = C_3^{(1)}$ and $C_3^{(2)} = L_3^{(1)}$.

## Step 3

The aim of the third and fourth steps is to allow the filter designer to choose arbitrary lumped elements values. For that purpose, the inverter values must be properly chosen. Firstly it is important to notice that the partial blocks under consideration are the same as in the two preceding steps. Therefore, again the second partial block remains the same ($B_2^{(3)} = B_2^{(2)}$, and hence $L_2^{(3)} = L_2^{(2)}$ and $C_2^{(3)} = C_2^{(2)}$).

With respect to the first partial block, its value once again will be calculated as:

$$B_1^{(3)} = \begin{bmatrix} \frac{K_{01}^{(3)}}{K_{12}^{(3)}} & 0 \\ \\ \frac{Z_1^{(3)}}{K_{01}^{(3)} K_{12}^{(3)}} & \frac{K_{12}^{(3)}}{K_{01}^{(3)}} \end{bmatrix} \tag{E.3}$$

This partial block must preserve the same value as the preceding partial block $B_1^{(2)}$:

$$B_1^{(2)} = \begin{bmatrix} 1 & 0 \\ \\ Z_1^{(2)} & 1 \end{bmatrix} \tag{E.4}$$

At this point it is highly convenient to develop the expression of $Z_1^{(2)}$:

$$Z_1^{(2)} = j\omega L_1^{(2)} + \frac{1}{j\omega C_1^{(2)}} = j\sqrt{\frac{L_1^{(2)}}{C_1^{(2)}}}\left(\frac{\omega}{\omega_0} - \frac{\omega_0}{\omega}\right) = j\frac{g_1}{\triangle}\left(\frac{\omega}{\omega_0} - \frac{\omega_0}{\omega}\right) \tag{E.5}$$

If equations E.3 and E.4 are compared, it is clear that the new inverters must satisfy $K_{01}^{(3)} = K_{12}^{(3)}$.Additionally it must be chosen $K_{01}^{(3)} = K_{12}^{(3)} = \sqrt{\frac{\triangle}{g_1}\sqrt{\frac{L_{01}}{C_{01}}}}$ so that:

$$\frac{Z_1^{(3)}}{K_{01}^{(3)} K_{12}^{(3)}} = \frac{j\sqrt{\frac{L_{01}}{C_{01}}}\left(\frac{\omega}{\omega_0} - \frac{\omega_0}{\omega}\right)}{\frac{\triangle}{g_1}\sqrt{\frac{L_{01}}{C_{01}}}} = Z_1^{(2)} \tag{E.6}$$

The same reasoning applies to $B_3^{(3)}$, and hence, $K_{23}^{(3)} = K_{34}^{(3)} = \sqrt{\frac{\triangle}{g_3}\sqrt{\frac{L_{03}}{C_{03}}}}$.

## Step 4

As it has already been mentioned, it is desirable to be able to choose the intermediate lumped elements as well. To accomplish this objective, the partial blocks of the preceding circuit must be defined differently in this transition.

According to the new definitions of $B_1^{(3)}$ and $B_3^{(3)}$ are directly $B_1^{(4)} = B_1^{(3)}$ and $B_3^{(4)} = B_3^{(3)}$. Therefore, $K_{01}^{(4)} = K_{01}^{(3)}$, $L_1^{(4)} = L_1^{(3)}$,$C_1^{(4)} = C_1^{(3)}$, $K_{34}^{(4)} = K_{34}^{(3)}$, $L_3^{(4)} = L_3^{(3)}$ and $C_3^{(4)} = C_3^{(3)}$. Now, according to the new definition of $B_2^{(3)}$:

$$B_2^{(3)} = \begin{bmatrix} \frac{K_{12}^{(3)}}{K_{23}^{(3)}} & 0 \\ \frac{Z_2^{(3)}}{K_{12}^{(3)}K_{23}^{(3)}} & \frac{K_{23}^{(3)}}{K_{12}^{(3)}} \end{bmatrix} = \begin{bmatrix} \frac{\sqrt{\frac{\triangle}{g_1}\sqrt{\frac{L_{01}}{C_{01}}}}}{\sqrt{\frac{\triangle}{g_3}\sqrt{\frac{L_{03}}{C_{03}}}}} & 0 \\ \frac{j\frac{g_2}{\triangle}\left(\frac{\omega}{\omega_0}-\frac{\omega_0}{\omega}\right)}{\sqrt{\frac{\triangle}{g_1}\sqrt{\frac{L_{01}}{C_{01}}}}\sqrt{\frac{\triangle}{g_3}\sqrt{\frac{L_{03}}{C_{03}}}}} & \frac{\sqrt{\frac{\triangle}{g_3}\sqrt{\frac{L_{03}}{C_{03}}}}}{\sqrt{\frac{\triangle}{g_1}\sqrt{\frac{L_{01}}{C_{01}}}}} \end{bmatrix} \tag{E.7}$$

The matrix of the partial block $B_2^{(4)}$ is:

$$B_2^{(4)} = \begin{bmatrix} \frac{K_{12}^{(4)}}{K_{23}^{(4)}} & 0 \\ \frac{Z_2^{(4)}}{K_{12}^{(4)}K_{23}^{(4)}} & \frac{K_{23}^{(4)}}{K_{12}^{(4)}} \end{bmatrix} = \begin{bmatrix} \frac{K_{12}^{(4)}}{K_{23}^{(4)}} & 0 \\ \frac{j\sqrt{\frac{L_{02}}{C_{02}}}\left(\frac{\omega}{\omega_0}-\frac{\omega_0}{\omega}\right)}{K_{12}^{(4)}K_{23}^{(4)}} & \frac{K_{23}^{(4)}}{K_{12}^{(4)}} \end{bmatrix} \tag{E.8}$$

Comparing equations E.7 and E.8, it can be seen that they are equal if $K_{12}^{(4)} = \sqrt{\frac{\triangle}{g_1}\sqrt{\frac{L_{01}}{C_{01}}}\frac{\triangle}{g_2}\sqrt{\frac{L_{02}}{C_{02}}}}$ and $K_{23}^{(4)} = \sqrt{\frac{\triangle}{g_3}\sqrt{\frac{L_{03}}{C_{03}}}\frac{\triangle}{g_2}\sqrt{\frac{L_{02}}{C_{02}}}}$.

---

**Step 5**

---

At this point it is considered convenient to allow the filter designer to choose the two loads (the source load and the end load) as well. In this case, and from the point of view of dipoles, it is pursued not to find an equivalent matrix but to keep the impedance seen.

The value of the impedance seen immediately after the first inverter when the source load is equal to $g_0$ is:

$$Z_{in}^{(4)} = \frac{(K_{01}^{(4)})^2}{g_0} = \frac{\frac{\Lambda}{g_1}\sqrt{\frac{L_{01}}{C_{01}}}}{g_0} \tag{E.9}$$

If the designer uses a generic source load $R_A$, the properly value of $K_{01}^{(5)}$ is $K_{01}^{(5)} = \sqrt{\frac{\triangle}{g_1}\sqrt{\frac{L_{01}}{C_{01}}}\frac{R_A}{g_0}}$ so that:

$$Z_{in}^{(5)} = \frac{(K_{01}^{(5)})^2}{g_0} = \frac{\left(\sqrt{\frac{\triangle}{g_1}\sqrt{\frac{L_{01}}{C_{01}}}\frac{R_A}{g_0}}\right)^2}{R_A} = Z_{in}^{(4)} \tag{E.10}$$

Similarly, it is chosen $K_{34}^{(5)} = \sqrt{\frac{\triangle}{g_3}\sqrt{\frac{L_{03}}{C_{03}}}\frac{R_B}{g_4}}$.

The final network has the following ideal inverter values:

$$
\begin{aligned}
K_{01}^{(5)} &= \sqrt{\frac{\triangle R_A}{g_0 g_1}\sqrt{\frac{L_{01}}{C_{01}}}} \\
K_{12}^{(5)} &= \triangle\sqrt{\frac{1}{g_2 g_3}\sqrt{\frac{L_{01}L_{02}}{C_{01}C_{02}}}} \\
K_{23}^{(5)} &= \triangle\sqrt{\frac{1}{g_2 g_3}\sqrt{\frac{L_{02}L_{03}}{C_{02}C_{03}}}} \\
K_{34}^{(5)} &= \sqrt{\frac{\triangle R_B}{g_3 g_4}\sqrt{\frac{L_{03}}{C_{03}}}}
\end{aligned}
\tag{E.11}
$$

Therefore, a lumped element ladder network has already been transformed into a lumped element ladder inverter network, where the lumped elements and the two loading resistors are arbitrary chosen by the filter designer. The generalised formulas can be found in chapter 5 in subsection 5.1.2.

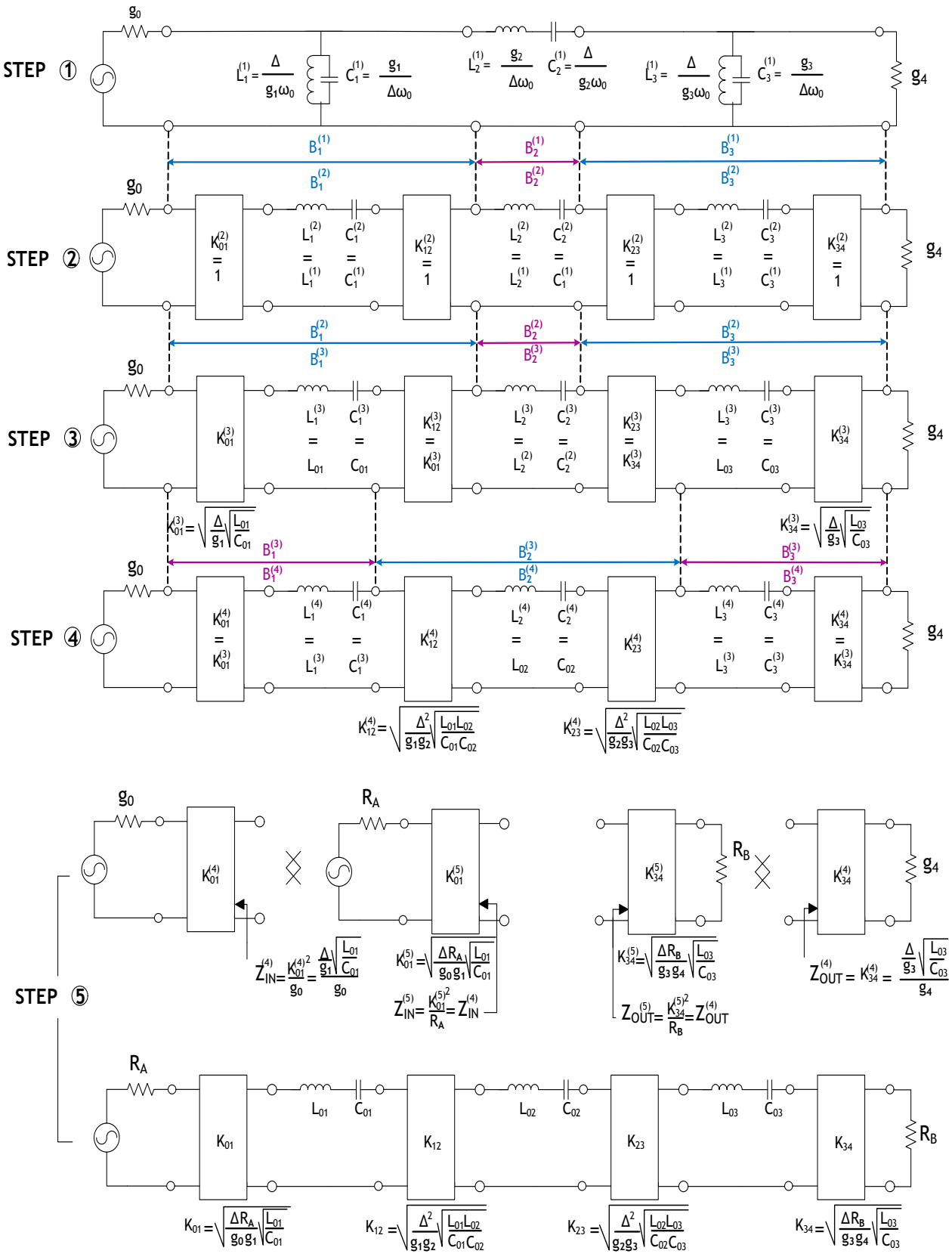


**Figure E.1: Development of the bandpass inverter model ladder network**

# F
# Optimization Tool

Enlarged images of the optimization tool developed are included in this appendix. Please continue to the next page.

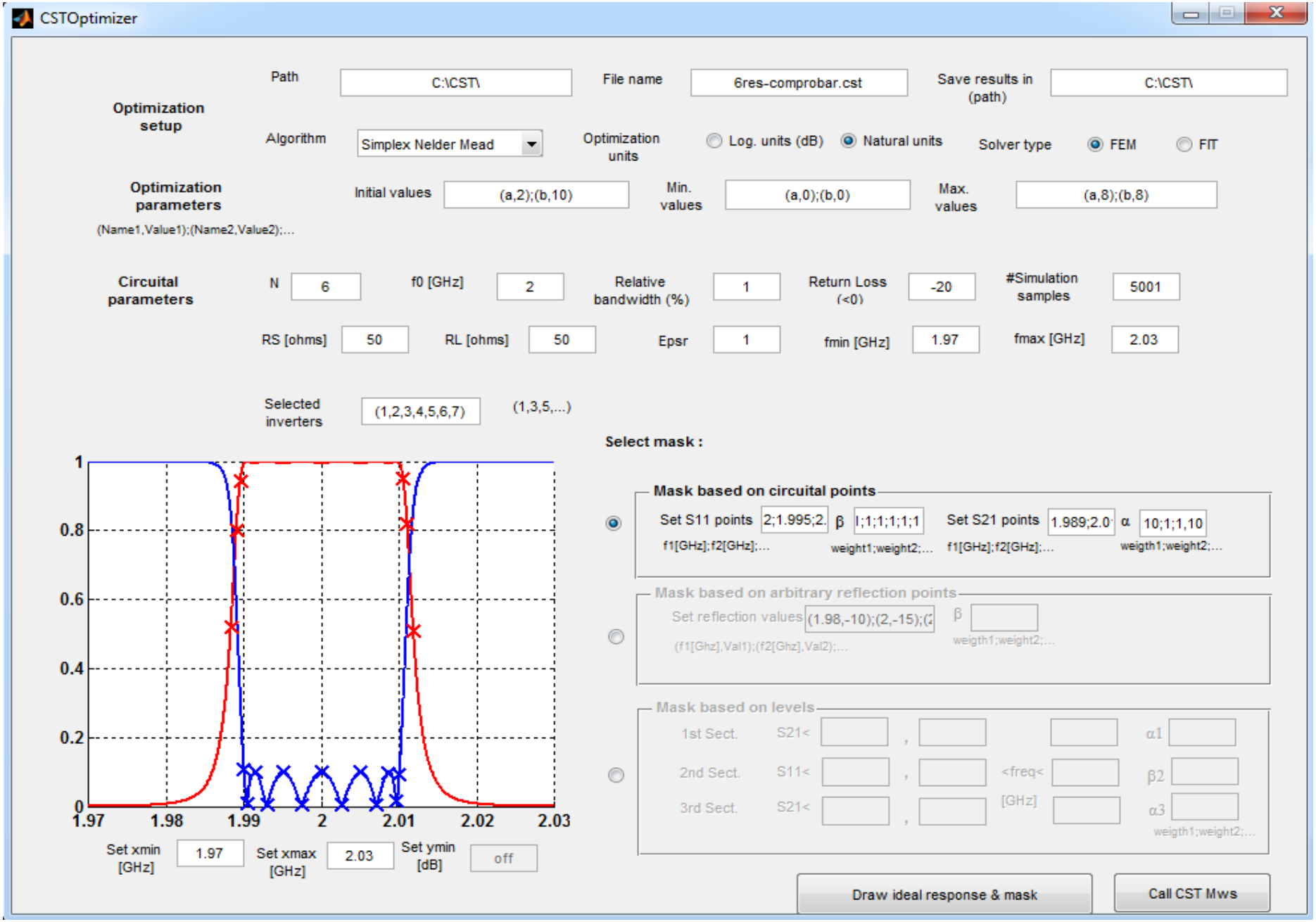


**Figure F.1:** Optimization tool first example

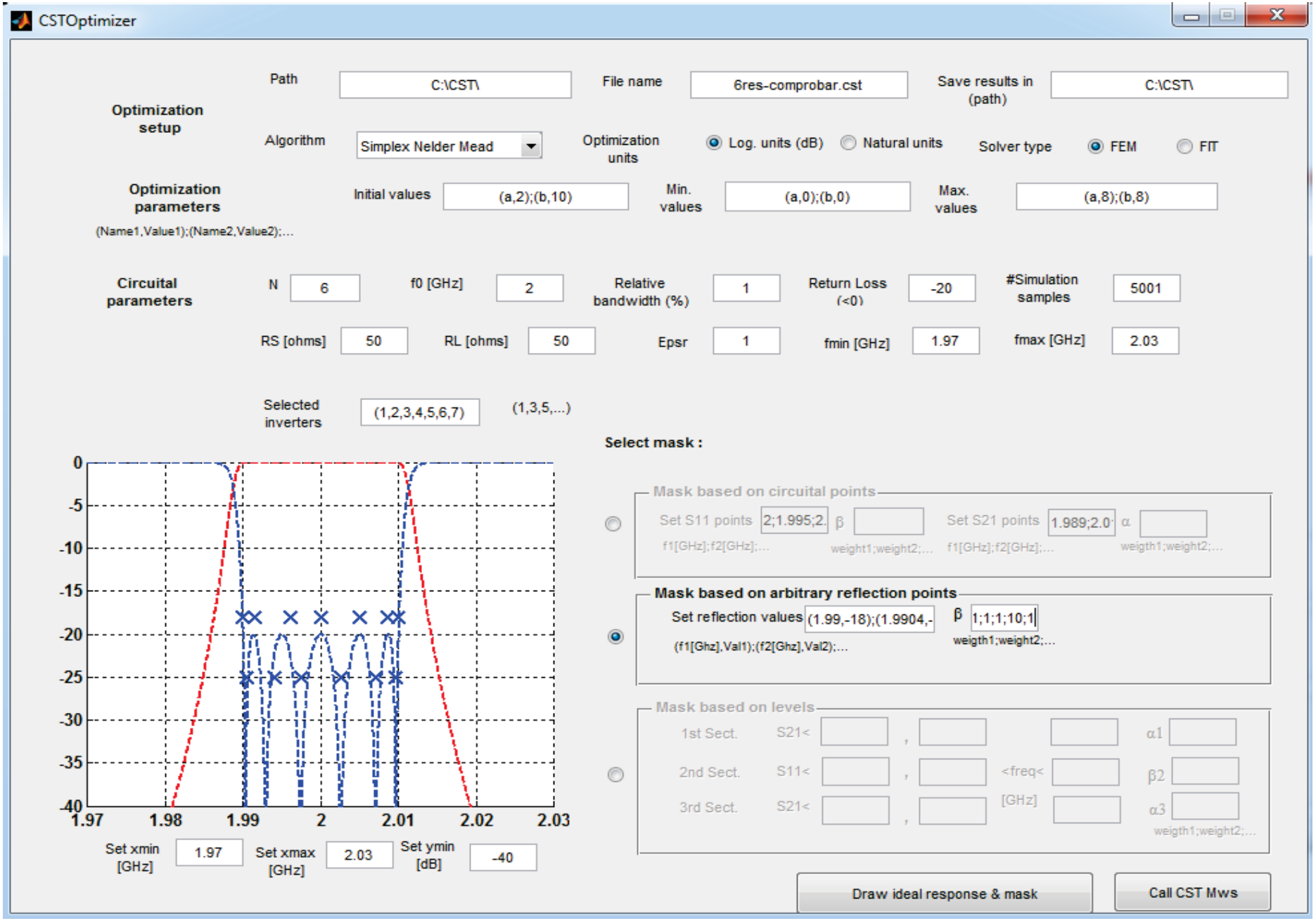


**Figure F.2:** Optimization tool second example

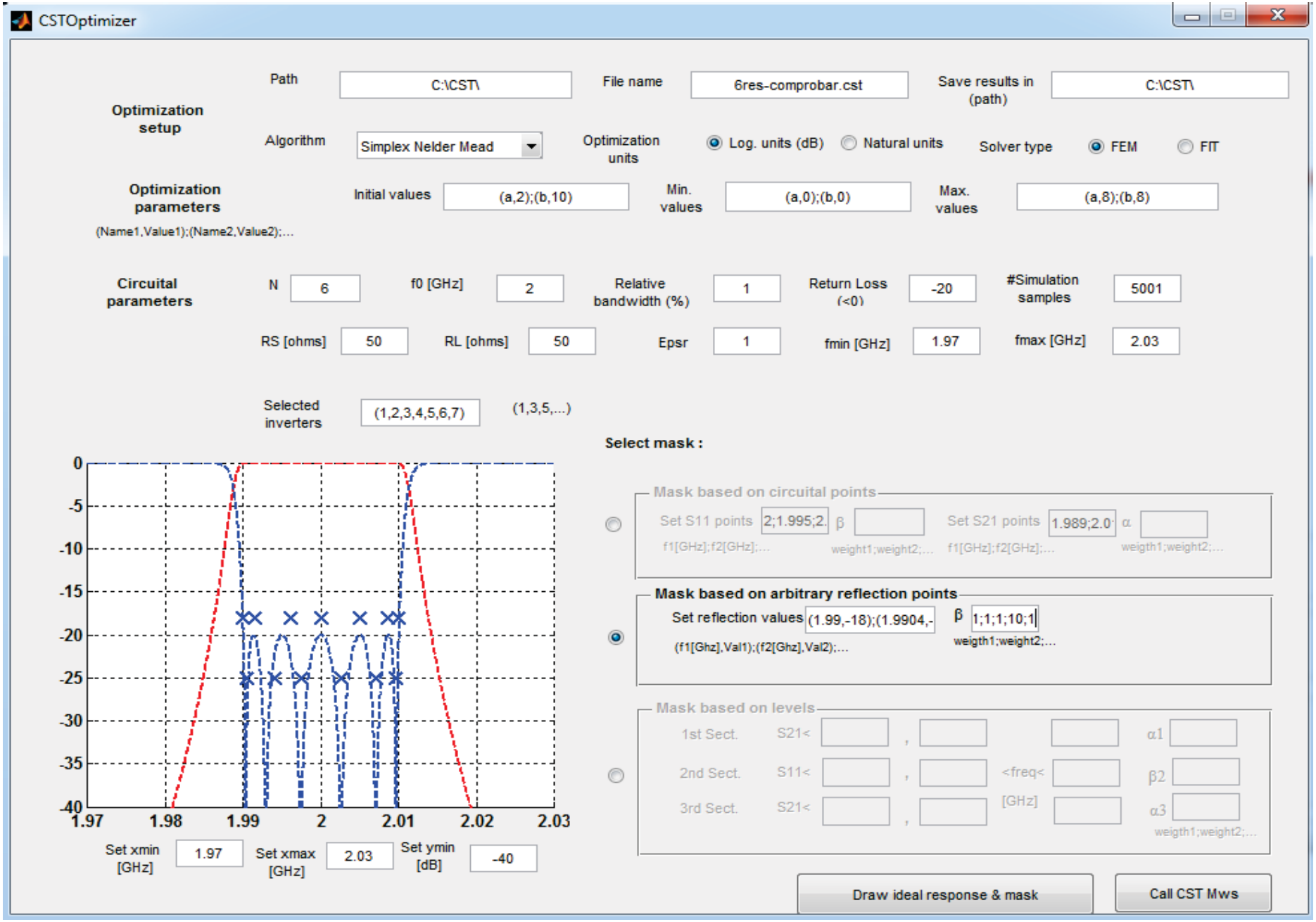


**Figure F.3:** Optimization tool third example

# G
# Published article

The article entitled *"Optimization method for the design of microwave filters based on sequential stages"*, published in the Congress on Numerical Methods (Lisbon, 2015) is here included.

Congresso de Métodos Numéricos em Engenharia 2015
Lisboa, 29 de Junho a 2 de Julho, 2015


# OPTIMIZATION METHOD FOR THE DESIGN OF MICROWAVE FILTERS BASED ON SEQUENTIAL STAGES

**Ana Morán-López[1], Jorge A. Ruiz-Cruz[1]**

1: Escuela Politécnica Superior,
Universidad Autónoma de Madrid
Calle Francisco Tomás y Valiente, 11. 28049 Madrid
e-mail: ana.moran.lopez@gmail.com, web: http://rfcas.eps.uam.es

**Keywords:** Combline filter, Microwave cavity, Optimization method by stages.

**Abstract** *Microwave filter design can be done using different approaches. These types of filters are typically found in the front-end of high-frequency transceivers of very diverse systems such as radar, satellite TV or microwave links. This paper addresses the strategy of subdividing the design process into minor stages, each of which takes into account less degrees of freedom (i.e. parameters of design) than in a direct global design. This work evidences how optimization divided into simpler stages becomes an excellent approach to accomplish this task, making it possible to achieve the level of refinement that the physical design parameters require to reach the desired partial responses. The advantages of this approach are discussed with a case of study based on a sixth-order combline cavity bandpass filter for application in base stations of wireless communications.*

## 1. INTRODUCTION

A microwave filter is a passive device in charge of the signal frequency selection in the context of a communication system [1][2]. Filter design can be addressed by means of electromagnetic solvers implemented in Computer Aided Design (CAD) tools, together with the use of a circuital approach. The use of an equivalent circuit model allows not only to identify (when possible) the different parts of the physical structure under design with their circuital counterpart, but to set the whole desired response that has to be achieved with the cavity filter structure [2].

In this work different stages of approximation are proposed to design microwave cavity filters [2] with the aim of reducing the complexity of the problem. It is important to note that the accurate analysis of a microwave filter involves solving Maxwell´s equations in the structure under analysis and, thus, the evaluation of cost functions in optimization methods may take several minutes. The performance of a microwave cavity filter is determined by its Scattering S-parameters [1][2], which are typically obtained (depending on the solver) by a Finite-Element Method or Finite Difference Method. The response of a microwave filter (i.e., its S-parameters) obtained using a numerical method solving Maxwell´s equations in the physical

structure is called *full-wave response*. Although circuit responses are very fast to obtain, full-wave responses (the response closest to what you would measure after an eventual construction of the filter) are very time consuming and demand a lot of RAM in the computer.

Therefore, design and optimization methods for microwave cavity filters should avoid problems with a large number of variables and involving many evaluations of the cost function. On the other hand, a "divide and conquer" strategy, as the approach in this paper, could be more efficient. Each stage uses the results obtained in the previous one, which takes into account a lower number of design elements. The evolution from one stage to another occurs when the full wave response (i.e. that accurate response obtained with an electromagnetic simulator) and the one obtained from the equivalent circuit model are ideally coincident after a refinement optimization process.

The purpose of this work is to emphasize the advantages of an optimization process subdivided into stages with a practical example of a so-called combline filter for base station applications in wireless communications [3][4]. This approach is an excellent alternative to a direct global design, indeed more complex in conceptual and computational terms.

## 2. STATEMENT OF THE PROBLEM

A combline cavity filter is shown in figure 1 [1]-[4]. The cylindrical cavities correspond to resonators and each resonator has two metallic elements: an internal post and the outer enclosure. The metallic post is shorted at one end with the enclosure, and its length is slightly shorter than a quarter of wavelength at the center frequency of the filter [3]. The cavities are not fully isolated since they have an open region between them that is used to couple them [2]. In the circuit model, these apertures, also called irises or windows are represented by circuit elements called inverters. Moreover, the first/last cavities are also coupled to the coaxial lines used for the input/output of the microwave signal.

In particular, figure 1 is a six order filter that can be used to realize filtering functions of the Chebychev-type [1]-[3]. The goal of this paper is to present a method to design a filter by dividing the whole design into simple stages. The design process must provide the physical dimensions of a structure like that in figure 1, whose full-wave response must fulfill (i.e. *approximate*) the aimed circuital filtering response set as goal. The physical dimensions involved in the design process of this filter are: the inner lengths of the posts ($Li_n$, $n$ is used to reference each post, since they can be different in each resonator), the height of the coaxial feed lines at the input/output ($h_f$) and the distance between resonators ($dc_n$). The radius of the cavities ($R_e$), the inner posts ($R_i$) and the feeds ($R_{ce}$, $R_{ci}$) are considered as fixed parameters previously set. Figure 2 depicts all these parameters for the physical structure representing a six order filter (having six cavities). The filter is symmetric with respect to plane yz and plane xy; thus, only the dimensions of half of the filter need to be specified. In figure 1 it is only represented the model to be analyzed with the full-wave method; the outer walls of an eventual physical construction are not plotted.

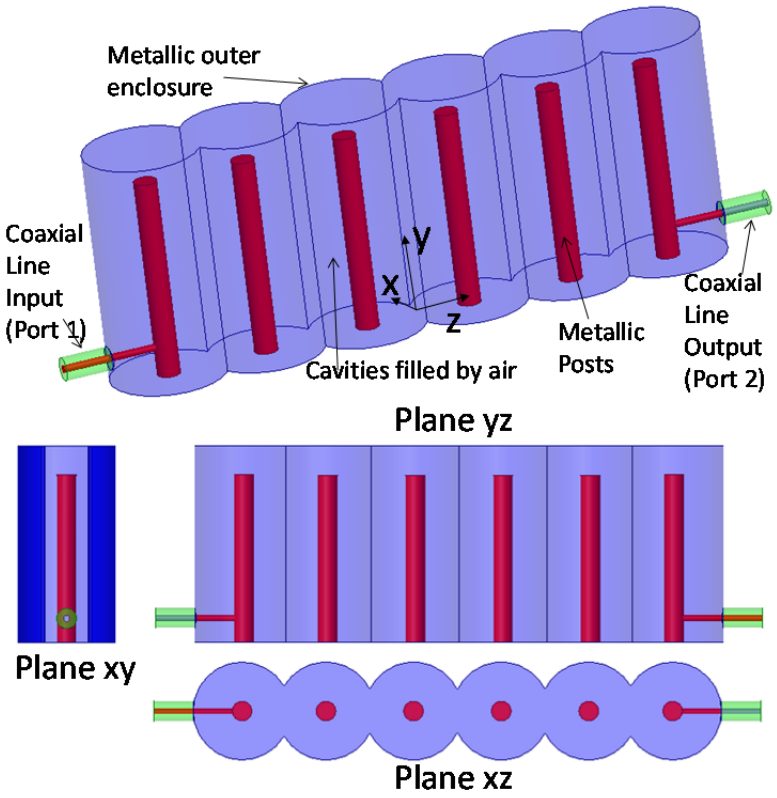


Figure 1. Six-order cavity combline microwave filter. Main views of the physical structure.

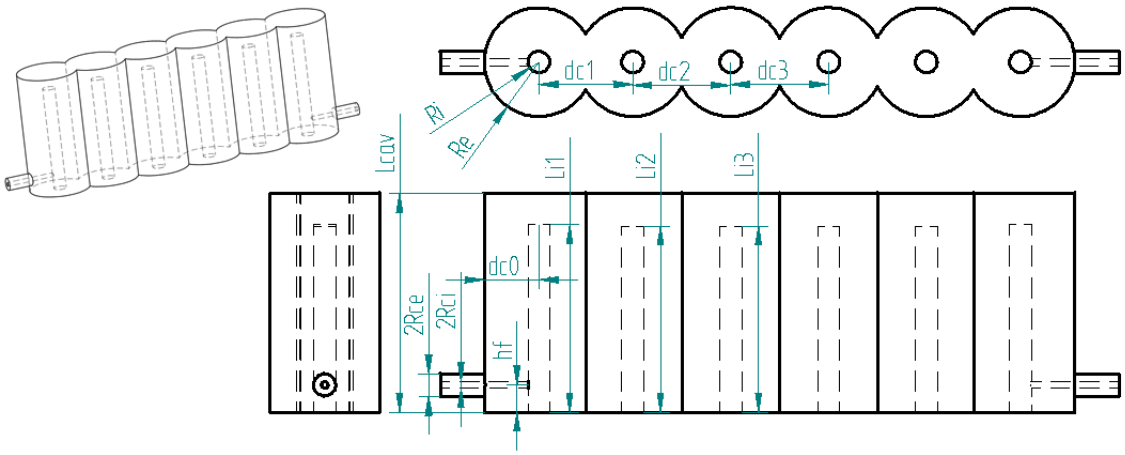


Figure 2. Physical dimensions involved in the design of a combline microwave filter.

The filtering response to be achieved with this physical structure is specified by the so-called coupling matrix **M** [3][5]. The case under consideration is an inline structure [3], where the coupling matrix reduces to only the couplings between adjacent resonators. For a symmetric six-order filter, only three values are needed $M_{1,2}=M_{5,6}$, $M_{2,3}=M_{4,5}$, $M_{3,4}$, that are mainly controlled by $dc_1$, $dc_2$, $dc_3$, respectively. Input-output couplings $M_{in}=M_{out}$ are controlled by $h_f$. The resonant frequency of the cavities will be determined by $L_{i1}$,$L_{i2}$,$L_{i3}$. It is emphasized here that although these parameters control the response of the filter, their values affect not only to one circuit parameter, but to several of them. As a summary, the filter design problem can be stated as: given the coupling values $M_{1,2}$, $M_{2,3}$, $M_{3,4}$, $M_{in}$, center frequency $f_0$ and bandwidth $bw$ of the desired circuit filtering response, find the dimensions $L_{i1}$, $L_{i2}$, $L_{i3}$, $h_f$, $dc_1$, $dc_2$, $dc_3$ of a physical combline structure whose full-wave response matches (approximates) the desired circuit response. The next sections will explain how to approach this problem by stages.

## 3. DESCRIPTION OF THE DESIGN METHOD

### 3.1. Stages

In each design stage a part of the structure is selected and the electromagnetic simulation is compared with the ideal circuital response correspondent to that part. For convenience the following stages can be represented by means of the pertinent diagram of figure 3, in which circles represent cavities and $M_{i,j}$ describes the coupling (inverters in the circuit model [2]) between resonators. In this way, the four stages selected in this design are represented schematically in figure 3, where $M_{in}=M_{out}$.

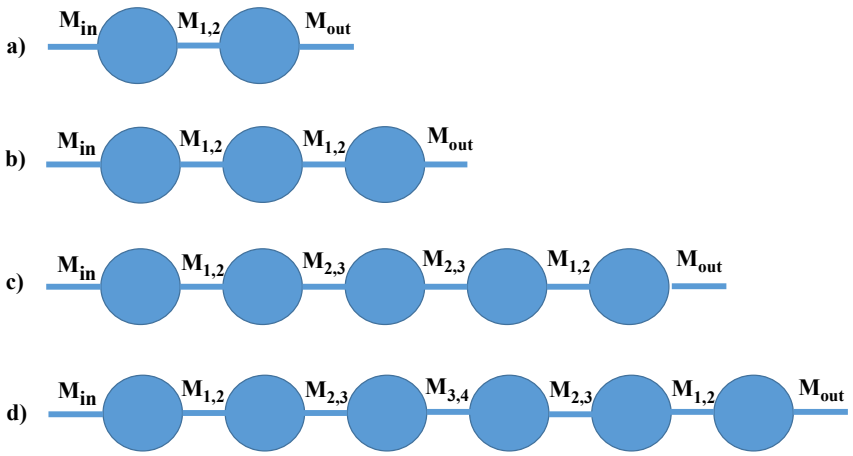


Figure 3. Schematic representation of the stages of the filter design: a) first stage, b) second stage, c) third stage, d) fourth stage (final desired filter).

### 3.2. Optimization method

Each stage design can be mathematically understood as a problem in which the physical parameters of the structure are variables which lead to an optimal solution – the one implementing the circuit response identified as a target. Three tools are involved in the optimization process: the cost function, the target mask and the optimization algorithm.

The physical dimensions presented in the preceding section are the variables upon which the cost function is dependent. The function to be minimized in this article is the following, comparing the full-wave and circuit responses (given by its S-parameters) at some selected critical frequencies:

$$f(\vec{x}) = \sum_{i=1}^{N} \alpha_i (|S_{21}^{full\ wave}(f_i)| - |S_{21}^{circuital}(f_i)|)^2 + \\ + \sum_{j=1}^{M} \beta_j (|S_{11}^{full\ wave}(f_j)| - |S_{11}^{circuital}(f_j)|)^2, \quad (1)$$

where $\vec{x}$ will be the optimization variables at each stage. The previous cost function is assessed in terms of discrete frequencies conveniently chosen by the designer depending on the optimization stage [6]. These frequencies are also involved in the second tool, which is fundamental for the optimization process – the mask. This article presents several mask types in order to attain the target circuit responses. Finally, the algorithm [7] used to minimize the cost function is the third and last tool of the process. In this particular case, a local-deterministic algorithm able to find minima in no-linear functions is enough.

## 4. APPLICATION OF THE DESIGN METHOD TO A MICROWAVE FILTER FOR BASE STATIONS

In order to validate the proposed design approach, a sixth-order Chebychev filter, with 20 dB of return loss is proposed. It is centered at $f_0$=2 GHz with a fractional bandwidth $bw$=1%, and $M_{1,2}$=0.843, $M_{2,3}$=0.611, $M_{3,4}$=0.583, $M_{in}$=$M_{out}$=1.002. This would be a typical scenario for narrow-band filters used in base stations for wireless communications [4]. The combination of the three optimization tools (cost function, mask and algorithm) during the fourth selected stages of design is presented below. In the stages over which the optimization process takes place, simplex algorithm by Nelder Mead is used [7], except in the second stage, in which Trust Region Framework is used.

Dimensions obtained at the end of each stage become the starting point of the next one. In all the stages, an initial task of coarse approximation of the physical parameters incorporated at that stage (and not used in previous stages) is done before the starting the optimization process. Initial values for all the variables can be found using models as those in [8],[9]. During the stages, the cost function (1) will be evaluated with S-parameters in natural units or in logarithmic (dB) units [2]. The representation in the figures will be realized in the domain used for the optimization.

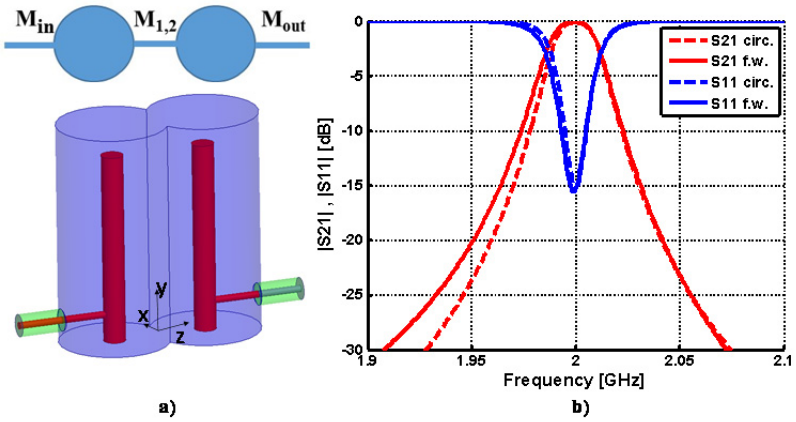


Figure 4. a) Simulated physical structure. b) End of the first stage.

### 4.1. First stage

The first step in the design process takes exclusively into account the two resonators placed at both ends of the structure (see figure 3.a and 4.a). Thanks to the small number of variables present at this stage (i.e. only $h_f$, $dc_1$ and $L_{i1}$, because of the xy-plane symmetry of the structure), even the optimization tool can be replaced by a parametric sweep. The result is shown in figure 4.b, where from now on the label *f.w.* refers to full wave response and the label *circ.* to circuit response.

### 4.2. Second stage

At this stage the three resonators shown in figures 3.b and 5.a are studied, and therefore the physical design parameters involved are $h_f$, $dc_1$, $L_{i1}$ and $L_{i2}$. This last variable is the only dimension that was not present at previous stage. Thus, the goal of this stage is to set the right value for $L_{i2}$, while the values of $h_f$, $dc_1$, $L_{i1}$ are slightly refined due to the loading effect of the new resonator not considered at the first stage. This is one of the advantages of this strategy: at each stage, new variables are introduced gradually, while previous ones are refined at the same time, and the complexity is increased very smoothly.

For our particular case, the target circuit response at this stage is very similar to the response of a three order filter designed to achieve the same reflection. Since their values do not differ greatly, and the bandwidth obtained in the former is much wider than in the latter, it is decided to use a section mask based on the latter, which is less restrictive. Additional resonators incorporated in the following stages will cooperate to achieve the desired mask. In this particular premature partial stage this is not essential. The result of the optimization process is shown in figure 5.b. together with the details of the mask used by sections only for the reflection. The following weights are used for the cost function by sections $\beta_{section\ 1,3,5} = 0.4$, $\beta_{section\ 2,4} = 0.75$.

For convenience hereinafter the physical structure selected at each stage will be depicted in the same figure where either the starting or ending point of the stage is showed.

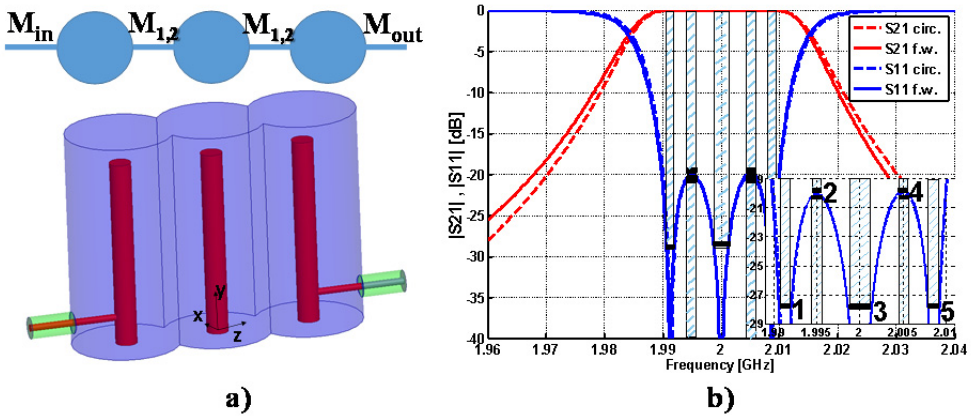


Figure 5. a) Simulated physical structure. b) End of the second stage.

### 4.3. Third stage

In the third stage, the five resonators detailed in figure 3.c are used. The physical design parameters involved now are $h_f$, $dc_1$, $dc_2$, $L_{i1}$, $L_{i2}$ and $L_{i3}$ (again only half of the structure because of the xy-symmetry). Figure 6.a shows the immediately preceding point to the optimization process. Changing from three to five resonators entails a large variation of the loading effect seen by each resonator, which implies a more cumbersome refining process than in the previous stage. Therefore, the optimization work is carried out in several iterations by masks seeking to enhance and correct several aspects of the full-wave response until a trade-off situation is reached. In this context, it is fundamental to define suitable weights $\alpha_i$ and $\beta_i$ in the cost function. To this end dotted masks instead of section masks are widely used, because the complex nature of this stage requires a more precise control over the selected weights. When dotted masks are used, such dots are depicted by crosses on the target response to which they belong.

Figure 6.b. shows how a dotted circuital optimization mask overlaps with the starting point response in natural units. This mask aims at recovering the transmission bandwidth, and therefore the selected weights are $\alpha_{1\ldots6,\neq3,4} = 1$, $\alpha_{3,4} = 10$, $\beta_{1\ldots11} = 1$.

Figure 6.c. depicts a circuital optimization mask based on levels that has been selected with the purpose of allowing the remaining two reflection zeros to appear. This aims at avoiding that the highly restrictive dotted mask prevents them from appearing. The following weights by sections are used: $\alpha_{section\,1} = 100$, $\alpha_{section\,2} = 150$, $\beta_{unique\ section} = 1$.

Figure 6.d. shows the response obtained after the use of the preceding mask, whose primary objective was to locate the remaining two reflection zeros. The algorithm evolution over that iteration did not show the five reflection zeros, but at least a fourth zero was obtained (figure 6.d is detailed in logarithmic units for the purpose of noticeably displaying the achieved reflection zeros).

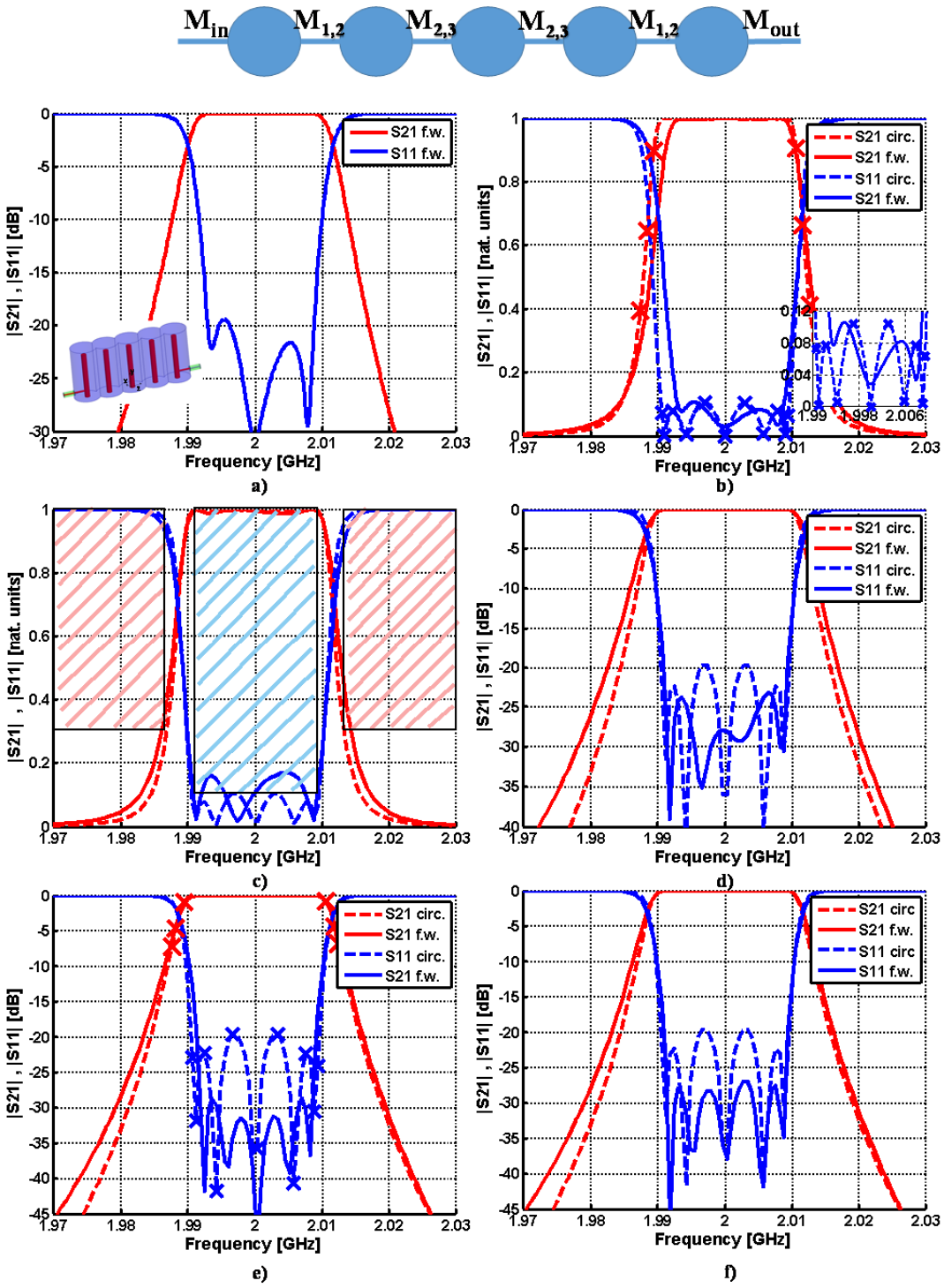


Figure 6. Responses of the most representative iterations of the second stage.

Several intermediate iterations are done with dotted circuital masks whose main goal is to obtain the remaining reflection zeros and to keep the achieved transmission bandwidth. It is important to highlight that sometimes the weights ($\alpha_i$, $\beta_i$) selected lead to the lack of one of the reflection zeros, but this iterative process requires taking such decisions in order to avoid a stalled process.

Once the reflection adjustment reaches the desired five reflection zeros without an unreasonable bandwidth widening in transmission, the response depicted in figure 6.e is obtained. This response is shown overlapped with *a family scanning* dotted circuital optimization mask. It aims at observing the natural evolution of the algorithm in order to locate filters within the same family of solutions. To this end all dots present unit weight:$\alpha_{1\ldots6,} = 1,\ \beta_{1\ldots11} = 1$.

Upon completion of the previous mask, the filtering response is represented in 6.f. It is considered a response close enough to the ideal objective circuital response as to put an end to the iterative optimization process of the third stage.

### 4.4. Fourth stage

This is the last stage in which the optimization process is involved, where the whole filtering structure is considered (see figure 3.d). In this case natural units are used to optimize the response, with unitary weights in both transmission and reflection ($\alpha_i$,$\beta_i$=1). Although this stage involves the same number of design parameters as in a direct global strategy (i.e. $h_f$, $dc_1$, $dc_2$, $dc_3$, $L_{i1}$, $L_{i2}$ and $L_{i3}$ due to the symmetry of the structure), those variables which were involved in the foregoing stage already have a value very close to the final optimal solution. This was the goal of previous stages.

It is important to mention that this stage differs from the preceding ones in the sense that whereas the previous stages sought the specific number of reflection zeros, at this stage this is not mandatory, as the aim of the whole filter design process from the industry side may be formulated in terms of a mask of reflection and rejection, and not to the aforementioned zeros. The visibility of the zeros becomes therefore a secondary objective. Notwithstanding, in this case study the implemented mask was point-based and the optimization process led to a response with six reflection zeros (figure 7.a) with a very good matching with the circuit response. However, it would have been perfectly correct to use a level-based mask at this stage instead.

At this point, it is important to mention that the electromagnetic simulation software used throughout the design process used settings oriented to the attainment of fast but relatively imprecise results. The underlying reason of this decision is that it was considered preferable to allow the optimization process to make more evaluations and therefore grant the possibility of finding out the behavior of the selected mask to correct it if needed.

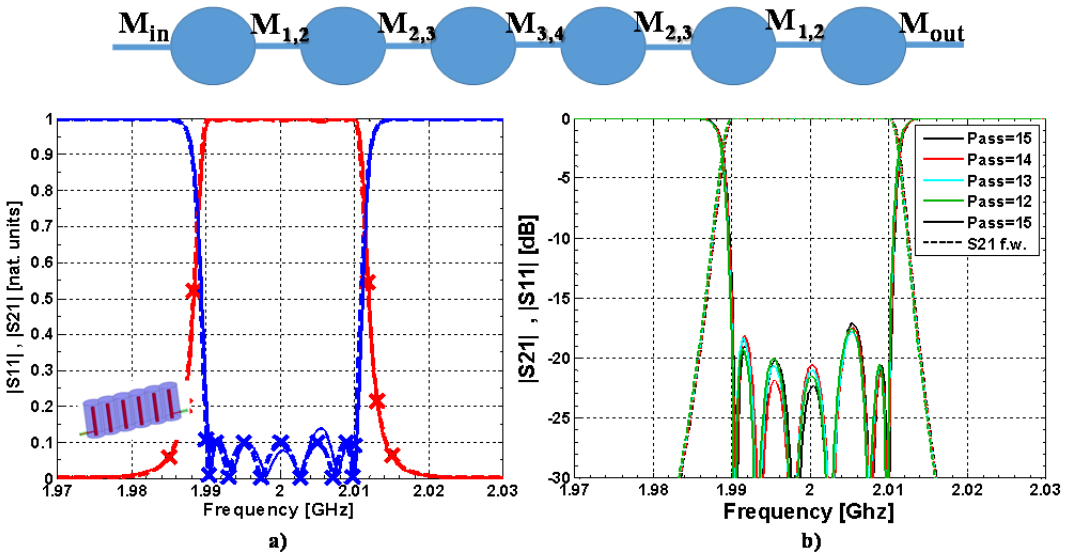


Figure 7. a) End of fourth stage b) Convergence of the FEM simulation for the final filter, where each pass has associated a finer mesh.

However, any final design must guarantee that the simulated response matches with reality. Accordingly, studying the convergence of the designed structure is a must. Since the FEM algorithm was used, this is directly translated as an increased number of meshing passes. Figure 7.b. shows the aforementioned convergence process. Table 1 gathers the final physical parameters of the designed filter (as defined in figure 2), and the final response is depicted in figures 8.a (narrowband response) and 8.b (wideband response, showing first spurious band at approximately $3f_0$=6 GHz, typical of combline filters [2]).

## 5. CONCLUSION

Filter design method based on stages has been used throughout this work. A sixth-order cavity combline bandpass filter was designed in four stages. Each of them used the preceding one as the starting point of a manual-coarse adjustment, after which the optimization tool is used as a process of refinement to achieve the desired partial response.

The stage approach offers one main benefit: these designs show lower uncertainty levels in terms of the physical parameters of the structure as opposed to designs that take into account the full structure from the very beginning. In this way a coarse adjustment is more easily obtained as a good starting point for optimization, which in turn translates into the optimization tool being closer to the optimal solution. This does not only mean a lower number of iterations, but also that a local-deterministic algorithm suffices to obtain the desired response. This process may result in even more benefits for filters with more complex coupling arrangements.

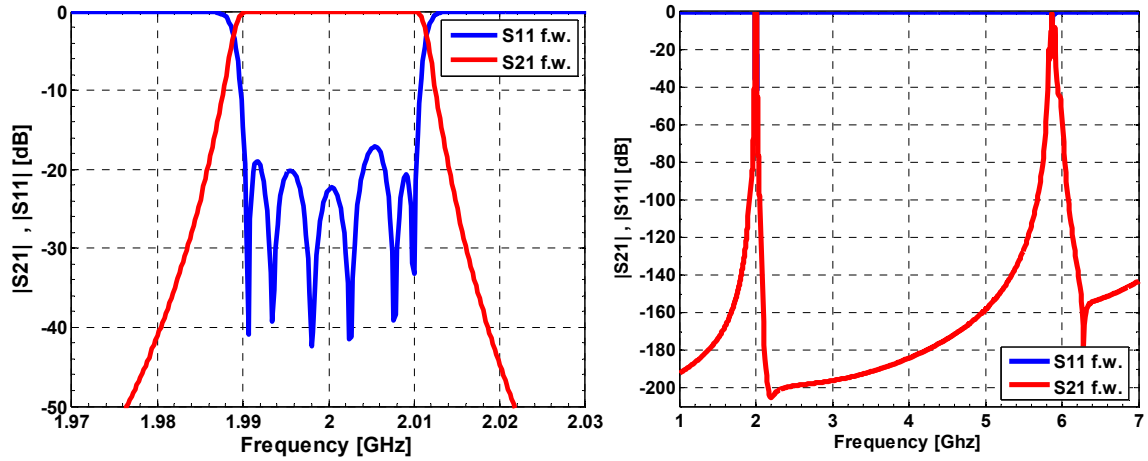


Figure 8. a) Filter response of the final structure obtained with the proposed optimization strategy (dimensions in Table 1); b) Wideband response of the filter.

| [mm] | | | | | | | | | | | | |
|---|---|---|---|---|---|---|---|---|---|---|---|---|
| $L_{cav}$ | $R_e$ | $R_i$ | $h_f$ | $L_{i1}$,$L_{i6}$ | $L_{i2}$,$L_{i5}$ | $L_{i3}$,$L_{i4}$ | $dc_1$,$dc_5$ | $dc_2$,$dc_4$ | $dc_3$ | $R_{ci}$ | $R_{ce}$ | $\varepsilon_{rcoax}$ |
| 40.2 | 10 | 2 | 1.901 | 34.397 | 34.147 | 34.172 | 17.150 | 17.850 | 17.935 | 0.638 | 2.03 | 1.88 |

Table 1. Final physical design parameters as defined in figure 2 for the microwave combline filter used to validate the optimization approach.

## REFERENCES

[1] G. L. Matthaei, L. Young, and E. M. T. Jones, Microwave Filters, Impedance-Matching Networks and Coupling Structure. New York: McGraw-Hill, 1984.

[2] R. J. Cameron, C. M. Kudsia, R. R. Mansour, "Microwave filters for communication systems fundamentals, design, and applications", Wiley-Interscience, 2007

[3] G. L. Matthaei, "Comb-line band-pass filters of narrow or moderate bandwidth," Microwave Journal, vol. 6, pp. 82–91, Aug. 1963.

[4] R. R. Mansour, "Filter technologies for wireless base stations", IEEE Microwave Magazine, vol 5, pp.68-74, March 2004.

[5] A.E. Atia and Williams, Narrow-band waveguide filters. I*EEE Trans. Microwave Theory Tech.* MTT-20, 258-265 (Aprol 1972).

[6] X. Shang, W. Xia, and M. J Lancaster, "The design of waveguide filters based on cross-coupled resonators," Microwave and Optical Technology Letters, Wiley Online Library, vol.

56, no. 1, pp. 3-8, 2014.

[7] W. H. Press, S. A. Teukolsky, W. T. Vetterling, B. P. Flannery, Numerical Recipes in Fortran. Cambridge University Press, 1986.

[8] Chi Wang, and K.A. Zaki, "Full-wave modeling of electric coupling probes in comb-line resonators and filters," Microwave Theory and Techniques, IEEE Transactions on, vol. 48, no. 12, pp. 2459 -2464, dec 2000.

[9] H.W. Yao, K. A. Zaki, A. E. Atia, and R. Hershtig, “Full wave modeling of conducting posts in rectangular waveguides and its applications to slot coupled combline filters,” IEEE Trans. Microwave Theory Tech., vol. 43, pp. 2824–2830, Dec. 1995

# H

# Motivación y estructura

## H.1 Motivación

El propósito de este trabajo es estudiar el diseño de filtros de radiofrecuencia (esto es, de filtros diseñados para el rango de 300 MHz a 300 GHz). Los filtros de radiofrecuencia son dispositivos pasivos encargados de la selección de señales en el dominio de la frecuencia, limitando el ruido y rechazando en la medida de lo posible las señales interferentes. Este tipo de filtros se suelen encontrar en los *front-end* de los transceptores de alta frecuencia, en sistemas tan diversos como radar, enlaces de televisión por satélite, etc.

Habitualmente estos sistemas están sujetos a estrictas restricciones, demandando por ello filtros de altas prestaciones. Desde el punto de vista eléctrico, las características deseables de un filtro son: alta selectividad, bajas pérdidas de inserción, amplia ventana libre de espúreos y buen manejo de potencia. Desde el punto de vista mecánico, el peso y el volumen pueden ser críticos dependiendo del sistema al que se destine el filtro.

Este trabajo se titula "Diseño de filtros en cavidad coaxial", dado que tiene como objetivo último el diseño de un filtro *combline* paso banda en cavidad coaxial. No obstante, el término *combline* alude al tipo de estructura física empleada, y sin embargo el diseño de filtros dista mucho de la resolución exclusiva de las dimensiones físicas de la estructura final de microondas. Tal y como muestra la figura H.1, el diseño completo de un filtro involucra varias etapas. En filtros de altas prestaciones, cada etapa es clave para que el diseño final pueda cumplir con las especificaciones. De hecho, cada una de estas etapas tiene tal complejidad que es considerada un área de conocimiento distinta.

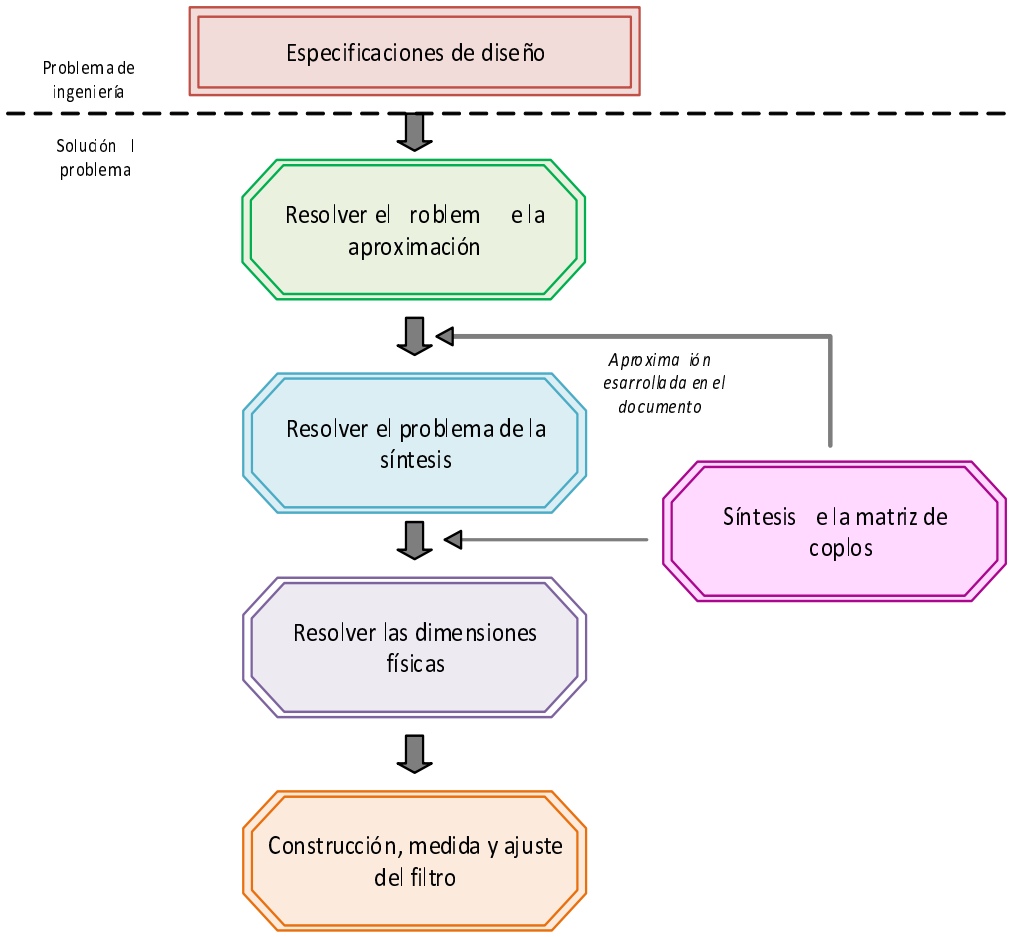


**Figure H.1: Etapas en el diseño de filtros**

Sin embargo, no son áreas independientes, y para que el diseño funcione cada etapa ha de tener en cuenta las sucesivas. El objetivo global de este trabajo es obtener una visión teórica y práctica del proceso global del diseño de filtros, aunando las etapas presentadas. Únicamente por falta de presupuesto y tiempo no se lleva a cabo la última etapa, en la que se construiría, mediría y ajustaría el prototipo diseñado.

## H.2 Objetivos y estructura del documento

Este documento se organiza de acuerdo con las etapas existentes en el diseño de filtros.

⇒ El capítulo 2 aborda el problema de la aproximación (esto es, el método de las pérdidas de inserción), el cual se preocupa de la consecución de una función racional que cumpla con las especificaciones dadas. En este capítulo se incluyen las propiedades que han de cumplir los polinomios de diseño involucrados. Se expone así mismo la relación entre dichos polinomios y los parámetros S empleados típicamente en dispositivos de radiofrecuencia. Al final del capítulo se presenta el método generalizado de Chebychev. Se trata de una herramienta valiosa, ya que le proporciona libertad al diseñador para establecer ceros de transmisión finitos, con los que incluso se pueden obtener respuestas asimétricas. El objetivo de este capítulo es implementar este método en MATLAB para poner en evidencia sus increíbles capacidades y flexibilidad. Se incluyen cuatro casos prácticos al final del capítulo.

⇒ El capítulo 3 está dedicado a la síntesis de la matriz de acoplos. En este caso, y a diferencia del capítulo anterior, la teoría presentada en el proyecto es un objetivo en sí misma. Aunque la teoría de síntesis de la matriz de acoplos puede encontrarse en varios libros (como por ejemplo en [1], [2]), resulta tediosa su comprensión, dado que normalmente la información se distribuye a lo largo de varios capítulos y se presentan normalmente varios métodos. Sólo tras la recopilación de información y su estudio ha sido posible desarrollar el capítulo 3 de este proyecto, y con él, el código de MATLAB asociado. La herramienta programada calcula los valores de la matriz de acoplos a partir de los polinomios de diseño. Nuevamente algunos ejemplos de validación se presentan al final del capítulo.

⇒ Los capítulos 4 y 5 abordan las etapas de síntesis y de realización de filtros. Los filtros paso bajo se estudian en el capítulo 4, mientras que el capítulo 5 está dedicado a los filtros paso banda.

El problema de la síntesis se presenta en la primera sección de ambos capítulos dado que las redes de elementos concentrados constituyen la base de los modelos de radiofrecuencia. El capítulo 5 incluye además una breve sección donde se introducen las rotaciones como herramienta para transformar la topología de un circuito descrito por la matriz de acoplos. Nuevamente se implementan e incluyen algunos ejemplos desarrollados en MATLAB.

En el capítulo 4, el principal objetivo es el diseño de un filtro de secciones cortas en tecnología coaxial. El capítulo 5 tiene por objetivo el estudio de la aproximación paso banda basada en inversores y el diseño de varios filtros en diferentes tecnologías de guía de onda. También en este capítulo se aborda el problema del cambio uniforme de dieléctrico en un filtro de radiofrecuencia.

⇒ Finalmente, el capítulo 6 se centra en el diseño de un filtro combline de banda estrecha de altas prestaciones. Se diseña para comunicaciones móviles en la Banda S. El objetivo de este capítulo es desarrollar un método para diseñar eficientemente filtros donde la caracterización de las discontinuidades no es siempre una tarea asequible. Este método se basa en la subdivisión estratégica del problema de diseño completo en etapas secuenciales.

En este método la optimización adquiere un papel esencial, dado que las dimensiones físicas de las estructuras de las etapas intermedias han de conseguir que idealmente la respuesta del simulador electromagnético y la del modelo circuital equivalente sean coincidentes. Si el nivel de refinamiento de los parámetros físicos tuviese que alcanzarse por medio de la variación manual de los parámetros, este método no sería en absoluto práctico.

# I

# Conclusiones y trabajo futuro

## I.1 Conclusiones

Este trabajo se ha centrado en el diseño de filtros de microondas. El proceso de diseño se divide en varias etapas: aproximación, síntesis de la matriz de acoplos, síntesis de la red circuital, selección de las dimensiones físicas de la estructura de microondas y fabricación, medida y ajuste de la estructura. Todas estas etapas , a excepción de la última (principalmente por tiempo y presupuesto), han sido abordadas (aunque con distintos grados de profundidad). De esta forma, este trabajo ofrece una visión global de casi todo el proceso de diseño. Se ha aprendido a lo largo del proyecto la complejidad que envuelve al problema completo de ingeniería, y se han aprendido y desarrollado algunas estrategias para abordarlo.

En el capítulo 2 se estudió el método generalizado de Chebychev como una herramienta muy valiosa a la hora de alcanzar la respuesta en frecuencia deseada. Se ha mostrado a través del código implementado cómo este método ofrece al diseñador la flexibilidad de perseguir un compromiso entre selectividad y linealidad de fase. Además, ha quedado demostrado que este método permite dar lugar a respuestas asimétricas, lo cual se traduce en diseños más compactos (es decir, de menor orden para las mismas especificaciones).

Una vez que se obtuvieron los polinomios de diseño por medio del método generalizado de Chebychev, se estudió la síntesis de la matriz de acoplos en el capítulo 3. La matriz de acoplos es una herramienta poderosa que permite, a partir de los polinomios de diseño, identificar la influencia que cada resonador ejerce sobre sí mismo y sobre los restantes en el circuito. Además, se ha podido ver que su versatilidad reside en que su síntesis no está ligada a ninguna tecnología en particular, por lo que puede usarse tanto para filtros de cavidades como para filtros de tecnología impresa. En este capítulo se incluyeron algunos ejemplos de validación del software desarrollado.

Además, se introdujeron las rotaciones como herramienta de transformación de la matriz de acoplos para garantizar una topología práctica en las estructuras típicamente empleadas en radiofrecuencia. Varios ejemplos de MATLAB se incluyeron en el capítulo correspondiente.

Una vez calculada la matriz de acoplos que cumple con las especificaciones eléctricas, se aborda el siguiente paso en el diseño de filtros: la obtención de las dimensiones físicas de la estructura de radiofrecuencia que implementa idealmente esa respuesta. Con este fin, la estructura física se selecciona teniendo en cuenta que, además de las especificaciones eléctricas, el filtro tendrá también restricciones en cuanto a peso, volumen, pérdidas de inserción y manejo de potencia. En el contexto de la realización física, se diseñó un filtro de secciones cortas en tecnología coaxial (capítulo 4), así como varios filtros de acoplos directos en guía de onda (capítulo 5). En ambos casos los diseños se llevaron a cabo siguiendo las aproximaciones típicas del diseño de filtros de radiofrecuencia. Adicionalmente se llevó a cabo un proceso de optimización para mejorar sus prestaciones.

En este mismo escenario de realización de filtros de radiofrecuencia, se diseñó en el capítulo 6 un filtro combline de cavidades de altas prestaciones para estaciones base. Para ello se propuso un método basado en la subdivisión del diseño de la estructura completa en etapas secuenciales. De esta manera, en cada paso de diseño se tuvieron en cuenta menos parámetros de diseño que en el problema global. Para poder llevar a cabo este método, de definió como función de coste la diferencia entre la respuesta del simulador electromagnético y la respuesta circuital de la estructura seleccionada en cada etapa. La validez de este método ha quedado demostrada en el capítulo correspondiente.

## I.2 Trabajo futuro

Siempre es posible mejorar y proponerse nuevos retos. Desde mi punto de vista, los puntos más importantes a desarrollar en el futuro serían los siguientes:

⇒ Aplicar el conocimiento obtenido en el área de la optimización al problema de la aproximación. Conceptualmente no supondría ningún reto, pero ahorraría tiempo a la hora de posicionar los ceros de transmisión finitos en el método generalizado de Chebychev.

⇒ Ampliar la teoría aprendida en el contexto de la matriz de acoplos y desarrollar el código de MATLAB correspondiente para la matriz de acoplos $(N+2) \times (N+2)$.

⇒ Estudiar la validez del método de extracción de acoplos como alternativa al método propuesto para el diseño del filtro combline.

⇒ Analizar si el uso de algoritmos heurísticos puede merecer la pena a la hora de afrontar el problema de la convergencia relativa. Podría ser una alternativa interesante a las múltiples iteraciones llevadas a cabo en una de las etapas de diseño del filtro combline.

⇒ Construcción y medida de los prototipos diseñados, para así completar el ciclo completo de diseño de filtros de radiofrecuencia. Aunque hoy en día los simuladores electromagnéticos son muy precisos, en el diseño de filtros de radiofrecuencia es común necesitar una etapa posterior de ajuste de la estructura construida para alcanzar la respuesta deseada. En ese sentido, es una etapa que no se debería subestimar.

# J

# Pliego de condiciones

## Pliego de condiciones

Este documento contiene las condiciones legales que guiarán la realización, en este proyecto,tanto de software de síntesis de filtros como de los planos de los distintos filtros diseñados en guía de onda. En lo que sigue, se supondrá que el proyecto ha sido encargado por una empresa cliente a una empresa consultora con la finalidad de realizar dicho sistema. Dicha empresa ha debido desarrollar una línea de investigación con objeto de elaborar el proyecto. Esta línea de investigación, junto con el posterior desarrollo de los programas está amparada por las condiciones particulares del siguiente pliego.

Supuesto que la utilización industrial de los métodos recogidos en el presente proyecto ha sido decidida por parte de la empresa cliente o de otras, la obra a realizar se regulará por las siguientes:

***Condiciones generales.***

A. La modalidad de contratación será el concurso. La adjudicación se hará, por tanto, a la proposición más favorable sin atender exclusivamente al valor económico, dependiendo de las mayores garantías ofrecidas. La empresa que somete el proyecto a concurso se reserva el derecho a declararlo desierto.

B. El montaje y mecanización completa de los equipos que intervengan será realizado totalmente por la empresa licitadora.

C. En la oferta, se hará constar el precio total por el que se compromete a realizar la obra y el tanto por ciento de baja que supone este precio en relación con un importe límite si este se hubiera fijado.

D. La obra se realizará bajo la dirección técnica de un Ingeniero Superior de Telecomunicación, auxiliado por el número de Ingenieros Técnicos y Programadores que se estime preciso para el desarrollo de la misma.

E. Aparte del Ingeniero Director, el contratista tendrá derecho a contratar al resto del personal, pudiendo ceder esta prerrogativa a favor del Ingeniero Director, quien no estará obligado a aceptarla.

F. El contratista tiene derecho a sacar copias a su costa de los planos, pliego de condiciones y presupuestos. El Ingeniero autor del proyecto autorizará con su firma las copias solicitadas por el contratista después de confrontarlas.

G. Se abonará al contratista la obra que realmente ejecute con sujeción al proyecto que sirvió de base para la contratación, a las modificaciones autorizadas por la superioridad o a las órdenes que con arreglo a sus facultades le hayan comunicado por escrito al Ingeniero Director de obras siempre que dicha obra se haya ajustado a los preceptos de los pliegos de condiciones, con arreglo a los cuales, se harán las modificaciones y la valoración de las diversas unidades sin que el importe total pueda exceder de los presupuestos aprobados. Por consiguiente, el número de unidades que se consignan en el proyecto o en el presupuesto, no podrá servirle de fundamento para entablar reclamaciones de ninguna clase, salvo en los casos de rescisión.

H. Tanto en las certificaciones de obras como en la liquidación final, se abonarán los trabajos realizados por el contratista a los precios de ejecución material que figuran en el presupuesto para cada unidad de la obra.

I. Si excepcionalmente se hubiera ejecutado algún trabajo que no se ajustase a las condiciones de la contrata pero que sin embargo es admisible a juicio del Ingeniero Director de obras, se dará conocimiento a la Dirección, proponiendo a la vez la rebaja de precios que el Ingeniero estime justa y si la Dirección resolviera aceptar la obra, quedará el contratista obligado a conformarse con la rebaja acordada.

J. Cuando se juzgue necesario emplear materiales o ejecutar obras que no figuren en el presupuesto de la contrata, se evaluará su importe a los precios asignados a otras obras o materiales análogos si los hubiere y cuando no, se discutirán entre el Ingeniero Director y el contratista, sometiéndolos a la aprobación de la Dirección. Los nuevos precios convenidos por uno u otro procedimiento, se sujetarán siempre al establecido en el punto anterior.

K. Cuando el contratista, con autorización del Ingeniero Director de obras, emplee materiales de calidad más elevada o de mayores dimensiones de lo estipulado en el proyecto, o sustituya una clase de fabricación por otra que tenga asignado mayor precio o ejecute con mayores dimensiones cualquier otra parte de las obras, o en general, introduzca en ellas cualquier modificación que sea beneficiosa a juicio del Ingeniero Director de obras,

no tendrá derecho sin embargo, sino a lo que le correspondería si hubiera realizado la obra con estricta sujeción a lo proyectado y contratado.

L. Las cantidades calculadas para obras accesorias, aunque figuren por partida alzada en el presupuesto final (general), no serán abonadas sino a los precios de la contrata, según las condiciones de la misma y los proyectos particulares que para ellas se formen, o en su defecto, por lo que resulte de su medición final.

M. El contratista queda obligado a abonar al Ingeniero autor del proyecto y director de obras así como a los Ingenieros Técnicos, el importe de sus respectivos honorarios facultativos por formación del proyecto, dirección técnica y administración en su caso, con arreglo a las tarifas y honorarios vigentes.

N. Concluida la ejecución de la obra, será reconocida por el Ingeniero Director que a tal efecto designe la empresa.

O. La garantía definitiva será del 4

P. La forma de pago será por certificaciones mensuales de la obra ejecutada, de acuerdo con los precios del presupuesto, deducida la baja si la hubiera.

Q. La fecha de comienzo de las obras será a partir de los 15 días naturales del replanteo oficial de las mismas y la definitiva, al año de haber ejecutado la provisional, procediéndose si no existe reclamación alguna, a la reclamación de la fianza.

R. Si el contratista al efectuar el replanteo, observase algún error en el proyecto, deberá comunicarlo en el plazo de quince días al Ingeniero Director de obras, pues transcurrido ese plazo será responsable de la exactitud del proyecto.

S. El contratista está obligado a designar una persona responsable que se entenderá con el Ingeniero Director de obras, o con el delegado que éste designe, para todo relacionado con ella. Al ser el Ingeniero Director de obras el que interpreta el proyecto, el contratista deberá consultarle cualquier duda que surja en su realización.

T. Durante la realización de la obra, se girarán visitas de inspección por personal facultativo de la empresa cliente, para hacer las comprobaciones que se crean oportunas. Es obligación del contratista, la conservación de la obra ya ejecutada hasta la recepción de la misma, por lo que el deterioro parcial o total de ella, aunque sea por agentes atmosféricos u otras causas, deberá ser reparado o reconstruido por su cuenta.

U. El contratista, deberá realizar la obra en el plazo mencionado a partir de la fecha del contrato, incurriendo en multa, por retraso de la ejecución siempre que éste no sea debido a causas de fuerza mayor. A la terminación de la obra, se hará una recepción provisional previo reconocimiento y examen por la dirección técnica, el depositario de efectos, el interventor y el jefe de servicio o un representante, estampando su conformidad el contratista.

V. Hecha la recepción provisional, se certificará al contratista el resto de la obra, reservándose la administración el importe de los gastos de conservación de la misma hasta su recepción definitiva y la fianza durante el tiempo señalado como plazo de garantía. La recepción definitiva se hará en las mismas condiciones que la provisional, extendiéndose el acta correspondiente. El Director Técnico propondrá a la Junta Económica la devolución de la fianza al contratista de acuerdo con las condiciones económicas legales establecidas.

W. Las tarifas para la determinación de honorarios, reguladas por orden de la Presidencia del Gobierno el 19 de Octubre de 1961, se aplicarán sobre el denominado en la actualidad "Presupuesto de Ejecución de Contrata" y anteriormente llamado "Presupuesto de Ejecución Material" que hoy designa otro concepto.

***Condiciones particulares.***

La empresa consultora, que ha desarrollado el presente proyecto, lo entregará a la empresa cliente bajo las condiciones generales ya formuladas, debiendo añadirse las siguientes condiciones particulares:

A. La propiedad intelectual de los procesos descritos y analizados en el presente trabajo, pertenece por entero a la empresa consultora representada por el Ingeniero Director del Proyecto.

B. La empresa consultora se reserva el derecho a la utilización total o parcial de los resultados de la investigación realizada para desarrollar el siguiente proyecto, bien para su publicación o bien para su uso en trabajos o proyectos posteriores, para la misma empresa cliente o para otra.

C. Cualquier tipo de reproducción aparte de las reseñadas en las condiciones generales, bien sea para uso particular de la empresa cliente, o para cualquier otra aplicación, contará con autorización expresa y por escrito del Ingeniero Director del Proyecto, que actuará en representación de la empresa consultora.

D. En la autorización se ha de hacer constar la aplicación a que se destinan sus reproducciones así como su cantidad.

E. En todas las reproducciones se indicará su procedencia, explicitando el nombre del proyecto, nombre del Ingeniero Director y de la empresa consultora.

F. Si el proyecto pasa la etapa de desarrollo, cualquier modificación que se realice sobre él, deberá ser notificada al Ingeniero Director del Proyecto y a criterio de éste, la empresa consultora decidirá aceptar o no la modificación propuesta.

G. Si la modificación se acepta, la empresa consultora se hará responsable al mismo nivel que el proyecto inicial del que resulta el añadirla.

H. Si la modificación no es aceptada, por el contrario, la empresa consultora declinará toda responsabilidad que se derive de la aplicación o influencia de la misma.

I. Si la empresa cliente decide desarrollar industrialmente uno o varios productos en los que resulte parcial o totalmente aplicable el estudio de este proyecto, deberá comunicarlo a la empresa consultora.

J. La empresa consultora no se responsabiliza de los efectos laterales que se puedan producir en el momento en que se utilice la herramienta objeto del presente proyecto para la realización de otras aplicaciones.

K. La empresa consultora tendrá prioridad respecto a otras en la elaboración de los proyectos auxiliares que fuese necesario desarrollar para dicha aplicación industrial, siempre que no haga explícita renuncia a este hecho. En este caso, deberá autorizar expresamente los proyectos presentados por otros.

L. El Ingeniero Director del presente proyecto, será el responsable de la dirección de la aplicación industrial siempre que la empresa consultora lo estime oportuno. En caso contrario, la persona designada deberá contar con la autorización del mismo, quien delegará en él las responsabilidades que ostente.

# K
# Presupuesto

**A**) **Ejecución Material**

- Compra de ordenador personal (Software incluido) — 2.000 €
- Material de oficina — 150 €
- Total de ejecución material — 2.150 €

**B**) **Gastos generales**

- 16% sobre Ejecución Material — 344 €

**C**) **Beneficio Industrial**

- 6% sobre Ejecución Material — 129 €

**D**) **Honorarios Proyecto**

- 2000 horas a 15 €/ hora — 30000 €

**E**) **Material fungible**

- Gastos de impresión — 250 €
- Encuadernación — 50 €

**F**) **Subtotal del presupuesto**

- Subtotal Presupuesto — 32.923 €

**G) I.V.A. aplicable**

- 21% Subtotal Presupuesto — 6913.83 €

**H) Total presupuesto**

- Total Presupuesto — 39.836.83 €

Madrid, Julio de 2015
La Ingeniera Jefe de Proyecto

Fdo.: Ana Morán López
Ingeniera de Telecomunicación